Noise Limits due to Light Mixing in Optical Code-Division Multiple-Access Systems

Elwyn D. J. Smith BE *(1st Class Hons)*

A thesis presented for the degree of
Doctor of Philosophy
in
Electrical and Electronic Engineering
at the
University of Canterbury,
Christchurch, New Zealand.

30 September 1998

ABSTRACT

This thesis is concerned with the performance limits arising in optical code-division multiple-access (OCDMA) networks due to the mixing of light from the independent sources of each user. The scheme of spectral-amplitude OCDMA is shown here to be significantly limited by the phase-induced intensity noise arising from such mixing, and the corresponding signal-to-noise ratio and network capacity limits are of the same order as those arising in coherence-multiplexing systems, also due to such noise. Mixing can only occur between spatially coherent light, and this typically takes place through the combination of the signals into a single-mode fibre. The use of multimode fibre instead of single-mode can thus significantly reduce the levels and effects of phase-induced intensity noise, and this is experimentally demonstrated.

It is shown that in general, assuming independent sources, there are only four possible ways in which to alleviate or eliminate noise limits of the form found for spectral-amplitude OCDMA. These are to separate the signals from each user in either the temporal, spectral, or spatial domains, or else to coherently despread the received signal. Neither spectral separation nor coherent despreading are practical for spectral-amplitude OCDMA, but spatial separation via multimode fibre may be applied. The use of pulse-position modulation (PPM) with spectral-amplitude OCDMA is shown to be able to improve the performance beyond the limits found earlier, and this is because of the temporal separation it introduces. However, unlike the direct reduction of source duty cycle, PPM signalling can be applied without increasing, relative to the bit rate, the modulation or detection bandwidths, nor the dispersion sensitivity. Such PPM signalling and the associated decoding can also be applied to other similarly limited systems, including those based upon coherence multiplexing.

If an OCDMA system is incoherent, has independent sources of the same spectrum, and has only a single-mode fibre to and from each user, then it can only avoid the significant noise limits found for spectral-amplitude OCDMA by the temporal separation of the signals from each user. This is the case for incoherent unipolar OCDMA systems, since the sparse codes of these systems rely on such temporal separation. Bipolar codes are not sparse, and in bipolar systems there is ordinarily no significant temporal separation between the signals from each user. Consequently, assuming sole single-mode-fibre paths and independent sources with identical spectra, every incoherent bipolar OCDMA system must encounter performance limits at least as bad as those found for spectral-amplitude OCDMA. These worst-case limits are identified for each of the incoherent bipolar OCDMA proposals to date.

PREFACE

My interest in optical communications was first sparked during my undergraduate days by Professor Peter Gough, through the descriptions of some of his research into coherent optical communication systems. Upon discussion of possible postgraduate studies with him, the field of optical code-division multiple access (OCDMA) was suggested as an area to which my attention could be directed.

At the time my research began, the optical code-division multiple-access field included many interesting and ambitious ideas, but significant practical problems remained to be overcome in most of these proposals. One of the earliest such schemes was based upon the spectral-phase encoding of ultrashort coherent pulses, and the use of an ideal coherent matched filter at the receiver to decode the transmitted signals. However, this scheme is particularly demanding in many ways, and another research group proposed an incoherent variation of the scheme that was much less demanding, and used cheap and simple broadband incoherent sources. These facts, along with the promising initial estimates of its performance, drew my attention to this scheme, and the experimental demonstration of such a system appeared within the capabilities of the resources available here. However, experimental demonstration to the degree necessary to verify the original performance estimates was not within these capabilities, and so an analytical approach to this scheme was taken. This thesis presents this analysis of the scheme known as spectral-amplitude OCDMA, and all the research that has stemmed from it.

Chapter 1 gives an introduction to optical communications and to network multiple-access schemes, and it describes the fundamentals of code-division multiple-access (CDMA) systems. Chapter 2 presents a literature review of the different approaches to optical CDMA that are being followed, and particular attention is paid to those schemes which are both incoherent and bipolar, and these include spectral-amplitude OCDMA. Although there are a number of astute observations in this chapter, there is no significant original content in Chapters 1 and 2.

Chapter 3 begins with a summary of the statistics of thermal noise and the effects of interference between independent light fields, as credited therein, but the rest of this chapter, in which these results are applied to spectral-amplitude OCDMA, and the associated appendix, are completely original. Such systems are thus shown to be limited to performance levels that are significantly lower than those initially predicted, even under best-case assumptions.

Chapter 4 describes an experimental investigation of the phase-induced intensity noise (PIIN) due to the interference between light from a source of broadband amplified spontaneous

emission. The measured levels are shown to be in agreement with theoretical expectations, unlike those of an earlier such investigation. The experimental use of multimode fibre to reduce this intensity noise is described, and the theoretical expectations of the PIIN reductions possible using multimode fibre are examined and compared. This chapter is original except for the summary of the mode structures of cylindrical dielectric waveguides, as credited therein.

In Chapter 5, the effects of reducing the duty cycles of the incoherent sources in spectral-amplitude OCDMA is investigated, and two alternative sources are considered. It is shown that similar performance limits also arise with these alternative sources, unless their spectra are dissimilar. This chapter and the associated appendices are entirely original.

In Chapter 6 the use of pulse-position modulation (PPM) together with spectral-amplitude OCDMA is proposed and investigated. It is shown that the use of PPM allows performance beyond the limits found in Chapter 3, and only a few simple changes to the original structure are necessary in the simplest case. This performance increase through PPM can also be obtained in other OCDMA systems which are limited in the same manner, including those based upon coherence multiplexing. This chapter is also original in its entirety.

Although Chapter 7 begins with the OCDMA framework from another work, this is then analysed in a more general sense and in greater detail, paying particular attention to the terms that are incorrectly dismissed in that work. This opening analysis therefore contains significant original contribution, and furthermore, the rest of this chapter and the associated appendices are completely original. The work in Chapter 7 thus analyses the general form of most OCDMA schemes, and it clearly identifies the conditions under which performance limits of the form found in Chapter 3 do or do not occur. The known such limit for coherence multiplexing with balanced detection is shown to arise from this analysis. All incoherent OCDMA systems using bipolar codes are shown to be ultimately limited by the mixing between light from different users. In particular, if such incoherent bipolar OCDMA schemes use independent sources with the same spectrum, and only one single-mode-fibre path to and from each user, then performance limits at least as bad as that found in Chapter 3 always occur.

Finally, in Chapter 8, a summary of the contributions and conclusions from the previous chapters is presented, together with suggestions for future work.

The following papers have been written as a result of the work presented in this thesis:

Smith, E.D.J., Gough, P.T. and Taylor, D.P. (1995), "Noise limits of optical spectral-encoding CDMA systems," *Electronics Letters*, Vol. 31, No. 17, August 1995, pp. 1469–1470.

Smith, E.D.J., Gough, P.T., Taylor, D.P. and Blaikie, R.J. (1996), "Spectral-Amplitude-Coding Optical CDMA with Pulse-Position Modulation,", In *Proceedings of the 21st Australian Conference on Optical Fibre Technology, ACOFT'96*, December 1996, pp. 189–192.

Smith, E.D.J., Blaikie, R.J. and Taylor, D.P. (1998), "Performance Enhancement of Spectral-Amplitude-Coding Optical CDMA using Pulse-Position Modulation," *IEEE Transactions on Communications*, Vol. 46, No. 9, September 1998, pp. 1176–1185.

ACKNOWLEDGEMENTS

I would like to thank Professors Peter Gough and Desmond Taylor, and also Dr. Richard Blaikie for their guidance, much fruitful discussion, and the editing of many draft manuscripts through the course of this thesis.

I thank my parents for their unending love and support in many ways, and thanks also to John and Barbara Smith for the opportunities to have a complete change of scene by spending time with them and their children, and for the numerous hearty meals I received. I would like to acknowledge the friendship and support of numerous flatmates and other friends through the years, and in particular the love and support of my close friends Jonathan and Meredith Thorpe, TjunWie Theng, and Michelle Nevill.

Outdoor activities seem almost compulsory in the Electrical and Electronic Engineering Department of the University of Canterbury, and I have spent many enjoyable study breaks rock climbing, mountain climbing, and caving with fellow students. I want to thank David Hawkins and Matthew Hebley in particular for their enthusiasm and company on many of these occasions, and their friendship and encouragement in general. I have also cycled many miles with Tasha Northcott, climbed indoors and on the Port Hills with Fiona Hunt, and explored old and new passages underground with Jon Terry, and I thank each of them for these opportunities and the friendships that have developed. Thanks also to all the other students and staff who have offered encouragements towards, and/or timely distractions from, the work in this thesis. In the latter respect, acknowledgement is probably also due to *The Times* and *The Sunday Times* (London) for their cryptic crosswords, which have challenged both staff and student alike during lunch and tea breaks.

Finally, I wish to acknowledge the financial support of the University of Canterbury Doctoral Scholarship, without which I would not have embarked on doctoral research at the university.

GLOSSARY

Mathematical Notation

$\sum$	Summation Operator
$e^{\cdot}, \exp(\cdot)$	Exponential Operator
j	Complex Quantity $\sqrt{-1}$
$\Re\{\cdot\}$	Real Part
$\Im\{\cdot\}$	Imaginary Part
$\cdot^*$	Complex Conjugate
d	Differentiation Operator
∂	Partial Differentiation Operator
$\cdot^T$	Matrix Transpose
$\lvert\cdot\rvert$	Absolute Value Operator
$\mathrm{E}[\cdot]$	Expectation Operator
$\circledast$	Convolution Operator
$\odot$	Temporal or Spectral Multiplication Operator
$\forall$	For All
ϵ	Is a Member Of
$\binom{n}{r}$	Binomial Coefficient ${}^{n}\mathrm{C}_{r}$
$\mathrm{erfc}(\cdot)$	Complementary Error Function
$p(\cdot)$	Probability or Probability Density
$\Gamma(\cdot)$	Gamma Function
$\mathrm{J}_{\xi}(\cdot)$	Bessel Function of the First Kind, of Order ξ
$\mathrm{K}_{\xi}(\cdot)$	Modified Bessel Function of the Second Kind, of Order ξ
$\mathrm{L}_{p}^{(\xi)}(\cdot)$	Generalised Laguerre Polynomial, of Degree p

List of Symbols

$\boldsymbol{A}, \bar{\boldsymbol{A}}, \boldsymbol{B}, \bar{\boldsymbol{B}}$	(Typically Unipolar) Code Sequences
$A_i, \bar{A}_i, B_i, \bar{B}_i$	ith Elements of Above Sequences
a	Fibre Core Radius

$\boldsymbol{a}, \boldsymbol{b}$	Bipolar Code Sequences
a_i, b_i	ith Elements of Above Bipolar Code Sequences
B_{e}	Noise-Equivalent Electrical Bandwidth
c	Speed of Light
$\boldsymbol{c}_k$	Unipolar Sequence
$c_k(i)$	ith Element of Above Unipolar Sequence
$\boldsymbol{D}, \bar{\boldsymbol{D}}$	General Decoder Operators
d	Binary Data
d_{thr}	Binary Decision Threshold
E	Electric Field Component
$\boldsymbol{E}$	Optical Field
$\boldsymbol{E}_{\mathrm{lo}}$	Local Oscillator Optical Field
$\boldsymbol{E}_{\mathrm{d}}, \bar{\boldsymbol{E}}_{\mathrm{d}}$	Optical Fields at the Photodetectors
e	Electronic Constant
f	Electrical Frequency
G	Total Network Capacity
$G(\nu)$	Single-sided Optical Power Spectral Density
$\tilde{G}(\nu)$	Double-sided Optical Power Spectral Density
$\hat{G}(\nu)$	Normalised Single-sided Optical Power Spectral Density
$\boldsymbol{H}$	Hadamard Matrix
H	Magnetic Field Component
h	Planck's Constant
$\boldsymbol{h}_k$	Bipolar Sequence of kth Row of Hadamard Matrix
$h_k(i)$	ith Element of Above Bipolar Sequence
I	Photocurrent from Detector or Balanced Detector Pair
I_{sig}	Signal Component of Photocurrent
K	Number of Active Users
K_{sp}	Spontaneous Emission Factor
$\mathcal{L}$	Number of Transmitting Users
L	Number of Interfering Users that are Transmitting
M	Total Number of Network Users
M	Pulse-Position-Modulation Order
$\mathcal{M}$	Temporal Degree of Freedom
m	Row Number of the Hadamard Matrix for a Particular User Code
N	Code Length
NA	Numerical Aperture
n	Refractive Index
P	Degree of Polarisation
P_{be}	Probability of Bit-Error
P_{c}	Chip Power Level

P_G	Total Power with Spectral Density $G(\nu)$
P_p	Spectrally-Encoded Pulse Power
P_r	Received Optical Power
P_s	Source Power
p	Natural-Number Index Denoting the pth Mode Solution for Each ξ
q	Spectrally-Encoded Pulse Waveform
R	Photodiode Responsivity
r	Polar Radius
$\boldsymbol{S}$	Source Optical Field
T	Time Interval
T_bit	Bit Period
T_c	Chip Period
T_D	Photodiode Integration Time
t	Time Variable
V	Normalised Frequency
W	Integrated Optical Intensity
$\overline{W}$	Mean Integrated Optical Intensity
w	Gaussian Beamwidth
X	Photoelectron Counts
$\overline{X}$	Mean Photoelectron Counts
Z_o	Vacuum Impedance
z	Length
α	Coupler Splitting Ratio
β	Phase Propagation Constant
γ	Mode Eigenvalue in Fibre Cladding
$\gamma(\tau)$	Complex Degree of Coherence
Δ	Refractive Index Difference
$\Delta\lambda$	Optical Bandwidth
$\Delta\nu$	Optical Bandwidth
ϵ	Electrical Permittivity
ζ	Index of Power-Law Variation of Refractive Index
η	Quantum Efficiency
θ	Polar Angle
κ	Mode Eigenvalue in Fibre Core
λ	Wavelength
μ	Magnetic Permeability
ν	Optical Frequency
ν_o	Centre Frequency
ξ	Azimuthal Index
ρ	Signal-to-Noise Ratio

σ^2	Variance
τ	Time Variable or a Time Delay
τ_c	Coherence Time
τ_{cc}	Chip Coherence Time
ϕ	Phase
ω	Angular Optical Frequency

Common Acronyms

ASK	Amplitude-Shift Keying
BPSK	Binary Phase-Shift Keying
CDMA	Code-Division Multiple Access
DS-BPSK	Direct-Sequence Binary Phase-Shift Keying
EDFA	Erbium-Doped Fibre Amplifier
FDMA	Frequency-Division Multiple Access
FWHM	Full Width at Half Maximum
LED	Light-Emitting Diode
MAI	Multiple-Access Interference
MMF	Multimode Fibre
MZI	Mach-Zehnder Interferometer
OCDMA	Optical Code-Division Multiple Access
OOK	On-Off Keying
PBS	Polarisation-Beam-Splitter
PIIN	Phase-Induced Intensity Noise
PolSK	Polarisation-Shift Keying
PPM	Pulse-Position Modulation
PSD	Power Spectral Density
PSK	Phase-Shift Keying
SA-OCDMA	Spectral-Amplitude Optical Code-Division Multiple Access
SIR	Signal-to-Interference Ratio
SLD	Superluminescent Diode
SMF	Single-Mode Fibre
SNR	Signal-to-Noise Ratio
TDM	Time-Division Multiplexing
TDMA	Time-Division Multiple Access
WDM	Wavelength-Division Multiplexing
WDMA	Wavelength-Division Multiple Access

CONTENTS

Chapter 1

INTRODUCTION

1.1 HISTORICAL PERSPECTIVE

At least some humans and many other creatures have been communicating with each other using various methods for countless centuries, and light is an essential part of many of these methods. Communication over large distances using light is also ancient, having been performed with fire and smoke signals in most civilisations. More advanced forms of such signalling have been used, including signalling lamps and flags, and the associated systems of message coding. The discovery and application of electricity led to the telegraph with digital Morse code becoming the dominant form of long-distance communication over fixed paths, until superseded by the analogue telephone in the late nineteenth century, which survives to this day. The invention of the wireless allowed long-distance radio communication over arbitrary paths through the use of electromagnetic radiation propagating in all directions. The telegraph and telephone transmissions over conductor pairs are usually considered simply as electron flow, but it is also electromagnetic radiation, where the electric and magnetic fields exist within, around and between the two conductors, and this radiation is effectively guided by the flow of electrons in the conductors. Throughout this century, the transmission frequencies of both guided and non-guided electromagnetic radiation have been increased regularly due to the growing demand for more communication and entertainment around more of the globe. Optical frequencies were duly reached, and are now widely used throughout the world, so humanity is back to signalling primarily with light for long-distance communication. The methods of such are, however, greatly advanced from fires and smoke signals, and the development and main components of optical communication systems are outlined in the following sections. The main types of channel sharing amongst the many users of a communications network are outlined, and of these, code-division multiple-access systems are described in more detail. Certain classes of optical code-division multiple-access systems are the focus of this thesis, as detailed in Section 1.5.

1.2 OVERVIEW OF OPTICAL-FIBRE COMMUNICATIONS

The two crucial developments which began the modern revolution of optical communications are the development of low-loss silica optical fibres, and the invention of the semiconductor diode laser.

The major incentive for using light for communication rather than radio or microwave signals is due to optical frequencies being many orders of magnitude higher than achievable electrical frequencies. This means that the possible bandwidth, which represents the information rate, is also very much larger. The development of optical fibres that have very low loss over bandwidths that are orders of magnitude higher than any electronic speeds means that enormous amounts of information can be sent many tens of kilometres along a single fibre. Even limited to electronic speeds, the product of the corresponding bandwidth and the maximum fibre length between transceivers or amplifiers is still much larger than the bandwidth-length products of any other long-distance terrestrial communication technology. In addition to this, fibre is lighter than any electrical cable, and multiple fibres can be packed together very densely due to their small size. Fibre does not conduct electricity, and the light signals within it are immune to almost all external electromagnetic interference (EMI). This isolation and immunity are particularly useful for communication within and from situations or installations where large electric fields and EMI levels make metal cables unattractive and potentially dangerous.

The invention of the laser provided a high-power light source giving a narrow beam of coherent light, having basically the same direction, phase, and polarisation, and hence the laser is a particularly attractive light source for optical communication. However, early lasers were based on lasing within gas-filled tubes or large crystals, and they were generally bulky, sensitive, fragile, and rather inefficient. The semiconductor diode laser arrived at about the same time as low-loss fibres were developed, and it provided a very small, robust and convenient light source, driven simply by forward biasing and the supply of a small current. It is simply produced through the same type of semiconductor fabrication steps used to produce the transistor, which was also revolutionary. The same form of semiconductor diode, when reverse-biased, provides a light detector rather than a light source, and these are generally termed photodiodes. Such diode lasers and photodiodes are now widely used throughout the world in CD players and shops for example, to read encoded audio sound-tracks and product identification labels respectively.

1.2.1 Increasing Capacity

The push towards higher bandwidth-length products led to the use of single-mode fibre rather than multimode, and it also motivated the development of semiconductor diodes with wavelengths of about 1.3 μm, near the wavelength of minimum dispersion in silica. These fibre types and properties are described in more detail in Section 1.3.1. Due to the lowest fibre loss occurring at wavelengths of about 1.55 μm, modified single-mode fibres having minimum

dispersion in this region were developed. Over the same period, diode lasers were being improved by further feedback structures and other modifications to reduce the spectral width and to permit straightforward wavelength tuning. The integration of these diode lasers together with associated driving and monitoring circuitry, including temperature control, into single small packages with fibre pigtails became commonplace, with direct laser modulation to several gigahertz possible. The error rate within digital fibre links of one in 10^9 became the commonplace standard, with links able to achieve one error in 10^{15} being considered for some applications, and these performance levels are mainly due to the immunity of signals within optical fibre to almost all forms of external interference.

Optical-fibre links have thus come to dominate the field of long-distance fixed point-to-point communication, and the use of fibre simply to replace copper has also occurred in local- and metropolitan-area networks. In this first generation of optical networks, the fibre is merely being used as a superior form of cable, having very little noise and greater bandwidth, but the signals are essentially the same as those in a non-fibre implementation.

To utilise the potential bandwidth in the low-loss regions of optical fibre requires the use of optical means, since this bandwidth of many terahertz greatly exceeds electronic speeds. The simplest method to extend the usable fibre capacity beyond electronic limits is to combine the light from multiple sources with different wavelengths into the same optical fibre. At the receiver, wavelength-selective devices are necessary to separate the light again for individual photodetection. Such wavelength-division multiplexing (WDM) has become the mainstream approach to achieving ever-increasing capacities for both point-to-point links, for example $50 \times 20\,\mathrm{Gb\,s^{-1}} = 1\,\mathrm{Tb\,s^{-1}}$ over 600 km [Aisawa *et al.* 1998], and to the next generation of optical networks. Many commercial installations and a wide range of tunable filters and other wavelength-dependent optical devices have resulted from this development.

1.2.2 Optical Amplification

Despite the very low loss of fibre, the limits of signal detectability are soon reached in long-distance links or, for example, if the transmitted light has to be split amongst many receivers in a network situation. In the electrical environment the equivalent problem is solved by having appropriate amplification, and thus much research into the development of suitable optical amplifiers was undertaken. The resulting invention of the erbium-doped fibre amplifier (EDFA) has further revolutionised optical communications. Long-distance links now have EDFAs periodically spaced throughout to compensate the fibre losses, rather than the electrical repeaters previously necessary. Such repeaters performed optical-to-electrical conversion, electrical retiming and amplification in general, and then electrical-to-optical conversion again for the next fibre section. The simplicity of the EDFA offers much greater flexibility to system designers, and it has enabled many useful devices to be constructed through providing the optical power to exploit fibre nonlinearities. When WDM is considered for long-distance links, then optical amplifiers are even more attractive, since they are able to amplify at once all the signals at

different wavelengths within the spectral range of the amplifier. This is vastly superior to a repeater which must filter and detect each wavelength separately, recover the signals, and then launch them all again at their respective optical wavelengths. EDFAs are thus used in WDM fibre links around the world. This huge advantage of keeping all the processing in optical form applies in general when large fractions of the fibre capacity are being used, since electronics simply cannot keep up without massive (and expensive) parallelism, and this is only possible in some circumstances. This is known as the electronic bottleneck, and to avoid it, the appropriate processing and amplification at all inter-link or network nodes must be implemented optically.

1.2.3 Multiple-Access Network Development

As optical-fibre links began to take over as the primary technology for communications trunking, and to be used in place of copper in the first generation of optical networks, much research into exploiting the enormous fibre capacity for completely optical networks was being performed. In a fibre network many users must share the capacity of each fibre in general, and there are three different ways in which this can occur. The two simplest ways in which to do this, at least conceptually, are to allocate either different time slots or different frequency ranges to each user, and these are termed time-division multiple access (TDMA) or frequency-division multiple access (FDMA) respectively. In the field of optical networking, the term wavelength-division multiple access (WDMA) has generally been used for the spectral-division case, since it is common to refer to optical sources by their free-space wavelength rather than by their frequency, which may be hundreds of terahertz. The third manner in which a communications channel can be shared is termed code-division multiple access (CDMA), and this is used in some mobile radio and telephone systems.

In contrast to TDMA and FDMA, in a CDMA system each user is generally permitted to transmit asynchronously using all of the available frequency range. However, the transmission from each user is encoded with a unique signature sequence, or user code, and a receiver with the knowledge of any one of these codes can extract the corresponding signal from amongst the transmissions from other users. A CDMA system in general cannot permit as many simultaneous users as the equivalent TDMA or WDMA system, although the optimum receiver performance is not far off. However, a much larger number of users with unique codes can be in the network than the number of divisions in the alternative TDMA or WDMA cases, and provided that each user only transmits for some fraction of the time on average, this allows a much larger number of users to have uncoordinated and asynchronous access to the network. In addition to this, as the number of simultaneous users in a CDMA network increases, the performance degrades smoothly as the interference from these users grows, unlike the hard limit at the number of divisions in the TDM and WDM cases.

WDM was the first optical multiplexing method to be used in fibre links because it simply used much existing technology in parallel, and it motivated much research into improved tunable lasers, filters, and other wavelength-selective devices. Frequency-division multiplexing

in the electrical domain before optical transmission is also possible, either in isolation or in conjunction with WDM, and this sub-carrier multiplexing (SCM) is particularly suited to one-to-many distribution systems. In order to avoid the electronic bottleneck arising in the nodes of networks, the operations at each node must become fully optical, and much fruitful research and development has been and is still being performed on the necessary components, including such devices as add-drop WDMs and optical cross-connects. In the case of fibre networks, as also for fibre links, WDMA has a big advantage with respect to both TDMA and CDMA in terms of fibre dispersion, which is a temporal spreading of the signal with fibre length. Unlike the atmosphere used in radio transmission, single-mode fibre has dispersion proportional to both fibre length and to the bandwidth of the signal in general, as detailed in Section 1.3.1.2. In TDMA and CDMA systems each signal extends across the whole utilised spectrum, but only a small fraction of the spectrum is used by each signal in WDMA, and hence the effect of dispersion in WDMA is correspondingly smaller. WDMA thus remains the multiplexing method of choice for long-distance links and networks.

TDMA requires time synchronisation between transmitters and receivers and all the signals from each user. Achieving this network-wide synchronisation in the fibre case is technically demanding, particularly if one wishes to utilise a significant proportion of the available optical bandwidth, since the timing and switching devices must then be optical, beyond electrical bandwidths. The need for synchronisation has restricted current optical TDM proposals and experiments to point-to-point links, where synchronisation between the co-located signals is straightforward. Optical demultiplexing of each signal is possible through the use of non-linear interaction between the received light and a sequence of sampling pulses, as detailed in Section 1.3.1.3.

In the following section the main optical components of optical communication systems and their characteristics are reviewed, and in Section 1.4 the basic requirements and structure of electrical and optical CDMA systems are outlined.

1.3 CRUCIAL COMPONENTS AND THEIR CHARACTERISTICS

The two components which began the optical communications revolution are the low-loss silica fibre and the semiconductor laser, and the doped-fibre optical amplifier has led to further significant advances. In this section the important characteristics of typical optical fibres, optical sources and optical amplifiers are described.

1.3.1 Optical Fibre

One of the essential ingredients in most optical communication systems is optical fibre, which guides the light from transmitter to receiver. Systems without such fibre are typically either very local and usually line-of-sight, using incoherent infra-red light (appliance remote controls for example), or else they are long-distance and with a safe line-of-sight path, where coherent

laser beams can be employed. The basic principle causing the guiding in an optical fibre is that of total internal reflection. This describes the fact that light approaching an interface with a medium of lower refractive index at a near-tangential angle to the interface does not pass through into the other medium, but is reflected from the interface. In this manner, light can be confined within a medium of higher refractive index than that of its surroundings, provided the incident angle of the light at the medium edge does not exceed the critical angle beyond which total internal reflection no longer occurs.

Early in the twentieth century, fibres were made from a single type of glass, where the air around the fibre was the medium of lower refractive index, but in the 1950s the use of a cladding layer of glass around the glass core of higher refractive index was introduced. This improved fibre characteristics considerably, and is considered the birth of the field of fibre optics [Agrawal 1989]. Although total internal reflection ideally confines the light within the fibre, in practice there is always some attenuation with fibre length due to bends, imperfections and various losses in the fibre. During the 1960s the silica fibre attenuation levels were very high, in excess of $1\,\mathrm{dB\,m^{-1}}$, but in 1970 optical fibre with only $20\,\mathrm{dB\,km^{-1}}$ was achieved, and by the end of that decade, fabrication technology had improved to the point where the intrinsic loss limits of less than $1\,\mathrm{dB\,km^{-1}}$ were being reached at some infra-red wavelengths [Agrawal 1989].

Standard communications-grade optical fibres today consist of a cylindrical core of silica, surrounded by silica of slightly different composition that has a marginally lower refractive index, with outside diameter $125\,\mu\mathrm{m}$. A thin protective plastic jacket encloses the fibre, and more protective sheathing, along with strength members of carbon fibre and plastic jacketing, may also be placed around the fibre, and this is termed the buffer. Alternatively, jacketed fibres may be lightly sheathed according to a colour code and bundled together as part of multi-fibre cable. If both the cladding and core refractive indices are constant with fibre radius, then this is called a step-index fibre due to the stepped index profile across the fibre. The refractive index of the core may instead be chosen to decrease with radius, and such fibres are termed graded-index [Green Jr 1993]. More-complicated refractive-index profiles are sometimes used to obtain different dispersion characteristics, as mentioned in Section 1.3.1.2. The core diameter for such fibres is either $50\,\mu\mathrm{m}$, and these are classed as multimode, or else about $9\,\mu\mathrm{m}$, and these fibres are classed as single-mode. As the name implies, single-mode fibres (SMF) permit only a single guided mode by making the core small enough with respect to the light wavelength, and the spatial distribution of the light across the fibre section is then fixed. However, this single mode is actually composed of two orthogonally polarised components, which ideally have the same propagation speed. Multimode fibres (MMF) have a core diameter of many more wavelengths, so there are many possible different standing-wave patterns corresponding to the modes of the fibre. Each MMF mode can also be thought of as a ray propagating via total internal reflection down the fibre, but at different angles and amounts of possible skew with respect to the fibre axis. The lengths of each of these paths are different, and hence there are relative time delays between light of the same frequency propagating within different modes,

and this is termed modal or intermodal dispersion. For step-index 50/125 μm MMF this modal dispersion is of the order of 50 ns km^{-1} of fibre length, whereas having a graded index reduces the dispersion to the order of 1 ns km^{-1} [Agrawal 1992]. This reduction of modal dispersion is in fact the primary motivation behind the use of graded-index profiles, since it avoids the much smaller core size of an SMF needed to eliminate modal dispersion completely. Other forms of dispersion are then significant in SMF, as discussed in Section 1.3.1.2.

1.3.1.1 SMF Attenuation

Restricting attention now to silica SMF in particular, the intrinsic limits of fibre attenuation are that due to Rayleigh scattering, which decreases as the fourth power of wavelength, and that due to material absorption, which is less than 0.1 dB km^{-1} in the wavelength range 0.8 μm to 1.6 μm, but becoming very significant above 1.6 μm [Agrawal 1992]. Rayleigh scattering is a fundamental loss mechanism due to the random density variations on a microscopic scale when the molten silica sets during fabrication, and these cause random fluctuations in the refractive index on a scale much smaller than optical wavelengths. The material absorption in silica above about 1.6 μm is due to vibrational resonances of the silica molecule. The presence of impurities in the silica imposes further extrinsic material absorption, the most significant being that of the OH^- ion, which imposes strong absorption at 0.95 μm, 1.24 μm, and 1.39 μm due to residual water vapour in the silica [Agrawal 1992]. Either side of the 1.39 μm OH^- loss peak the loss is dominated by Rayleigh scattering, and at 1.3 μm the attenuation of approximately 0.5 dB km^{-1} is achievable in practice, and at 1.55 μm the loss minimum of 0.2 dB km^{-1} is practical. The low loss about these two wavelengths has contributed strongly to them being the predominant wavelengths for optical-fibre communication, although dispersion and optical amplification have also had significant effect, as discussed in Sections 1.3.1.2 and 1.3.3.

1.3.1.2 SMF Dispersion

Although modal dispersion within SMF is ideally zero, inhomogeneities and other departures from an ideal cylindrical fibre do result in a slight birefringence between the two orthogonally polarised modes of an SMF, and a small amount of dispersion may result. However, this polarisation dispersion is generally negligible compared to the chromatic dispersion that also arises in SMF.

Chromatic dispersion, also called group-velocity dispersion or intramodal dispersion, represents the fact that the propagation speed in the fibre is frequency dependent. Chromatic dispersion consists of both material dispersion, which is that arising from the frequency dependence of the refractive index of the fibre, and also waveguide dispersion. The two modes propagate with an effective refractive index which lies between the core and cladding indices, and the function relating the effective index to the actual media indices is also wavelength dependent. This wavelength dependence is the basis of waveguide dispersion, and its level includes dependence upon the refractive-index difference and the fibre core radius.

Dispersion is typically expressed in terms of picoseconds of dispersive spreading per kilometre of fibre, per nanometre of spectral width. In what is usually termed standard SMF, the material and waveguide dispersion components are equal and opposite at about 1.3 μm, giving zero nett dispersion at that wavelength. However, the slope of the dispersion curve at that point, also referred to as second-order dispersion, and of the order of 85 fs km^{-1}nm^{-2}, still gives rise to dispersion with real signals of finite spectral width [Agrawal 1992]. The dispersion parameter is positive at wavelengths longer than the zero-dispersion wavelength, and this is often termed anomalous dispersion, as opposed to normal dispersion with a negative parameter. The dispersion parameter of standard SMF in the lowest-loss region around the wavelength of 1.55 μm is about 16 ps km^{-1}nm^{-1} [Agrawal 1992]. In order to better utilise the low-loss wavelength region around 1.55 μm, SMFs can be designed with slightly different radii and other parameters in order to increase the waveguide dispersion, thus relocating the wavelength of zero dispersion to around the 1.55 μm region. Such SMFs are known as dispersion-shifted fibres (DSF), and the dispersion slope is of the order of 50 fs km^{-1}nm^{-2} at the dispersion zero [Agrawal 1992]. In particular circumstances, flattening of the dispersion curve and other such adjustments may be desired, which can be achieved by using multiple claddings and other complex refractive-index profiles.

1.3.1.3 SMF Nonlinearity

The response of all dielectrics to light becomes nonlinear when the intensity is sufficiently high. Although the nonlinear response of silica is very low, the small core of SMF and the low attenuations possible mean that the light can be highly concentrated over very long fibre lengths, thus giving significant nonlinear behaviour.

There are two important inelastic scattering processes that occur in SMF, that of Raman scattering and Brillouin scattering, although for low optical powers these are generally insignificant, apart from possibly the small contribution to the fibre loss. Raman scattering is a scattering of an incident photon by a molecule into a lower frequency photon, where the energy difference is absorbed by the molecule making a transition to a higher-energy vibrational state. Brillouin scattering describes the interaction where a photon is again shifted down in frequency to what is termed the Stokes frequency, but this is due to the generation of a phonon, the quantum unit of an acoustic wave. At a sufficiently high intensity, however, the scattered photons become likely to stimulate further such scattering, and the majority of the incident power then becomes shifted to the peak Stokes frequency. In the case of stimulated Raman scattering (SRS) in silica SMF, the threshold is of the order of 500 mW, the Stokes frequency shift is about 13 THz, and the stimulated light may propagate in either direction [Agrawal 1992]. However, as the number of wavelengths in a WDM system increases, the effective threshold level is reduced. For stimulated Brillouin scattering (SBS) in silica SMF, the threshold level may only be of the order of 1 mW, above which most of the energy is transferred to a backwards-propagating wave at the Stokes frequency, which is only about 10 GHz

lower [Agrawal 1992]. Both SBS and SRS can be used to provide optical amplification of signals at the Stokes wavelength, but only over many kilometres of fibre, compared to the few metres of fibre necessary for strong stimulated emission in rare-earth-doped fibre amplifiers, and these are considered in Section 1.3.3.

The silica molecule SiO_2 is symmetric, and from this fact it follows that ideally there are no second-order-based nonlinearities in SMF. The other two significant nonlinear effects arising in silica SMF are therefore due to the third-order susceptibility, which results in the refractive index being intensity dependent. This intensity dependence of the refractive index is described as nonlinear refraction, or the Kerr nonlinearity, and it results in a nonlinear phase shift also dependent upon intensity. This is termed either self phase modulation (SPM) or cross phase modulation (XPM), according to whether the signal causing the phase modulation and that undergoing the phase modulation are the same signals or not [Agrawal 1992]. A particularly useful optical switching device based upon SPM and XPM within a Sagnac interferometer is the nonlinear optical loop mirror (NOLM), which can be used for optical time demultiplexing [Andrekson *et al.* 1992].

At wavelengths for which the dispersion is anomalous, it is possible for SPM to counteract the anomalous dispersion, and pulses of certain shape can propagate without any dispersion- or SPM-induced spreading, and these are called solitons. With periodic amplification to counteract the fibre losses, it is possible for solitons to be transmitted many thousands of kilometers without any temporal spreading, on average, and hence soliton systems are expected to be used for some very long fibre communication links [Mollenauer *et al.* 1993].

The other nonlinear effect arising from the third-order susceptibility is that usually termed four-wave mixing (FWM), and sometimes four-photon mixing. This simply expresses the fact that due to third-order nonlinearity, any three co-propagating fields of frequencies ν_1, ν_2 and ν_3 can generate mixing frequencies in the same spectral vicinity of the form $\nu_4 = \nu_1 + \nu_2 - \nu_3$ [Agrawal 1992]. This can also be used for optical switching and sampling, as in time demultiplexing [Andrekson *et al.* 1991]. FWM is particularly significant when there are many optical signals at close and regularly spaced discrete wavelengths, since for each of many such mixing terms, ν_4 coincides with another signal wavelength, and the mixing level is significant due to the similar propagation rates of each wavelength. Hence, FWM can be a source of significant inter-channel interference in closely spaced WDM systems [Maeda *et al.* 1990].

1.3.2 Optical Sources

Optical sources can generally be classified as either incoherent or coherent. For incoherent sources, such as most light-emitting diodes (LED), the light is generated by spontaneous emission occurring independently and at random amongst the excited medium, and hence each photon has random phase, polarisation, and direction in general. Such sources have a very broad spectral shape due to this random-phase characteristic, and in general the instantaneous

output intensity also fluctuates due to the independent emission events. Unless the diode structure is designed to confine this spontaneous emission, LEDs are very inefficient in generating light in a particular direction, as desired for fibre transmission [Agrawal 1992].

Coherent optical sources or lasers, however, are based upon stimulated emission in which each stimulated photon has the same frequency, phase, polarisation, and direction, as the incident photon causing the emission. The emission of a photon, whether spontaneous or stimulated, occurs as a carrier makes the transition from one energy level to a lower level, where the energy difference is that of the photon, and hence corresponds to the photon frequency. The opposite transition may also occur due to the absorption of such a photon. The carriers in a semiconductor diode laser are electron-hole pairs, but they are electrons in gas lasers, and in doped-fibre amplifiers they are the dopant rare-earth ions. There are two requirements that are necessary for a laser to operate. The first is that there must be a gain medium in which a population inversion is maintained. This describes the situation in which there are sufficient excited carriers at the higher energy level that any spontaneous or stimulated incident photon of the appropriate frequency is more likely to stimulate another photon emission than to be absorbed by returning a carrier to the upper energy level, and hence amplification occurs. There must be an electrical or optical input which pumps the carriers to the upper energy level in order to maintain the population inversion. The second laser requirement is that of optical feedback, and this is provided by reflective devices at each of the ends of the gain medium. With sufficient gain, the reflection loss and other losses are overcome, and highly coherent light emission (lasing) occurs at the wavelengths which match the round-trip length between reflections. By having wavelength-selective reflection, rather than simple mirrors, it is possible to ensure lasing at only a single wavelength or mode, and diffraction gratings are usually used to provide this selectivity. Diode lasers which use such reflective gratings are called distributed Bragg reflector (DBR) lasers, and the distributed-feedback (DFB) diode laser actually has a grating for wavelength selection imposed along the length of the gain medium. Further modifications and improvements are possible so that these gratings can be effectively controlled, thus providing tunable single-mode diode lasers [Green Jr 1993].

Direct modulation of the diode-laser drive current can be used to modulate the laser output, although the changing drive current also causes the output wavelength to chirp up and down, and this is undesirable in many situations. However, this can be done at rates higher by an order of magnitude than those for LED sources, and the power levels able to be launched into SMF can be several orders of magnitude higher also.

Lasers are often arranged to directly produce pulses of light rather than continuous wave (cw) output. One such method is to modulate the laser cavity length at radio frequencies (RF), which mode-locks the laser into producing pulses of light at the RF period, whose temporal extent is determined by the gain bandwidth of the laser medium. Another optical pulse source is the soliton oscillator, or soliton laser. This consists of a ring of fibre that has anomalous dispersion, and included in the ring are both an optical amplifier and a filter. At sufficient amplification there is a gain greater than unity around the ring for the peak filter wavelength,

so the noise from the optical amplifier starts to build up at this wavelength. This is shaped by the anomalous dispersion and the self phase modulation in the fibre, as well as the filter, and over the appropriate range of conditions the result is a circulating soliton pulse or series of pulses.

Edge-emitting LEDs (ELED) use the different refractive indices of the diode layers to confine the light within a dielectric slab waveguide, exactly as in many diode lasers, and thus most of the emission is from the edge of the diode and can be better coupled into a fibre.

It is also possible to use stimulated emission to amplify the spontaneous emission within a diode, but without sufficient power or optical feedback for lasing to occur. In this manner, the broadband spontaneous-emission profile is maintained, but with increased power and directivity due to the stimulated emission, and such diodes are termed superluminescent diodes (SLD). Such amplified spontaneous emission (ASE) also arises in other optical amplifiers and laser media in general, and in particular from doped-fibre optical amplifiers.

1.3.3 Optical Amplifiers

Any stimulated emission in general provides optical amplification, and thus optical amplifiers based upon stimulated Brillouin scattering and stimulated Raman scattering are possible. The stimulated emission of a semiconductor diode laser without a resonant cavity gives a semiconductor diode optical amplifier, and this is often termed a semiconductor laser amplifier (SLA). However, the stimulated emission possible within a few metres of rare-earth doped fibre, pumped optically at particular wavelengths, has a number of advantageous characteristics. In particular, the erbium-doped fibre amplifier (EDFA) has a moderately broad gain profile (30 nm or so) in the 1.55 μm low-loss region, and it only requires regular fibre splicing for insertion into any network, whereas the fibre coupling losses are high for SLAs. A simple wavelength-selective coupler for insertion of the pump power is required, and high-power semiconductor diode lasers for pumping at appropriate wavelengths have been developed and are readily available [Agrawal 1992]. These favourable characteristics, amongst others, have led to the EDFA being used to eliminate electrical repeaters in long-distance links around the world, and whole new optical network architectures using optical amplifiers are now considered. The high output powers available using EDFAs has also allowed the straightforward exploitation of fibre nonlinearities to create many useful devices and system components. The ultra-long-distance soliton transmission possible using EDFAs is one example of the use of these nonlinearities. Optical amplification within the 1.3 μm low-loss window using rare-earth doped fibre is possible using praseodymium doping, but unfortunately the fluoride-based fibres required cannot be simply spliced to standard silica fibre. The EDFA has increased the motivation to use the 1.55 μm low-loss window rather than that at 1.3 μm, which also has slightly higher loss, and hence the use of dispersion-shifted fibre is increasing.

As the demand continues for broader amplification bandwidths within the 1.55 μm window, modified EDFAs and fibre amplifiers with alternative dopants such as thulium have been

developed, and the broader gain bandwidth of Raman amplification (based upon stimulated Raman scattering) can also be combined with doped-fibre amplifiers. For example, gain-shifted EDFAs providing amplification around 1.58 μm rather than 1.55 μm have been developed, and with such an amplifier in parallel with an EDFA, a WDM link with 20×100 GHz-spaced channels about 1550 nm and 30×100 GHz-spaced channels about 1585 nm has been demonstrated [Aisawa *et al.* 1998]. Also, the combination of an EDFA with Raman amplification over 50 km of dispersion-shifted fibre has been used to provide a gain spectrum which is flat to 1 dB over 90 nm, and centered about 1.605 μm [Masuda *et al.* 1998].

1.4 CODE-DIVISION MULTIPLE ACCESS

Although less bandwidth-efficient than TDMA or FDMA, CDMA has become established in mobile radio communication due to the soft performance degradation with the number of users, and its asynchronous transmission. It thus avoids the alternative of contention amongst a large number of potential users for a fixed number of frequency or time slots. Due to the enormous fibre bandwidth available, researchers have looked to optical CDMA (OCDMA) to utilise this in providing a flexible optical network with the same asynchronous uncoordinated access and soft performance degradation. In this section the requirements and structure of CDMA systems are outlined, along with indications of how they relate to the optical environment, and this serves as the basis for the review of OCDMA approaches and systems in Chapter 2.

The basic requirement of CDMA is that termed spread spectrum (SS), which describes any process by which the data signal is encoded or spread in such a way that it occupies a much greater bandwidth than the minimum required to represent the data signal. This is necessary since many separable such spread-spectrum signals are required to occupy the same bandwidth in a CDMA system. At the receiver a corresponding despreading or decoding process is typically performed in order to recover the transmitted data signal, and this is reflected in the structure of Figure 1.1. In a CDMA system this type of spread-spectrum receiver is called a single-user detector, since it only uses a single code in the detection process. Each user has a unique code, and would be represented by an otherwise identical transmitter and receiver connected to the communications channel in Figure 1.1. The alternative multi-user detector is described in Section 1.4.1.

There are three basic methods of generating a spread-spectrum signal, termed direct sequence (DS), frequency hopping (FH), and time hopping (TH), although combinations of these methods are possible. All these possibilities are collectively expressed as code modulation in Figure 1.1.

Direct-sequence spreading is the simple multiplication in time of the non-spread data signal with the spreading code of much higher rate. Each element of the spreading code is often referred to as a chip, and hence the terms chip time or chip period, which represent the fraction of the bit period for which each code element applies. In radio CDMA systems using direct sequence, both the data and code modulations are typically represented by binary phase-shift

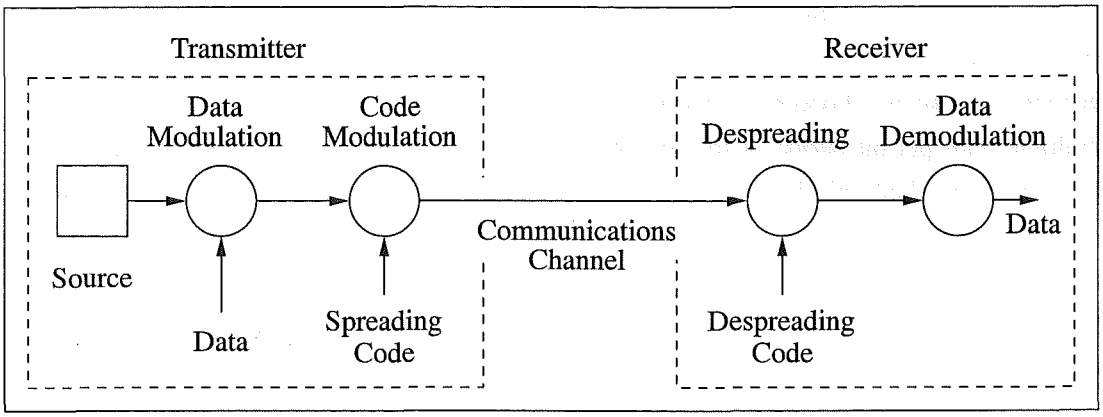

Figure 1.1 Spread-Spectrum Structure

keying (BPSK), where the source simply generates the sinusoidal carrier, and the whole spreading code or a long sub-sequence is keyed during each bit period. Binary keying between phase shifts of 0 and π radians is equivalent to a modulation of the carrier sinusoid with a sequence of elements of $+1$ or -1 respectively, and spreading codes for BPSK systems are termed bipolar codes due to this bipolar nature.

An important class of bipolar codes of pseudorandom nature are those known as maximal-length shift-register sequences, or m-sequences. These are ± 1 sequences of length $2^m - 1$, where m is a positive integer, and they have a periodic autocorrelation function that is only two-valued, of in-phase level equal to $2^m - 1$, and all out-of-phase levels equal to -1. These m-sequences are simply produced by a binary shift-register of length m, with linear feedback, and they have the maximum length possible from such a shift-register. There are not, however, a particularly large number of m-sequences, and their cross-correlation levels are not necessarily small. Certain pairs of m-sequences have periodic cross-correlation functions that are three-valued, where these values are within a factor of 2 or $\sqrt{2}$ of the minimum size limit possible, and these are called preferred pairs. From such a preferred pair, it is possible to generate a set of $2^m + 1$ sequences of length $2^m - 1$ for which all the cross-correlation levels and out-of-phase autocorrelation levels also have this limited three-valued property, and these correlation values are the smallest possible for this number of such sequences [Simon *et al.* 1985]. These sequences are the well known and widely used Gold codes. Note that all these are periodic correlation properties, but due to the data keying in a direct-sequence BPSK system, adjacent sequences often have opposite polarity, and hence the aperiodic correlation properties of the spreading sequences must also be examined.

Direct-sequence BPSK (DS-BPSK) using bipolar codes is possible in OCDMA, although more demanding because of the higher carrier frequencies, but the keying rate is still limited to electrical-domain bandwidths in general. However, in many OCDMA systems both the data and the spreading-code elements are represented simply by the presence or absence of a light pulse, which is unipolar rather than bipolar coding, and this has significant consequences, as detailed in the review of OCDMA systems in Chapter 2, and discussed further in Chapter 7.

The spread-spectrum method of frequency hopping is simply what it says, where the carrier frequency is regularly changed in a pseudorandom fashion amongst a fixed set of frequencies. Frequency hopping is designated either fast or slow, according to whether there are multiple hops per bit period or multiple bit periods per hop respectively. Frequency hopping is generally applied only in radio spread-spectrum systems or subsystems, although a few exceptions to this are noted in Chapter 2 on OCDMA systems. Time hopping is the temporal counterpart of frequency hopping, where transmission from a single user occurs across the whole frequency range during only a small fraction of the time in total, where the transmission times are chosen according to the particular spreading code, which generally has a pseudorandom form. Time hopping is also mainly confined to radio-domain systems or part systems thereof, although one of the earliest OCDMA proposals can be viewed as using forms of time hopping, as described in Chapter 2.

1.4.1 Receiver Structure

The despreading process at the receiver can be viewed as either correlating or matched filtering, which are equivalent. A filter matched to a particular signal has an impulse response primarily given by that signal reversed in time, and the filter performs a convolution of the input waveform with its impulse response. This convolution with the time-reversed desired signal is equivalent to a correlation with the desired signal.

In the ideal matched-filtering case, the receiver is exactly matched to the desired transmitted waveform. Just as in the electrical domain, in the optical domain this requires coherent sources and coherent detection, and the data and coding modulations can then take the same DS-BPSK form. It is also possible to encode the optical spectral phase rather than temporal phase, and to construct the corresponding exactly-matched filter at the receiver. However, if incoherent sources are used, an exact match to the transmitted signal cannot be determined due to the stochastic phase of the source. In this situation, the next best option is to have a receiver which is exactly matched to the encoder that modulates the light from the source. The exact matching in both of these cases can be termed coherent matching, since it requires optical phase and polarisation matching, and in general this requires precision and stabilisation to small fractions of the optical wavelength.

In order to avoid the precision of coherent matching, many OCDMA systems are incoherent and they use sources that have a very short coherence length. In order to eliminate coherent recombination, the nominally matched filter pairs actually must mismatch by greater than this coherence length. Hence, merely the impulse response power of the receiver matched filter is required to be approximately equal to the time reversal of the power response of the encoder, with sufficient mismatch to avoid coherent recombination.

While the matched filter is optimum for detecting the desired signal amongst additive white noise, in CDMA it is the signals from each user out of which the receiver must extract the desired signal. The matched filter is generally no longer optimum in this situation since

it ignores the information associated with the structure of the other signals in the channel, especially if an interfering signal has a much greater power level. In order to approach the performance of the optimum maximum-likelihood detector, it is necessary to make use of all the codes in the system, and this is then termed multi-user detection. In contrast to Figure 1.1, a multi-user detector typically involves the simultaneous estimation of the signals from all the active users in order to iteratively improve the estimate of each single signal. The susceptibility of matched filtering or correlation detection to a high-power interfering signal is termed the near-far problem, since in a mobile environment the channel attenuation is predominantly determined by the distance between transceivers. In such cases, some form of power control is usually implemented, but multi-user detection also offers near-far resistance. In a fibre network, however, balancing the power from each user is much simpler due to the fixed channels, and thus most OCDMA proposals and analyses assume equal power from each user, and follow the simple single-user detection structure of Figure 1.1. The spreading codes are designed to minimise the contributions from unmatched users after the despreading process, and these contributions are termed multiple-access interference (MAI).

The matched filtering in the receiver is equivalent to performing a correlation between the receiver code and the codes of all the incident signals, regardless of the type of spreading or matching. The only exception to this is if wavelength division is combined with the OCDMA system, in which case a bandpass optical filter can reject mismatched signals regardless of code correlation. The goal of temporal coding design in asynchronous CDMA systems is thus to minimise the cross-correlation levels between different codes and the out-of-phase autocorrelation levels of each code, thus minimising the MAI and increasing the distinction of a match. In the special case where the coding is spectral rather than temporal, the transmitted and receiver codes always remain in phase, and it is possible to have a set of ideally orthogonal codes with this restriction. The receiver correlation detection or matched filtering is generally either performed passively by a filter of appropriate structure, or actively by the direct modulation and filtering of the received signal, as indicated in Figure 1.2. In the case

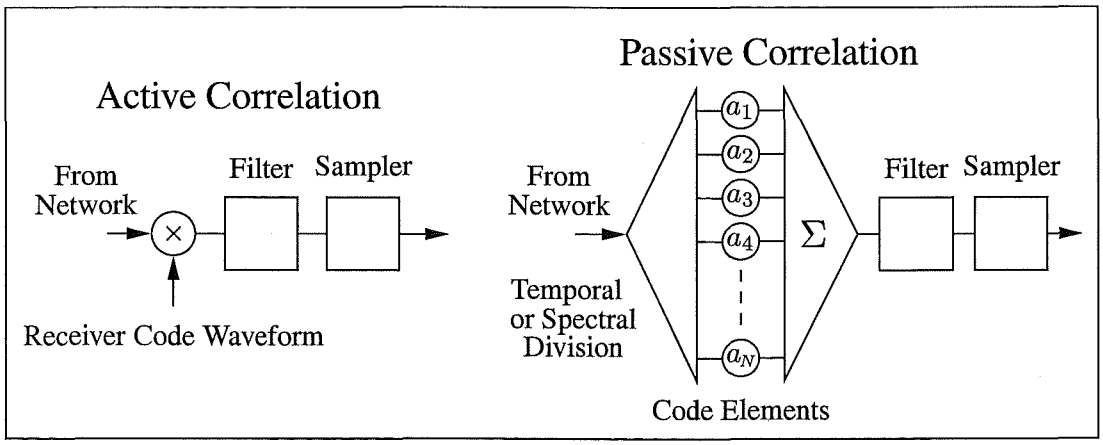

Figure 1.2 Active and Passive Correlation Structures

of active correlation, the receiver code waveform may simply be the appropriate unipolar or bipolar code sequence, or it may also include an optical carrier, as in the case of heterodyne or homodyne detection. The filter type in the active case has not been specified since it can be either optical (bandpass) or electrical (either bandpass or lowpass), depending upon the type of system. In the case of passive correlation, as indicated in Figure 1.2, the incoming signals are distributed in the appropriate domain and then each output is weighted by the corresponding receiver code element, clearly showing the correlation structure. These weighted outputs are then recombined and filtered appropriately, where this filtering may be either spectral or temporal, and suitable sampling of the output to get the decision variable for each data bit is again indicated. While the labelled filters in Figure 1.2 simply pass a certain spectral band or temporal extent, the passive correlation structure in Figure 1.2 that splits, weights, and then recombines the signal is usually termed a filter also. Here this is referred to as a filter structure when necessary to avoid confusion.

Although appearing simple, active correlation at the receiver of OCDMA systems has the disadvantages of being limited to electronic modulation bandwidths in general, and of needing to first obtain synchronisation between the receiver code and the desired signal. In order to be unconstrained by electronic bandwidths, most OCDMA systems use an optical filter structure both to encode the light at the transmitter and to perform the passive correlation at the receiver. While synchronisation is also generally necessary with passive correlation in order to sample at the appropriate instant, this can be achieved simply by monitoring the output of the passive filter structure in general. It is also possible to mix the two approaches and avoid electronic bandwidth constraints, for example by using a passive optical filter structure to generate the receiver code waveform, which then optically modulates the received signal.

Although the optical filter structures that are typically used to encode the light at OCDMA transmitters are termed passive, such a filter must be able to be switch from one code sequence to another in order to address other network users. The arrangement of receivers having fixed code sequences and the transmitters having adjustable sequences is most commonly considered, but code adjustability at the receivers may be considered either as an alternative or in order to add extra flexibility. The code switching speed should be as high as possible in general, thus minimising the bandwidth lost if switching occurs regularly.

1.5 THESIS AIM AND OUTLINE

Due to the huge available fibre bandwidth, the use of CDMA in optical networks appears to be able to exploit this bandwidth to offer asynchronous and uncoordinated network access to many potential users, with soft performance degradation as the number of simultaneous users increases. However, standard and successful electrical-domain CDMA techniques can only make use of a small fraction of the available fibre bandwidth, and much research in the last decade has gone into developing alternative OCDMA systems and the associated code designs in order to use much greater optical bandwidths. This research field is still very active, and in

the space of this decade many novel devices and techniques have been developed that continue to broaden the possibilities both now and presumably into the future also. This thesis continues the development and analysis of OCDMA systems by drawing attention to the fundamental performance limits arising in some types of OCDMA systems due to their basic structure, regardless of whatever devices are used to implement them either now or in the future. Such limits do not necessarily rule out these systems, but the limits and their origins need to be clearly understood in order to direct future OCDMA development.

Chapter 2 of this thesis reviews the different incoherent and coherent OCDMA approaches that have been followed by researchers as OCDMA has developed, and particular attention is paid to the schemes that are incoherent but nonetheless use the bipolar codes of coherent systems.

In Chapter 3 a proposed incoherent OCDMA system based upon spectral-amplitude coding with bipolar codes is analysed in detail. It is shown that this system is limited by the interference between the light from the different broadband sources, and consequently the total network capacity is approximately inversely proportional to the number of simultaneous users.

An experimental investigation of the intensity noise due to the interference between light from a source of broadband amplified spontaneous-emission (ASE) is described in Chapter 4, and the results confirm the theoretical expectations. The experimental use of multimode fibre (MMF) to reduce this intensity noise is described, and the theoretical expectations of the reductions possible using MMF are examined and compared with the measured results.

In Chapter 5 the effects of reducing the duty cycle of the thermal sources used in spectral-amplitude OCDMA (as per Chapter 3) is considered. The performance of this system under the use of a number of non-thermal broadband sources is also considered, and it is shown that similar limits still arise unless the source spectra are dissimilar.

In Chapter 6 the use of pulse-position modulation (PPM) together with spectral-amplitude OCDMA is proposed and investigated. It is shown that the use of PPM allows performance beyond the limits found in Chapter 3, and only a few simple changes to the original structure are necessary in the simplest case. This performance increase through PPM can also be obtained in other OCDMA systems which are limited in the same manner, including those based upon coherence multiplexing.

In Chapter 7 OCDMA is approached and analysed in a general manner, and the conditions under which limits of the form in Chapter 3 do or do not occur are examined carefully. The different types of OCDMA systems are then considered in the light of this analysis. Assuming sole single-mode-fibre paths and independent sources with identical spectra, it is shown that every incoherent bipolar OCDMA system must encounter performance limits at least as bad as those found for spectral-amplitude OCDMA. These worst-case limits are identified for each of the incoherent bipolar OCDMA proposals to date.

The thesis is concluded by Chapter 8, which summarises the contributions of this thesis to OCDMA and presents topics for future work.

Chapter 2

OPTICAL CDMA

2.1 INTRODUCTION

OCDMA research has ranged from completely incoherent systems to the completely coherent, and this history is reviewed here. The main categories of OCDMA systems are described and discussed in detail, and particular attention is paid to those systems which are both incoherent and that utilise bipolar coding, to which this thesis is primarily directed.

2.2 NETWORK TOPOLOGY

There are many possibilities for the topology of an optical network, but the vast majority of OCDMA system proposals and experimental demonstrations have assumed that of a *star*, where each terminal is connected to a central distribution unit. The general structure of a star-topology OCDMA network is shown in Figure 2.1. It consists of many terminals, each with an encoder and decoder, and the outputs of every encoder are combined and then distributed amongst every decoder. The star topology is simple, it does not waste optical power, and it is arranged so that each user sees the same relative signal strengths. These are the main reasons for the popularity of the star topology, but, as optical amplifiers become cheaper, less power-efficient topologies such as bus and tree topologies may be more widely considered.

The optical paths from each encoder and to each decoder are usually provided by one single-mode fibre (SMF). Other possibilities include multiple fibres and free-space transmission. The combination and redistribution of the light from each encoder is usually performed by a single star-coupler, which can be either fibre-based, or performed with integrated optical waveguides on a planar lightwave circuit (PLC). As indicated in Figure 2.1, the encoding and decoding can be performed in either the electrical or optical domains. The term photonic CDMA has been used to denote those OCDMA systems which fully perform both the signal encoding and decoding in the optical domain [Pendock *et al.* 1995]. The main potential advantage of such OCDMA systems is that the total network capacities are not necessarily constrained by electronic processing speeds, since much more of the available optical bandwidth can be effectively utilised with optical processing.

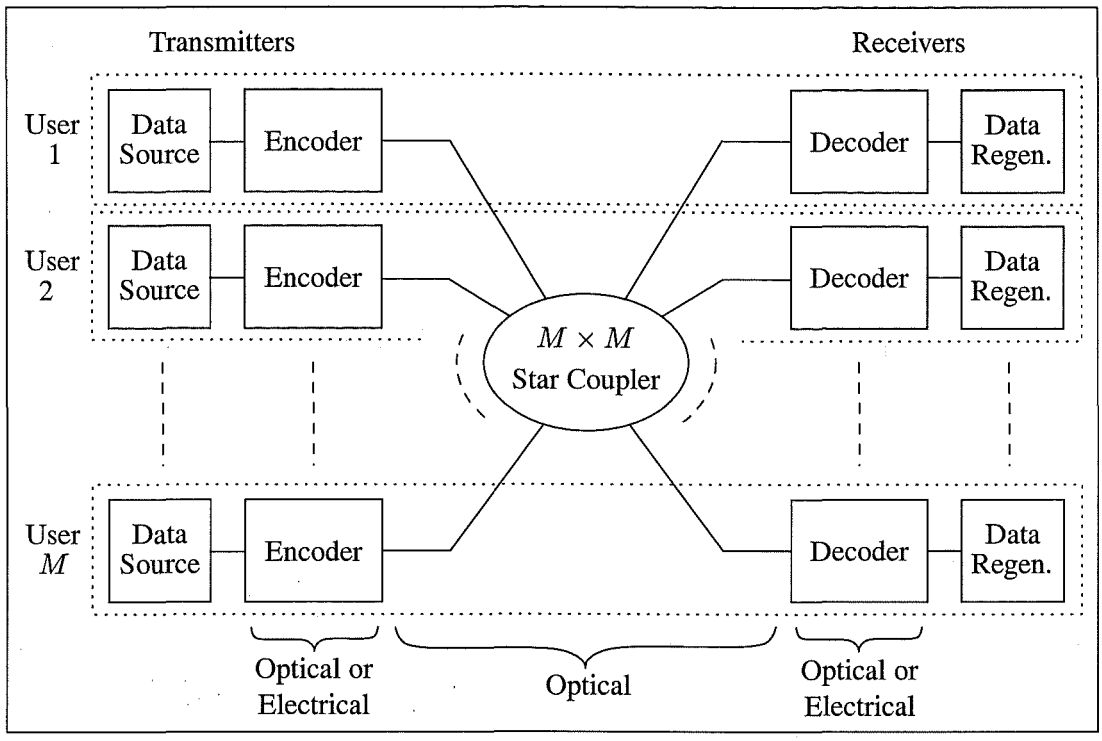

Figure 2.1 Star-Topology OCDMA Structure

2.3 THE EARLIEST OCDMA SCHEMES

The earliest OCDMA schemes and experimental demonstrations [1] merely used optical means to transmit electronically encoded signals, and the receiver decoding was performed after photodetection, also in the electrical domain, and these works include [Peterson and Gardner 1981, Davies and Shaar 1983, Hasegawa and Hirosaki 1983, Tamura *et al.* 1985].

The proposal and analysis of [Peterson and Gardner 1981] is for terrestrial-satellite communication, and it assumes direct-sequence bipolar coding represented by either left-circular or right-circular polarised laser light. The receivers consist of a polarisation splitter, balanced photodetection, and standard electrical-domain bipolar despreading. This work is examined in more detail in Section 2.9.1.

The work of [Davies and Shaar 1983] proposes what is effectively an asynchronous time-hopping OCDMA network. The system is described as an asynchronous multiplexing system, and it is based upon a form of pseudorandom pulse-position modulation (PPM), which is arranged to minimise the chance that transmissions from any group of users could be misinterpreted as belonging to any other user.

The work of [Hasegawa and Hirosaki 1983] presents a proposal, an analysis, and a simple experiment of a loop system where each spread-spectrum node uses direct-sequence BPSK to encode and decode signals electrically using m-sequences, and the sum of all these is sim-

[1] The earliest demonstrations of coherence transmission and coherence-multiplexed communication systems predated these OCDMA schemes [Delisle and Cielo 1975, Cielo and Delisle 1976], as detailed in Section 2.4.

ply passed from node to node by an optical-fibre link using intensity modulation and direct detection.

The work of [Tamura *et al.* 1985] presents a proposal, an analysis and an experiment of optical code-multiplexing by the intensity modulation of light sources with Gold-code-based DS-BPSK signals. At the receivers, direct photodetection is performed, with standard electrical-domain correlation detection to recover the data. The signals from each user in this scheme are separately transmitted into the optical network, unlike the previous scheme, where the spread-spectrum signals are combined electrically before the optical-fibre link.

Each of these systems assumes that any combination of light signals is on an intensity basis, and hence any mixing effects are neglected. This is reasonable for the particular situations and signalling rates considered therein, but this should not be assumed in general. The term incoherent is used here to describe these and other systems which are based upon the manipulation of light purely on an intensity or power basis only, and thus such schemes pay no attention to optical phase or polarisation. Due to the electrical-domain processing of each of the aforementioned schemes, their maximum network capacities are directly related to practical electronic bandwidth limits, rather than the much greater fibre bandwidths.

2.4 INCOHERENT SYSTEMS USING UNIPOLAR CODING

This section begins with a historical outline of the crucial works in the literature upon which this section is based, and many subsequent works are briefly categorised and listed. This is followed by detailed descriptions of the structure and characteristics of the typical incoherent OCDMA system that uses unipolar coding. If the reader is not familiar with the OCDMA field, the reader may prefer to skip Section 2.4.1 in order to first familiarise themselves with the terminology and the structure subsequently outlined in Section 2.4.2.

2.4.1 Historical Review

At the same time as a number of the early OCDMA proposals were being made, the work of [Jackson *et al.* 1985] reviewed earlier proposals and demonstrations of optical-fibre delay-line signal processing using multimode fibre, and the potential of single-mode optical-fibre delay-line signal processing was demonstrated. The low loss and dispersion of SMF at 1.3 μm was observed to allow much greater signal-processing capabilities than the multimode fibre of previous works.

In the work of [Hui 1985], a proposal was made for an OCDMA system based upon single or multiple fibres from and to each user. Using the fibre delay-line structures subsequently published in [Jackson *et al.* 1985], incoherent unipolar time-domain coding was proposed. In conjunction with the spatial (multi-fibre) dimension, the optical processing of the delay-lines was seen to permit much flexibility in the design of system configurations and code patterns.

However, such processing and the light modulation and detection were limited to electrical bandwidths in all the proposed configurations.

Following the work of Jackson *et al.*, another optical spread-spectrum network proposal was made [Prucnal *et al.* 1986a, Santoro and Prucnal 1987]. They proposed to use the optical-processing capabilities of fibre delay-lines to enable OCDMA performance beyond the conventional electronic limits. In this work, codes known as prime codes [Shaar and Davies 1983] were considered a class of codes potentially suitable for their OCDMA system. However, the poor autocorrelation properties of prime codes were observed, and this led to the synchronous OCDMA proposal of [Prucnal *et al.* 1986b], where a master clock signal would control when each receiver was to perform its threshold detection, rather than being based upon distinctive autocorrelation peaks.

The works of [Salehi 1989a, Salehi 1989b, Salehi and Brackett 1989, Chung *et al.* 1989] then considered the optimum unipolar-code correlation characteristics, defined bounds on the existence of codes with such characteristics, and presented some constructions of such codes, which were termed *optical orthogonal codes* (OOC). These codes and their characteristics are detailed in Section 2.4.2, but it is noted here that they are not, as their name implies, strictly orthogonal, - they are merely as near-orthogonal as is possible with unipolar binary sequences, and *near-orthogonal optical codes* or *pseudo-orthogonal optical codes* would have been better terms [Kwong *et al.* 1991].

Following the works of Prucnal *et al.* using prime codes, and Salehi *et al.* defining OOCs, a myriad of subsequent papers have followed, including [Azizoglu *et al.* 1990, Petrovic and Holmes 1990, Chung and Kumar 1990, Kwon 1991b, Kwon 1994b, Lam and Hussain 1992, Marić 1993, Kostić and Titlebaum 1994, Yang and Jaw 1994, Argon and Ergül 1995, Marić *et al.* 1995, Wu and Wu 1995, Yang and Fuja 1995, Zhang 1996]. These papers either provide further code constructions, or various modified code forms which make a whole range of trade-offs between certain code properties, according to the particular OCDMA system configuration considered.

The fibre delay-line structure used in [Prucnal *et al.* 1986a], and assumed in many of the coding works just listed, is particularly inefficient power-wise, especially when the desire for programmability is taken into account. Alternatively, ladder-like lattices of cascaded Mach-Zehnder interferometers (MZI) (Figure 2.3), first investigated in [Marom and Ramer 1978], allow pulse sequences to be generated much more efficiently, but with certain constraints on pulse positions [Chang and Marhic 1990, Holmes and Syms 1992]. Consequently, the unipolar codes designed in the papers above cannot, in general, be generated with such a lattice encoder. Hence, a number of works have developed desirable codes specifically for such lattice networks, or have modified earlier unipolar codes to fit within the constraints of lattice codes [Chang and Marhic 1990, Holmes and Syms 1992, Kwong *et al.* 1992, Kwong *et al.* 1994, Yang and Kwong 1995a, Kwong and Yang 1995, Tančevski and Andonovic 1995], and an experimental demonstration of the programmability of such lattice encoders is described in [Holmes

and Syms 1991].

Many of the aforementioned papers provide analyses of their OCDMA configuration with their particular codes and conditions. There have also been numerous papers specifically analysing the performance of previously published OCDMA configurations and code sets [Kwon 1991a, Petrovic and Holmes 1991, Kwon 1994a, Lam and Hussain 1992, Ho and Wu 1994, Letaief 1995, Mandayam and Aazhang 1994, Yang and Kwong 1995b, Ho 1996, Mezger and Brandt Pearce 1996]. Typically these have used more-realistic system models or analytical assumptions and methods than the original papers. A number of works have also addressed the optimum multi-user decoder, and practical near-optimum multi-user decoders [Brady and Verdú 1991, Nelson and Poor 1995a, Nelson and Poor 1995b, Brandt Pearce and Aazhang 1994].

2.4.2 System Structure and Characteristics

A typical incoherent unipolar OCDMA proposal follows the form of Figure 2.1, where the encoders and decoders are implemented optically, and the transmitter and receiver structure of each user is shown in Figure 2.2. Each data bit 'one' is represented by a coded sequence of light pulses, generated from a single narrow pulse by a network of fibre delays and couplers. The coding networks, consisting in Figure 2.2 of the splitter, delays, and combiner, are usually referred to as tapped delay-lines. In Figure 2.2, each path from the splitter to the combiner represents a tap of unity weight, at the delay determined by the path length, and all other tap

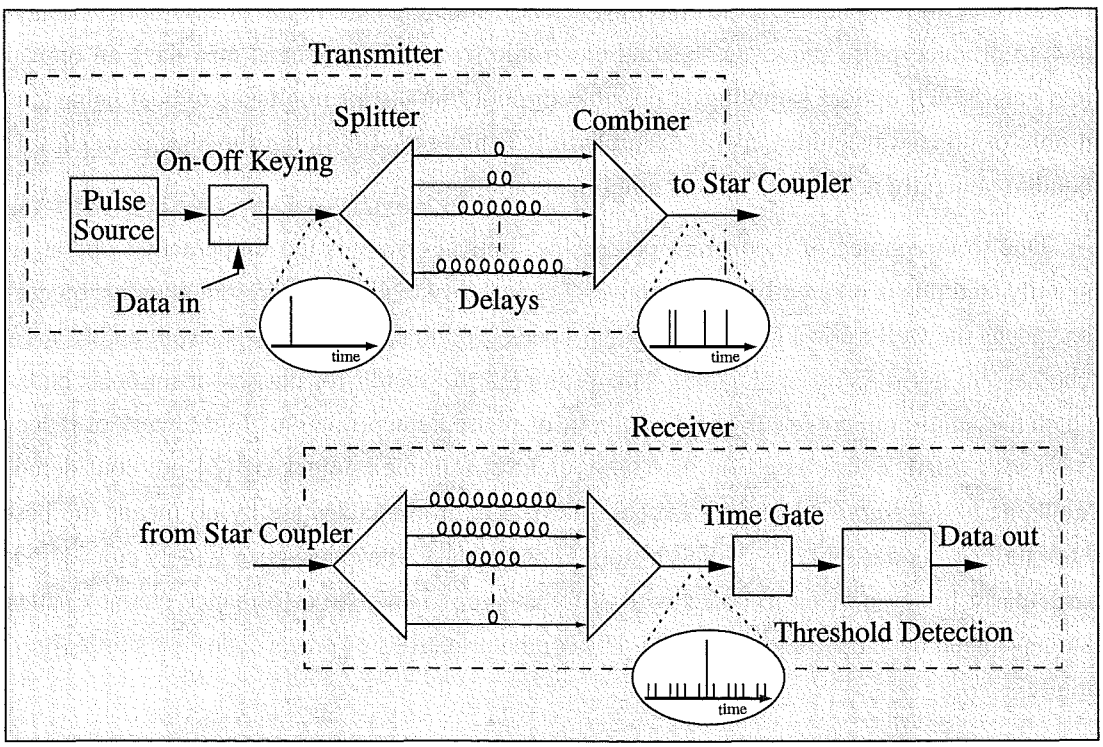

Figure 2.2 Incoherent OCDMA System using Optical Tapped Delay-Lines

weights are zero. The delays indicated in Figure 2.2 show the receiver delay-line impulse response is approximately equal to the time-reversed transmitter delay-line response, as required for matched filtering.

The recombination of pulses performed by the receiver delay-line is chosen to be on an incoherent basis, in order to avoid the complexities of optical phase and polarisation matching. This necessitates pulse coherence times that are much less than the actual pulse width, and it is also necessary that the delays in the receiver delay-line do not exactly match the time-reversed transmitter delay-line response. The encoder and decoder delays have to match to within a small fraction of the pulse width, but they need to differ by at least a few coherence times, in order that the pulses from the matched encoder, which are generated from a single pulse, add purely on a power basis.

Inset into Figure 2.2 are idealised illustrations of the temporal light-intensity variation at various points in the system. The insets illustrate the case of an isolated 'one' being transmitted by a single user, showing the original pulse, the encoded pulse sequence and the autocorrelation with the matched delay-line. Note that the light intensity is not-to-scale between insets. Also shown in Figure 2.2, immediately prior to threshold detection, is a 'time gate'. The time gate is to ensure that its output level depends only upon the input light level during a single chip time, and in particular, the chip time when an autocorrelation peak is expected if the data bit is a 'one'. The time-gate function is exactly analogous to the narrowband filter used in radio direct-sequence-spread receivers, to extract the despread signal from the other spread signals. Such a time gate has to be chip-synchronised to the incoming signal, and it must have a bandwidth corresponding to the chip time. Hence, if an OCDMA system uses optical delay-lines to produce pulse sequences beyond electronic frequencies, it must also have an optical time gate. Such optical sampling is possible through the use of nonlinear optical behaviour in fibre or other waveguides, as for example in [Chang *et al.* 1998], but the high power levels required generally necessitate optical amplification.

Due to the choice of incoherent processing, optical power is the fundamental operating quantity, and this is inherently non-negative. The inability to simply represent negative quantities means the well-known classes of bipolar codes used in radio spread-spectrum and CDMA schemes are not directly applicable. This prompted the search for classes of unipolar codes which had minimum cross-correlation and out-of-phase autocorrelation. In the work of [Prucnal *et al.* 1986a], codes based on the Galois field of a prime number GF$\{p\}$ are considered, known as *prime codes* [Shaar and Davies 1983]. The prime codes are by no means the best set of unipolar codes, but due to their historical precedence, they have been widely considered, particularly in comparison to codes with different properties and performance characteristics that have been developed more recently. Hence, the properties of prime codes are summarised briefly.

Prime codes are of length $N = p^2$, where p is a prime, and there are p such codes available. A prime code has a single unity element in each of the p groups of p sequential code elements,

and every other code element is zero. When such a code is used in an OCDMA system of the form of Figure 2.2, the code elements of unity correspond to the transmission of a light pulse at that temporal position, and zero elements correspond to no transmission. The positions of the p 'one's in each prime code assure that their periodic cross-correlation levels do not exceed 2, which is near the minimum sidelobe level of 1. The peak autocorrelation value of a prime code is given by p, but the out-of-phase autocorrelation can be as high as $p-1$. Note that the codes are only non-zero for the fraction $\frac{1}{p}$ of their total length, and hence are often termed *sparse*, and also the number of codes available is given by only the square root of the code length $p=\sqrt{N}$. Hence, it can be seen that the prime codes are sparse, there are not very many of them, and their autocorrelation functions are very poor. These properties compare poorly with those of typical bipolar CDMA sequences, such as the Gold codes outlined in Section 1.4.

The relatively poor performance of prime codes compared to the known classes of bipolar codes was followed by the definition of the best possible unipolar codes and bounds upon their existence [Salehi 1989a, Salehi 1989b, Salehi and Brackett 1989, Chung *et al.* 1989]. They considered codes of length n, with w unity elements, and all other elements zero. The maximum value of the out-of-phase periodic autocorrelation was denoted λ_a, and the maximum value of the periodic cross-correlation with any other such code as λ_c. The minimum values of λ_a and λ_c are readily seen to be unity, and codes that had this property were termed *optical orthogonal codes (OOC)*. A code family C was denoted by the $(n, w, \lambda_a, \lambda_c)$ quadruple, and the number of such sequences denoted as $|C|$. Bounds upon $|C|$ were given, and a number of constructions of such codes were reported. In the case of minimum λ_a and λ_c, the number of possible (n,w,1,1) codes is simply shown to be upper-bounded by

$$|C| \leq \left\lfloor \frac{n-1}{w(w-1)} \right\rfloor \tag{2.1}$$

where $\lfloor x \rfloor$ denotes the floor of x (round to the nearest integer towards $-\infty$). In the case when $\lambda_a = \lambda_c = \lambda$, the Johnson bound from algebraic coding theory can be used to show that

$$|C| \leq \left\lfloor \frac{(n-1)\ldots(n-\lambda)}{w(w-1)\ldots(w-\lambda)} \right\rfloor \tag{2.2}$$

The unipolar on-off keying (OOK) regime means that the use of periodic correlation properties is appropriate, since the adjacent sequences of each user are either identical, or one of them is zero, whereas aperiodic correlation properties must also be considered in bipolar DS-CDMA systems.

It should be noted that the bound of Equation 2.1 is quite restrictive. It is desirable to have the code weight w as large as possible, in order to reduce the likelihood of errors, and to increase the total fraction of the code length in which light is transmitted. Consequently, according to Equation 2.1, the number of available (n,w,1,1) codes must be significantly fewer than the code length. For example, with a code length $n = 1000$, and with weight $w = 10$, there can be no more than $|C| = 11$ such (n,w,1,1) codes.

It can be seen that OOCs with the smallest correlation sidelobes are very sparse in general, more so than prime codes, and again there are not very many of them. This prompted a number of groups to develop similar codes that trade larger correlation sidelobes ($\lambda_a, \lambda_c > 1$) for higher code weights and family sizes.

It is possible to significantly improve the theoretical error performance of a system such as Figure 2.2 by the inclusion of what is termed a 'hard limiter'. This is a component that would operate on the signal immediately prior to the receiver delay-line. The ideal function of the hard limiter is to give a constant output level whenever the input exceeds a certain threshold, and to give no output otherwise. This eliminates many cases which would otherwise cause errors, and it makes the system much more tolerant to differences in the power received from each user. For this reason, such a device would generally be required in practice, but to the author's knowledge no particularly suitable such device has yet been developed. It is highly likely, however, that such a device would require a high power level in order to exploit optical nonlinearities, and thus optical amplification would be necessary.

2.5 COHERENT OCDMA SCHEMES

In parallel to the large body of work on incoherent OCDMA systems that use unipolar time-domain coding, there have been a number of completely coherent approaches to OCDMA, and these are outlined in the following.

The experimental spreading and despreading of ultrashort pulses by the coherent bipolar coding of the spectral phase was reported in [Weiner *et al.* 1988], and an OCDMA system based on such encoding was proposed. More-detailed system proposals and performance analysis were forthcoming [Weiner *et al.* 1988, Salehi 1989a, Salehi *et al.* 1990], and later analyses incorporating further details were presented in [Hajela and Salehi 1992, Yao *et al.* 1993]. Another group also proposed various similar techniques of transform- and spectral-domain processing [DeCusatis and Das 1990]. In the scheme of [Weiner *et al.* 1988], in order for pulse reconstruction to occur, the encoder and decoder have to be a coherent optical matched-filter pair. However, the extremely-high-bandwidth time gating required at the receiver and the very high dispersion sensitivity are two of the practical issues which are likely to limit this scheme. A very recent encoding and decoding demonstration using programmable liquid-crystal masks, a nonlinear optical detection scheme, and dispersion compensation, shows that transmission over a couple of kilometres may be achievable [Chang *et al.* 1998]. The original demonstration of spectral-phase encoding led to a number of similar proposals based upon spectral-amplitude coding [Zaccarin and Kavehrad 1993, Brandt Pearce and Aazhang 1993, Kavehrad and Zaccarin 1995, Nguyen *et al.* 1995], and it is the scheme of Zaccarin and Kavehrad [1993] that is analysed in detail in Chapter 3 of this thesis. The similar encoding of spectral polarisation has also been considered [Griffin *et al.* 1995].

There have also been a number of straightforward coherent temporal-encoding OCDMA schemes. With the progress towards coherent heterodyne optical detection by the early eighties,

the work of [Tou 1987] proposed direct-sequence coherent bi-phase modulation (DS-BPSK) of optical carriers using Gold codes, together with heterodyne detection using a similarly keyed local optical source and bandpass filtering at the IF (intermediate frequency). The need for carrier frequency locking and code synchronisation was recognised, but these were not addressed in this early proposal. The scheme of [Foschini and Vannucci 1988] then proposed coherent DS-BPSK of laser sources of random wavelengths. The receiver consists of a phase-modulator driven by the spreading sequence and a narrow tunable optical filter before photodetection. The filter completely removes signals from any sources of significantly different wavelength, and if by chance, an unwanted interferer has approximately the same source wavelength, the interfering signal is not despread, so only a small fraction passes through the filter. The experimental demonstration of such optical DS-BPSK spreading and despreading was demonstrated in [Vannucci and Yang 1989], and since then, there have been a number of further analyses and proposals based upon the coherent coding of the temporal phase of light [Benedetto and Olmo 1991, Takushima and Kikuchi 1994, Zaccarin and Kavehrad 1994a, Karafolas and Uttamchandani 1994a, Karafolas and Uttamchandani 1994b, Karafolas and Uttamchandani 1995, Ayadi and Rusch 1997]. The scheme of [Kiasaleh 1991] simply used electrical frequency-hopped signals to successively phase-modulate the light from a single optical source, and then electrical despreading/dehopping after detection. Each of these systems is however, restricted by the electro-optic phase modulation, or injection locking in [Ayadi and Rusch 1997], to electrical-domain bandwidths, although some increase may be gained by cascading phase-modulators in some circumstances.

However, phase modulation does not have to be performed electro-optically or via injection locking, and an interesting alternative is to use cross phase modulation (XPM) within a fibre or some other single-mode waveguide with nonlinear refraction (Section 1.3.1.3). To utilise this effect, a high-power pulse sequence at another wavelength can be used to induce a corresponding phase modulation in the co-propagating carrier waveform, and the pulse sequence can then be simply filtered out, as suggested in [Neusy and Kavehrad 1990]. However, the treatment of this scheme by Neusy and Kavehrad [1990] is rather sketchy, and the deficiencies of this are outlined in Section 2.9.4, due to the closely related incoherent proposal in the same work. The receiver in [Neusy and Kavehrad 1990] modulates the phase of a local source in the same manner, and then uses heterodyne or homodyne detection. Neither XPM nor the generation of this pulse sequence are constrained by electrical bandwidths, since the pulse sequence can be generated by an optical delay-line structure such as that illustrated in the transmitter of Figure 2.2. Apart from the use of another dimension such as wavelength [Foschini and Vannucci 1988], or space (multi-fibre for example), this is the only type of configuration which permits network throughput beyond electrical-domain bandwidths using coherent direct-sequence spreading.

2.6 SYSTEMS USING COHERENTLY MATCHED TEMPORAL CODING

In view of the relatively poor distinction between the autocorrelation peaks of unipolar codes and the sidelobes of both the auto- and cross-correlations, two groups investigated and demonstrated the possibilities of the coherent recombination of light pulses with fibre lattices of cascaded MZIs [Marhic and Chang 1989, Sampson and Jackson 1990a, Sampson and Jackson 1990b]. The coherent recombination of light pulses results in a sum of field amplitudes, rather than the sum of field intensities in the incoherent case. The result is an autocorrelation peak that is n times larger than in the incoherent case, where n is the number of pulses combined, and there is a reduction in some sidelobe levels due to destructive interference. However, in order to achieve coherent recombination with a lattice encoder and decoder pair, such as those illustrated in Figure 2.3, the optical phase delays in each branch of the encoder and decoder must match, and the relative polarisations must also be maintained. The decoder then has an impulse response given exactly by the temporal reverse of the impulse response of the matching encoder, and is thus a matched filter. Having such lattices implemented with polarisation-maintaining waveguides in an optical integrated circuit was seen as the most practical manner in which the phase and polarisation matching could be regularly achieved [Sampson and Jackson 1990a].

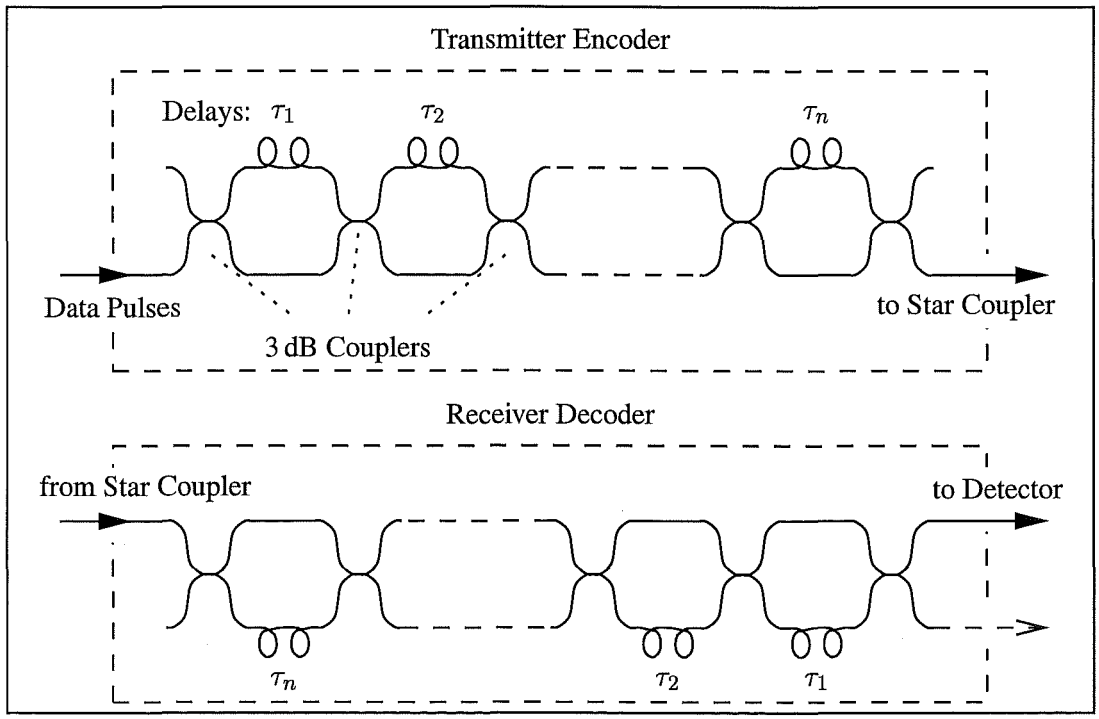

Figure 2.3 Lattice Encoding and Decoding

The first experimental demonstrations used the same lattice for both the encoding and decoding, thus assuring that they were coherently matched, but coherent matching of a remote encoder and decoder pair was then reported in both [Griffin *et al.* 1992a] and [Chang and

Marhic 1992]. In the experimental arrangement of [Griffin *et al.* 1992a], electro-optic phase-modulators were inserted into one arm of each lattice stage of the decoder, and these were controlled by straightforward feedback systems using slight phase-dithering and locking to the corresponding modulation in the detected output. In this manner, the relative phase-delays in both the encoder and decoder remained matched despite their environmental fluctuations. Single-ended detection was used in all these early experimental demonstrations, but balanced detection of both outputs of the final decoder coupler (Figure 2.3) is superior in general.

In the configurations of [Marhic and Chang 1989, Chang and Marhic 1992], both of the outputs of the final 3 dB coupler of the encoder are connected to the two coupler inputs of the decoder (only a single such connection is indicated in Figure 2.3). In this case, described as inverse decoding, the system is lossless and complete reconstruction of the original pulse sequence ideally occurs, provided the polarisation of, and the phase relationship between, the two encoder outputs are maintained. In their experimental demonstration of remote inverse decoding, Chang and Marhic [1992] use the two orthogonally polarised modes within SMF to convey both encoder output waveforms. Further analysis and discussion of inverse decoding, their experimental demonstrations, and other similar configurations were presented in the review of [Marhic 1993]. However, the practical difficulties in fibre transmission of both encoder outputs over a real fibre network, while retaining the phase-matching between them, mean that inverse decoding is unlikely to be used in practice [Sampson *et al.* 1997].

In the work of [Sampson *et al.* 1994], data transmission using coherent correlation with matched coders of the form in Figure 2.3 is analysed in detail. The configuration considered in [Griffin *et al.* 1992b] follows Figure 2.3 with each delay $\tau_1 \ldots \tau_n$ equal, but with binary phase selection in each interferometer to differentiate signals from each user. This eliminates both the need to have differing interferometer delays for each coder, and the corresponding requirement to change these delays to address other users, which is advantageous since large delay changes generally are very much slower than electro-optic phase modulation. Sampson *et al.* [1994] show that the SNR limits due to crosstalk from other users in such coherently matched systems are much higher (and hence better) than for systems based upon incoherent correlation.

2.7 SYSTEMS USING COHERENCE MULTIPLEXING

The transmission of information using the coherence of a broadband light source was first reported in [Delisle and Cielo 1975], and the use of this technique for multiplexing two signals was demonstrated in [Cielo and Delisle 1976]. This technique became known as coherence multiplexing, and its use was proposed for multiplexing sensors and also for communications purposes. For a comprehensive review of the history of coherence multiplexing the work of [Sampson *et al.* 1997] is recommended, whereas here only selected works are noted before the recent resurgence of this technique.

The proposals and analyses of systems of coherence-multiplexed sensors were presented in [Brooks *et al.* 1985] and [Wentworth 1989], with many different configurations and noise

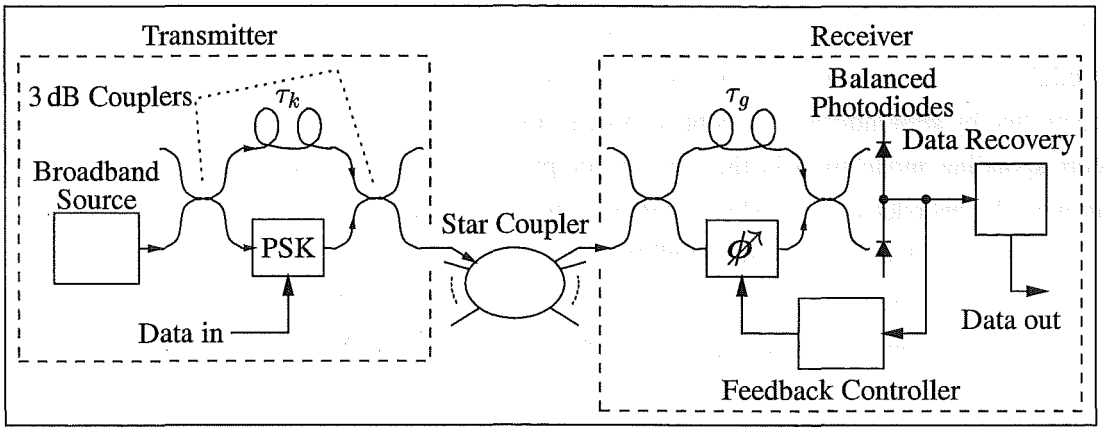

Figure 2.4 Multiple-Access System based upon Coherence Multiplexing

considerations addressed therein. The first demonstration of coherence multiplexing with parallel encoders and decoders (corresponding to Figure 2.1) for communication purposes was reported in [Goedgebuer and Hamel 1987]. The first analysis of the SNR limits arising in a multiple-access system based upon coherence multiplexing, especially considering sources of the same optical spectra, was reported in [Healey 1987]. The work of [Chu and Dickey 1991] proposed coherence multiplexing for increased inter-processor bandwidth, and it detailed the capacity limit due to mixing between incoherent optical fields, assuming spectrally similar thermal sources and single-ended detection.

Shown in Figure 2.4 is a typical multiple-access system based upon coherence multiplexing. The information is encoded into the coherence of the light by the phase-shift keying (PSK) of the transmitter interferometer, whose path-length difference τ_k must significantly exceed the source coherence time τ_c. For any receiver where τ_g differs from τ_k by significantly more than τ_c, the light appears completely incoherent, and hence the light power is split equally between the two receiver photodiodes, ideally giving no signal. If the encoder and decoder delays match to within the source coherence time, that is $|\tau_k - \tau_g| < \tau_c$, then there is some coherence between the light entering the two arms of the second receiver 3 dB coupler, and hence the light may not split equally between the two photodiodes. If the difference between τ_k and τ_g is maintained at an integer number of optical wavelengths, and less than τ_c, then the light from the matched user is incident upon only one of the receiver photodiodes, according to the transmitted data. Hence, a bipolar signal is recovered at the receiver, and a threshold of zero is optimum for the binary data decisions. As indicated in Figure 2.4, locking of the receiver MZI phase to that of the transmitter MZI is accomplished through a simple feedback loop to a phase-modulator in one branch of the receiver MZI, as demonstrated in [Griffin *et al.* 1992a] for the coherent matching of multiple MZIs.

Coherence multiplexing has been identified as a multiple-access technique that is much simpler than most OCDMA schemes, but has a number of similarities to OCDMA, and demonstration of coherence multiplexing with two 1 Gb s^{-1} data signals has been classified as a multi-

gigabit per second demonstration of photonic code-division multiplexing [Pendock *et al.* 1995]. Further experimental and analytical work by the same authors also refer to their system as either a code-division multiple-access system based on coherence multiplexing, or just a code-division multiple-access system [Pendock and Sampson 1995, Pendock and Sampson 1996a]. In the review paper of [Sampson *et al.* 1997], this classification of coherence multiplexing as a CDMA technique is justified on the basis of its asynchronous and uncoordinated network access using signals of the same optical bandwidth.

The proposals, demonstrations, and analyses of coherence multiplexing up to and including the work of [Chu and Dickey 1991] used merely a single photodiode at the receiver. It was clear that the use of a balanced receiver would eliminate common-mode signals and noise terms in the same manner as in any other system where the coherence between two light fields mixing in a 3 dB coupler is to be determined. Measured performance levels with and without balanced detection were first reported and compared in the work of [Pendock and Sampson 1995], and the expected improvement was indeed observed. The use of balanced detection eliminates contributions from the source amplitude variations of each unmatched user, whether it be inherent source noise, or due to amplitude keying of the source. Hence, with balanced detection, it is possible to merely amplitude-shift key the light before the encoder MZI, rather than the phase-shift keying indicated in Figure 2.4, as demonstrated by the experiments reported in [Pendock *et al.* 1995].

The work of [Pendock and Sampson 1996a] presents the SNR expression arising from the application of the analysis of [Wentworth 1989] to coherence multiplexing using independent thermal sources and differential detection, and compares this to the experimental results reported in [Pendock and Sampson 1995], noting good agreement. The details of this analysis were then presented in [Pendock and Sampson 1997], along with analysis including the effects of fibre dispersion, and this work is in general agreement with the previous results for the case of single-ended detection. Other works of the same group include [Wacogne and Jackson 1996a], in which it was pointed out that coherence-multiplexed systems can easily be tapped with a simple optical filter. Various suggestions for imparting a degree of inherent security to the system were made, including that of incorporating a pseudorandom key with the data, as subsequently demonstrated and reported in [Wacogne and Jackson 1996b]. Such a scheme was also proposed in [Gupta *et al.* 1994], and a similar experiment reported in [Karafolas *et al.* 1996]. The combination of coherence multiplexing and coarse wavelength-division multiplexing was also proposed and demonstrated experimentally, as reported in [Cahill *et al.* 1997].

Another group recently addressed the limits of single-ended coherence multiplexing due to mixing noise between diode laser sources [Gupta *et al.* 1997]. These sources are assumed to have negligible self-intensity noise, and hence slightly better performance is expected in the case of single-ended detection compared to that using thermal sources. However, there are a number of deficiencies in [Gupta *et al.* 1997], and consequently the results differ from previous analyses with single-ended detection, as detailed in Section 7.3.1.1.

2.8 OTHER OCDMA SCHEMES

The other main category of OCDMA systems that has not yet been described is that of incoherent systems that use bipolar coding. These schemes are the main focus of this thesis, and they are examined in detail in Section 2.9. In this section, we briefly mention those system proposals that use a combination of the OCDMA techniques previously categorised, and those that use OCDMA along with other multiple-access or signalling regimes.

The OCDMA proposal of [Griffin *et al.* 1993] is termed coherence coding, and they describe therein a proof-of-concept experiment. Coherence coding incorporates the coherent spectral-phase encoder of [Weiner *et al.* 1988] into one branch of the MZI encoders and decoders of a coherence-multiplexed system, improving the security of the transmitted data. The performance of such a system was briefly indicated along with its proposal [Griffin *et al.* 1993], and was considered in detail in the subsequent treatment of [Griffin *et al.* 1995]. The performance is, however, limited to that of the coherence-multiplexing system alone [Sampson *et al.* 1997].

Following the initial space- and time-domain coding OCDMA proposal of [Hui 1985], further work by the same group on temporal/spatial OCDMA was reported in [Park *et al.* 1992], and an experimental demonstration was reported in [Mendez *et al.* 1994]. A holographic OCDMA system was proposed in [Salehi and Paek 1995], and a proof-of-concept experiment using free-space optics was performed. By using two spatial dimensions for the coding, the potential number of simultaneous users with such a scheme is claimed to be many thousand. The scheme proposed in [Riza *et al.* 1993] also uses two-dimensional coding, but these are simply 2-D on-off patterns used to mask coherent free-space beams directed towards an orbiting satellite (many-to-one). The proposal of [Kitayama 1994] is for image multiplexing through a multi-fibre cable, with one fibre per pixel. It uses optically addressable spatial light modulators (SLM) to impress on-off signature patterns onto input images, and similar masking operations and threshold detection are used to separately recover the images at the receiver.

The random-carrier OCDMA system of [Foschini and Vannucci 1988] is basically a mixture of wavelength-division and code-division multiple access. Both time hopping and time-and-wavelength hopping were proposed in [Gelman and Schilling 1988], using incoherent unipolar techniques, and the use of an ALOHA protocol was also considered. The work of [Ayadi *et al.* 1995] is also a hybrid of WDMA and CDMA in an optical network. The work of [Tančevski and Andonovic 1994] proposes a wavelength-hopping time-spreading system where incoherent unipolar temporal coding is used. There have been several later works by the same authors extending their treatment of this system, of which the work of [Andonovic and Tančevski 1996] is suggested as a reasonable starting point.

There have also been a number of works which utilise a combination of OCDMA using temporal coding with pulse-position modulation (PPM). PPM has received a lot of attention in optical communication systems, particularly for loss-limited systems where receiver sensitivity is paramount, since many bits of information are associated with a single light pulse, into

which the photons are concentrated. Such a pulse may then still be reliably detected at channel attenuation levels that would render undetectable the corresponding single-bit PCM (pulse-code modulation) symbols with the same total energy. Many works thus traded off the SMF bandwidth via PPM signalling in order to increase the receiver sensitivity, especially before optical amplifiers such as the EDFA were developed, as for example in [Garrett 1993]. The combination of PPM signalling with incoherent OCDMA systems using unipolar codes, as in Section 2.4, was investigated theoretically and experimentally after an earlier proposal by the same group [Gagliardi *et al.* 1993]. In this work the unipolar pulse sequence, generated by an optical delay-line, was transmitted in one out of M PPM slots in the PPM word or frame, according to the $\log_2 M$ bits of information thus represented. A similar arrangement was proposed in [Elmirghani and Cryan 1994], except that the unipolar sequence could then assume positions within the PPM word that were separated by only a fraction of the unipolar sequence length. Detailed analyses of PPM-OCDMA systems such as that of [Gagliardi *et al.* 1993], together with various receiver configurations, have been presented in a number of works by the same author, including [Shalaby 1995] and [Shalaby 1996]. The effects of an optical hard limiter and error-correction coding upon such PPM-OCDMA systems has been considered [Ohtsuki *et al.* 1995], and proposed in [Ohtsuki *et al.* 1996] is the deliberate introduction of a limit to the average network access time each user has, thus artificially imposing the regime in which CDMA is most effective.

2.9 INCOHERENT SYSTEMS USING BIPOLAR CODING

A crucial aspect of an incoherent OCDMA system that uses bipolar codes is the way in which the negative code elements are represented, since power is inherently non-negative. In most of such system proposals, negative code elements are represented by a power level of zero at the transmitter, and at the receiver, negative code elements are implemented by subtraction after photodetection.

OCDMA proposals that are both incoherent, and which use bipolar codes, can then be broadly classed as having the structure shown in Figure 2.5, or some subset or other slight variation thereof. The sequences $\boldsymbol{A}$ and $\bar{\boldsymbol{A}}$ are used to encode the light for data bits 'one' and 'zero' respectively. At the receiver, correlations with sequences $\boldsymbol{B}$ and $\bar{\boldsymbol{B}}$ in general are performed, and for the matched user $\boldsymbol{A} = \boldsymbol{B}$ and $\bar{\boldsymbol{A}} = \bar{\boldsymbol{B}}$. In many such schemes, $\boldsymbol{A}$ and $\bar{\boldsymbol{A}}$, and also $\boldsymbol{B}$ and $\bar{\boldsymbol{B}}$, are unipolar complementary sequences, derived simply from bipolar codes, as explained in the following.

If there is a bipolar code $\boldsymbol{a}$, whose elements $a_i = \pm 1; \forall i$, then unipolar versions of $\boldsymbol{a}$ and $-\boldsymbol{a}$ may be given by $A_i = \frac{(1-a_i)}{2}; \forall i$, and $\bar{A}_i = \frac{(1+a_i)}{2}; \forall i$. These unipolar sequences are merely scaled and offset from the bipolar sequences, and also $\boldsymbol{a} = \bar{\boldsymbol{A}} - \boldsymbol{A}$. Signalling by keying between such sequences $\bar{\boldsymbol{A}}$ and $\boldsymbol{A}$ corresponds to the signalling arrangement in a coherent direct-sequence spread-spectrum system (Section 1.4), but with the crucial difference that the transmitted power level is now zero wherever the signal would be negative in the coherent

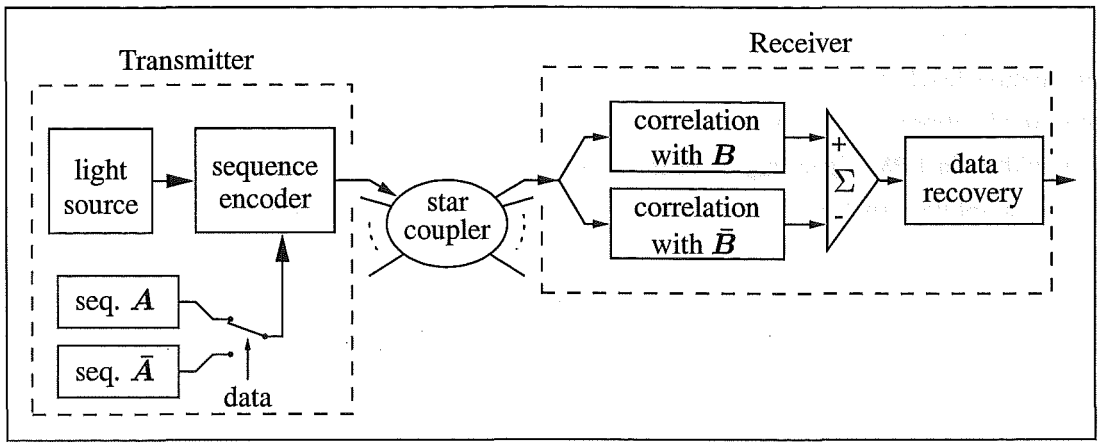

Figure 2.5 Incoherent OCDMA using Bipolar Codes - System Structure

system. As explained in the various works of O'Farrell *et al.*, if such unipolar sequences are correlated with a bipolar sequence $\boldsymbol{b}$, where $b_i = \pm 1; \forall i$, then

$$\boldsymbol{A} \cdot \boldsymbol{b} = \sum_i A_i b_i = \sum_i \frac{1 - a_i}{2} b_i = -\frac{1}{2}\boldsymbol{a} \cdot \boldsymbol{b} + \frac{1}{2}\sum_i b_i \tag{2.3}$$

It can be seen from Equation 2.3 that the unipolar-bipolar correlation $\boldsymbol{A} \cdot \boldsymbol{b}$ is equal to a scaled version of the bipolar correlation $\boldsymbol{a} \cdot \boldsymbol{b}$, plus an offset dependent upon the element-wise sum of the original bipolar code $\boldsymbol{b}$. Note that in practice, the elements of $\boldsymbol{A}$ represent optical power, and thus the offset term in Equation 2.3 generally results in an offset proportional to the received power. If balanced bipolar codes are used, the offset is equal to zero, and the scale factor of negative one half arises from each unipolar sequence having half of its elements equal to zero, together with the sign choice in the bipolar to unipolar mapping.

If the complementary unipolar sequences $\boldsymbol{B}$ and $\bar{\boldsymbol{B}}$ are derived from the bipolar sequence $\boldsymbol{b}$ exactly as for $\boldsymbol{a}$, then $\boldsymbol{b} = \bar{\boldsymbol{B}} - \boldsymbol{B}$, and the receiver structure in Figure 2.5 performs the following

$$\boldsymbol{A} \cdot \boldsymbol{B} - \boldsymbol{A} \cdot \bar{\boldsymbol{B}} = \boldsymbol{A} \cdot (\boldsymbol{B} - \bar{\boldsymbol{B}}) = -\boldsymbol{A} \cdot \boldsymbol{b} \tag{2.4}$$

assuming sequence $\boldsymbol{A}$ was transmitted. It is thus clear that the receiver in Figure 2.5 can perform the unipolar-bipolar correlation of Equation 2.3 through the use of two completely unipolar correlations. In this manner, these correlations can be performed using incoherent optical techniques, such as the optical delay-lines illustrated in Section 2.4.2, and these can also be used for generating the unipolar sequences at the transmitter. The difference between the outputs of the two correlations must be performed, and this is generally achieved by using a balanced photodiode pair. This gives a signal proportional to the difference between the light power incident on each photodiode. Assuming balanced codes, the keying between $\boldsymbol{A}$ and $\bar{\boldsymbol{A}}$ according to the data then simply changes the sign of the output, completing the appearance of

bipolar signalling. Since $\boldsymbol{A}$ and $\bar{\boldsymbol{A}}$ are the logical complements of each other in this arrangement, this signalling scheme is referred to here as complementary keying. In the various works of O'Farrell *et al.*, such signalling is described as code-inversion keying or sequence-inversion keying (SIK), but these terms are avoided here to eliminate confusion over the meaning of the term 'inverse'. The bipolar correlation process may also be described as performing the difference between the number of agreements (between the elements of two codes) and the number of such disagreements, since this is effectively what happens when two ± 1 sequences are multiplied and added.

The use of unbalanced codes in such a unipolar-bipolar correlation scheme may be reasonable if the received power levels from each user are constant, if each user starts and stops transmitting independently, and if the shortest possible transmission times for each user are equivalent to a large number of bits. In such a case, and using Gold codes, for example, the offset term in Equation 2.3 is significantly smaller than the signal, it has one of 3 known levels (according to $\sum_i b_i$), and it does not change very often, so it may be possible to adequately filter or track it out.

The original spectral-amplitude OCDMA proposal by Zaccarin and Kavehrad [1993], that is analysed in detail in Chapter 3 of this thesis, can be compared to the structure of Figure 2.5. This scheme implements the sequence coding as spectral-amplitude filtering of a broadband incoherent source, with the balanced complementary receiver structure of Figure 2.5. However, for practical reasons, the transmitter code is fixed and the source is simply on-off keyed (OOK), which corresponds to the assignment $\bar{\boldsymbol{A}} = 0$ in Figure 2.5. In a subsequent work, Kavehrad and Zaccarin [1995] note that complementary keying with $\boldsymbol{A}$ and $\bar{\boldsymbol{A}}$ would be more efficient (termed "orthogonal signalling" in their work). Due to the fact that this scheme is described and analysed in Chapter 3, this scheme is not detailed here.

2.9.1 The First Incoherent Bipolar OCDMA Proposal

One of the earliest OCDMA system proposals, if not the first to be described as such, was the work of [Peterson and Gardner 1981]. Their scheme is incoherent and bipolar coding is used, and this system is examined here to illustrate the principles and to facilitate comparison with the recent such proposals treated in this thesis.

Peterson and Gardner [1981] investigated the performance of a multiple-access satellite repeater system using bipolar coding, polarisation modulation and direct detection. The basic transmitter and receiver structure is shown in Figure 2.6. At a terrestrial station, each bipolar data bit is direct-sequence spread by a bipolar Gold code, and this is then used to polarisation-shift key (PolSK) a laser beam between left-circular (LC) and right-circular (RC) polarisations. At the satellite, the received light is split by a polarisation-beam-splitter (PBS) into left- and right-circular polarisations, and these are incident upon a balanced photodetector pair. Correlation detection on the subsequent photocurrent difference is then performed electrically, with bipolar matched filters for each user in the usual manner, although this is only shown for one

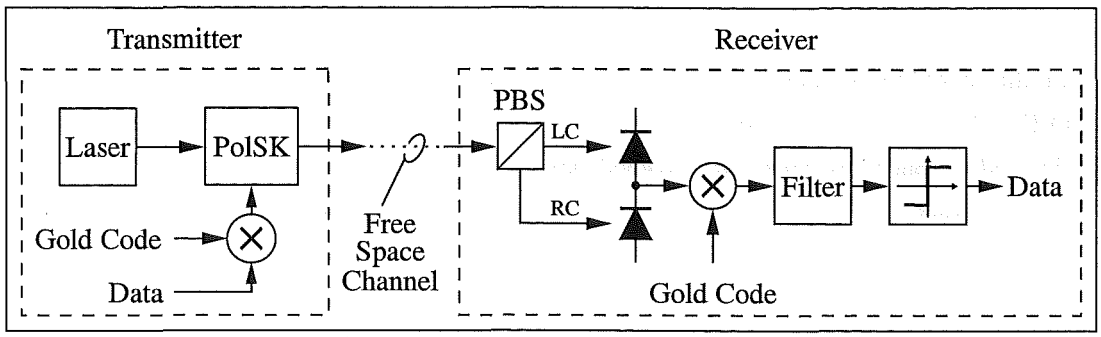

Figure 2.6 Terrestrial-Satellite OCDMA System

user in Figure 2.6. The downlink is very similar, with the laser being intensity-modulated according to the magnitude of the sum of all the regenerated signals from the uplink, and the polarity is again represented by the left- or right-circular polarisation of the light.

This system is classified here as incoherent, in the sense that it is only the light polarisation which conveys the information. It is noted that left- and right-circular polarised light has, by definition, complete coherence between the components extracted by any two orthogonal linear polarisers, with either $\frac{\pi}{2}$ or $-\frac{\pi}{2}$ phase difference between these components. However, the use of lasers and circular light polarisation is purely a practical requirement of the terrestrial-satellite link, and not because of any inherent coherence requirements of the system.

In the system of Figure 2.6, positive and negative code elements are represented by light power of left-circular and right-circular polarisations respectively. This is a very efficient and effective signalling system, since power is transmitted for code elements of both polarities, as in coherent direct-sequence systems, and it is possible since the free-space channel maintains the polarisation states, unlike standard single-mode optical fibres. The system is equivalent to two parallel implementations of Figure 2.5, one for each circular polarisation, where $\boldsymbol{A}$ and $\bar{\boldsymbol{A}}$ are the unipolar (offset) versions of Gold sequences and their negative, and $\boldsymbol{A}$ is transmitted by the left-circular section when the right-circular section is using $\bar{\boldsymbol{A}}$, and vice-versa. The photodetection takes place before the correlation in the receiver, so $\boldsymbol{B}$ can be the actual bipolar Gold sequence $\boldsymbol{b}$, with $\bar{\boldsymbol{B}} = 0$ (or equivalently $\bar{\boldsymbol{B}} = -\boldsymbol{B}$). The outputs from the effective parallel implementations of Figure 2.5 are given by both Equation 2.3 and Equation 2.4 with $\boldsymbol{A}$ replaced by $\bar{\boldsymbol{A}}$, and hence $\boldsymbol{a}$ replaced by $-\boldsymbol{a}$. By performing the difference between these outputs, the offset term in Equation 2.3 is cancelled, giving the ideal zero-offset bipolar signal $\boldsymbol{a} \cdot \boldsymbol{b}$, regardless of any code imbalance.

Interference between the light fields from different sources at the uplink detectors is considered not to occur. This is justified by assuming that there is sufficient geographical separation between the sources that their fields at the detectors are not spatially coherent. This spatial incoherence, like state-of-polarisation preservation, is another fortuitous characteristic of the free-space channel and the geographical arrangement of their network, and unfortunately, this too cannot be generally achieved with a single-mode fibre network. In the subsequent chapters

of this thesis, the important consequences of this difference are dealt with in detail.

Peterson and Gardner [1981] show that even in the ideal case of orthogonal codes, the presence of other users on the uplink degrades the uplink performance due to the increase in shot noise at the detectors. The shot-noise-limited performance on the downlink is shown to be better than the uplink. This can be understood by considering that the transmitted light intensity for the downlink exactly corresponds to the uplink signal immediately after the balanced detectors, but there is less shot noise at a downlink receiver, since light is not simultaneously transmitted in both circular polarisations. A weakness of this work is that the only error estimates displayed for more than two users are based upon the assumption of ideally orthogonal codes, which is quite misleading. In the case of asynchronous DS-CDMA with pseudorandom sequences, including Gold codes, the MAI is definitely not negligible [Viterbi 1995], and hence the improved shot-noise performance of the downlink is unlikely to be significant when there are many simultaneous users. Due to the fact that the satellite-based receiver decodes all of the signals on the uplink, a multi-user decoding structure is clearly applicable, and consequently uplink performance near the shot-noise limit may be achievable if the increased decoder complexity is possible and affordable. It is clear, however, that the maximum chip rate is limited by the bandwidth of the electro-optic modulators, and hence the total network capacity is similarly limited.

As well as eliminating the offset arising with unbalanced codes, the use of the parallel polarisation channel for power corresponding to the negative code elements means that 3 dB is gained in terms of the SNR with respect to shot noise and receiver thermal noise also. Unfortunately, standard optical fibre does not maintain any particular field polarisation, although orthogonal polarisations do remain orthogonal, and polarisation-maintaining fibres (PMF) generally support only a single field polarisation. However, there has been one suggested fibre-based OCDMA structure that does use orthogonal polarisations to represent the elements of bipolar codes, and this system uses polarisation-shift keying (PolSK) for the data, along with PolSK of the broadband optical source spectrum [Griffin *et al.* 1995]. At the receiver, the opposite spectral PolSK (matched filtering) is performed upon the received signal. The result of this keying is then either the desired PolSK signal, with arbitrary reference polarisation, or a mismatched signal with very small remaining polarisation. A PolSK receiver which can accommodate the arbitrary and slowly-varying reference polarisation is then required. The use of a separate channel for the power representing negative code elements has not currently been proposed in any other system, although the Manchester coding considered in Sections 2.9.3 and 2.9.4 effectively uses every other pulse position for the negative elements. Applying the two-channel PolSK system of [Peterson and Gardner 1981] to a fibre system using temporal optical coding is one approach which may be considered. As with many other PolSK systems, such a scheme would require active polarisation control to track the polarisation of the desired signal. However, it may not be easy, or perhaps even possible, to achieve such polarisation locking and subsequent tracking from among the many such signals received in a multiple-access network.

2.9.2 Systems using Electronic Processing

In the OCDMA works of [Hasegawa and Hirosaki 1983, Tamura *et al.* 1985, Kiasaleh 1989, Onoda and Miki 1991], the CDMA processing is all performed electronically, and hence the effective transmitter and receiver structures match that of Figure 2.5 with $\boldsymbol{A} = -\bar{\boldsymbol{A}}$ and $\boldsymbol{B} = -\bar{\boldsymbol{B}}$. In this case, the CDMA subsystem reduces to basic bipolar direct-sequence spreading and correlation detection, as described in Section 1.4. The electro-optic and opto-electric conversions then occur immediately after the transmitter and before the receiver shown in Figure 2.5. Consequently, the optical network is purely being used as an intensity-modulation direct-detection (IMDD) transparent pipe for the electrical signals, and any light interference effects are neglected. In Chapter 7 the conditions under which such interference may or may not be neglected are examined in detail.

2.9.3 Complementary Keying and Balanced Detection

The structure of Figure 2.5, with $\boldsymbol{A}$ and $\bar{\boldsymbol{A}}$ being unipolar sequences given by offsets of a bipolar code, and using balanced photodetection after correlation, is based upon the work reported by O'Farrell and Beale [1989], and subsequent works have dealt with various implementations of this structure [O'Farrell and Lochmann 1994a, O'Farrell and Lochmann 1994b, O'Farrell and Lochmann 1995]. The works of [Khaleghi and Kavehrad 1996] and [Nguyen *et al.* 1995] also use this structure, and it is used within the inner subset of the OCDMA proposal of [Zaccarin and Kavehrad 1994b]. A variant on this structure is proposed by Andonovic *et al.* [1994], but it is possible to modify their system to fit this structure more closely.

The works of O'Farrell *et al.* describe the relationship between unipolar-bipolar correlations and bipolar correlations as detailed early in Section 2.9, and both passive and active correlation configurations (Figure 1.2) are proposed. The sequence encoding is implemented as on-off keying (OOK) of an incoherent pulse source, and the first receiver configuration is simply a passive tapped delay-line, where each tap output is routed to one of a balanced photodetector pair[2], corresponding to a tap weight of $+1$ or -1. The second receiver configuration consists of the received signal being split in two, and then being directly on-off keyed by temporal sequences $\boldsymbol{B}$ and $\bar{\boldsymbol{B}}$ before incidence upon a balanced pair of photodiodes. However, this scheme incurs a 3 dB (optical) power penalty with respect to one which switches all the received light between the two photodiodes according to the code $\boldsymbol{b}$, which thus implements the receiver structure of Figure 2.5 in an ideally lossless manner. The use of an on-off-keyed semiconductor laser amplifier to perform both OOK of the received signal and also optical preamplification has been proposed and demonstrated [Wallace *et al.* 1995].

While the alternative scheme of [Vethanayagam and MacDonald 1991] does not use complementary keying, it is mentioned here since it efficiently implements the form of decoder proposed in [O'Farrell and Lochmann 1994a]. The decoder consists of a tapped delay-line,

[2]This configuration incurs significant loss if the tap outputs are combined into a single fibre before photodetection, and this along with other possible consequences are treated in Chapter 7.

one tap for each code element, and these are all incident upon a parallel array of symmetrical photodiodes, whose polarity is controlled by the applied voltage [Vethanayagam and MacDonald 1991]. In this manner, the bipolar code implemented by this passive decoder is simply programmable. The codes used in the $50\,\mathrm{Mb\,s^{-1}}$ demonstration with a 16-element decoder were not based upon standard bipolar spreading sequences, but rather upon Alberta codes, which allow the autocorrelation peak to be simply distinguished from all the auto- and cross-correlation sidelobes [Vethanayagam and MacDonald 1991]. These unipolar codes have significantly fewer 'one's than 'zero's, and hence the majority of the decoder taps are weighted as -1, corresponding to the 'zero's. Simple unipolar coding with on-off keying for the data is used at the transmitter, and with these codes the only condition in which a positive decoder output occurs is the autocorrelation peak [Vethanayagam and MacDonald 1991]. However, the number of such codes for a given code length has to be smaller as a result of this correlation restriction, - in [Vethanayagam and MacDonald 1991], for example, there are a set of 5 Alberta codes listed, of code length 16 and weight 4, but two of these actually have positive autocorrelation sidelobes. In addition, although this coding system allows an autocorrelation peak to be distinguished from any auto- and cross-correlation sidelobes, it appears to have this property only when there is a single received sequence, which renders it inapplicable to multiple-access schemes. For example, if several unmatched signals are received at the same time as the matched sequence, then the unmatched signals give a negative contribution on average (definitely non-positive due to the Alberta coding), and hence distinguishing the (positive) autocorrelation peak of the matched sequence is no longer simple.

Khaleghi and Kavehrad [1996] endeavour to overcome the restriction of needing to use balanced codes because of the offset term in Equation 2.3, which otherwise results in a DC level in the detected signal that is dependent upon the received power from each user. This is done by adjusting the splitting ratio of the coupler immediately preceding the separate correlations with $\boldsymbol{B}$ and $\bar{\boldsymbol{B}}$ in the receiver. The receiver correlation consists of direct on-off keying and balanced photodetection, as per [O'Farrell and Lochmann 1995]. Khaleghi and Kavehrad show that it is possible to choose a fixed splitting ratio, according to the sum of the receiver code, so as to greatly reduce the DC component in the received signal, and the consequent increase in multiple-access interference (MAI) is tolerable. In this manner, any bipolar code set can be used directly, with similar MAI characteristics to fully bipolar systems.

The proposal by Nguyen *et al.* [1995] differs from the previous systems in that the complementary amplitude coding is implemented in the frequency domain. Hence, the sequences $\boldsymbol{A}$ and $\bar{\boldsymbol{A}}$ determine the on-off filtering of the wavelength bands across a broad-spectrum incoherent source. At the receiver, each wavelength band is directed to one or other of the balanced photodiodes according to the receiver code $\boldsymbol{b}$. This proposal is an extension to the works of Zaccarin and Kavehrad that are analysed in detail in Chapter 3, and in which complementary keying in the manner of Figure 2.5 and [Nguyen *et al.* 1995] is considered. Nguyen *et al.* introduce a method to implement the high-rate keying between complementary spectral-amplitude codes $\boldsymbol{A}$ and $\bar{\boldsymbol{A}}$ that was noted as desirable, but dismissed as beyond current technological

limits in the configuration of [Kavehrad and Zaccarin 1995]. Nguyen *et al.* satisfy the requirement for balanced codes by generating balanced codes of twice the length of any unbalanced bipolar code. This is simply accomplished by concatenating the original bipolar code and its negative, which is equivalent to the concatenation of the unipolar code and its complement. Their analysis, however, merely considers the effect of shot noise on the theoretical system performance, and as shown in Chapter 3, this is not the dominant limitation for such systems. Hence, Nguyen *et al.* erroneously conclude that their system can be more bandwidth-efficient than a WDMA system using the same apparatus.

As an alternative to code balancing by concatenation of any unipolar sequence with its complement, such a unipolar sequence can be balanced by element-wise complementation, which has the form of Manchester encoding. In schemes using this encoding, each $+1$ of the original bipolar code may be represented by $[1, 0]$ and each -1 by $[0, 1]$, where [1] represents the transmission of a light pulse, and [0] represents the absence of a pulse. Both arrangements achieve balanced unipolar codes from any (especially unbalanced) bipolar code by the doubling of the code length, but the Manchester coding ensures the correlation properties of the resulting codes are very similar to that of the original bipolar code. If this Manchester encoding is performed but the sequences remain bipolar, then it is simple to show that the correlation levels at each even shift of the Manchester-encoded sequences correspond exactly to those of the original bipolar sequence. It can also be simply shown that the correlation levels at each odd shift of the Manchester-encoded sequences are given by the average of the two adjacent even-shift levels, but with opposite polarity, and these properties arise in their unipolar representations also [Tančevski *et al.* 1994]. The unipolar codes arising from such Manchester encoding of complementary Golay codes have been termed optical unipolar Golay codes [Wallace *et al.* 1995]. Simple concatenation or other appropriate arrangements of the complementary sequences can be used in schemes such as [Nguyen *et al.* 1995], without considering the modified correlation sidelobes, since the spectral code sequences always remain in phase.

The scheme of [Zaccarin and Kavehrad 1994b] uses Manchester encoding of short bipolar sequences, namely Barker codes or short m-sequences, along with an outer bipolar spreading sequence. In the form of Figure 2.5, the short Manchester-encoded sequences are produced by complementary fibre delay-lines, and matching delay-lines and a balanced photodiode pair are used for their correlation detection. The outer bipolar sequence is simply implemented electronically, and it may be used to provide all of the user-discrimination. In this case, each user can have the same short delay-lines, the losses and cost of which can then be kept to a minimum [Zaccarin and Kavehrad 1994b]. By using a single Barker code or m-sequence for the inner bipolar code, the autocorrelation sidelobes are either zero or they have unity magnitude for each even shift of the corresponding Manchester-encoded sequence, since these correspond to the autocorrelation of the bipolar code. Since the correlation sidelobes at each odd shift are given by the average of the two adjacent even-shift levels, but with opposite polarity [Tančevski *et al.* 1994], the two sidelobes adjacent to the autocorrelation peak always have approximately half the peak magnitude, but with opposite polarity to the peak, and the

other odd-shift sidelobes are either zero or of unity magnitude[3].

The proposal of [Andonovic *et al.* 1994] uses directional coupler switches to build a programmable incoherent correlator architecture. It is shown that for their correlator architecture, Manchester encoding of the signature sequences is required, but they use an extra empty pulse spacing, so each element of the bipolar sequence is represented by pulse sequences of either [0,1,0] or [1,0,0], according to the element polarity. Hence, the code lengths are 50% longer than those with Manchester encoding as described earlier. However, it is possible to slightly modify their correlator structure so that only this Manchester encoding is necessary, while retaining the same correlator function and programmability (Appendix E). Their correlator structure is designed to route a proportion of the light power corresponding to each agreement between the transmitted code and the receiver code to one photodiode. The same proportion of the power corresponding to each disagreement between the transmitted code and the receiver code is routed to the other photodiode. The correlator delays assure that these quantities of light are incident on the balanced photodiodes during the same pulse time, and hence the photocurrent in that interval corresponds to the difference in these two power levels. In this manner, the bipolar correlation with the receiver code is achieved. It is not, however, simple to determine from the correlator the correct pulse time in which the desired correlation level is present. Hence, some external method of synchronisation is necessary for this system.

2.9.4 Complementary Keying and Single-Ended Detection

Here the OCDMA schemes of [Neusy and Kavehrad 1990] and [Tančevski *et al.* 1994] are considered, and unlike the schemes discussed in Section 2.9.3, both of these use single-ended detection schemes, but this is detrimental to performance in general.

The work of [Neusy and Kavehrad 1990] proposes two OCDMA configurations based upon an optical device which performs the logical exclusive-or (XOR) operation. The first configuration assumes both unipolar data and a unipolar spreading sequence, and it uses a nonlinear optical XOR gate to generate time-domain pulse sequences from these. The XOR function is achieved through the use of high power levels, at which the intensity dependence of the refractive index of the medium is sufficient to change the phase matching within an interferometer. In this manner, keying between complementary incoherent pulse sequences is achieved, corresponding to the transmitter of Figure 2.5. Assuming that optical representations of the unipolar spreading sequence and the actual data are available, then the optical XOR gate allows data modulation at rates unconstrained by electronic bandwidths. At the receiver, an XOR operation between the received pulse stream and the unipolar receiver code is performed, and the result detected. As noted by Neusy and Kavehrad, the high power levels necessary for the function of the XOR gate necessitate significant optical amplification in this system. Comparison with Figure 2.5 shows that their transmitter has the same form, but their receiver

[3]The Barker code of length 4 has autocorrelation sidelobes of zero, and hence the only non-zero autocorrelation sidelobes for the Manchester-encoded version of this code are the sidelobes adjacent to the peak.

structure only performs the correlation with $\boldsymbol{B}$, and it does not perform the correlation with $\bar{\boldsymbol{B}}$. Using the notation of Equation 2.3, this is equivalent to the correlation of two unipolar sequences $\boldsymbol{A} \cdot \boldsymbol{B}$, which, as shown in Equation 2.5, is equal to a scaled version of the bipolar correlation $\boldsymbol{a} \cdot \boldsymbol{b}$, along with three offset terms.

$$\boldsymbol{A} \cdot \boldsymbol{B} = \sum_i A_i B_i = \sum_i \frac{1-a_i}{2}\frac{1-b_i}{2} = \frac{1}{4}\left[\boldsymbol{a} \cdot \boldsymbol{b} + \sum_i 1 - \sum_i a_i - \sum_i b_i\right] \tag{2.5}$$

The constant offset and that due to the sum of the receiver code result in DC levels in the detector current that depend upon the received power and the known level of receiver code imbalance. There is also an offset term that depends upon the sum of the transmitted bipolar code, and this represents the difference in signal level due to code imbalance. Even if balanced codes are used, there is still a non-zero offset in the detected signal which depends upon the received power. Another point of note is that the transmitted light power is only used when the data bit is 'one' and $\bar{\boldsymbol{A}}$ is transmitted (rather than $\boldsymbol{A}$ due to the inversion of the XOR function), since for a bit 'zero', $\boldsymbol{A}$ is transmitted, but the correlation with the matched sequence $\boldsymbol{B} = \boldsymbol{A}$ then gives zero since both XOR inputs are equal. The fact that none of these matters are even alluded to in [Neusy and Kavehrad 1990] is a serious shortcoming of this work. However, it does appear possible that the receiver XOR gate in this proposal could be modified simply to provide the correlations with both $\boldsymbol{B}$ and $\bar{\boldsymbol{B}}$ simultaneously, and hence with balanced detection, such a system would have the structure of Figure 2.5, and could thus be categorised with the schemes of Section 2.9.3.

The second configuration proposed in [Neusy and Kavehrad 1990] uses their XOR gate to generate a complementary-keyed pulse sequence as before, and then cross phase modulation is used to effectively generate a direct-sequence, binary phase-shift-keyed (DS-BPSK) light signal, and the potential of this is discussed in Section 2.5. Here the deficiencies of this work are noted, and these are primarily related to the use of a coherent detection system with a local oscillator at the receiver. The deficiencies with the treatment of this scheme in [Neusy and Kavehrad 1990] are that no attention has been paid neither to the coherence or otherwise of the light sources, nor to any restrictions on their relative wavelengths, nor to the 3 dB SNR advantage of balanced detection, nor to the necessity of a narrowband RF filter to complete the despreading. The need for phase-matching of the local-oscillator light source to that of the desired transmitter is touched upon, but the practical difficulties of this are not addressed, and neither is the manner in which synchronisation between the transmitter and receiver code sequences is achieved. Consequently, although there are some novel ideas in the work of [Neusy and Kavehrad 1990], crucial aspects of the function of both of their proposed configurations have not been addressed.

Following the work of [Andonovic *et al.* 1994] considered in Section 2.9.3, this group then presented the work of [Tančevski *et al.* 1994]. In this paper, a scheme is presented which is also based upon Manchester encoding, but unlike the scheme of [Andonovic *et al.* 1994],

it does not require such a complicated receiver, nor the external synchronisation, and nor the extra [0] between each Manchester-encoded chip. In [Tančevski *et al.* 1994], the transmitted signals consist of unipolar Manchester-encoded versions of bipolar sequences, and hence they are twice as long as the bipolar sequences. These unipolar sequences can be generated by an incoherent optical delay-line, and the receiver consists of a similar incoherent delay-line, which is matched to the Manchester-encoded unipolar version of the receiver code. Their receiver thus only performs the correlation with $\boldsymbol{B}$ in Figure 2.5, and not the correlation with $\bar{\boldsymbol{B}}$, and hence the correlation described by Equation 2.5 for the first scheme from [Neusy and Kavehrad 1990] also applies here. However, since balanced codes are assured via the Manchester encoding, the only non-zero offset remaining in Equation 2.5 is the first one, of value $\frac{N}{4}$, where N is the code length, and the actual offset depends upon the received power level in practice. Tančevski *et al.* [1994] do recognise that this offset occurs, and they propose that a balanced detection system is used, whereby the opposite branch has incident power of exactly this offset level at the appropriate time, thus cancelling it out, but they do not describe how to achieve this. However, if the parallel correlation with $\bar{\boldsymbol{B}}$ indicated in Figure 2.5 were to be implemented in the same manner as that with $\boldsymbol{B}$ in this scheme, then this would not only provide the desired offset exactly, but it would double the signal level also. The resulting system would then have identical structure to that of the inner coding system of [Zaccarin and Kavehrad 1994b] (Section 2.9.3).

Tančevski *et al.* [1994] show that in every even time-shift, the output level of the balanced receiver corresponds to that of the correlation of the bipolar codes, and that in every odd shift, the output level magnitude is given by the average of the two adjacent even-shift output levels. Hence, the correlation sidelobes of the Manchester-encoded unipolar sequences are no worse, on average, than that of the bipolar codes on which they are based. As noted in Section 2.9.3, however, the two adjacent sidelobes to the peak have approximately half its magnitude, and both have opposite polarity to the peak. Two possible reconfigurable delay-line architectures are also presented in [Tančevski *et al.* 1994], but this work does not consider the necessity of a time-gate of some form for the selection of the single pulse interval at which the correlation peak occurs.

2.10 SUMMARY

In this chapter the OCDMA research field has been reviewed, and the structure and characteristics of the main categories of OCDMA systems have been described. The earliest OCDMA systems merely used optical means to transmit electrically-encoded CDMA signals, and hence were limited by the electrical encoding. Optical coding methods are thus necessary to exploit the available fibre bandwidth, and such OCDMA systems can be broadly categorised on the basis of whether the optical coding is incoherent or coherent. Most of the incoherent schemes are based upon unipolar code sequences, but compared to the bipolar sequences used in radio CDMA, such unipolar codes tend to have poor duty cycles and correlation properties, and the

number of such codes is also limited, although trade-offs amongst these are possible. Coherent OCDMA schemes can use bipolar sequences exactly as in radio CDMA schemes, but direct electro-optic phase modulation is limited to a few tens of gigahertz at most, so the available optical bandwidth cannot be fully utilised in this manner alone. An alternative coherent OCDMA system using bipolar spectral-phase modulation has been investigated and demonstrated, but the critical coherent matching and dispersion compensation necessary for each path in this system are unattractive. The use of coherently-matched lattice coders to encode and coherently decode pulse sequences has been demonstrated, and such systems appear much more attractive than their incoherent counterparts. Another optical encoding scheme is that of coherence multiplexing, and the system demonstrations and performance measurements using this OCDMA-like technique have been more practical and attractive than any OCDMA demonstration to date. There has also been another group of proposals which, while performing the optical coding in an incoherent manner, have endeavoured to utilise the structure and hence the correlation properties of bipolar codes, since these are much better than that of typical unipolar codes. The structure of each of these schemes has been described, and the unipolar manners in which they implement bipolar code structures have been explained. One of these schemes is analysed in detail in Chapter 3, with related material in subsequent chapters, and the common characteristics of all these schemes and their consequences are treated together in Chapter 7.

Chapter 3

SPECTRAL-AMPLITUDE OCDMA

3.1 INTRODUCTION

In this chapter the performance of an OCDMA system based upon spectral-amplitude coding is analysed. The system structure is based upon the proposal of [Zaccarin and Kavehrad 1993], but the analyses therein and in their subsequent works ignore source intensity noise and the intensity noise arising from the interference between light fields from different users. In contrast, the analysis presented in this chapter focuses primarily on these effects. It is shown that intensity noise alone limits the system performance to a level significantly below the estimates reported in [Zaccarin and Kavehrad 1993] and [Kavehrad and Zaccarin 1995].

In Sections 3.2 and 3.3 thermal source intensity noise and the interference of independent light fields are reviewed and quantified. The system configuration is described in Section 3.4, and Section 3.5 contains the analysis of this idealised spectral-amplitude OCDMA system, concentrating in particular upon the effects detailed in Sections 3.2 and 3.3. This analysis shows that the interference between incoherent fields leads to an SNR limit that is significantly lower than that of a wavelength-division system using the same spectral range and divisions. The SNR dependence of spectral-amplitude OCDMA is shown to be similar to that found for sub-carrier-multiplexed (SCM) systems and coherence-multiplexed systems, and this is because the dominant noise or interference arises in precisely the same manner. In Section 3.5.3 the dominant noise statistics are examined, and for reasonable system parameters a Gaussian approximation is shown to be sufficiently accurate to permit realistic error-rate estimates. The signalling system in the original spectral-amplitude OCDMA proposal is considered in Section 3.5.4 under various possible conditions, assuming Gaussian noise, thus allowing direct comparison between the original performance estimates and the limits derived here. Many of the performance comparisons are presented in Section 3.5.5, and in Section 3.6 a discussion of a number of important practical issues is included. The work of this chapter is then summarised in Section 3.7.

3.2 THERMAL SOURCE INTENSITY NOISE

Broadband thermal sources may be used in wavelength-division and code-division multiple-access systems, and the amplified spontaneous emission (ASE) from optical amplifiers also has thermal properties.

A thermal source contains large numbers of electrons or other entities in excited states, which randomly and independently drop to lower energy states by emitting photons. This is termed spontaneous emission. Hence, the instantaneous intensity of the light from such a thermal source is actually a random process, very different from the near-constant-amplitude light from a stabilised single-mode laser. The characteristics of such thermal light are well known, and the appropriate descriptions are presented here.

3.2.1 Noise Distribution

A standard single-mode fibre (SMF) actually supports two modes, these being modes of orthogonal polarisation. Apart from this, however, it is assumed that the light incident upon a photodetector at the end of SMF is fully spatially coherent. Under this assumption, using W to represent the time-integrated light intensity, over time T, from a polarised thermal source, the probability density function $p_W(W)$ is closely approximated by a Gamma probability density function, given by [Goodman 1985]

$$p_W(W) = \begin{cases} \dfrac{\left(\frac{\mathcal{M}}{\overline{W}}\right)^{\mathcal{M}} W^{\mathcal{M}-1} \exp\left(-\mathcal{M}\frac{W}{\overline{W}}\right)}{\Gamma(\mathcal{M})}, & W \geq 0 \\ 0 & \text{otherwise} \end{cases} \tag{3.1}$$

where $\overline{W}$ is the mean integrated intensity, $\Gamma(\mathcal{M})$ is a gamma function of argument $\mathcal{M}$, and $\mathcal{M}$ is given by

$$\mathcal{M} = \left[\frac{1}{T}\int_{-\infty}^{\infty} \Lambda\left(\frac{\tau}{T}\right) |\gamma(\tau)|^2 \mathrm{d}\tau\right]^{-1} \tag{3.2}$$

In Equation 3.2,

$$\Lambda(x) = \begin{cases} 1 - |x|, & |x| \leq 1 \\ 0 & \text{otherwise} \end{cases} \tag{3.3}$$

and $\gamma(\tau)$ is the complex degree of coherence of the light, given by

$$\gamma(\tau) = \int_0^{\infty} \hat{G}(\nu) e^{j2\pi\nu\tau} \mathrm{d}\nu \tag{3.4}$$

where ν is optical frequency and $\hat{G}(\nu)$ is the one-sided normalised power spectral density (PSD) of the light. The variable $\mathcal{M}$ is the temporal degree of freedom, which is closely related

to the coherence time of the light τ_c, which is defined as [Goodman 1985]

$$\tau_c = \int_{-\infty}^{\infty} |\gamma(\tau)|^2 d\tau = \int_0^{\infty} [\hat{G}(\nu)]^2 d\nu \tag{3.5}$$

where the second equality follows from the fact that $\gamma(\tau)$ and $\hat{G}(\nu)$ are a Fourier-transform pair. For the case when $T \ll \tau_c$, the temporal degree of freedom $\mathcal{M} \approx 1$, and for $T \gg \tau_c$, $\mathcal{M} \approx T/\tau_c$, and hence $\mathcal{M}$ can be interpreted as the number of coherence 'cells' of the light wave that influence the measurement over time T. When light is incident upon a semiconductor-based photodetector, the energy of each photon may generate an electron-hole pair within a depletion region. The electric field within this region causes such pairs to separate, usually travelling to the region boundaries, and this current is detected. The quantum efficiency η is the ratio of how often this happens on average compared to the number of incident photons. The term photoevent is used here to represent an incidence of a photon that excites an electron-hole pair which contributes to the photocurrent. The photon arrival statistics are Poisson, conditioned upon the light intensity. When the light intensity is not constant, as for a thermal source, the unconditional photoevent distribution can be evaluated using Mandel's formula as follows [Goodman 1985]

$$p(X) = \int_0^{\infty} \frac{(\alpha W)^X}{X!} e^{-\alpha W} p_W(W) dW \tag{3.6}$$

where X is the number of photoevents in the time interval T, $\overline{X}$ is the mean number of photoevents, and $\overline{X} = \alpha \overline{W}$. The constant α is given by $\alpha = \frac{\eta}{h\nu}$, where h is Planck's constant. For a thermal source, the intensity fluctuates according to Equation 3.1, and substituting this in Equation 3.6, it is found that

$$\begin{aligned} p(X) &= \int_0^{\infty} \left[\frac{(\alpha W)^X}{X!} e^{-\alpha W}\right] \frac{\left(\frac{\mathcal{M}}{\overline{W}}\right)^{\mathcal{M}} W^{\mathcal{M}-1} \exp\left(-\mathcal{M}\frac{W}{\overline{W}}\right)}{\Gamma(\mathcal{M})} dW \\ &= \frac{\Gamma(X+\mathcal{M})}{\Gamma(X+1)\Gamma(\mathcal{M})} \left[1+\frac{\mathcal{M}}{\overline{X}}\right]^{-X} \left[1+\frac{\overline{X}}{\mathcal{M}}\right]^{-\mathcal{M}} \end{aligned} \tag{3.7}$$

The distribution in Equation 3.7 is known as negative binomial, and this has been found to quite accurately match actual measurements [Goodman 1985]. For completely unpolarised light, Equation 3.7 applies but with degree of freedom $2\mathcal{M}$ rather than $\mathcal{M}$. For partially polarised light, the photoevent distribution is given by a convolution of two such negative binomial distributions, however, it is sufficient for the purposes here to consider either fully polarised or completely unpolarised light. It should also be noted that both the gamma distribution of Equation 3.1 and the negative binomial distribution of Equation 3.7 are asymptotically Gaussian as the degree of freedom $\mathcal{M}$ tends to infinity.

3.2.2 Photocurrent Variance

If the average number of photoevents in a photodetector during an interval T is denoted $\overline{X}$, and this light is from a thermal source with degree of polarisation P, then the variance of the photocount fluctuations is given by [Goodman 1985]

$$\sigma_X^2 = \overline{X} + \frac{(1+P^2)\overline{X}^2}{2\mathcal{M}} \tag{3.8}$$

where $\mathcal{M}$ is the parameter defined in Equation 3.2. When the measurement interval T is much greater than the coherence time τ_c, or equivalently, when the optical bandwidth is much larger than the detector bandwidth, $\mathcal{M} \approx T/\tau_c$, and so

$$\sigma_X^2 = \overline{X} + \frac{(1+P^2)\overline{X}^2\tau_c}{2T} \tag{3.9}$$

Assuming that the optical bandwidth greatly exceeds the electrical bandwidth results in a theoretical receiver noise spectrum that also greatly exceeds the actual receiver bandwidth (a more general case of this is detailed in Section 3.3). Hence, the noise PSD is sufficiently wide that it can be considered flat over the receiver bandwidth. Using the facts that the noise-equivalent bandwidth B_e of an ideal integrator operating over time T is given by $B_e = \frac{1}{2T}$, and that the average current over the interval T is given by $I = e\overline{X}/T$, where e is the electronic constant, the photocurrent variance then becomes

$$\sigma_I^2 = \frac{e^2\sigma_X^2}{T^2} = 2eIB_e + (1+P^2)I^2\tau_c B_e \tag{3.10}$$

This equation is in agreement with that given in [Morkel *et al.* 1990] for the unpolarised case ($P = 0$), where the optical bandwidth is defined as the reciprocal of the coherence time τ_c. The first term of Equation 3.10 is the usual shot noise component, whereas the second term expresses the increased variation due to the intensity fluctuations of the source, and is sometimes referred to as the excess noise term. It is also common to express the mean photocurrent in the form $I = RP_r$, where P_r is the average incident optical power, and R is the photodiode responsivity, which is given by $R = \frac{e\eta}{h\nu}$.

Analysis by Taylor [1990] indicates that the intensity noise of superluminescent diode (SLD) sources may be less than that of an ideal thermal source, according to the value of the source spontaneous-emission factor K_{sp}, giving the modified noise variance

$$\sigma_I^2 = 2eIB_e + \frac{(1+P^2)I^2\tau_c B_e}{K_{sp}} \tag{3.11}$$

For such sources that are purely index-guided within the active region, a value of $K_{sp} = 1$ is predicted, so that Equations 3.10 and 3.11 are equal. Gain-guided SLDs may have $K_{sp} > 1$, and consequently Equation 3.11 must be used in this case. Measured K_{sp} values for SLDs are

predominantly between 1 and 2, although a value as high as $K_{sp} = 7.6$ has been reported [Lee and Taylor 1991]. External feedforward compensation of source intensity noise is also possible to some extent [Keating and Sampson 1997]. Rare-earth-doped fibre amplifiers produce amplified spontaneous emission (ASE) in a similar manner to SLDs, and they are index-guided single-mode devices. Hence, their noise characteristics should behave according to Equation 3.10, and this has been experimentally demonstrated [Morkel *et al.* 1990, Burns *et al.* 1990]. Unless otherwise stated, all sources in the following are assumed to be ideally thermal, so effectively $K_{sp} = 1$, and Equation 3.10 applies directly.

3.3 INTERFERENCE BETWEEN INCOHERENT SOURCES

When two or more incoherent light fields are mixed and incident upon a photodetector, the phase noise of the fields causes an intensity-noise term in the photodetector output, termed phase-induced intensity noise (PIIN) [Griffin *et al.* 1995]. The level of this PIIN is found in the following manner.

If two statistically independent, zero-mean stationary random processes $x_1(t)$ and $x_2(t)$ are input to a square-law device, giving output $y(t) = a(x_1(t) + x_2(t))^2$, with a constant, then the double-sided PSD of $y(t)$ contains the component [Davenport Jr and Root 1958]

$$\tilde{G}_{1\times2}(\nu) = 4a^2 \int_{-\infty}^{\infty} \tilde{G}_1(\nu')\tilde{G}_2(\nu - \nu')\mathrm{d}\nu' \tag{3.12}$$

where $\tilde{G}_1(\nu)$ and $\tilde{G}_2(\nu)$ are the double-sided PSDs of processes $x_1(t)$ and $x_2(t)$. Equation 3.12 represents the PSD component of $y(t)$ due to the interaction of process $x_1(t)$ with $x_2(t)$, and the other PSD components, those purely at $\nu = 0$ and those due to the interaction of each process with itself, are not represented here. Equation 3.12 shows that the square-law output PSD due to the interaction of the two independent processes is simply given by the convolution of the PSDs of these processes.

Applying this result to the case of two statistically-independent identically-polarised light fields, that are spatially coherent and incident together upon a photodetector, then $x_1(t)$ and $x_2(t)$ simply correspond to the zero-mean optical fields, a represents the photodiode responsivity R, and $y(t)$ represents the photocurrent. Equation 3.12 then represents the PSD of the photocurrent noise due solely to the mixing of the two fields, but it ignores the finite electrical bandwidth of the detector. If each optical field has the same PSD $\tilde{G}(\nu)$, then the spectral width of the components of $\tilde{G}_{1\times2}(\nu)$ in the vicinity of $\nu = 0$ is approximately twice the optical bandwidth of the fields. Under the assumption that the optical bandwidth is significantly larger than the detector electrical bandwidth, then this PIIN PSD extends far beyond the detector bandwidth, and it can be considered approximately constant at the $\nu = 0$ level across the whole detector bandwidth. Since double-sided PSDs are symmetrical about $\nu = 0$, the photocurrent

noise PSD at $\nu = 0$ is then expressed as

$$\tilde{G}_I(0) = 4R^2 \int_{-\infty}^{\infty} \left[\tilde{G}(\nu')\right]^2 \mathrm{d}\nu' \tag{3.13}$$

Converting from the single-sided normalised PSD of Equation 3.5 to a double-sided PSD $\tilde{G}(\nu)$ of power $P_{\tilde{G}}$, Equation 3.5 becomes

$$\tau_\mathrm{c} = \frac{2}{P_{\tilde{G}}^2} \int_{-\infty}^{\infty} \left[\tilde{G}(\nu)\right]^2 \mathrm{d}\nu \tag{3.14}$$

With two sources of the same PSD being incident on the photodetector, $P_{\tilde{G}}$ is simply equal to half the total incident optical power P_r. Hence, Equation 3.13 becomes

$$\tilde{G}_I(0) = \frac{R^2 P_\mathrm{r}^2 \tau_\mathrm{c}}{2} \tag{3.15}$$

Assuming that the PSD is approximately flat across the double-sided detector bandwidth $2B_\mathrm{e}$, and expressing the mean photocurrent as $I = RP_\mathrm{r}$, the photocurrent noise variance due to the mixing fields is then

$$\sigma_I^2 \approx 2B_\mathrm{e}\tilde{G}_I(0) = I^2 \tau_\mathrm{c} B_\mathrm{e} \tag{3.16}$$

If the two sources have polarisation degree P, but are not otherwise changed, then the PIIN term resulting from the mixing of the fields is given by Equation 3.16 with the extra multiplicative factor $\frac{1+P^2}{2}$.

The noise power of Equation 3.16 corresponds to that found by Moslehi [1986] for the detection of laser light that has passed through a power-balanced interferometer with a delay significantly greater than the laser coherence time, where the laser linewidth is much larger than the receiver bandwidth. In this case the two optical fields being mixed in the interferometer have the same PSD but can be considered independent, and negligible laser intensity noise is assumed, so that only the phase-induced intensity noise of Equation 3.16 is found.

Each of the two light fields that mix to give the PIIN of Equation 3.16 generate mean photocurrents of $I/2$, and if they were thermal, then using Equation 3.10, they would each cause a photocurrent variance of $eIB_\mathrm{e} + I^2\tau_\mathrm{c}B_\mathrm{e}/2$. Since the intensity noise of each source is independent of the PIIN from their mixing, the variances due to each source intensity noise and the PIIN term of Equation 3.16 can be added, giving a total of $\sigma_I^2 = 2eIB_\mathrm{e} + 2I^2\tau_\mathrm{c}B_\mathrm{e}$, which is exactly as expected for a single such thermal source generating a photocurrent I. From this it can be seen that the PIIN generated by two independent light fields has the same power as that from two incoherent thermal sources.

If the fields from many similar incoherent sources are mixed at a photodetector, then the PIIN power matches that of thermal sources. The intensity noise from individual sources may of course be non-thermal, but the PIIN dominates for many similar sources. Hence, as the

number of sources increases, the noise power rapidly approaches that of a thermal source with the same total power. Consequently, even with SLD sources having a high K_{sp} value, or sources with significant intensity-noise suppression in some other manner, the noise generated by the interference of the light from many such sources has approximately the same power as from a thermal source. However, the noise distribution is not necessarily that from a thermal source until the number of sources tends to infinity.

3.4 SPECTRAL-AMPLITUDE OCDMA DESCRIPTION

The ideal spectral-amplitude OCDMA system is shown in Figure 3.1, following the structure of the proposal in [Zaccarin and Kavehrad 1993]. Each user spectrally encodes the light from a broadband source with its data, and this is distributed to every receiver via a star coupler. Note that only one transmitter and one receiver are shown in Figure 3.1. The transmitted spectrum is divided into N rectangular slices, and this is amplitude masked according to the user's code. Ideal complementary keying is initially assumed, using codes based upon Hadamard matrices, in accordance with the further work of [Kavehrad and Zaccarin 1995].

Using complementary keying, the source spectrum is encoded either with the user code or its complement, according to the binary data to be transmitted. As indicated in Figure 3.1, when the transmitter code matches that of the receiver, all the light from this transmitter is incident upon either photodiode D_1 or D_2, according to whether the user code or its complement has been transmitted. In this manner, either a positive or negative signal appears at the output of the balanced receiver, providing bipolar signalling. The orthogonality properties of Hadamard

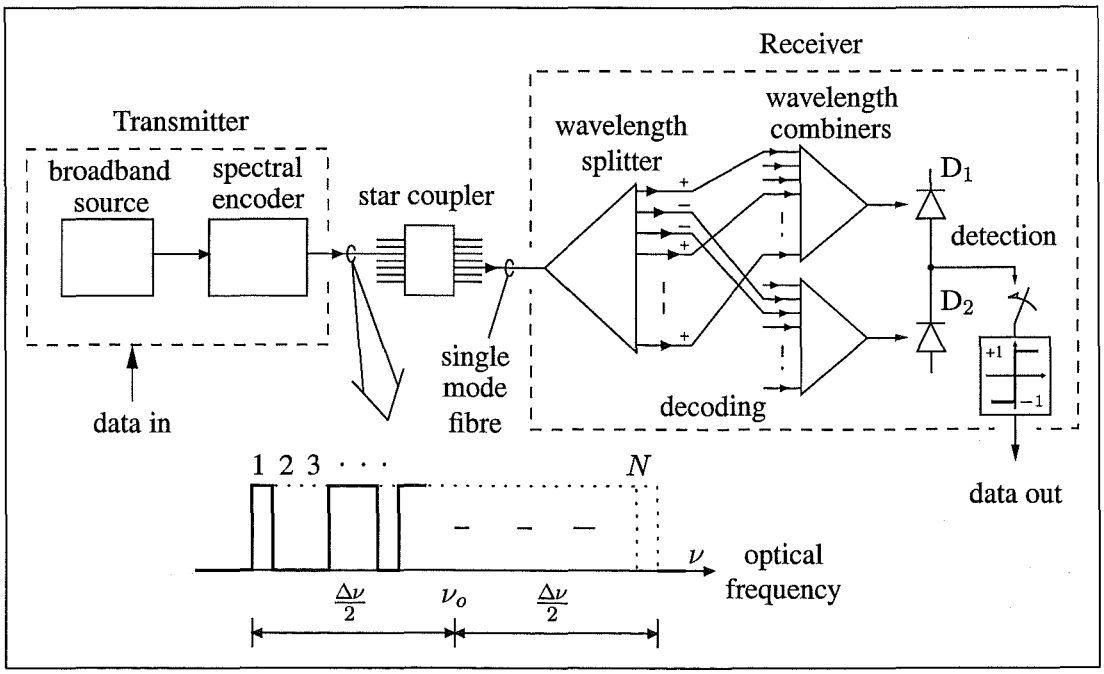

Figure 3.1 Ideal Spectral-Amplitude OCDMA System

codes ensure that light from any user whose code does not match is split equally between D_1 and D_2, giving ideally no signal. In practice, complementary keying could be achieved at high bit rates by having two spectral encoders and sources, which are on-off keyed in complement [Nguyen *et al.* 1995], although a 3dB power loss would be incurred.

A simpler keying arrangement is possible by having the spectral code fixed, and merely on-off keying the source [Zaccarin and Kavehrad 1993]. Any user transmitting using a different code ideally produces no signal at the receiver as before, but the signal from the desired user is now only unipolar.

The system portrayed in Figure 3.1 is considered ideal due to the following best case assumptions, which are made in order to obtain an upper bound on the system performance. Each source is assumed to have a spectrum that is ideally flat over the bandwidth range $\Delta\nu$ used by the system. Ideal rectangular spectral filtering (amplitude masking) of the source light into the desired amplitude code at each transmitter is assumed. The wavelength division and recombination in each receiver is also assumed to be ideally rectangular, and exactly matched to every other receiver and to the transmitters. Unpolarised sources are assumed, and each user is considered to have equal power at the receivers. The ideal receiver in Figure 3.1 detects all of the received light, whereas the configuration in [Zaccarin and Kavehrad 1993] performs the same function, but at the expense of half the optical power.

Note that incoherent light from every user is combined into the same single-mode fibre before incidence upon the receiver photodiodes, and the light covers the same spectral range, so the interference between this light must be considered.

3.5 ANALYSIS OF SPECTRAL-AMPLITUDE OCDMA

In this section the spectral-amplitude OCDMA system of Figure 3.1 is analysed in order to determine the performance limits due to intensity noise. The case of complementary keying is initially considered, and then the OOK arrangement originally proposed is treated, allowing direct comparison with the original performance estimates. It is shown that the assumption of Gaussian noise statistics is justified for reasonable system parameters, and hence most of the performance comparisons later in this section are based upon Gaussian noise distributions.

3.5.1 Complementary Keying

An $N \times N$ normalised Hadamard matrix, in ± 1 form, is denoted $\boldsymbol{H}$, where N is the number of slices the available optical spectrum is divided into (illustrated in Figure 3.1). The kth row of $\boldsymbol{H}$ is expressed as $\boldsymbol{h}_k$, whose ith element is written as $h_k(i)$. The unipolar sequences used to code the spectral amplitude of the sources are expressed as $\boldsymbol{c}_k$. These sequences correspond to the rows of $\boldsymbol{H}$, and they are complemented according to the transmitted data, hence

$$c_k(i) = \frac{1 - d_k h_k(i)}{2} \qquad i = 1, 2, \ldots, N; \qquad k = 2, 3, \ldots, N, \tag{3.17}$$

where $d_k = \pm 1$ represents the binary data of the kth user. The case $k = 1$ has been excluded since the first row of the Hadamard matrix is all 'ones'. The set of K active users ($K \leq N-1$) is expressed as $\{m_1, m_2, \ldots, m_K\}$, corresponding to transmission using the spectral codes $\boldsymbol{c}_{m_1}, \ldots, \boldsymbol{c}_{m_K}$, where $m_k \epsilon \{2, 3, \ldots, N\}$, $k = 1, 2, \ldots, K$. Each unpolarised source PSD is ideally flat over the system bandwidth of $\nu_o \pm \frac{\Delta\nu}{2}$, with magnitude $\frac{P_r}{\Delta\nu}$, where P_r is the received power from a single source. Any excess losses in the receiver are assumed to be incorporated in P_r.

The orthogonality property $\boldsymbol{H}\boldsymbol{H}^T = N\boldsymbol{I}$, where $\boldsymbol{I}$ is the identity matrix, means that for any pair of distinct rows of $\boldsymbol{H}$, the number of elements in agreement is equal to the number in disagreement. This also holds for the unipolar representations of these rows, and their complements, and hence the following property is found, independent of d_k and d_l

$$\sum_{i=1}^{N} c_k(i)c_l(i) = \begin{cases} \frac{N}{2}, & k = l \\ \frac{N}{4}, & k \neq l \end{cases} \qquad k, l \epsilon \{2, 3, \ldots, N\} \tag{3.18}$$

Without loss of generality, the receiver is assumed to have masks corresponding to the code $\boldsymbol{h}_{m_1}$. Both bit synchronism and negligible dispersion are also assumed at this stage. This allows the PSDs at the photodiodes D_1 and D_2, during one bit period, to be expressed as

$$G_1(\nu) = \frac{P_r}{\Delta\nu} \sum_{k=1}^{K} \sum_{i=1}^{N} \frac{1 - h_{m_1}(i)}{2} c_{m_k}(i) \left\{ u\left[\nu - \nu_o - \tfrac{\Delta\nu}{2N}(-N + 2i - 2)\right] - u\left[\nu - \nu_o - \tfrac{\Delta\nu}{2N}(-N + 2i)\right] \right\} \tag{3.19}$$

and

$$G_2(\nu) = \frac{P_r}{\Delta\nu} \sum_{k=1}^{K} \sum_{i=1}^{N} \frac{1 + h_{m_1}(i)}{2} c_{m_k}(i) \left\{ u\left[\nu - \nu_o - \tfrac{\Delta\nu}{2N}(-N + 2i - 2)\right] - u\left[\nu - \nu_o - \tfrac{\Delta\nu}{2N}(-N + 2i)\right] \right\} \tag{3.20}$$

where $u[\nu]$ is the unit step function:

$$u[\nu] = \begin{cases} 0, & \nu < 0 \\ 1, & \nu \geq 0 \end{cases} \tag{3.21}$$

It is assumed that either each source is thermal, or that there are sufficient sources that their combination, via a single-mode star coupler and single-mode fibre (SMF), appears thermal. Hence, as in [Chu and Dickey 1991], it is assumed that the total single-mode output is equivalent to that of one thermal source, with a PSD equal to the sum of the PSDs from each of the users. Consequently, the receiver intensity noise is calculated directly on the basis of the total PSD at each photodiode.

Using Equations 3.18 and 3.19, the mean power incident on photodiode D_1 is given by

$$P_{G_1} = \int_0^\infty G_1(\nu)\mathrm{d}\nu = \frac{P_\mathrm{r}}{4}(K + d_{m_1}) \tag{3.22}$$

and also

$$\int_0^\infty [G_1(\nu)]^2\mathrm{d}\nu = \frac{P_\mathrm{r}^2}{N\Delta\nu}\sum_{i=1}^{N}\left\{\frac{1-h_{m_1}(i)}{2}\left[\sum_{k=1}^{K} c_{m_k}(i)\right]\left[\sum_{l=1}^{K} c_{m_l}(i)\right]\right\} \tag{3.23}$$

Similarly, for photodiode D_2, the mean incident power and mean squared power are given by

$$P_{G_2} = \int_0^\infty G_2(\nu)\mathrm{d}\nu = \frac{P_\mathrm{r}}{4}(K - d_{m_1}) \tag{3.24}$$

and

$$\int_0^\infty [G_2(\nu)]^2\mathrm{d}\nu = \frac{P_\mathrm{r}^2}{N\Delta\nu}\sum_{i=1}^{N}\left\{\frac{1+h_{m_1}(i)}{2}\left[\sum_{k=1}^{K} c_{m_k}(i)\right]\left[\sum_{l=1}^{K} c_{m_l}(i)\right]\right\} \tag{3.25}$$

Since the light incident on each photodiode is from complementary spectral regions, the intensity noise from each diode is independent. Using the second term in Equation 3.10, the sum of the intensity noise from the two photodiodes is then given by

$$\sigma_I^2 = B_\mathrm{e}(I_1^2\tau_{\mathrm{c}_1} + I_2^2\tau_{\mathrm{c}_2}) \tag{3.26}$$

where $I_1 = RP_{G_1}$ and $I_2 = RP_{G_2}$ are the photodiode currents, and τ_{c_1} and τ_{c_2} are the coherence times of the light incident on each photodiode. Normalising the PSDs and using Equation 3.5, it is found that

$$\begin{aligned}\sigma_I^2 &= B_\mathrm{e}I_1^2\frac{\int_0^\infty [G_1(\nu)]^2\mathrm{d}\nu}{P_{G_1}^2} + B_\mathrm{e}I_2^2\frac{\int_0^\infty [G_2(\nu)]^2\mathrm{d}\nu}{P_{G_2}^2} \\ &= B_\mathrm{e}R^2\left\{\int_0^\infty [G_1(\nu)]^2\mathrm{d}\nu + \int_0^\infty [G_2(\nu)]^2\mathrm{d}\nu\right\}\end{aligned}$$

where R is the photodiode responsivity. From Equations 3.23 and 3.25, this becomes

$$\begin{aligned}\sigma_I^2 &= \frac{B_\mathrm{e}R^2P_\mathrm{r}^2}{N\Delta\nu}\sum_{i=1}^{N}\left\{\left[\sum_{k=1}^{K} c_{m_k}(i)\right]\left[\sum_{l=1}^{K} c_{m_l}(i)\right]\right\} \\ &= \frac{B_\mathrm{e}R^2P_\mathrm{r}^2}{N\Delta\nu}\sum_{i=1}^{N}\left[\sum_{k=1}^{K}[c_{m_k}(i)]^2 + 2\sum_{k=1}^{K-1}\sum_{l=k+1}^{K} c_{m_k}(i)c_{m_l}(i)\right]\end{aligned}$$

where the first term is identified as the self-intensity noise contribution, and the second is seen to represent the PIIN from the interference between pairs of independent light fields. Using Equation 3.18, this becomes

$$\begin{aligned}\sigma_I^2 &= \frac{B_e R^2 P_r^2}{N\Delta\nu}\left[\frac{KN}{2} + \frac{K(K-1)N}{4}\right] \\ &= \frac{B_e R^2 P_r^2 K(K+1)}{4\Delta\nu}\end{aligned} \tag{3.27}$$

Note that since Equation 3.18 holds regardless of the polarity of the data of any active user, Equation 3.27 is independent of the data of all the active users. Hence, the timing of transitions in the users' data should not have a significant effect, so Equation 3.27 is considered to apply for a completely asynchronous system also.

The signal from the desired user is given by the difference of the photodiode currents

$$I_{\text{sig}} = I_1 - I_2 = \frac{RP_r d_{m_1}}{2} \tag{3.28}$$

Equations 3.27 and 3.28 give an SNR limit due to intensity noise of

$$\rho = \frac{I_{\text{sig}}^2}{\sigma_I^2} = \frac{\Delta\nu}{K(K+1)B_e} \tag{3.29}$$

This can be termed a high-power SNR limit since with sufficient signal power the intensity noise becomes the dominant limitation. Note that unlike most other CDMA systems, the SNR limit of Equation 3.29 does not depend upon the code length N. This is because the effective processing gain is given by the bandwidth ratio $\frac{\Delta\nu}{B_e}$, and N merely determines the number of available codes. In [Smith *et al.* 1995] the same spectral-amplitude coding was considered, but with a receiver based upon a single wavelength demultiplexer and an ideal photodiode array, under which the same SNR limit was determined. Hence, despite some claim to the contrary [Kavehrad 1995], there is no fundamental performance difference between these two receiver structures.

Using the relationship $B_e = \frac{1}{2T_{\text{bit}}}$ in the ideal case, where T_{bit} is the bit period, the total network capacity G is given by

$$G = K.\frac{1}{T_{\text{bit}}} = \frac{2\Delta\nu}{\rho_d(K+1)} \tag{3.30}$$

where ρ_d is the desired SNR. The total network capacity is seen to be approximately inversely proportional to the number of active users. Plotted in Figure 3.2 is the network capacity of Equation 3.30 for a range of optical bandwidths $\Delta\nu$, along with their equivalent widths in the 1550 nm region, and at the fixed value $\rho_d = 15.6$ dB, which corresponds to an error rate of 10^{-9} if the noise is Gaussian. Note that the smaller optical bandwidths in Figure 3.2 may represent narrower (and thus more realistic) spectral-slice profiles rather than a reduction in

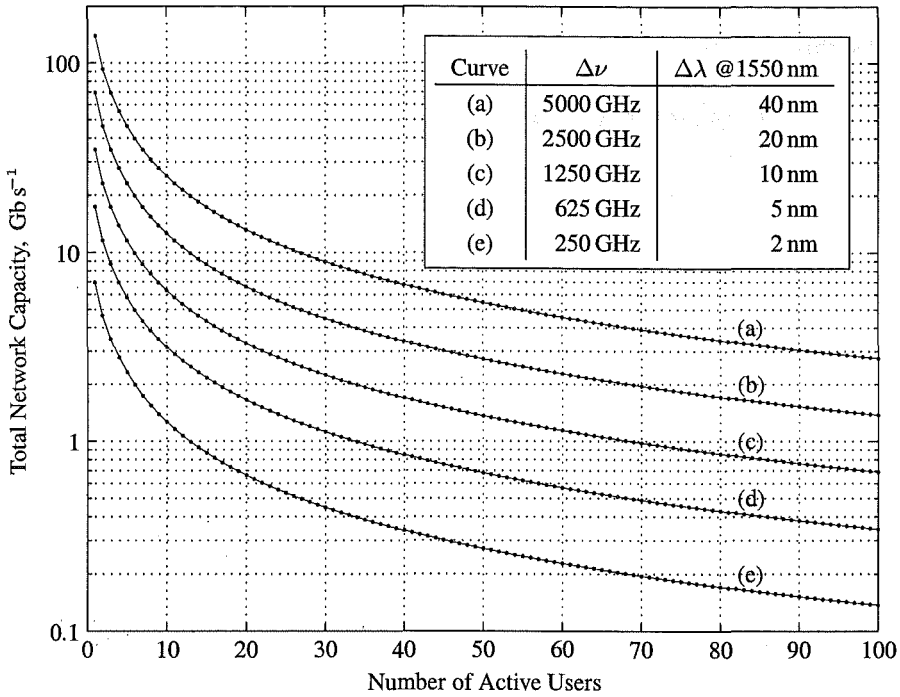

Figure 3.2 Total Network Capacity of Ideal Spectral-Amplitude OCDMA, $\rho_d = 15.6$ dB

the total range of all the spectral coding. This issue is discussed further in Section 3.6.3.

The general form of the capacity limit in Equation 3.30, being approximately inversely proportional to the number of active users, has also been found for sub-carrier-multiplexed (SCM) systems [Desem 1988] and coherence-multiplexed systems [Chu and Dickey 1991]. This similarity is because the limiting noise arises in the same manner. Each of these systems has spatially coherent light from every user incident together on the same receiver photodiode(s), which measures the incident optical intensity. Furthermore, each user has an independent light source, so there is no temporal coherence between fields, but they occupy the same optical bandwidth. As a consequence, the interference between each pair of spectrally similar independent fields causes intensity noise which is within the receiver bandwidth, and the corresponding photocurrent noise then has a power level proportional to approximately the square of the number of active users.

The analysis leading to Equations 3.29 and 3.30 assumed that the detected power from each spectral slice of each user was identical. Therefore, using orthogonal Hadamard codes, there is ideally no signal received from any unmatched user, so in this case the multiple-access interference (MAI) is ideally zero. This highlights the fact that these SNR and capacity limits are not related to MAI at all, unlike those of most radio CDMA systems. Since the dominant SNR limit arises here with ideally zero MAI, a multi-user detection structure (Section 1.4) cannot provide any performance improvement. The crucial difference is that the transmissions in a radio CDMA system are completely coherent, and can be exactly specified with knowledge

of the carrier frequency and phase, along with the actual data, whereas the optical phase from a thermal source is a random process. Hence, even complete knowledge of the data streams of all the unmatched users at best only determines the noise variance, or power level, but its actual value is still a random variable. In the case of complementary keying, the actual data of the unmatched users does not even affect the receiver noise level, since this depends merely upon the total number of active users.

3.5.2 Comparison with Spectrally-Sliced WDM

A spectrally-sliced WDM system simply allocates a single spectral slice of a broadband source to each user, and hence the receiver filter allows only the signal from the desired user to reach the photodetector. In this manner, there is no significant mixing between signals from independent sources, and the intensity noise of the signal itself is then the critical issue. Assuming spectrally-flat sources and ideal rectangular filtering, as in Section 3.5.1 for spectral-amplitude OCDMA, then each user has optical bandwidth $\frac{\Delta\nu}{N}$. If each source is thermal and unpolarised, then from Equations 3.10 and 3.5 the intensity noise inherent in the signal gives an SNR limit of

$$\rho = \frac{\Delta\nu}{NB_{\mathrm{e}}} \tag{3.31}$$

which is simply the ratio of the optical and electrical bandwidths. Since all N users can be active simultaneously, and using $B_{\mathrm{e}} = \frac{1}{2T_{\mathrm{bit}}}$, the total network capacity for this system at an SNR ρ_{d} is simply

$$G = \frac{2\Delta\nu}{\rho_{\mathrm{d}}B_{\mathrm{e}}} \tag{3.32}$$

which is independent of the number of spectral slices. Although spectrally-flat sources and ideal rectangular filters were assumed in reaching Equations 3.31 and 3.32, these equations still apply for more realistic spectral profiles provided each slice has the same profile and that the optical bandwidth measure is defined as the reciprocal of the coherence time of Equation 3.5 [Morkel *et al.* 1990]. Comparing Equations 3.29 and 3.30 with Equations 3.31 and 3.32, and assuming that $N = K$ in the spectrally-sliced WDM system, it can be seen that both the high-power SNR limit and the corresponding capacity limit of the spectral-amplitude OCDMA system are worse than those of a spectrally-sliced WDM system by the factor $(K + 1)$. It was claimed in [Nguyen *et al.* 1995] that a spectral-amplitude OCDMA scheme could be more efficient than a WDM system, but this was purely on the basis of shot noise, and it has been shown here that spectral-amplitude OCDMA is definitely not shot-noise limited.

3.5.3 Receiver Noise Distribution

When detecting light from a broadband thermal source, the actual noise distribution is often approximated as Gaussian, since as the SNR increases, the actual distribution is asymptotically Gaussian. However, as illustrated in [Nguyen *et al.* 1996], when the ratio of optical to electrical bandwidth is only of the order of 30, a Gaussian approximation to the actual distribution is a poor one. This has lead to some pessimistic system performance predictions for spectrally-sliced systems [Nguyen *et al.* 1996]. Clearly then, any approximations to the actual noise distribution need to be justified for the particular conditions considered.

In the spectral-amplitude OCDMA system of Figure 3.1, each user is transmitting in a coded manner across half the available spectrum, whereas in a spectrally-sliced system, only a narrow slice of the spectrum is available to each user. Hence, the noise distribution in the OCDMA case should be much closer to Gaussian. As a verification of this, the noise distribution was evaluated for reasonable system parameters, using the negative binomial model of Equation 3.7. This assumes that the combined spectrally-encoded light from all the users has the characteristics of light from a thermal source. The spectral-amplitude OCDMA system of Figure 3.1 was considered, using complementary keying, and with the parameters as listed in Table 3.1. The Hadamard code matrix was based upon every cyclic shift of the m-sequence indicated in Table 3.1.

Optical Centre Frequency	$\nu_o = 194\,\text{THz}$ (1550 nm)
Optical Bandwidth	$\Delta\nu = 2.5\,\text{THz}$ (20 nm)
Per-User Bit Rate	$1\,\text{Gb s}^{-1}$
Receiver Electrical Bandwidth	$B_\text{e} = 500\,\text{MHz}$
Single Source Power at Receiver	$P_\text{r} = 10\,\mu\text{W}$
Photodiode Quantum Efficiency	$\eta = 0.8$
Code length	64
m-sequence generator polynomial [Holmes 1982]	$1 + x + x^6$

Table 3.1 System Parameters

In Figure 3.3 the calculated distribution of the receiver current is compared with a Gaussian approximation of the same variance. The photoelectron count distribution at each photodiode is assumed to be negative binomial, following Equation 3.7, and dark current and receiver thermal noise have been neglected. The coherence times of the light at each photodiode are calculated directly from Equations 3.23 and 3.25, and the noise at each photodiode is independent, since the light is from different spectral regions. Consequently, the noise distribution at the balanced detector output is given by the convolution of the individual probability density functions (pdf) at each photodiode. In the case of only eleven simultaneous users, it is seen that the difference between the calculated distribution and the Gaussian approximation is extremely small, even in the tails of the distribution. The system bit-error probability is given by the area under the pdf and to the left of zero. The calculated pdf gives an error probability estimate of between

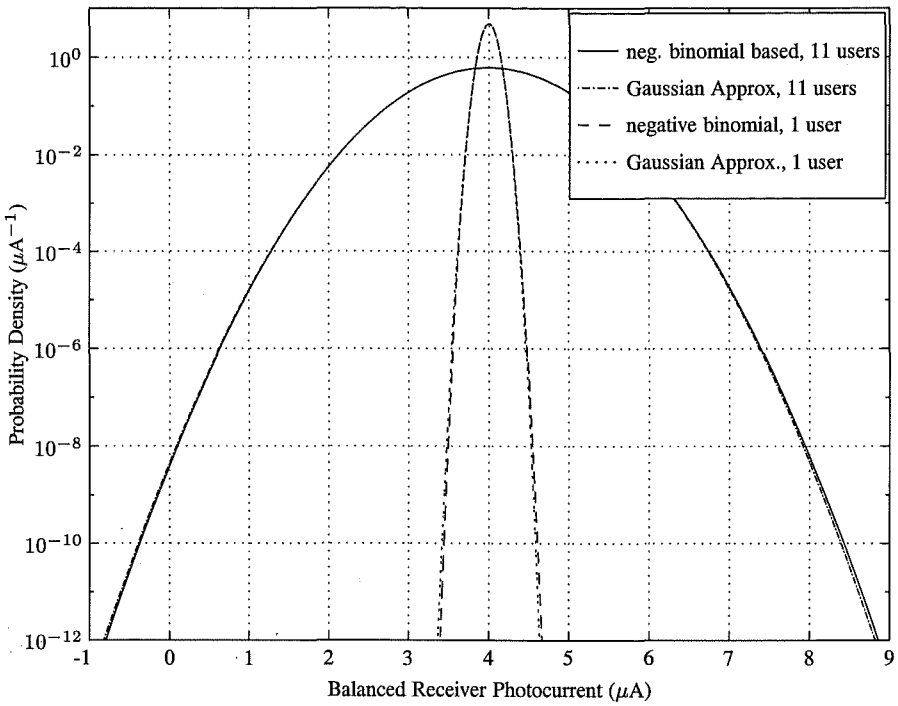

Figure 3.3 Photocurrent Probability Density Function (pdf), Conditions as per Table 3.1

3.8×10^{-10} and 4.1×10^{-10}, whereas the Gaussian approximation predicts 4.9×10^{-10}. The variation in the calculated estimate is due to different combinations of active users, which cause a slight variation in the coherence time of the detected light. Assuming Gaussian noise, Equation 3.29 predicts an error probability of 3.8×10^{-10}, which is smaller since Equation 3.29 does not include shot noise.

In the case of a single user, which is also shown in Figure 3.3, the transmitted light is incident on only one photodiode, and hence the current is of a single polarity. The calculated distribution is purely negative binomial, and it has significantly more asymmetry than the distribution when other users are transmitting as well. Even in this worst case, at an error probability of 10^{-9}, the conservative Gaussian approximation introduces an SNR penalty of only 0.34 dB. Hence, the assumption of Gaussian noise is found to be very reasonable for the chosen system parameters.

Under the Gaussian noise assumption, the error probability can be calculated directly from Equation 3.29. In Figure 3.4 the error-probability dependence upon the number of users is displayed for various ratios of optical to electrical bandwidth. This may be compared to Figure 3.2, in which the error probability is effectively fixed, and the total network capacity is then given for various values of the optical bandwidth. To more easily grasp the bandwidth ratios listed in Figure 3.4, the reader may wish to refer back to Figure 3.2, where various values of $\Delta\nu$ are expressed in both gigahertz and nanometres of wavelength about 1.55 μm. The conversion is that 1 nm of optical bandwidth in the 1.55 μm region is almost exactly 125 GHz, or equiva-

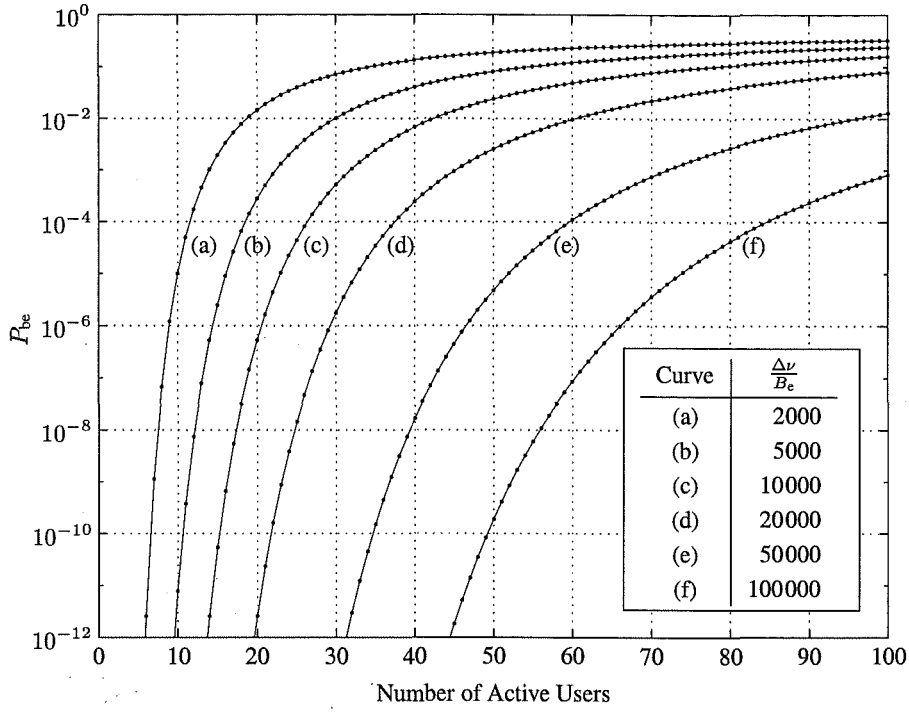

Figure 3.4 Error Probability of Ideal Spectral-Amplitude OCDMA, using Complementary Keying

lently, a 1 THz bandwidth corresponds to 8 nm. Curve (e) of Figure 3.4 thus corresponds, for example, to per-user bit rates of between 10 Mb s^{-1} and 200 Mb s^{-1} when the effective optical bandwidth is between 2 nm and 40 nm about 1.55 μm respectively, assuming B_e is equal to half the per-user bit rate. At a raw bit-error rate of 10^{-9} or less, curve (d) shows that up to 23 active users are permitted with $\frac{\Delta\nu}{B_e} = 20000$, which corresponds, for example, to a per-user bit rate of 50 Mb s^{-1} when the effective optical bandwidth is 4 nm near 1.55 μm. Curves (e) and (f) of Figure 3.4 show that at a raw bit-error rate of 10^{-9} or less, up to 36 and 52 active users respectively are permitted at the corresponding bandwidth ratios.

3.5.4 On-Off Keying

In the original spectral-amplitude OCDMA proposal [Zaccarin and Kavehrad 1993], the spectral codes were fixed, and data keying was to be achieved by on-off keying (OOK) of the source. The analysis of the system using OOK is simply performed by making the appropriate comparisons with the previous analysis in Section 3.5.1.

Initially, exactly the same receiver structure and Hadamard-based codes as used for the case of complementary keying are assumed here, along with bit-synchronism. Since there is no light transmission for a data 'zero', the complements of each code are not required, and the representation of a data 'one' is exactly as for the case of complementary keying. Consequently, if $\mathcal{L}$ is the number of bit-synchronous users that are transmitting during a single

bit interval, then it can simply stated from Equation 3.27 that

$$\sigma_I^2|_{\mathcal{L}} = \frac{B_e R^2 P_r^2 \mathcal{L}(\mathcal{L}+1)}{4\Delta\nu} \tag{3.33}$$

Note that apart from the code restrictions due to OOK, all other assumptions made in reaching Equation 3.27 in Section 3.5.1 apply to Equation 3.33 also. The signal current due to the desired user is given by $I_{\text{sig}} = \frac{RP_r}{2}$ when a data 'one' is transmitted and $I_{\text{sig}} = 0$ otherwise. Since each interfering user also transmits data by OOK, the number of users actually transmitting within any bit interval depends upon the data of each user. Assuming equiprobable binary data, it is possible to average the photocurrent variance over the data distribution to get the following average noise estimate (Appendix A)

$$\mathrm{E}[\sigma_I^2] = \frac{B_e R^2 P_r^2 K(K+3)}{16\Delta\nu} \tag{3.34}$$

Note that Equation 3.34 has been averaged over the data of the desired user as well as that of the interfering users. Together with the choice of a fixed decision threshold $d_{\text{thr}} = \frac{RP_r}{4}$, these approximations allow the following simple estimate of the signal-to-average-noise ratio

$$\rho_{\text{avg}} \approx \frac{(I_{\text{sig}} - d_{\text{thr}})^2}{\mathrm{E}[\sigma_I^2]} = \frac{\Delta\nu}{B_e K(K+3)} \tag{3.35}$$

Comparing Equations 3.35 and 3.29, it can be seen that the estimated SNR limit in the OOK case is, on average, slightly worse than for the case of complementary keying. In [Kavehrad and Zaccarin 1995] it is claimed that complementary keying (termed "orthogonal signalling" therein) would gain 3 dB with respect to the OOK case. This is true simply with respect to shot and receiver noise, however, due to the interference between light signals, the dominant SNR limit is seen here to be very similar for the cases of both complementary and on-off keying. Note, however, that the average SNR of Equation 3.35 does not give a direct indication of the error performance due to the highly nonlinear relationship between SNR and bit-error rate. The actual bit-error rate has to be found from

$$P_{\text{be}} = \sum_{L=0}^{K-1} p(L).P_{\text{be}}|_L \tag{3.36}$$

where L is the number of interfering users transmitting in a bit period, $p(L)$ is the probability of L such users, and $P_{\text{be}}|_L$ is simply the bit-error probability conditioned upon L. To proceed beyond Equations 3.36 and 3.33, the statistics of the noise must be known. In Section 3.5.3 the Gaussian noise assumption was shown to be very reasonable, and hence, assuming that the photocurrent noise is Gaussian and that the transmitted data is equiprobable, Equation 3.36 becomes

$$
\begin{aligned}
P_{\mathrm{be}} &= 2^{-K} \sum_{L=0}^{K-1} \binom{K-1}{L} \left[P_{\mathrm{be}}|_{L,d=1} + P_{\mathrm{be}}|_{L,d=0} \right] \\
&= 2^{-(K+1)} \sum_{L=0}^{K-1} \binom{K-1}{L} \left[\mathrm{erfc}\left(\sqrt{\frac{I_{\mathrm{sig}}^2 (1-d_{\mathrm{thr}})^2}{2\sigma_I^2|_{L+1}}} \right) + \mathrm{erfc}\left(\sqrt{\frac{I_{\mathrm{sig}}^2 d_{\mathrm{thr}}^2}{2\sigma_I^2|_{L}}} \right) \right] \\
&= 2^{-(K+1)} \sum_{L=0}^{K-1} \binom{K-1}{L} \left[\mathrm{erfc}\left((1-d_{\mathrm{thr}}) \sqrt{\frac{\Delta\nu}{2B_{\mathrm{e}}(L+1)(L+2)}} \right) + \right. \\
&\qquad \left. \mathrm{erfc}\left(d_{\mathrm{thr}} \sqrt{\frac{\Delta\nu}{2B_{\mathrm{e}}L(L+1)}} \right) \right]
\end{aligned}
\tag{3.37}
$$

where d_{thr} represents the decision threshold as a fraction of the signal current I_{sig}. The case $d_{\mathrm{thr}} = 0.5$ is the simplest to implement, since for equiprobable transmitted data the average receiver photocurrent should equal the detection threshold. However, when the total number of active users is small, there is a significant difference between the noise levels when a 'one' or a 'zero' is transmitted by the matched user, so $d_{\mathrm{thr}} = 0.5$ is sub-optimum in this case. In Section 3.5.4.1 the potential performance improvements from optimising the detection threshold are briefly considered.

From the code construction of Equation 3.17, when a data 'one' is transmitted, the values [+1,-1] in the Hadamard matrix are mapped to the values [0,1] in the spectral-amplitude code. Since each element of the first column of the Hadamard matrix is unity, and code complements are not used in an OOK system, each spectral code starts with zero. This means that light is never transmitted in the first spectral slice, and hence the bandwidth of this slice is being wasted. To most effectively utilise the available bandwidth $\Delta\nu$ with this system, it is clear then that the codes can be shortened by one element with no loss in performance, and there is a slight increase in spectral efficiency. In the proposal of [Zaccarin and Kavehrad 1993] that used OOK, the user codes consisted of all the cyclic shifts of a single m-sequence. This is merely a particular case of such shortened Hadamard codes, and many other code forms can be taken from different Hadamard-matrix constructions [Harwit and Sloane 1979]. An OOK system using Hadamard-based codes in this manner can then be written as having an optical bandwidth of $\tilde{\Delta\nu} = \frac{\Delta\nu N}{N-1}$, and a received power level $\tilde{P}_{\mathrm{r}} = \frac{P_{\mathrm{r}} N}{N-1}$, but it actually only requires the optical bandwidth of $\Delta\nu$, and the received power in this bandwidth is P_{r}. Consequently, for an OOK system that uses codes of length $N-1$, Equations 3.27 - 3.30 and Equations 3.33 - 3.37 apply to this system also, merely by replacing P_{r} and $\Delta\nu$ by $\tilde{P}_{\mathrm{r}}$ and $\tilde{\Delta\nu}$ respectively. Note, however, that this possible efficiency improvement is generally neglected in the OOK performance estimates throughout the rest of this chapter, in order to keep the comparisons independent of code length N. This does not introduce a major error assuming that N is of the order of 100 or more.

3.5.4.1 Determination of Detection Threshold

If there are L bit-synchronous interfering users transmitting a 'one' in a given bit period, then when the data bit of the matched user is also a 'one', the intensity noise is given simply by Equation 3.33 with $\mathcal{L}$ replaced by $L+1$, and when the data bit of the matched user is 'zero', the noise is simply given by Equation 3.33 with $\mathcal{L} = L$. Hence, in the high-power limit the noise level is always higher when a 'one' is transmitted, so a threshold level slightly less than 0.5 may be advantageous.

Ideally, if the receiver has the knowledge of how many bit-synchronous users are transmitting during a single bit period, then the decision threshold could be optimised for the detection of each bit. However, to determine how many users are transmitting in any bit period is almost a full multi-user detection problem, and requires significant complexity. Ignoring the complexity issue at this stage, if the probability of error is to be identical for both binary symbols, then the optimum threshold can be simply found for the Gaussian noise case. For binary signals received with additive zero-mean Gaussian noise, with variances σ_0^2 and σ_1^2 when the signal is a 'zero' or 'one' respectively, the optimum threshold for symmetric errors is easily shown to be $d_{\text{thr}} = \sigma_0/(\sigma_0 + \sigma_1)$, where d_{thr} is the fraction of the separation between the 'zero' and 'one' signals. Hence, if there are L other users transmitting a 'one' during a bit period, then the optimum threshold is given by

$$d_{\text{thr}} = \frac{\sqrt{L(L+1)}}{\sqrt{(L+1)(L+2)} + \sqrt{L(L+1)}} \tag{3.38}$$

In Figure 3.5 this threshold level is plotted versus L. It is also possible to derive analytically the threshold level that minimises the error probability without assuming that it must be the

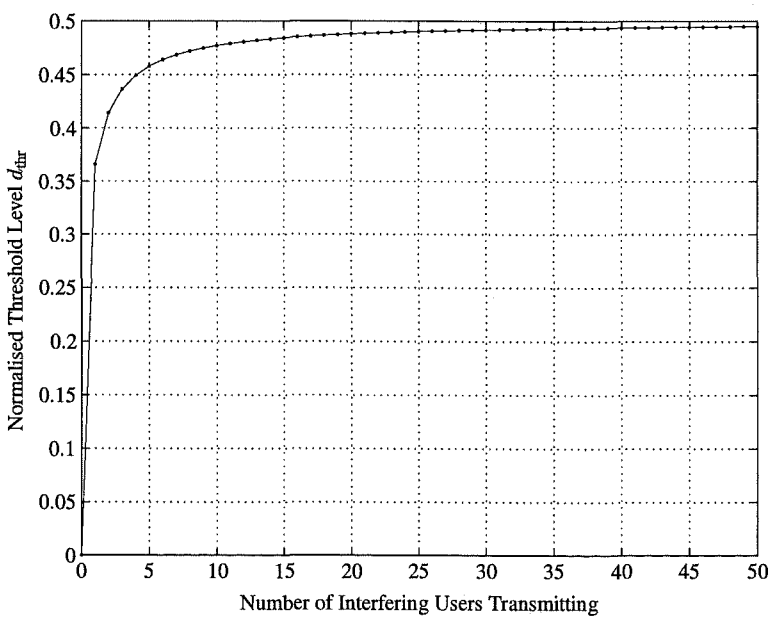

Figure 3.5 Optimum High-Power Detection Threshold for Bit-Synchronous OOK

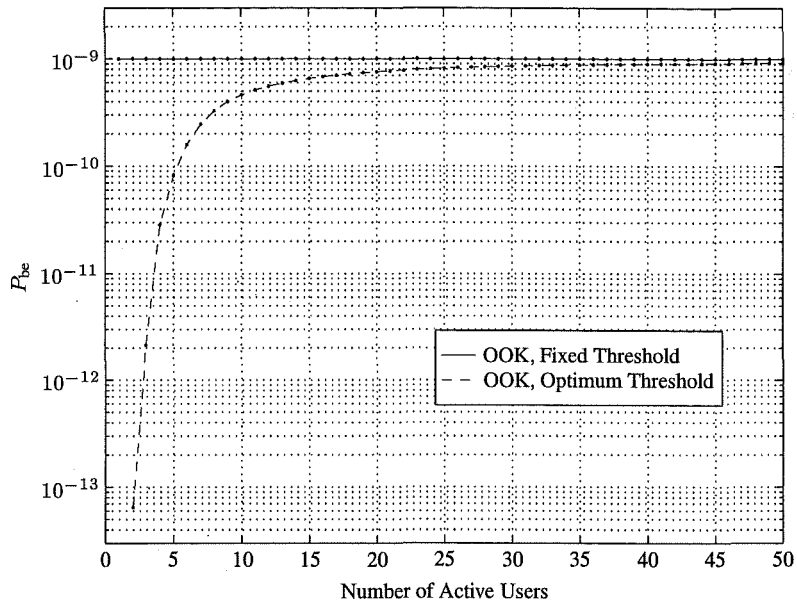

Figure 3.6 Error Probability Comparison of Bit-Synchronous OOK using Fixed and Optimum Thresholds

same for both symbols. However, over the bandwidth ratios of interest, there is no practical difference between the threshold so obtained and that of Equation 3.38. As the number of users increases, the optimum threshold gets closer to 0.5, and so the performance improvement over a fixed threshold $d_{\text{thr}} = 0.5$ is expected to be small in this region. Indeed this is the case, as can be seen from Figure 3.6, in which the ratios of optical to electrical bandwidth are chosen so that the system has an error probability of 10^{-9} under OOK with $d_{\text{thr}} = 0.5$, regardless of the number of users. These are calculated directly from Equation 3.37 with the threshold d_{thr} either fixed at 0.5 or dependent upon L according to Equation 3.38. Clearly, the performance difference is only significant when the number of users is small, as expected.

Note that when the number of users is small, the sum in Equation 3.37 tends to be dominated by the term with $L = K - 1$, since this is the most noisy case and the erfc function decreases exponentially. Hence, there should be little difference in the probability of error if the threshold is set according to Equation 3.38 with $L = K - 1$. Indeed, this is the case such that the difference cannot be distinguished on the scale of Figure 3.6. This is also the basis on which the case of d_{thr} becoming zero ($L = 0$ in Equation 3.38) is not dwelt upon, even though this is clearly impractical. Hence, a receiver merely with knowledge of the total number of active users in the system, regardless of their data, can adjust the detection threshold to achieve the advantage for small numbers of users indicated in Figure 3.6. However, as shown in Section 3.5.5, this may be of no practical advantage. Section 3.5.5 also shows the effect of optimising the threshold level upon network capacity, and in summary, significant gains of 20-50% are possible when there are less than five active users, but once the number of active users exceeds 10-15, there is practically no difference. It is therefore concluded that OOK

using a fixed threshold of $d_{\text{thr}} = 0.5$, corresponding to the average photocurrent, is the simplest OOK detection scheme and there is generally insufficient advantage to be gained from the complexity of an adjustable threshold.

3.5.4.2 Asynchronous OOK

All the previous OOK performance analysis and threshold optimisation has been for the bit-synchronous case, but the asynchronous performance is of most interest. Due to the asynchronism, the noise level during any given bit period depends not only upon the data of each user but upon their relative delays. Assuming that each user has a similar bit rate, the relative delays between users change little between adjacent bits, and so some correlation in noise level between adjacent bits may be expected. However, it is assumed here that the OOK regime with the assumption of equiprobable data symbols introduces sufficient differences between the detection of adjacent bits that such correlation can be neglected.

In the asynchronous case, with only 2 or 3 active users, assuming equiprobable symbols and assuming relative time delays that are uniformly distributed over a bit period, it is possible to analytically obtain the expected distribution of the noise variance. From these distributions, assuming Gaussian noise, an estimate of the error probability can be found, and this in general is lower than the corresponding bit-synchronous error probability. The reason for this is that the noise variance distribution is now continuous rather than discrete, but still within the same limits as in the synchronous case. Hence, the noise distribution in the asynchronous case is narrower, on average, primarily due to the lack of discreet probabilities at the distribution extremes. Due to the highly nonlinear relationship between SNR and error probability, low SNR events dominate the average error probability, and hence such a narrower variance distribution results in a lower average error probability. Numerical simulation is used to determine the distribution of the noise variance for larger numbers of asynchronous users, and this is discussed further in the following section.

3.5.5 Performance Comparisons

In Figure 3.7 the asynchronous performance estimates are compared to the bit-synchronous case, assuming equiprobable symbols, relative time delays that are uniformly distributed over a bit period, and a fixed threshold $d_{\text{thr}} = 0.5$. Monte Carlo simulation was used to get the estimates of the noise variance, and these corresponded accurately with the analytical distributions for the case of two and three users. Furthermore, the asynchronous simulation-based performance tends toward the bit-synchronous performance as the number of users becomes very large, which is reasonable. The performance when the threshold is set according to the number of active users ($L = K - 1$ in Equation 3.38) is also shown on Figure 3.7, but it is clear that this gives no practical advantage.

In Figure 3.8 the network capacity limits of spectral-amplitude OCDMA are shown for

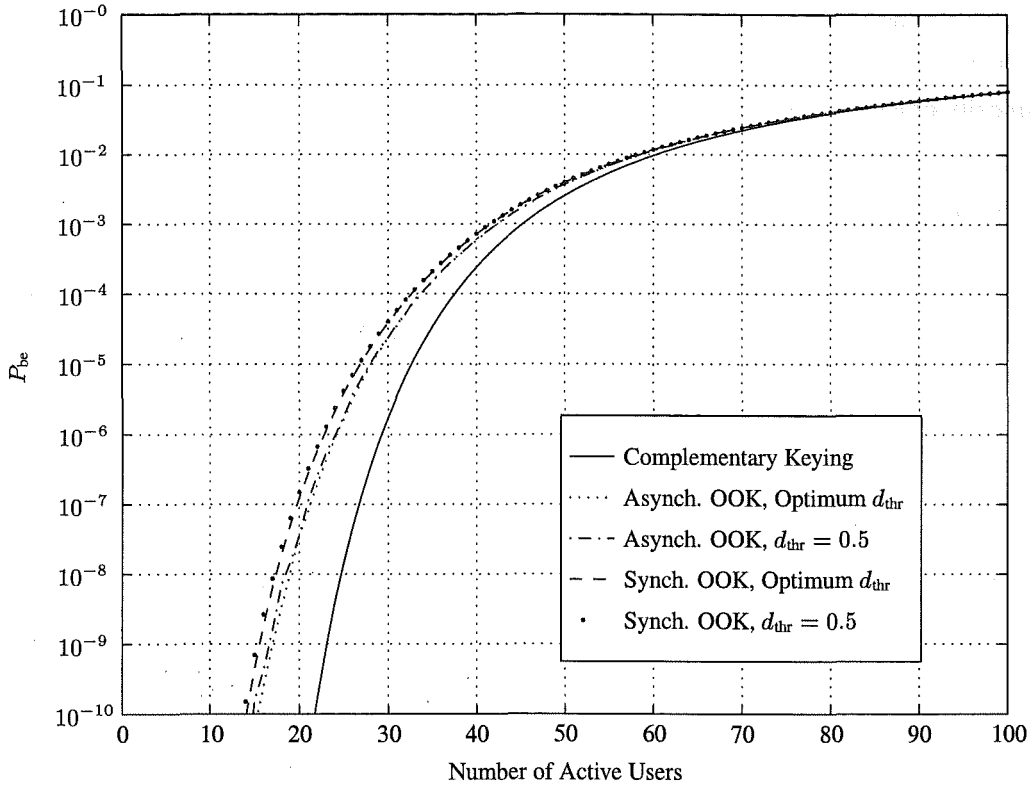

Figure 3.7 Comparisons of Bit-Error Rate at $\frac{\Delta\nu}{B_e} = 20000$

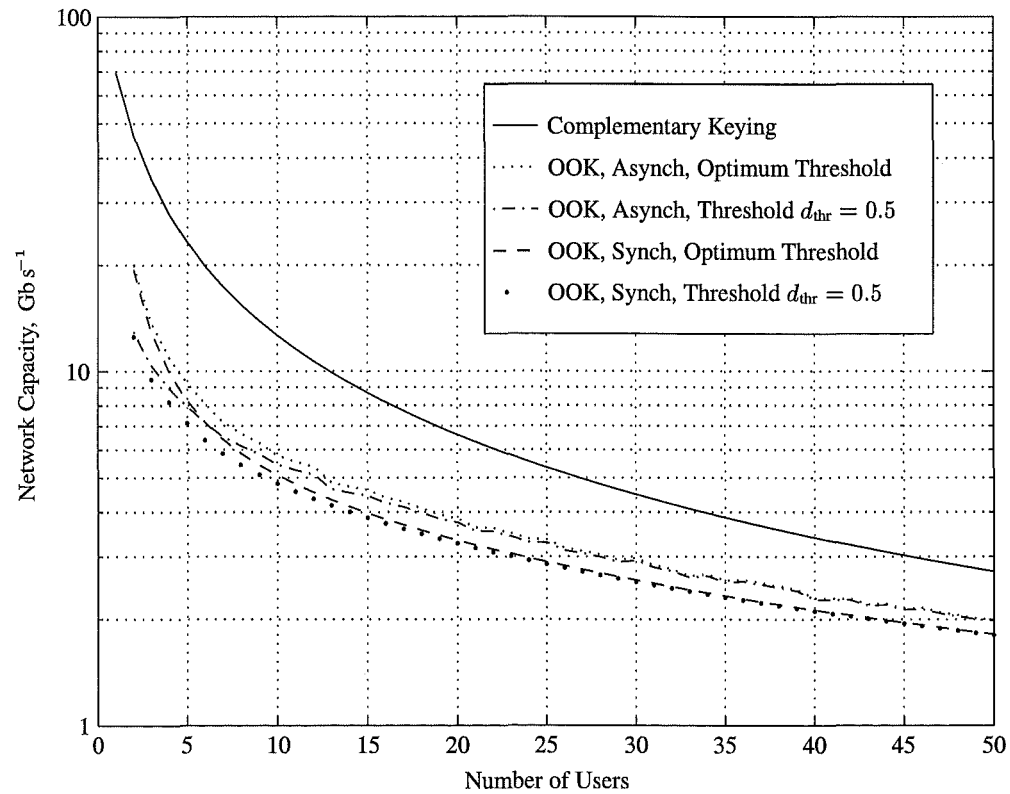

Figure 3.8 Throughput Comparisons for Intensity-Noise-Limited On-Off Keying, $\Delta\nu = 2.5$ THz

both the complementary keying and OOK cases. The synchronous and asynchronous OOK performance differ, unlike the complementary-keying case, and the effect of basing the OOK detection threshold on the number of active users is also shown. These are all calculated for the case of $\Delta\nu = 2.5\,\text{THz}$, and at an error rate of 10^{-9}. In the same manner as Figure 3.2, differing values of $\Delta\nu$ simply move all the curves up or down, assuming the error rate of 10^{-9} is maintained.

In Figure 3.9, comparison is made between the SNR limit from Equation 3.29 and the performance estimates from the original spectral-amplitude OCDMA proposal and those in the more detailed work of [Kavehrad and Zaccarin 1995]. The bit-error rates corresponding to the SNR levels under the assumption of Gaussian noise are also indicated. The error rates and effective SNRs are also shown for the OOK case assuming Gaussian noise, from Equation 3.37 and via simulation for the asynchronous case, assuming a fixed detection threshold $d_{\text{thr}} = 0.5$, and Hadamard codes of length $N = 128$ as per the data from [Kavehrad and Zaccarin 1995]. The term effective SNR is used since unlike the complementary-keying case, the actual SNR in any bit period under OOK can take on a wide range of values, depending upon the current data bit(s) of each active user. The effective SNR is the constant SNR level which corresponds to the average bit-error rate, which is calculated on the basis of the SNR distribution. The two curves from [Zaccarin and Kavehrad 1993] simply indicate the best and worst error probability estimates out of all the cases considered therein. The performance estimates from Figure 7 of [Kavehrad and Zaccarin 1995] incorporate shot noise, receiver thermal noise, non-ideal source spectra, and system losses, but the intensity noise of the detected light is not considered at all. The asynchronous OOK performance in Figure 3.9 is based purely on the intensity noise of the light, assuming thermal sources, ideal source spectra, and ignoring the shot and receiver noises. The optical bandwidth of 40 nm in the 1550 nm region (5 THz) was chosen as a reasonable maximum in order to clearly indicate the maximum performance that might be possible when the system is intensity-noise limited, and any bandwidth less than this only lowers the intensity-noise limit further. Clearly, the estimates from both [Zaccarin and Kavehrad 1993] and [Kavehrad and Zaccarin 1995] are overly optimistic due to the neglect of the intensity noise. Kavehrad and Simova [1996] have experimentally demonstrated spectral-amplitude OCDMA with two users, each with a bit rate of $10\,\text{kb}\,\text{s}^{-1}$, where the 62 nm FWHM bandwidth of 830 nm LEDs was encoded, and 200/240 μm multimode fibre was used. Even if single-mode fibre had been used in this experiment, the number of users and the optical-to-electrical bandwidth ratio are such that the limit of Equation 3.29 would still have been orders of magnitude away.

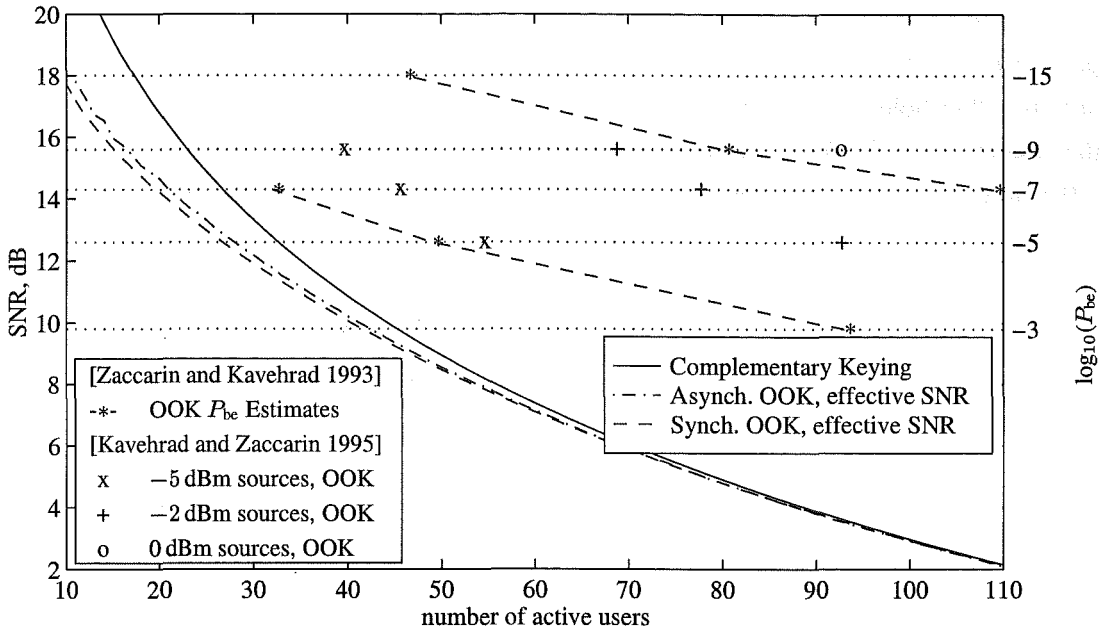

Figure 3.9 Comparison of the SNR Limits with the Original Performance Predictions, Bit Rate 500 Mb s^{-1}, Optical Bandwidth 5 THz (40 nm @1550 nm)

3.6 PRACTICAL ISSUES

3.6.1 Polarisation Dependence

In the analysis of Section 3.5.1 the sources were all assumed to be unpolarised, and it was assumed that the light remains unpolarised right to the detectors. This is a best-case condition, since thermal light intensity noise increases with the degree of polarisation (Equation 3.10). The worst case condition is that the light from each user is fully polarised, and that these polarisation states are all perfectly aligned at the receiver. In this worst case, the intensity noise is simply 3 dB larger than in the unpolarised case (Equation 3.27), and this degradation by a factor of two can then be carried through into all the subsequent equations and comparisons. A more likely scenario is that polarised light from each user arrives at the receiver in a random state of polarisation, due to environmental fluctuations along the different SMF paths. In this case the intensity noise of each single user's light is increased by 3 dB, but now the interference between the light from different users is highly dependent upon their relative state of polarisation. As the number of users increases, the polarisation degree of the overall received light decreases, so the average PIIN level approaches that in the unpolarised case. Note however that since the environmental fluctuations typically have much longer time constants than the data bit interval, any SNR variation due to the relative polarisation states is rather slow.

In the work of [Sampson *et al.* 1997], the dominant SNR limit of coherence multiplexing is observed to be worse than that of Equation 3.29[1] by a factor of four. This factor of four

[1] As published in [Smith *et al.* 1995], following an alternative derivation.

is attributed to the four different paths between each source and photodiode in the case of coherence multiplexing, since both the transmitter and receiver contain an interferometer, as shown in Figure 2.4. However, the SNR limit given for coherence multiplexing assumes the worst case of fully polarisation-matched signals at the receiver [Sampson *et al.* 1997], whereas Equation 3.29 must be reduced by 3 dB to apply for this case. Attributing a reduction in SNR by a factor of four to the number of paths in coherence multiplexing is nonetheless correct, but in spectral-amplitude OCDMA, each user only ever transmits in ideally half the available optical bandwidth, whereas coherence-multiplexing transmission uses all of it. Hence, the SNR limit of spectral-amplitude OCDMA is greater than that of coherence multiplexing by only a factor of two, at most.

3.6.2 Dispersion

The analysis in this chapter has not considered dispersion at all. Clearly, however, with very broad optical spectra the dispersion is going to limit transmission distances significantly. The first-order dispersion of standard single-mode fibre is around $16\,\mathrm{ps\,km^{-1}nm^{-1}}$ in the 1550 nm region [Agrawal 1992], so for an optical bandwidth of 20 nm, the dispersion is $320\,\mathrm{ps\,km^{-1}}$. Using the heuristic reckoning of ensuring this dispersion length is no more than 10% of the bit period, the bit-rate-length product is restricted to the order of $0.3\,\mathrm{Gb\,s^{-1}\,km}$. By using dispersion-shifted fibre (DSF) in the 1550 nm region, which typically has second-order dispersion of $50\,\mathrm{fs\,km^{-1}nm^{-2}}$ [Agrawal 1992], the dispersion for a 20 nm bandwidth is of the order of $20\,\mathrm{ps\,km^{-1}}$. The same reckoning then gives a bit-rate-length product of the order of $5\,\mathrm{Gb\,s^{-1}\,km}$. Clearly, these calculations only give a rough idea of the effects since the spectral shape and the signalling method have not been specified at all, amongst other limitations. In the case of Gaussian optical spectra, and especially if the pulse shapes are also Gaussian, then accurate calculations of dispersion penalties can be performed relatively simply, as for example in [Gimlett and Cheung 1986], but this does not apply to the spectral-amplitude OCDMA system considered here. However, this heuristic reckoning is not far wrong, since Pendock and Sampson [1995] demonstrated coherence multiplexing over 8 km of dispersion-shifted fibre (DSF), using EDFA-boosted amplified spontaneous emission of 17 nm FWHM and coherence time 250 fs, and where the bit rate was $1\,\mathrm{Gb\,s^{-1}}$ per user. Hence, using DSF, it is considered that bit-rate-length products of between 2 and $10\,\mathrm{Gb\,s^{-1}\,km}$ are possible with minimal dispersion penalty for reasonable optical bandwidths in the 1550 nm region.

Due to the reduction in intensity noise with increasing optical bandwidth, but also increasing dispersion penalty, some optimum optical bandwidth for a given bit rate and link length can be expressed as in [Pendock and Sampson 1997], but this is not attempted here.

Analytical and experimental work reported in [Pendock and Sampson 1996b] shows that as pulses of amplified spontaneous emission are dispersed beyond the bit period, the intensity-noise limited SNR, as measured over the bit period, suffers an additional degradation. This penalty is because the spectral extent of the pulse fraction within the bit period is less than

that of the original pulse, due to the chirping produced by the dispersion. This applies directly to spectral-amplitude OCDMA using OOK, but the effects of this are less clear in the complementary-keying case.

3.6.3 Spectral Profiles and Filters

The intensity-noise limits found in this chapter assume perfect spectral division into N slices of width $\frac{\Delta\nu}{N}$, whereas any real filtering technique must incorporate at least slightly narrower slices in order to allow filter roll-off while ensuring that adjacent slices do not overlap significantly. Assuming that it is still valid to treat each slice as having the same spectral profile, and that there are no significant differences in these amongst all the users, then the effect of the non-ideal profiles is to simply reduce $\Delta\nu$ in all the analysis here. This is the reason that the optical bandwidths used in Figure 3.2 are smaller than that which can be resolved into an adequate number of spectral slices by some filtering methods, and in particular, the arrangement of lenses and diffraction gratings considered in [Zaccarin and Kavehrad 1993].

The assumption of equal detected power from each spectral slice of each user is idealistic, since there are many components in the system that contribute some level of variation from this ideal. The initial and most obvious of these are the broadband sources themselves, and the characteristics of the spectral filtering at the transmitters and receivers are also important. Other realities include the different fibre lengths to each user, the variation of photodiode responsivity with wavelength, the degree of mismatch between the nominally balanced photodiodes, and in general, any other source of wavelength-dependent or user-dependent attenuation.

In [Zaccarin and Kavehrad 1993] broadband thermal sources (LED) with a Gaussian spectral profile were assumed, and the coded optical bandwidth was restricted to the 3 dB width or a fraction thereof in order to obtain near-flat useful spectra. However, this reduces the available power and necessitates narrower spectral filtering. Other possibilities include rare-earth-doped fibre amplifiers, particularly the EDFA, used purely as a source of amplified spontaneous emission (ASE). These can be designed to give high-power broadband spectrally-flat outputs, as shown in [Sampson and Holloway 1994], and an experimental demonstration using an EDFA as a source has been performed [Nguyen *et al.* 1997].

The proposals of OCDMA based upon either spectral-phase or spectral-amplitude coding both used a well-known arrangement of lenses and diffraction gratings to spread the light across the focal plane of the lenses according to wavelength. The encoding was then performed by simply placing the appropriate phase or amplitude mask at this point [Weiner *et al.* 1988, Zaccarin and Kavehrad 1993]. By using a liquid crystal array, commonly termed a spatial light modulator (SLM), rather than a fixed mask, the spectral coding becomes programmable. The use of acoustically-tunable optical filters (ATOF) for spectral-amplitude coding has also been proposed, since it is possible to have multiple passbands corresponding to multiple applied radio frequencies [Hinkov *et al.* 1995]. Both of these filtering methods allow the amplitude

of each spectral slice to be individually controlled, and hence some compensation of spectral power variation is possible at the expense of the overall transmitted power.

As noted in [Kavehrad and Zaccarin 1995], the extinction ratio of an SLM is not infinite, but the degradation of their calculated performance was considered minimal. Also, for Hadamard-based codes, the residual light levels of each unmatched user are still ideally orthogonal. Here, the effect of a finite filter extinction ratio on the intensity-noise limit can be determined by modifying both the signal level and the levels in Equation 3.18 to account for the non-zero representations of the 'zero' code elements. Following this through, for a nominally zero level $r \ll 1$, the intensity-noise SNR limit then includes the multiplicative factor $(\frac{1-r}{1+r})^2$, assuming the receiver still has an infinite extinction ratio, and if the receiver has the same finite ratio, then this factor should be multiplied by $(1-2r)^2$. Numerically, a 10 dB extinction ratio ($r = 0.1$) at the transmitter reduces the SNR limit by 1.7 dB, and a 20 dB extinction ratio gives only 0.17 dB penalty. If the receiver has the same extinction ratio, then these penalties approximately double.

Along with programmable transmitter codes, in [Kavehrad and Zaccarin 1995] the receiver codes were fixed, since this allowed the use of fixed masks with negligibly large extinction ratio. For a fixed spectral-amplitude filter, there are a number of recently developed methods that could also achieve this, including in-fibre gratings and arrayed waveguide grating multiplexers (AWGM). An AWGM is basically a wavelength multiplexer, and hence it can form the basis of the receiver structure of Figure 3.1. Successive in-fibre gratings tuned to different spectral lines would reflect those spectral lines, but pass all others, and hence this could be incorporated into the balanced receiver of Figure 3.1 also. If the dispersion in the reflected light is too large, then two complementary filters used in transmission only may be used, but with the 3 dB power loss that also occurs in the receiver configuration of [Zaccarin and Kavehrad 1993, Kavehrad and Zaccarin 1995]. Further development and refinement of such filters and multiplexers is expected as the trend toward wavelength-division multiplexing (WDM) for large optical networks continues.

Using an acousto-optic filter or any form of grating-based filter for the spectral coding, the residual light level transmitted for any zero code element is then determined by the sidelobes of any neighbouring unity code elements, rather than being fixed. Hence, the sidelobes of unmatched users are not orthogonal in general, and this results in some fraction of the unmatched users' signals appearing at the receiver, - such MAI does of course occur when any other real deviation from the ideal case causes a loss in orthogonality also.

The cancellation of signals common to both photodiodes is an essential part of the receiver filtering. Balanced photodiode receivers such as the New Focus No. 1617, which has a common-mode rejection ratio (CMRR) of 25 dB, have been commercially available for several years. It is therefore expected that CMRRs greater than this can be readily achieved, although it is quite possible that non-uniformity in optical power splitting and/or wavelength splitting before photodetection are more significant than any photodiode mismatch.

3.6.4 Power Control

The photocurrent intensity-noise power at the receiver is roughly proportional to the square of the total received optical power. This gives a reasonable idea of how the intensity-noise limit behaves if the power levels received from each user are not equal. Unlike most, if not all, radio CDMA systems, the channels are generally fixed in an optical network, and indeed that is the case assumed here. With single-mode fibre of attenuation as little as 0.2 dB km^{-1} readily available, and assuming the network to be less than ten kilometres in size, due to dispersion, the variation in power levels due to differing distances from the star coupler is minimal. If power matching is of concern either initially or over the long term, it should be a simple matter to occasionally adjust the power level of a particular source on the basis of the received power level when matched to its own transmission, assuming equal attenuation to and from the star coupler.

3.7 SUMMARY

This chapter has presented a performance analysis of an OCDMA system based upon spectral-amplitude coding of broadband thermal sources, and attention has been concentrated upon source-intensity noise and the phase-induced intensity noise (PIIN) caused by the mixing of fields from independent sources. It has been shown that the intensity noise at the receiver is dominated by the PIIN, which results in an SNR limit that is approximately inversely proportional to the square of the number of active users. This causes the total network capacity to be approximately inversely proportional to the number of active users. The original proposals and analyses of spectral-amplitude OCDMA did not consider intensity noise at all, and hence their performance estimates are significantly greater than the limits found here, and are thus incorrect. Both the original on-off keying and the more efficient complementary keying have been treated, and complementary keying has been seen to perform better than OOK in the intensity-noise limit. However, the improvement using complementary keying is not as much as the 3 dB increase in SNR that was claimed in an earlier analysis which did not consider intensity noise.

The SNR and capacity limits that were found here due to intensity noise were shown to be worse than those of an equivalent wavelength-division system which uses the same sources and spectral divisions, and this is by a factor of approximately the number of active users. These limits correspond to similar limits found for sub-carrier-multiplexed and coherence-multiplexed communication systems, since the dominant limitation arises in the same manner. The order of SNR and capacity limits found here, assuming ideal optical bandwidth use, are 3 dB greater than those of the corresponding coherence-multiplexed system. A 6 dB improvement on the basis of the four paths through the interferometers in a coherence-multiplexed system is expected, but each user in spectral-amplitude OCDMA only ever transmits in half the optical bandwidth at one time, so the overall advantage is only 3 dB.

Finally, the various practical realities of a spectral-amplitude OCDMA system, such as

fibre dispersion and realistic spectral profiles, have been discussed, and hence the idealised treatment here has been brought into perspective.

Chapter 4

EXPERIMENTAL INVESTIGATION OF PIIN

4.1 INTRODUCTION

In Chapter 3, the SNR limit of spectral-amplitude OCDMA was found under the assumption that the received light appeared as from a single thermal source, whose intensity noise characteristics are described in Section 3.2. However, the majority of the limiting noise power of Equation 3.27 is actually phase-induced intensity noise (PIIN), due to the interference between the light from the independent incoherent sources (Section 3.3), regardless of whether the sources are thermal or not.

The filtering of source intensity noise and the generation of PIIN in interferometric systems and their characteristics have been well covered in theoretical works such as [Moslehi 1986, Wentworth 1989] and [Tur *et al.* 1990]. The first experimental measurements using a broadband superluminescent diode (SLD) source with a Michelson interferometer clearly showed that with the source intensity noise eliminated, PIIN was generated and its level significantly exceeded that of the shot noise [Yurek *et al.* 1987]. However, it was observed that the measured level of PIIN was lower by 2.7 dB from that theoretically expected according to the measured source coherence time [Wentworth and Moslehi 1989]. Subsequent experimental measurements with the growing range of SMF-output broadband incoherent sources tended to focus simply on the levels of source intensity noise, comparing these with each other and with those from an ideal thermal source [Burns *et al.* 1990, Morkel *et al.* 1990]. It was decided to experimentally investigate the levels of PIIN generated by the mixing of two independent incoherent broadband light fields, with the aim of showing that the actual PIIN levels do correspond to those expected theoretically. Section 4.2 describes this experimental investigation and the verification that the actual PIIN level does correspond to that expected from theoretical analysis, within the limits of the experimental uncertainty.

At the same time that the experiments described in this chapter were being performed, the first experimental demonstration of a coherence multiplexing system where the effects of PIIN could be seen was reported [Pendock and Sampson 1995]. However, these measurements were not compared to theoretical predictions until the work of [Pendock and Sampson 1996a], wherein reasonable correspondence was indeed observed.

In Section 4.3 the use of multimode fibre (MMF) to reduce the PIIN level is investigated. The experimental PIIN measurement described in Section 4.2 is repeated using available graded-index MMF rather than SMF, and the PIIN level is observed to be reduced by about 7 dB using only 14 m of graded-index MMF. The mode structures of step-index and graded-index cylindrical dielectric waveguides are reviewed, and these are used to estimate the modal power distribution of the light launched into the MMF, which is in general agreement with the experimental results. The PIIN reductions expected for much longer typical step-index and graded-index MMFs are discussed, and heuristic estimates are made. The contents of this chapter are then summarised in Section 4.4.

4.2 PHASE-INDUCED INTENSITY NOISE FROM A BROADBAND SOURCE

4.2.1 Source Characterisation

The source used in the following investigations was a 1300 nm superluminescent diode (SLD), Oki OE360S, packaged within a Fibernet stabilised-light-source unit, containing power supplies, temperature stabilisation, and modulation control. It launches −4 dBm into SMF, and has a spectral width of 51 nm (FWHM). It has the calibrated power spectrum shown in Figure 4.1, as measured by the manufacturer after assembly and before shipping. A suitable optical spec-

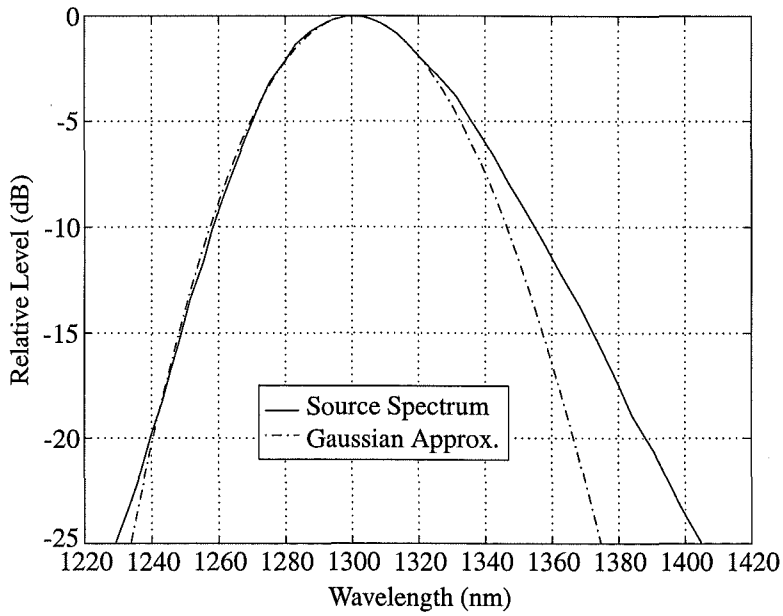

Figure 4.1 Spectrum of Superluminescent Diode

trum analyser was not available after shipping to recheck this spectrum. It was assumed that the spectral characteristics of the solid-state SLD would not have been significantly affected by the transportation of the source unit. Also shown in Figure 4.1 is a Gaussian curve through the 3 dB points of the actual spectrum. It can be seen that the source has a near-Gaussian

spectrum except for a larger tail toward longer wavelengths. The source coherence time corresponding to this Gaussian approximation is given by $\tau_c = \frac{1}{\Delta\nu}\sqrt{\frac{2\ln 2}{\pi}}$ where $\Delta\nu$ is the FWHM bandwidth [Goodman 1985], which gives $\tau_c = 73.8\,\text{fs}$. Since the actual source spectrum is slightly broader than the Gaussian, it should have a slightly shorter coherence time. Equipment for direct measurement of the coherence time was not available, so numerical evaluation of Equation 3.5 was performed for the actual spectrum of Figure 4.1, giving $\tau_c = 71.2\,\text{fs}$, which is reasonable. The numerical integrations were performed using Simpson's rule after cubic-spline interpolation. It was confirmed that the same numerical evaluation also gave a coherence time of 73.8 fs when applied to the Gaussian curve over the range shown in Figure 4.1.

The arrangement of Figure 4.2 was set up in order to measure the degree of polarisation of the superluminescent source. The polarisation controller was manually adjusted to provide maximum power-imbalance at the receiver, and the power ratio was recorded. The polarisation controller was then adjusted to give the maximum output at the opposite polarisation-beam-splitter (PBS) port, and the power ratio recorded again. This permitted the compensation of any power or measurement imbalances between the two paths from the PBS. Over a number of successive such measurements, the degree of polarisation of the source was determined to be $P = 0.32 \pm 0.01$.

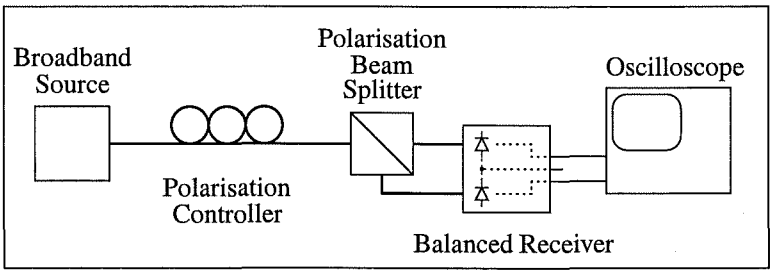

Figure 4.2 Setup for Measurement of the Polarisation Degree of the Source

The initial configuration to measure the source intensity noise consisted of simply the source, an attenuator, and a DC-125 MHz low-noise receiver (New Focus 1811), connected with SMF. The received signal was then fed into a 150 MHz spectrum analyser (HP3588A) for measurement. A polarisation controller and PBS were then included as in Figure 4.2 to investigate the polarisation dependence. In Figure 4.3 a typical spectrum of the received signal is shown, along with the receiver noise floor. The particular case is that of polarised light of -13 dBm optical power at the receiver, and the spectra have been averaged over 10 successive sweeps. Since the source bandwidth is so large, the intensity-noise spectrum at the receiver is expected to be completely flat over the receiver bandwidth. Clearly, there are some discrete tones in the measured intensity spectrum, and these are thought to be due to imperfect RF isolation of the source power supply and modulation circuitry. The peak at just below 100 MHz corresponds to the FM radio station 98RDU broadcasting at 98.3 MHz from the University of Canterbury.

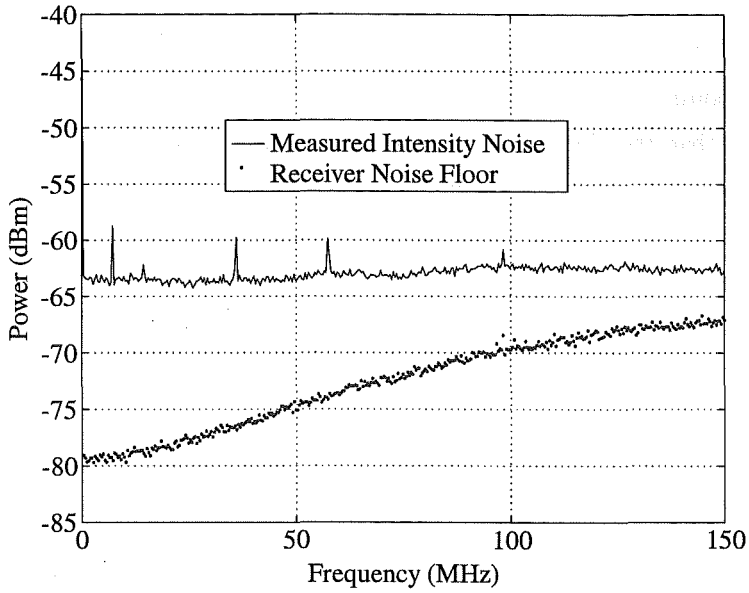

Figure 4.3 Intensity-Noise Spectrum

The noise level was measured at 10 MHz for various power levels in both the unpolarised and polarised cases. 10 MHz was chosen as a convenient setting well away from any $\frac{1}{f}$ noise, with no discrete lines immediately nearby, and not far from the receiver-noise minimum. In Figure 4.4, comparison is made between the expected noise level from a thermal source, with degree of polarisation $P = 0.32$ and coherence time $\tau_c = 71$ fs, and the directly measured intensity noise, after subtracting the levels of shot noise and receiver noise. The error bars

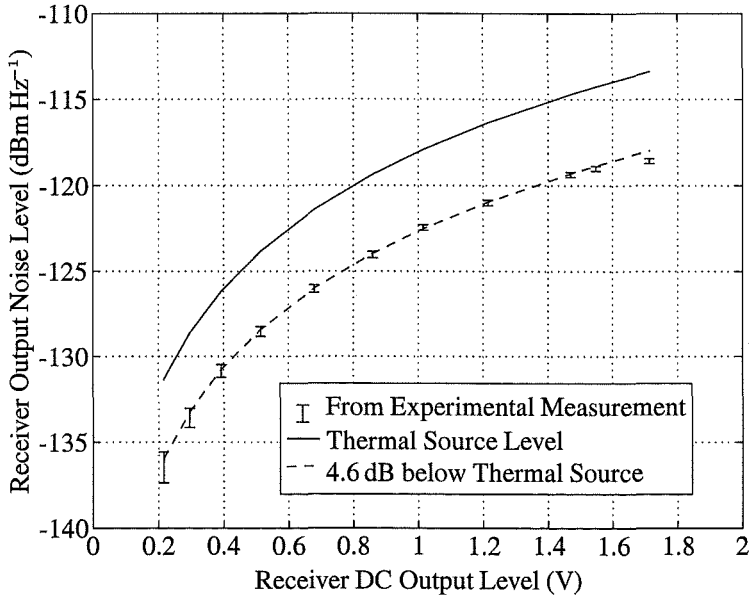

Figure 4.4 Comparison of Measured Noise Level with that from a Thermal Source, at 10 MHz

are dominated by the ± 0.1 dB uncertainty in the actual noise measurements, although other uncertainties are included. The DC coupled receiver starts to saturate above about 1.5 V, and

hence the measured noise levels are less than expected for high powers. The error bars become larger as the power is reduced since the receiver noise floor is being approached. Unfortunately, the receiver was not AC-coupled, since this would have allowed measurement at higher powers, further from the receiver noise floor.

It can be seen that the light intensity noise of the diode is suppressed by about 4.6 dB from that of an ideal thermal source. However, when measuring the intensity noise through a PBS, and with the polarisation controller adjusted for maximum power difference between the PBS outputs, the relative intensity noise of each output was found to be different, with the light of the polarisation state with the majority of the power having the lower noise level. Furthermore, adding these levels independently gave more noise than that without the PBS as in Figure 4.4, so the intensity noise of each polarisation appeared to be correlated, with some degree of cancellation when the two were summed, unlike that of an ideal thermal source.

Clearly, the actual intensity-noise levels and polarisation dependencies of this source are quite different from those of a thermal source with identical characteristics otherwise, although the noise levels all have the same power dependence. However, this is not dwelt on or investigated closely here, since demonstrating the generation of PIIN through interference was the primary aim, and all source intensity noise can be greatly attenuated at a particular frequency, as described in the following section.

4.2.2 PIIN Measurement

Due to the fact that only a single broadband source was available, PIIN was generated by combining part of the SLD output with a time-delayed component from the same source, according to the arrangement shown in Figure 4.5. The path-length difference between the two 3 dB couplers was nominally 10 m, corresponding to a time delay of approximately 50 ns. Since the source coherence time is only 71 fs, there was no coherence between the light from the paths being combined in the second coupler. In this respect, PIIN is generated as though the light was from two independent sources of the same specifications. However, due to the use of a single source, the intensity noise of the light in each path is correlated, which would not have been the case if two separate sources had been used.

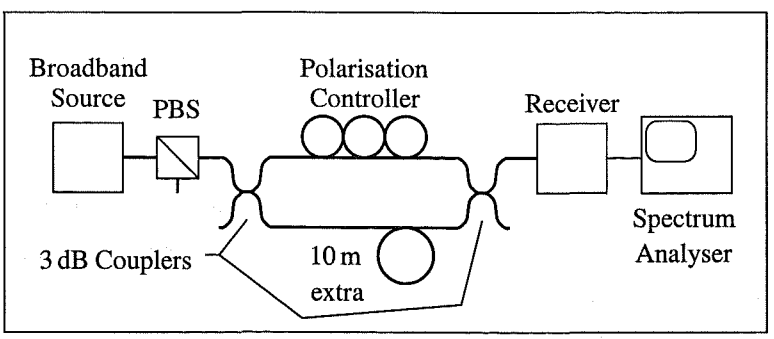

Figure 4.5 Experimental Arrangement for PIIN Measurement

The interferometer structure of Figure 4.5 acts as a spectral filter, and it is simple to show that the spectral-intensity transmission of such an interferometer is given by $\frac{1}{2}(1+\cos(2\pi f \tau_d))$, where τ_d is the time delay between the two paths of the interferometer, f is frequency, and assuming equal power in each interferometer arm. The intensity transmission spectrum shown in Figure 4.6 was recorded through direct modulation of the source drive current, which was swept across the spectrum. By slightly attenuating the interferometer path with the larger power, a good power balance was obtained in the interferometer of Figure 4.5, as indicated by the null depth of -42 dB apparent in Figure 4.6. The shape of the response closely matches the theoretical shape expected, and the position of the first null at 9.86 MHz corresponds to a interferometer delay of 50.92 ns. The insertion loss of the polarisation controller was observed to vary very slightly as the polarisation was changed. However, the null at 9.86 MHz remained below -30 dB across the full range of polarisation manipulation. Consequently, by measuring the noise levels at 9.86 MHz with the source unmodulated, the intensity noise is attenuated by at least 30 dB, rendering it insignificant compared to the receiver noise floor. This occurs regardless of whether the intensity variation is from the source itself or from any residual modulation due to incident RF signals. A balanced detection system would ideally balance out any source intensity noise at all frequencies simultaneously, rather than just at discrete frequencies, as in the configuration of Figure 4.5. However, a balanced receiver with sufficiently low noise was not available.

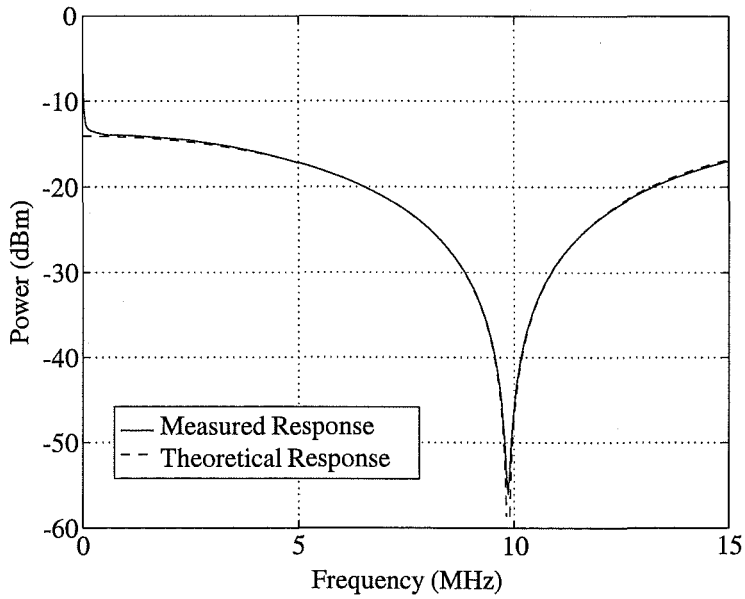

Figure 4.6 Intensity Transmission Spectrum

The plot in Figure 4.7 is calculated by subtracting the levels of shot noise and receiver noise from the noise measured at 9.86 MHz in the arrangement of Figure 4.5, with the polarisation controller adjusted for maximum noise. This ensures that the light polarisation is the same in each input to the second 3 dB coupler, and the degree of polarisation at this point was measured to be $P = 0.98$. Consequently, the remaining noise should be solely due to the

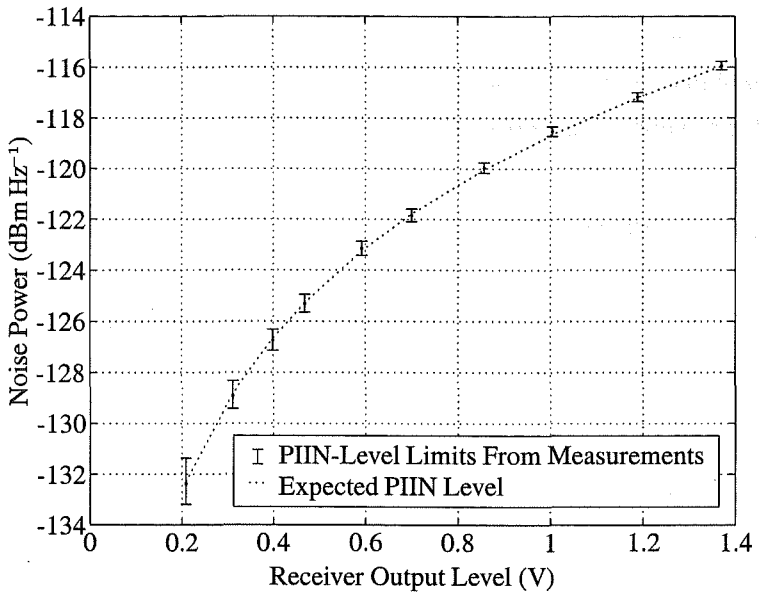

Figure 4.7 Comparison between Measured and Theoretical PIIN Levels

two identically-polarised incoherent fields interfering at the second 3 dB coupler. The error bars in Figure 4.7 represent the total uncertainty assuming that the noise measurements are all ± 0.1 dB, the receiver voltage levels are $\pm 2\%$, the coherence time is $\tau_c = 71 \pm 1$ fs, and the combined responsivity of the receiver and its transimpedance gain are $32 \pm 1.6\,\mathrm{V\,mW^{-1}}$. The difference between the measured noise levels with the polarisation controller adjusted for maximum and minimum noise actually corresponds to a degree of polarisation of $P = 0.95$, and this value is used in calculating the expected PIIN level in Figure 4.7. The difference in PIIN level from that with $P = 1$ is barely noticeable on the scale of Figure 4.7, and the PIIN levels in both cases are still within the experimental limits. With the polarisation controller adjusted so that the measured noise level is minimised, the light in each arm is near-orthogonally polarised, so shot and receiver noise predominate, and the measured noise levels are within 0.4 dB of that thus expected. It is therefore clear that the theoretically expected PIIN level matches the actual measurements to within the limits of the experimental uncertainty.

As with the experimental configuration used in [Yurek *et al.* 1987], here the source intensity noise has been balanced out when the PIIN was measured, clearly illustrating that the PIIN level is quite distinct from any source intensity noise. This highlights the minor error in [Smith *et al.* 1995], in which the factor K_{sp}, representing the factor by which the source intensity noise is suppressed with respect to that of a thermal source, remained in the noise level and SNR expressions when PIIN was the dominant form of noise. However, the graphs and conclusions in [Smith *et al.* 1995] are nonetheless correct, since $K_{sp} = 1$ was subsequently assumed. At best, the factor K_{sp} only applies to the source-intensity-noise components of the noise expressions, and as can be seen from Equation 3.29, these are dominated by the PIIN except when there are very few users. At most, the effect upon the total intensity noise of $K_{sp} > 1$ is to replace

$(K+1)$ by $(K-1+\frac{2}{K_{sp}})$ in Equation 3.29. However, it is expected that for any broadband incoherent source with its intensity noise suppressed below that of a thermal source ($K_{sp} > 1$), the spectral-amplitude filtering reduces this level of suppression somewhat. Unfortunately, it was not possible to verify or quantify this experimentally with the available equipment.

4.3 PIIN REDUCTION USING MMF

The generation of PIIN occurs when uncorrelated fields are mixed, and this requires the fields to be spatially coherent. The use of SMF ensures that any light transmitted along the fibre is completely spatially coherent within each of two (spatially) orthogonal polarisation states. By using MMF rather than SMF, any transmitted light becomes spread amongst the many propagation modes in the fibre, and mixing can only occur between fields within each spatially coherent mode. Hence, the use of MMF rather than SMF is expected to significantly reduce PIIN levels. In the following sections, experimental investigation of this PIIN reduction is described, and the results are compared with theoretical predictions.

4.3.1 PIIN Measurement with MMF

The experimental arrangement used for measuring the PIIN is shown in Figure 4.8. The only difference between this arrangement and that for the SMF case (Figure 4.5), is that the final 3 dB coupler is now an MMF 3 dB coupler, with 14 m of MMF in each path of the interferometer before the final coupler. Other MMF lengths (0.5 m and 105 m) were also used for comparison, as discussed later in this section. As in Section 4.2.2, the power balance in the interferometer was adjusted so that any source intensity noise was attenuated by at least 30 dB at the measurement frequency, which was again 10 MHz.

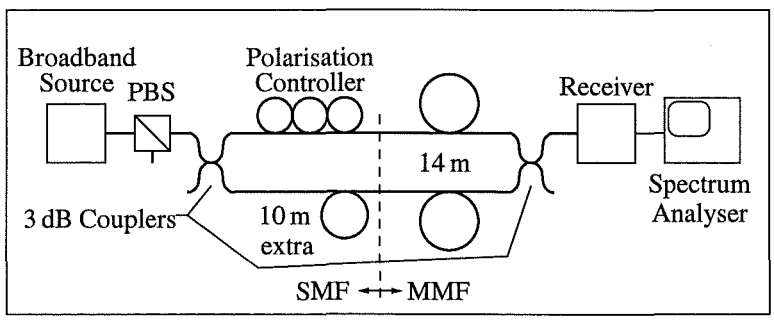

Figure 4.8 Experimental Arrangement for PIIN Measurement with MMF

In Figure 4.9 the PIIN levels are compared to those expected when using SMF, where again the nominal levels of receiver and shot noise have been subtracted from the actual noise measurements. These noise measurements were made with the polarisation controller adjusted for maximum noise. The error bars represent the uncertainty arising from reasonable tolerances in measurements and specifications or calibrations, as in Section 4.2.2. These error bars are

larger than those in Figure 4.7, and this is primarily due to the lower PIIN level, since it is closer to the receiver noise floor.

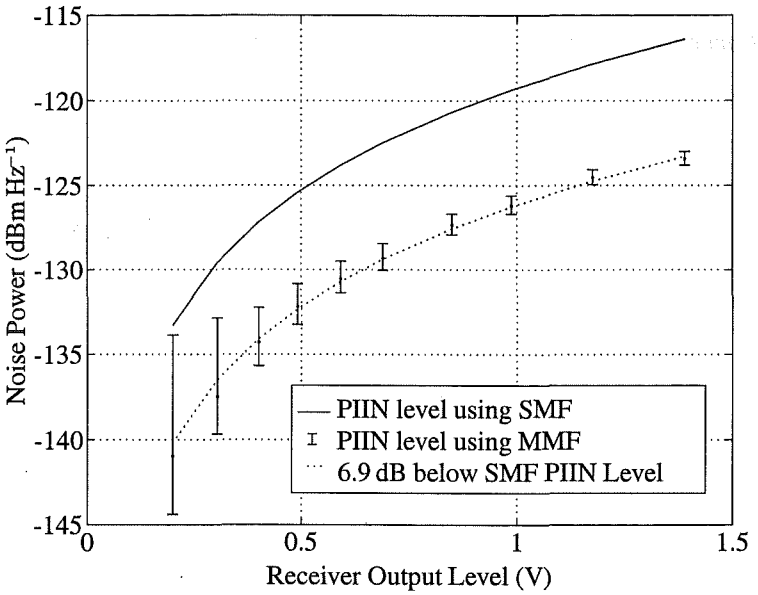

Figure 4.9 Comparison between PIIN Levels with Single-Mode and Multimode Fibre

Since the available polarisers all had SMF pigtails, accurate direct measurement of the overall degree of polarisation P at the MMF coupler was not possible. However, the degree of polarisation of the light coupled from 14 m of MMF back into SMF was measured, giving the approximate value $P \approx 0.85$. Hence, there was a reduction in polarisation degree of at least some of the light over the 14 m of MMF. Furthermore, the difference between the noise levels measured with the polarisation controller adjusted for maximum and minimum noise can be used to estimate the degree of polarisation at the MMF coupler. The degree of polarisation was thus estimated to be $P = 0.82 \pm 0.01$, which is slightly less than that measured from the light fraction launched back into SMF. This is not unreasonable, assuming a general reduction in overall degree of polarisation with MMF length. The value $P = 0.82 \pm 0.01$ is then used in determining the PIIN level with SMF in Figure 4.9, following Equation 3.16.

By weaving various MMF sections through a bed-of-nails arrangement, together with other fibre manipulations, it was attempted to modify the coupling between modes in the fibres. However, no significant differences in noise spectra or levels were observed during this.

The experiment was repeated with the MMF coupler directly connected to the SMF, so the MMF lengths before the coupler were simply the 0.5 m MMF pigtails. The noise variation with polarisation state adjustment was within the experimental error of that expected for the degree of polarisation in the SMF ($P = 0.98$). The PIIN level measured with this 0.5 m MMF length was only 4.4 dB below that expected with SMF, which is significantly less than that found with 14 m of MMF. The experiment was repeated again with 105 m of MMF in each interferometer path, which was the greatest MMF length available. After this length of MMF, using an SMF-pigtailed PBS to estimate the polarisation degree, $P \approx 0.7$ was found. However,

the variation in noise level when adjusting the polarisation controller in the interferometer indicated $P = 0.9$, which was unexpectedly higher than both that of the fraction coupled into SMF, and of that measured with 14 m of MMF. Hence, the polarisation degree after 105 m of MMF was not accurately known. If it is assumed that this polarisation degree is in the range $0.6 < P < 0.8$, then the measured PIIN levels with 105 m of MMF were between 7.8 dB and 8.6 dB below that expected using SMF, and with the same degree of polarisation.

With the minimum MMF length, the PIIN level was reduced by about 4.5 dB, which indicates that most of the light in the MMF was spread amongst only a handful of modes. This is not unreasonable under the assumption of ideal alignment of the adjacent SMF and MMF connectors, since the MMF modes initially excited are likely to be only those which closely match the shape of the SMF mode. The PIIN level was observed to decrease as the MMF length was increased, and the polarisation degree decreased also, indicating that the light power was spreading out amongst the fibre modes.

In the following sections, the mode structures of the fibres are examined, and for the experimental configuration of Section 4.3.1, these are used to estimate the power in each of the modes initially launched into the MMF. The differences expected between step-index and graded-index MMF are discussed, and a heuristic approach to obtain an estimate of the PIIN reduction for much longer MMF lengths is also outlined.

4.3.2 Step-Index MMF Mode Structure

Applying Maxwell's equations to a cylindrical step-index fibre, assuming zero conductivity and negligible absorption, it is convenient to use cylindrical polar coordinates (z,r,θ), and in terms of the longitudinal component of electric field E_z, the wave equation is then expressed as [Agrawal 1992]

$$\frac{\partial^2 E_z}{\partial r^2} + \frac{1}{r}\frac{\partial E_z}{\partial r} + \frac{1}{r^2}\frac{\partial^2 E_z}{\partial \theta^2} + \frac{\partial^2 E_z}{\partial z^2} E_z + \omega^2 \epsilon \mu E_z = 0 \tag{4.1}$$

In [Agrawal 1992], E_z is implicitly assumed to be the Fourier transform of the time-varying field in general, but by assuming monochromaticity here, the fields simply have time dependence $\exp(j\omega t)$, of angular optical frequency ω. The medium permeability μ and permittivity ϵ are represented as usual. The solution of this equation is straightforward, and can be found in [Agrawal 1992] and in many other fibre-optics and electromagnetics texts, - the details are omitted here. In summary, the longitudinal and angular dependence of E_z are simply complex exponentials, and the radial dependence of E_z is governed by Bessel's differential equation. Under the constraints that E_z is finite for $r < a$, where a is the fibre core radius, that E_z tends

to zero for $r > a$, and that E_z is continuous at $r = a$, E_z is expressed as

$$E_z = \begin{cases} A\frac{\mathrm{J}_\xi(\kappa r)}{\mathrm{J}_\xi(\kappa a)} \exp(j\xi\theta) \exp\big(j(\omega t - \beta z)\big), & r \leq a \\ A\frac{\mathrm{K}_\xi(\gamma r)}{\mathrm{K}_\xi(\gamma a)} \exp(j\xi\theta) \exp\big(j(\omega t - \beta z)\big), & r > a \end{cases} \tag{4.2}$$

where

$$\kappa^2 = \left(\frac{\omega n_1}{c}\right)^2 - \beta^2 \tag{4.3}$$

and

$$\gamma^2 = \beta^2 - \left(\frac{\omega n_2}{c}\right)^2 \tag{4.4}$$

In Equation 4.2, $\mathrm{J}_\xi(\kappa r)$ is the ξth Bessel function of the first kind, $\mathrm{K}_\xi(\gamma r)$ is the ξth modified Bessel function of the second kind, and A is a constant relating to the power of the mode. The wave is assumed to propagate in the positive z direction, with propagation constant β, and hence wavelength $\lambda = \frac{2\pi}{\beta}$. The angular dependence is governed by azimuthal index ξ, which must be an integer. The variables n_1 and n_2 are the refractive indices of the fibre core and cladding respectively, and c is the speed of light in a vacuum. The variable κ is the transverse component of the wave vector in the core $\frac{\omega n_1}{c}$, with longitudinal component β. Similarly $j\gamma$ is the transverse component of the wave vector $\frac{\omega n_2}{c}$ in the cladding, with longitudinal component β also. Mode parameters are often displayed in terms of the normalised frequency V, which can be expressed as

$$V^2 = (\kappa a)^2 + (\gamma a)^2 = \frac{\omega^2 a^2}{c^2}(n_1^2 - n_2^2) = \frac{4\pi^2 a^2}{\lambda^2} NA^2 \tag{4.5}$$

where the equivalence from Equations 4.3 and 4.4 has been included, along with the implicit definition of the fibre numerical aperture NA.

A wave equation similar to Equation 4.1 exists for the z-component of the magnetic field H_z, and the solutions for H_z are the same as Equation 4.2, except for the appearance of a multiplicative factor $\frac{n_2}{n_1}$ in the cladding field expression, and a different constant A. The knowledge of both E_z and H_z is sufficient to specify any mode, since the radial and angular field components E_r, E_θ, H_r, and H_θ are uniquely determined by E_z and H_z through Maxwell's equations [Agrawal 1992]. The tangential field components at the core-cladding boundary (E_z, H_z, E_θ, H_θ) must be continuous, and this condition gives rise to a quadratic eigenvalue equation. In general, both E_z and H_z are non-zero, except when $\xi = 0$, so that the modes are described as hybrid (rather than transverse) modes. The eigenvalue solutions fall into two groups, one corresponding to hybrid modes for which H_z is dominant, which are termed HE modes, and the other corresponding to hybrid modes for which E_z dominates, which are termed EH modes

[Agrawal 1992][1]. These are generally denoted $HE_{\xi p}$ and $EH_{\xi p}$, where ξ is the azimuthal index, and $p = 1, 2, \ldots$ identifies the pth solution to the eigenvalue equation for each ξ, numbered from the smallest value of κ. In the particular case where $\xi = 0$, solutions do exist with either $E_z = 0$ or $H_z = 0$, so HE_{0p} and EH_{0p} can be represented as TE_{0p} (transverse electric) and TM_{0p} (transverse magnetic) respectively [Agrawal 1992].

If the relative difference between the refractive indices of the fibre core and cladding is very small, that is $\frac{n_1 - n_2}{n_1} \ll 1$, as is the case for optical fibres with small numerical aperture, then the fibre is said to be weakly guiding. In this case, both E_z and H_z are small with respect to the transverse field components, and it can be shown that there is a solution to the wave equation that is very nearly transverse and linearly polarised [Gloge 1971]. In this approximate solution, E_y is taken to have the form of Equation 4.2, $H_x = -\frac{n}{Z_0} E_y$, where $Z_0 = \sqrt{\frac{\mu_0}{\epsilon_0}}$ is the vacuum impedance, $n = n_1$ or $n = n_2$ for the core or cladding respectively, and E_x, H_y, E_z, and H_z are all considered negligible. These linearly polarised modes are denoted $LP_{\xi p}$ in the same manner as for the exact hybrid-mode notation, and finding the eigenvalues κ and γ in Equation 4.2 is reduced to solving the equation [Gloge 1971]

$$\frac{\mathrm{J}_\xi(\kappa a)}{\mathrm{J}_{\xi-1}(\kappa a)} = -\frac{\kappa}{\gamma} \frac{\mathrm{K}_\xi(\gamma a)}{\mathrm{K}_{\xi-1}(\gamma a)} \tag{4.6}$$

Each $LP_{\xi p}$ mode can have one of two orthogonal polarisations, and there is a further degeneracy of two due to the $\exp(j\xi\theta)$ term, so that there are actually four degenerate modes for each $LP_{\xi p}$ when $\xi > 0$, and two otherwise. Note that although the modes of the approximate and exact solutions are denoted similarly, in general each of the degenerate $LP_{\xi p}$ modes corresponds to a linear combination of the two degenerate forms of each of the exact modes $HE_{\xi+1,p}$ and $EH_{\xi-1,p}$, where $EH_{-1,p}$ is treated as zero [Gloge 1971]. This recombination of degenerate hybrid modes into approximate LP modes is possible since they have approximately the same β. In particular, the fundamental mode of the fibre is the HE_{11} mode, which is approximately represented by the LP_{01} mode, when $\frac{n_1 - n_2}{n_1} \ll 1$. The fundamental mode has the smallest κ value, but in particular, it has no low-frequency cutoff, and hence a step-index optical fibre can always support the HE_{11} mode. When the optical frequency is lower than the cutoff frequencies of all the higher modes, then only the HE_{11} mode remains, and the fibre is termed single-mode (SMF). This criterion for step-index SMF requires $V < 2.405$, corresponding to the ratio of wavelength to core radius

$$\frac{\lambda}{a} > 2.613NA \approx 2.613 n_1 \sqrt{2\Delta} \tag{4.7}$$

where Δ is the fractional difference $\Delta = \frac{n_1 - n_2}{n_1} \ll 1$.

[1]There is a conflict between this designation, (also used in [Ramo *et al.* 1984] and [Green Jr 1993]) and that in the analyses of [Gloge 1971] and [Snyder and Love 1983], in which both the modes TE_{0p} ($E_z = 0$) and TM_{0p} ($H_z = 0$) appear as the two degenerate modes of EH_{0p}

4.3.3 Graded-Index MMF Mode Structure

Graded-index MMFs are generally designed to have significantly lower modal dispersion than step-index MMF, while not requiring the small core radii of SMFs. As the name implies, the refractive index of the fibre core is not constant, but it varies with radial distance out to the cladding, which typically has constant refractive index. The refractive index generally has the form [Agrawal 1992]

$$n(r) = \begin{cases} n_1\left(1 - \Delta\left(\frac{r}{a}\right)^{\zeta}\right), & r < a \\ n_1(1-\Delta) = n_2, & r \geq a \end{cases} \tag{4.8}$$

where n_1 is now the refractive index at the fibre centre only, n_2 is the cladding refractive index as before, and Δ is the fractional difference between them ($\Delta \ll 1$). The modal-dispersion minimum occurs at $\zeta = 2(1-\Delta)$ theoretically, although it is modified somewhat by material dispersion, so most fibres have a near-quadratic index profile.

Under the assumption that $\Delta \ll 1$, and that the index profile is quadratic, given by the upper portion of Equation 4.8 with $\zeta = 2$, the square of the refractive index is then given by

$$n^2(r) = n_1^2\left(1 - 2\Delta\left(\frac{r}{a}\right)^2\right) \tag{4.9}$$

where the term in Δ^2 has been neglected. Assuming that the index profile follows Equation 4.9, that $\Delta \ll 1$, and that the index change over a wavelength is small, then an approximate wave equation is found that can be solved for a transverse component of the electric field E_t to get [Snyder and Love 1983]

$$E_t = A\left(\frac{r}{w}\right)^{\xi} \mathrm{L}_{p-1}^{(\xi)}\left(\frac{2r^2}{w^2}\right) \exp\left(\frac{-r^2}{w^2}\right) \exp(j\xi\theta) \exp\big(j(\omega t - \beta z)\big) \tag{4.10}$$

where A is a constant, $\mathrm{L}_p^{(\xi)}(u)$ is a generalised Laguerre polynomial of degree p, defined as [Gradshteyn and Ryzhik 1965]

$$\mathrm{L}_p^{(\xi)}(u) = \sum_{i=0}^{p} (-1)^i \binom{p+\xi}{p-i} \frac{u^i}{i!} \tag{4.11}$$

and w is the $\frac{1}{e}$ beam radius of the fundamental mode, given by

$$w^2 = \frac{a\lambda}{2\pi n_1}\sqrt{\frac{2}{\Delta}} = \frac{2a^2}{V} \tag{4.12}$$

where the normalised frequency V is given by

$$V = \frac{2\pi a n_1 \sqrt{2\Delta}}{\lambda} \tag{4.13}$$

The azimuthal index is again denoted ξ, and $p = 1, 2, \ldots$ represents the pth solution for each ξ. The propagation constant β of each mode is given by [Snyder and Love 1983]

$$\beta_{\xi p} = \frac{V}{a\sqrt{2\Delta}}\left(1 - \frac{4\Delta}{V}(2p + \xi - 1)\right)^{\frac{1}{2}} \tag{4.14}$$

This mode structure parallels that in the weakly guiding treatment of [Gloge 1971] for step-index fibre, where longitudinal field components are small, and modes of almost equal propagation constant can be paired to give modes of approximately linear polarisation.

This analysis and mode representation does not include the fact that the quadratic index dependence upon radius only applies for $r < a$, but this reality restricts the mode propagation constants, since a mode must have $\beta < \frac{2\pi n_2}{\lambda}$ in order to be guided by the fibre. This limit can be used along with Equation 4.14 to determine the possible ranges of ξ and p, but in general, for large V, the total number of guided modes supported by the fibre is given by $\frac{V^2}{4}$ [Snyder and Love 1983]. The representation of any mode which is not of insignificant level beyond the edge of the graded-index core is correspondingly limited with this structure. It can also be shown that a fibre with parabolic index profile becomes single-mode for $V < 3.5$ [Kao 1988].

4.3.4 Estimation of the Initial PIIN Reduction using MMF

If an incoherent source with no mode structure is adjacent to the end of an MMF, then it is expected that the power launched into the MMF is equally distributed amongst the modes of the fibre [Gloge 1971]. This is reasonable with a source that spontaneously emits incoherent light in all directions, such as many LEDs. In this case, the PIIN levels resulting from the mixing of the guided light with that from a similar source via MMF is expected to be reduced by the number of spatially orthogonal modes. The number of modes in a step-index MMF is approximately $\frac{V^2}{2}$ for large V, and for graded-index MMF with a power-law profile (Equation 4.8), the number of modes is approximately $\frac{V^2}{2}\frac{\zeta}{\zeta+2}$, also for large V [Snyder and Love 1983]. Typical values for such MMFs are a core radius of $a = 25\,\mu$m, a maximum refractive index $n_1 = 1.45$, relative refractive-index difference $\Delta = 0.01$, and $\zeta = 2$. For wavelengths in the range $1.2\,\mu\text{m} < \lambda < 1.6\,\mu\text{m}$, the normalised frequency is within the range $20 < V < 27$, so for such a step-index MMF, there are between 200 and 360 modes, according to the wavelength, and likewise between 100 and 180 modes for such a parabolic graded-index MMF. This suggests that the PIIN can be reduced by 20 dB or more, which is very significant. However, broadband sources to be used in SMF systems are either designed to couple as much power as possible into SMF, or they are built within SMF itself. In both of these cases, the resulting guided light is then confined within the single mode of the SMF, whose characteristics are easily specified. If such an SMF is butted to an MMF, assuming no angular or transverse displacement, then the modes initially excited in the MMF are intuitively expected to be primarily those with similar radial dependence, and with the same azimuthal index. Theoretically, assuming a weakly guiding MMF, the mode coefficients can be found by matching the incident

transverse field components with those of each mode, which can be simply performed due to the mode orthogonality [Kao 1988]. Hence, the intuitive picture is also reasonable theoretically, and only a subset of the modes in the MMF are initially excited with an incident field from SMF.

Using the known parameters of the actual source and fibres used in the experiment described in Section 4.3.1, along with the theoretical mode structure from Sections 4.3.2 and 4.3.3, and assuming ideal axial alignment of the single-mode and multimode fibres, the initial mode excitation in the MMF can be found. The MMF was standard graded-index MMF of 50/125 μm core/cladding diameter, with numerical aperture $NA = 0.2$, and the maximum refractive index is assumed to be $n_1 = 1.45$ (that of silica at about 1.3 μm [Kao 1988]), thus giving an index difference $\Delta = 0.01$. At the wavelength 1.3 μm, the normalised frequency is $V = 24.1$, so the number of modes in the MMF is approximately 145. The SMF has core diameter 8.7 μm, and is single-mode for at least the 1.3 μm band and longer. Using this diameter and again assuming $n_1 = 1.45$, the index difference must be about $\Delta = 0.0027$ for a step-index fibre to be single-mode for $\lambda > 1.2\,\mu$m, which gives numerical aperture $NA = 0.11$, and these are not atypical parameters [Agrawal 1992]. The value of Δ is certainly very much less than unity for both fibres, which means the weakly guiding approximations in Sections 4.3.2 and 4.3.3 are reasonable.

In the absence of any misalignment which modifies the angular dependence of the incident field, the HE_{11} mode in the SMF can only excite the HE_{1p} MMF modes, and it is assumed that the fibre end-faces are sufficiently close that all other effects can be simply modelled by the appropriate power loss (Fresnel reflection, for example). The SMF output was fully polarised in the experimental arrangement of Figure 4.8, and it is assumed that whatever the output polarisation state, any HE_{1p} MMF modes excited also have this polarisation initially. The modes in the MMF are approximately transverse, with radial dependence given by Equation 4.10 with $\xi = 0$ and $w \approx 7.2\,\mu$m using the parameters above, and angular dependence purely according to the polarisation of the incident SMF field. Note that although the source bandwidth (Figure 4.1) does not support the monochromatic assumptions in Sections 4.3.2 and 4.3.3, the mode field patterns in both the SMF and MMF have the same dominant wavelength dependence, which is sufficient to estimate the proportions of power in orthogonal groupings. It is also true that at the electronic bandwidths of interest, and certainly at the PIIN measurement frequency of 10 MHz here, that any two interfering optical frequency components that generate in-band PIIN must be extremely narrowband in terms of optical frequency. The fundamental HE_{11} MMF mode simply has a Gaussian profile, and the higher HE_{1p} modes have narrower main lobes, each undergoing $p-1$ phase reversals as r increases from zero, as shown in Figure 4.10 for $p \leq 4$.

The mode shapes corresponding to both step-index and parabolic graded-index SMFs with $a = 4.35\,\mu$m, $n_1 = 1.45$ and $\Delta = 0.0027$ are also shown for $\lambda = 1.302\,\mu$m in Figure 4.10. It can be seen that in the absence of any misalignments, the SMF mode shapes are going to excite mainly the first two or three MMF modes, and this is borne out by the modal decompo-

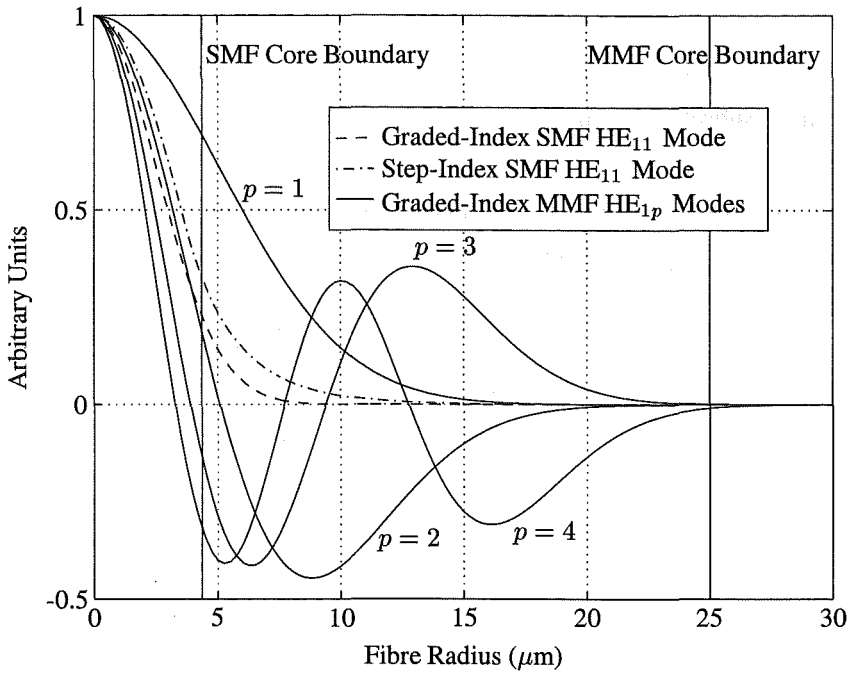

Figure 4.10 Radial Dependence of the HE_{11} SMF and HE_{1p} MMF Modes

sition results shown in Figure 4.11, which were obtained by integrating, with respect to area, the product of the incident field with each normalised-power MMF mode. From Equation 4.14

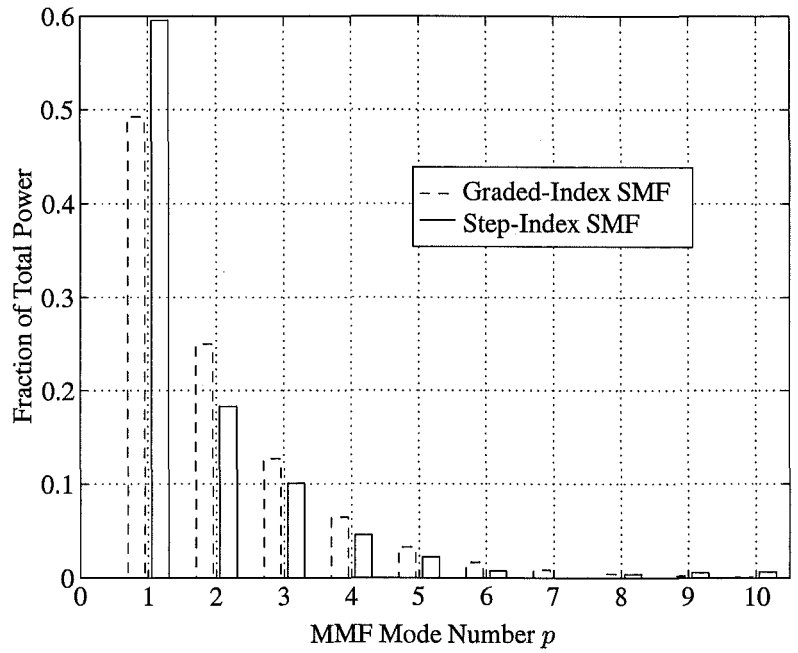

Figure 4.11 Initial MMF HE_{1p} Mode Excitation Due to Incident SMF Field

it can be determined that $p \leq 6$ is necessary for the HE_{1p} modes to be guided modes with the MMF parameters above, so the power in the higher modes of Figure 4.11 is lost. The expected PIIN levels for these distributions up to $p = 6$, with respect to that of a single mode, are

-4.9 dB and -4.0 dB for the graded-index and step-index SMF mode shapes respectively, and these levels are both in the vicinity of the 4.4 dB reduction measured experimentally. The connections between the MMF and SMF were made with fine-tolerance polished ceramic-ferrule terminations and sleeves, but they are nonetheless not perfect. While mechanical misalignment would definitely significantly alter the initially-excited MMF modes, it is assumed that unless the coupling loss is high, that the same order of mode excitation would occur as predicted here for the modes arising in the ideally aligned case. It is also true that the fibre characteristics are not fully known, but they are certainly somewhere close to those assumed here, and even if the unknown parameters depart significantly from typical values, the corresponding range of PIIN levels is still between -3.5 dB and -5.5 dB relative to that of SMF.

As the light within the initially excited modes propagates along the MMF, there are many bends, twists, impurities, and other imperfections which scatter or couple the light into different fibre modes (and their polarisations), and some light is also lost by scattering into non-guided modes. This is reflected in the experimental observation of further PIIN reduction with increasing fibre length, as the light spread amongst more orthogonal modes. The mode coupling is generally small, and assuming that the coupling is random, after a sufficient length of propagation the set of modes reaches a form of equilibrium. After this point, the dispersion then increases as the square root of distance rather than being proportional to distance, due to the coupling of power between fast and slow modes [Kao 1988]. Strong coupling between modes may occur whenever there is a periodic perturbation from the ideal cylindrical waveguide, where this period matches the difference between the propagation constants of the strongly coupled modes. During the experimental investigation various sections of MMF were bent in an approximately periodic fashion to try and introduce some such strong mode coupling that would noticeably modify the noise level, but this was not successful. The length at which the light becomes sufficiently spread amongst the modes to be in equilibrium depends on the quality of the fibre, and for graded-index MMF with a loss due to coupling into non-guided modes of 1 dB km^{-1} or less, this length is of the order of 1 km or more [Kao 1988]. The overall loss specification of the MMF used in the experimental investigation was 1 dB km^{-1}, and it is therefore concluded that the 100 m MMF lengths available were not long enough for this equilibrium to be reached. The experimentally observed increase in PIIN reduction with MMF length is therefore expected to have continued until the fibres were about a kilometre long. The question that naturally arises then is just what the PIIN level reduction is for a sufficiently long MMF, and in the following section a heuristic approach is used to get some idea of what this might be.

4.3.5 Heuristic Estimation of the Maximum PIIN Reduction using MMF

The greatest possible PIIN reduction occurs when the power in every MMF mode is equal, and this reduction is then given by the number of MMF modes, assuming comparison to the fully polarised SMF case (ie truly single-mode). Although the total number of modes in a step-index

MMF is twice that of a graded-index MMF with the same normalised frequency, the dispersion in a graded-index MMF is typically smaller by a factor of 50 or more [Green Jr 1993], so the use of step-index MMF is unlikely. In Section 4.3.1, the measured PIIN levels with MMF were compared with that of SMF with the same polarisation state, so the greatest such reduction is given by half of the total number of modes, giving a factor of about 72, or 18.6 dB. In this section two simple models are assumed for the mode coupling due to fibre deformations and other imperfections. These models are then applied to the initial power distributions of Figure 4.11, and iterated until the total mode power distributions approach shapes that are approximately constant under these mode-coupling models. Hence, an indication is obtained of what the MMF PIIN reduction may be in the large-length limit.

The first model for the mode coupling is simply that at each coupling point, there is a small amount of scattering from a single randomly selected mode into every other mode. The amount of power coupled out of the particular mode at such points is chosen to be 1%, and this power is spread amongst every mode according to an exponentially decreasing function (from $\exp(0)$ to $\exp(-x)$), where the exponent x is chosen as 10. This corresponds, for example, to half of the power being distributed among 10 out of 145 modes, a quarter of the power amongst the next 10, and so on. In addition, the modes into which the power is coupled are chosen randomly, so that those modes receiving the greatest contribution from another mode are not the same at each coupling point.

The initial power distributions were chosen to be those shown in Figure 4.11 for $p \leq 6$, and zero otherwise, and no other differences between the modes were modelled. After sufficient coupling points ($> 70\,000$), the limiting distribution found in both cases using this coupling model has the power spread quite evenly amongst all the modes, as indicated in Figure 4.12. This is an average of several of the mode-power histograms once the PIIN reduction reached its limit, which was within 0.05 dB of the 18.6 dB maximum reduction with respect to the unpolarised SMF case. Adjustment of the coupling power fraction and exponent varies the rate at which the limit is approached, but the limiting distributions are very similar to Figure 4.12, with only slight width variation, giving no more than 0.1 dB change in PIIN reduction. By adjusting the model so that the modes receiving the greatest contribution from another mode are fixed at each coupling point, after the first random choice, the resulting limiting distribution is slightly broader in comparison, but the PIIN reduction is still only about 0.1 dB smaller than that with equal power per mode.

The second coupling model investigated has weak coupling exactly as in the first model, with coupled power fraction 1% and the exponential index 10, but now after 50 weak coupling points, strong coupling between two randomly selected modes is introduced. This strong coupling is taken to have the form that the power from both modes is redistributed as $0.5(1 - \cos(u))$ and $0.5(1 + \cos(u))$, where u is a random variable uniformly distributed on 0-π. The resultant limiting distribution then has the form shown in Figure 4.13, after more than 70 000 coupling points, and the predicted PIIN reduction is now 2.2 dB less than that with equal power per mode. If this strong coupling is now introduced after only every 100 weak coupling points,

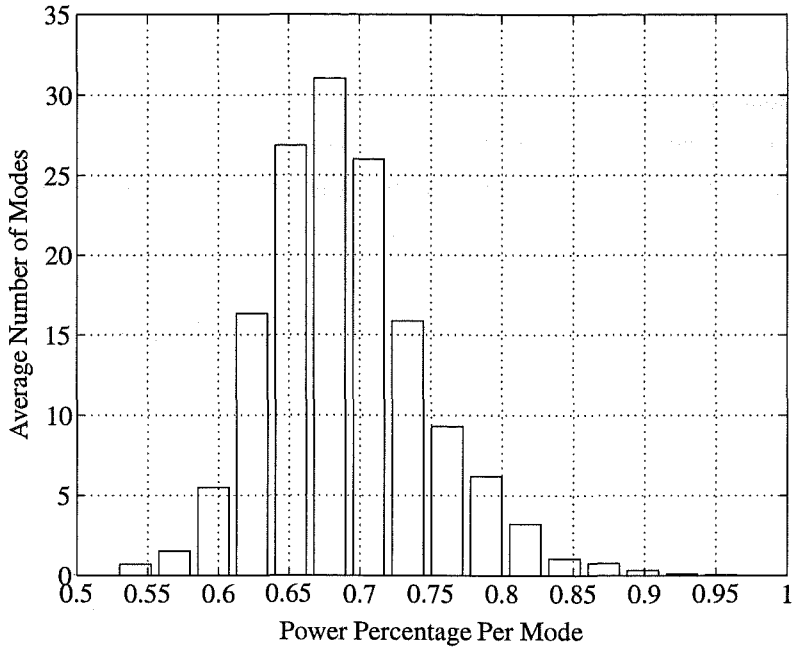

Figure 4.12 Mode Power Distribution in the Limit of Large Fibre Length, with the Weak-Coupling Model

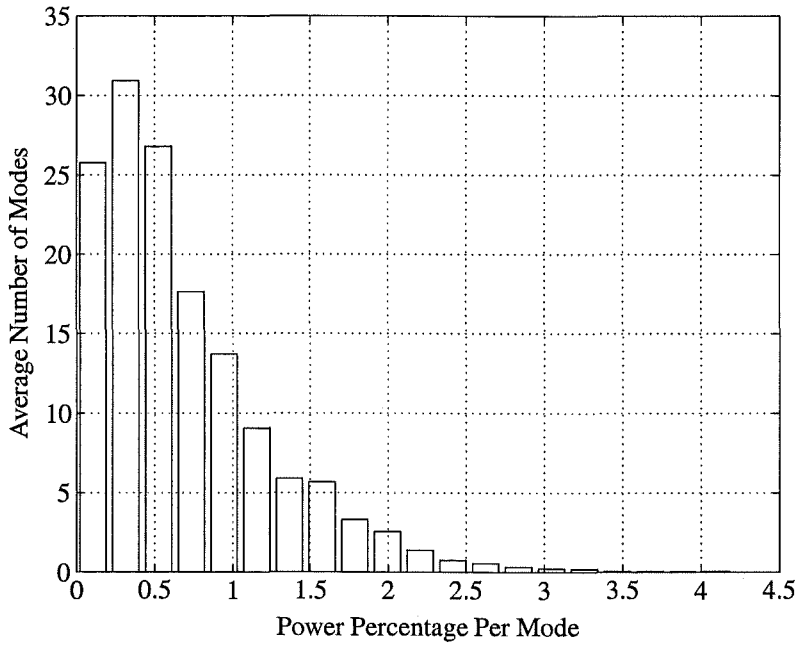

Figure 4.13 Mode Power Distribution in the Limit of Large Fibre Length, with Weak and Strong Coupling

for example, then the limiting distribution is not as broad, and the PIIN reduction is 1.4 dB less than that with equal power per mode. Hence, the introduction of the regular strong coupling into the model has countered the tendency of the weak coupling to spread the power evenly amongst the modes, resulting in a much-less-even power distribution in the limit of large fibre length. The difference in PIIN level reduction from the maximum possible is then basically determined by the relative amounts of strong and weak coupling.

The first indication from this heuristic approach is that if the MMF mode coupling is weak

and if the coupling behaviour does not favour any particular mode (at least on average), then the power eventually becomes evenly distributed amongst the MMF modes. With such a distribution in the long-MMF limit, the corresponding PIIN reduction is virtually at its maximum value. The second indication is that any mechanism which introduces strong coupling or other such strong structure (at least occasionally) can result in a much-less-even power distribution, and hence smaller PIIN reduction with respect to the SMF case. At best, the PIIN reduction with respect to unpolarised fields in SMF is given by half of the total number of modes in the MMF. For typical graded-index MMFs, this factor is of the order of 80, giving a maximum PIIN reduction of about 19 dB.

While these simple models have yielded plausible indications of the MMF PIIN reduction in the limit of large fibre length, this approach is very heuristic, and much better modelling and experimental verification of the reduction in PIIN with large MMF length is needed if this approach to reducing PIIN is seriously considered.

4.4 SUMMARY

This chapter has described the experimental measurement of PIIN levels using interfering beams in SMF from a broadband superluminescent diode, and has verified that the measured levels agree with those from theoretical analysis. The measurement of the PIIN levels was performed in a manner designed to eliminate any intensity variations arising from the source, which would otherwise contribute to measured noise levels.

The experiment to measure the PIIN was repeated with various lengths of MMF rather than SMF, and the PIIN level was observed to be reduced by between 4-8 dB, for MMF lengths between 0.5 m and 105 m respectively. The theoretical mode structures in cylindrical dielectric waveguides have been reviewed, and it has been shown that the measured PIIN reduction for very short MMF length is in accordance with that predicted by this theory. For maximum PIIN reduction, the length of MMF required was found to be an order of magnitude greater than the available MMF length. Via a heuristic approach it was suggested that the maximum PIIN reduction with sufficient lengths of MMF may be within a few decibels of that with equal power in each MMF mode, when the mode coupling is predominantly weak. This maximum reduction with respect to the unpolarised SMF case is about 19 dB for typical graded-index MMF parameters.

Chapter 5

ALTERNATIVE BROADBAND SOURCES

5.1 INTRODUCTION

In Chapter 3, spectral-amplitude OCDMA using broadband thermal sources was found to have a significant SNR limit that cannot be overcome by simply increasing the transmitted power. The limiting noise is proportional to the square of the number of simultaneous users, rather than having a linear dependence, so in this chapter the duty-cycle reduction of the sources is briefly considered. The corresponding conditions under which this may or may not affect the SNR limit are thus determined and discussed. In order to further clarify the origins of the SNR limit found in Chapter 3, the use of two alternative non-thermal broadband sources are also considered with spectral-amplitude coding. The first of these is a source producing ultra-short coherent pulses, which can be thought of as the ultimate low duty-cycle source. These pulses are assumed to be so short that their associated bandwidth extends well beyond the limits of the spectral coding, and hence it is then purely the spectral-amplitude coding that determines the encoded pulse spectrum and the corresponding temporal shape. The other form of broadband source considered in this chapter is that of an array of coherent diode lasers, one laser for each of the spectral elements of the spectral-amplitude coding. The forms of SNR limit that arise with this type of source depend upon the particular characteristics of the lasers in the arrays. These limits are determined and discussed for the various possible and likely source array configurations. The conclusions from all these alternative spectral-amplitude OCDMA configurations are then summarised in Section 5.5.

5.2 DUTY-CYCLE REDUCTION AND TIME GATING

Since the limiting noise of incoherent spectral-amplitude OCDMA is quadratic in the number of simultaneously transmitting users, rather than linear, a simple duty-cycle reduction that linearly reduces both the signal power and the number of simultaneously transmitting users appears advantageous. However, duty-cycle reduction alone cannot improve the SNR limit, as shown in the following example.

Consider the spectral-amplitude OCDMA system as in Chapter 3, but now each user re-

stricts their transmission to a fraction of the bit period $\frac{T_{\text{bit}}}{n}$, with the same maximum source output power. Clearly, the optical signal energy is then reduced by the factor n. At this point, it is easy to think that the original electrical power level now occurs for only $\frac{1}{n}$th of the bit period, and hence the electrical signal energy is only reduced by n also. However, this does not occur since the original receiver bandwidth is only of the order of the data rate, and hence the receiver photocurrent is effectively an average of the optical intensity during the bit period. Consequently, the receiver photocurrent is actually reduced in level by n, and the corresponding electrical signal level (energy or power) is thus reduced by n^2. If it is assumed that all the received optical power is roughly uniformly distributed across each bit period, which is not unreasonable if there are many asynchronous users, and that this light appears thermal, then the photocurrent intensity-noise power due to the incident light is also down by approximately n^2 from the full duty-cycle case. Consequently, there is no gain in the high-power SNR limit. Clearly, the SNRs with respect to shot noise and receiver noise are also reduced by the factor n in this example, but this would not be the case if the average optical power was able to be kept constant while reducing the duty cycle.

The assertion in the opening paragraph of this section is nonetheless correct, - a linear reduction in the electrical signal power along with a quadratic noise reduction does give an increase in the SNR limit. The problem is that it has just been shown that this does not actually occur when the duty cycle is reduced, since both the photocurrent signal power and noise power reductions have the same quadratic dependence.

Continuing with the example of ideal duty-cycle reduction by the factor n, the desired signal light now occurs only within $\frac{T_{\text{bit}}}{n}$, but the signals from the interfering users are expected to be scattered across the whole of the bit period T_{bit} if the system is asynchronous. Hence, the use of a device that ideally is transparent during the time $\frac{T_{\text{bit}}}{n}$ in which the signal is expected to occur, but opaque otherwise, would then exclude much of the light from the interfering users, and hence the associated mixing noise. Such a device is here referred to as a time gate, and ideally it would permit an increase in the high-power SNR limit of up to the factor n. However, this duty-cycle reduction requires a higher modulation bandwidth, along with a time gate of the same bandwidth, and it also increases the dispersion sensitivity of the system by the same factor n. Note that in general, time-gating exactly in synchronism with the signal location is effective in reducing *all* forms of noise that occur before the time gate and over a greater temporal extent than the signal [Sampson *et al.* 1997]. This is simply the temporal parallel to the more familiar spectral case of using a filter to exclude any noise not within the signal bandwidth.

It is possible that simple duty-cycle reduction alone could improve the SNR if the signals from each user have little intensity noise, that is, significantly less than if they were ideally thermal. In the full duty-cycle case this system is only marginally better than with pure thermal sources since the mixing between the light fields from many users makes the received signal appear near-thermal. However, in an asynchronous system with transmissions in a small fraction of the bit period, the likelihood of many signals arriving at a receiver simultaneously

is greatly reduced, and hence the received signal cannot be assumed thermal or near-thermal. Note that this actually requires that the light from every source within each spectral slice to have little or no intensity noise, since it is the mixing of light within the same slice that can generate PIIN within the receiver bandwidth. The least complex method of achieving such a light source is to have an array of diode lasers, one for each spectral slice. Such sources and the corresponding system performances are discussed in more detail in Section 5.4.

If duty-cycle reduction and time-gating are taken to extreme, then the SNR limit due to PIIN should become sufficiently large that it is insignificant, and the system tends toward a form of ultrashort coherent pulse OCDMA. The OCDMA scheme discussed in Section 2.5 is based on the spectral-phase coding of ultrashort coherent pulses, and it effectively has this very low duty cycle and narrow time-gating structure. While such sources are definitely not thermal, and there are significant differences between phase and amplitude coding, this simple comparison suggests that mixing between signals in the system of Section 2.5 is not a significant limitation. This is indeed the case, as discussed further in Section 7.4.

5.3 SPECTRAL-AMPLITUDE OCDMA WITH ULTRASHORT COHERENT PULSES

One may think of the SNR limit in spectral-amplitude OCDMA with thermal sources as a consequence of the mixing of fields with uncorrelated phase noise, and hence be curious about what happens when perfectly coherent sources are used. In addition, very short coherent pulses are required to provide the broadband spectrum required, so the source duty cycle is very low. The maximum expected performance of spectral-amplitude OCDMA with ultrashort coherent pulses is calculated here as a comparison to that with thermal sources.

In the same manner as in Chapter 3, several idealities are assumed in this first-order analysis. This allows direct comparison between the performance in Chapter 3 and that found here, and it gives an upper limit to the performance of a real such system.

It is assumed that the spectral encoding is ideal, with N adjacent rectangular spectral slots, across the total optical bandwidth $\Delta\nu$, centered at ν_o. For simplicity, it is assumed that the power in each slot is approximately equal, which requires either that the ultrashort pulses are sufficiently short, or that there is appropriate attenuation of each slot to achieve this. For convenience, it is assumed that each signal is fully polarised and that complete polarisation alignment between all users is achieved, since the effects of other polarisation conditions can be simply deduced. Hence, an encoded pulse centered at time zero can be represented as

$$q = \frac{\sqrt{P_\mathrm{p}}}{N} e^{j2\pi\nu_o t} \operatorname{sinc}\left(\frac{\Delta\nu t}{N}\right) \sum_{i=1}^{N} c_k(i) e^{-j\frac{2\pi\Delta\nu t}{N}\left(i-\frac{N+1}{2}\right)} \tag{5.1}$$

where P_p is the power of the uncoded pulse (with $c_k(i) = 1, \forall i$), $\operatorname{sinc}(x) = \frac{\sin(\pi x)}{\pi x}$, and $c_k(i), i = 1 \ldots N$ are the [0,1] amplitude code elements of the kth code.

5.3.1 Synchronous Case

If each user is bit synchronous, but not phase synchronous, then the signals of each user can be represented by Equation 5.1, where the only differences from user to user are the amplitude code elements $c_k(i)$, along with an additional random phase term $e^{j\phi_k}$. The synchronous case is first considered here because it is much simpler to analyse than the asynchronous case, and it also gives an insight into the interference levels when by chance a number of asynchronous users are near synchronous. If an ideally balanced receiver of the form of Figure 3.1 is assumed, together with Hadamard-based codes, and also assuming that $\frac{\Delta\nu}{N} \gg B_e$, where B_e is the receiver bandwidth, then it can be shown (Appendix B) that the interference from unmatched users leads to an SIR limit of

$$\frac{4}{3(K-1)} \leq \text{SIR} \leq \frac{2}{(K-1)} \tag{5.2}$$

where K is the number of active users. The severity of this limit is due to the ideality of the pulse spectra and spectral coding. Under the assumptions of ultrashort coherent pulses with ideal rectangular spectral coding, the only difference between the light from different synchronous users within a single spectral slot is the relative optical phase, that is they are highly coherent. Consequently, the coherent (and relative-phase-dependent) addition of optical signals from different users causes the receiver signal to be determined predominantly by the relative phase delays of each signal, and the actual signal level from the desired user is swamped, on the whole, as indicated by the very low SIR.

The linear dependence upon the number of simultaneous users, rather than quadratic, is due to the orthogonal Hadamard sequences and the bit-synchronous condition. For the incoherent-source case, each unique pair of transmitting users generates PIIN of the same order, giving quadratic dependence upon the number of users. However, as detailed in Appendix B, the primary interference in the bit-synchronous coherent-source case is due to each unmatched signal interacting with the matched signal. Each unmatched signal can also interact with at most one other unmatched signal, but all other signal pairings give zero interference. Consequently, the interference level for the bit-synchronous coherent-source case increases linearly with the number of interfering users.

The upper and lower limits in Equation 5.2 arise when the unmatched users are arranged to respectively minimise or maximise the number of pairings which generate interference. The SIR approaches the upper limit as the number of users K approaches the maximum $N-1$, since more such pairings are likely.

The limit of Equation 5.2 does not include B_e, N, or $\Delta\nu$, which may at first be surprising. The reason why the optical bandwidth does not appear explicitly is that for a sufficiently short pulse (ideally impulsive), the only variations in each encoded-pulse spectrum are due to the coding alone. Hence, one should expect N dependence in Equation 5.2, but here this is implicit since $K \leq N-1$ assuming Hadamard-based codes. Also, the likely level of the SIR with

respect to the limits in Equation 5.2 depends upon $\frac{K-1}{N}$. The receiver bandwidth dependence arises in the assumption of $\frac{\Delta\nu}{N} \gg B_e$, which means that mixing between light in different spectral slots is outside the receiver bandwidth. Practically, of course, B_e must be large enough to match the data rate, and preferably no larger, in order to minimise the receiver noise.

5.3.2 Asynchronous Case

Having observed that there is very strong interference between signals from different users when they are synchronous, it is expected that in the asynchronous case the interference should be much less on average because of the asynchronism. However, assuming that the bit rates of each user are nominally equal, then the relative time delays of each user only change rather slowly. Hence, if by chance several of the users are near-synchronous, and hence cause significant interference, then this situation may continue for many successive bit periods.

In the asynchronous case, the analysis becomes more cumbersome, and a judicious assumption is made in order to estimate the interference level . This assumption is justified upon the basis that the subsequent predictions match closely the performance indicated by Monte-Carlo simulations of the ideal asynchronous system. The details are contained in Appendix B, and for a coded optical bandwidth $\Delta\nu$ and bit period T_{bit}, the SIR is found to be

$$\text{SIR} \approx \frac{\Delta\nu T_{\text{bit}}}{K(K-1)} \tag{5.3}$$

This SIR is approximately equal to the SNR which occurs for ideal spectral-amplitude coding using incoherent broadband sources, when all signals have the same (full) polarisation. This order of limit is significantly worse than that for a system based upon spectral-phase coding of ultrashort coherent pulses, since the coherent detection scheme results in the dominant interference term having only linear dependence upon the number of interfering users.

The physical realities causing this limit for both coherent and incoherent sources can be viewed in the following manner: the signals from each user have significant spectral overlap and have the same power, and in the case of thermal sources they occur at the same time at the receiver. Hence, in the same single-mode fibre there is intensity noise due to each pair of such fields, which is approximately proportional to the square of the number of users. Due to the same source spectra, this intensity noise is centered about zero frequency, and the noise power within the photodetector bandwidth is then determined by the ratio of electrical to optical bandwidth. In the case of ultrashort coherent sources, however, the interference from any two signals arriving almost simultaneously at the receiver (on order of $\frac{1}{\Delta\nu}$ temporal offset or less) is of the same level as the signal power itself. For encoded signals with a moderate temporal overlap, of the order of $\frac{N}{\Delta\nu}$, the interference power is down by approximately N on the signal power level.[1] In an asynchronous system, the chance of these temporal overlaps between

[1]This 'two-level' effect is because the encoded pulse can be represented as a short coherent pulse, with temporal size of order $\frac{1}{\Delta\nu}$, along with a widely dispersed and lower level component, with temporal extent of order $\frac{N}{\Delta\nu}$.

received signals is determined by the ratio of the bit period to the order of temporal overlap under consideration. For both the near-synchronous and the moderate overlap cases, the overall effect is the same, giving an average SIR that still has the approximate form $\frac{\Delta\nu T_{\text{bit}}}{K^2}$. However, significant variation in SIR may occur according to the time offsets between asynchronous users in the case of coherent pulse sources, unless they are dispersed significantly.

The system representation here and the analysis in Appendix B assume zero dispersion, but this is not very realistic. However, significant dispersion serves only to temporally spread the encoded pulses according to wavelength, and the limit of Equation 5.3 arises without any dispersion, assuming uniformly distributed offsets between users. It is therefore expected that the only effect of dispersion, provided it remains less than the bit period, is to spread the signals temporally, thereby making the noise level due to interference (Equation 5.3) much less sensitive to the relative delays between each user.

The fact that the same form of limit as for thermal sources arises here is quite significant. It highlights the fact that eliminating thermal sources from a spectral-amplitude OCDMA system is not enough to overcome the serious SNR limit that arises therein. This is because the system is incoherent, and the unwanted interference that occurs between signals when coherent sources are used causes the same SNR limit as the interference between incoherent thermal sources. It suggests that spatially coherent fields from independent users cause a serious problem in any incoherent optical multiple-access system that does not employ some form of time or wavelength separation, and this is considered more closely in Chapter 7.

The limit of Equation 5.3 was found assuming balanced detection and effective integration over the bit period, as considered in Chapter 3. If it were feasible to perform the necessary power difference optically, rather than with balanced detection, and then to detect the very short signal pulse that remains after this scheme, then the limit of Equation 5.3 is overcome. However, the system has become a coherent scheme, since coherent matching of the spectral coders and dispersion compensation is then necessary to recreate the desired short pulse. This configuration is simply a less efficient implementation of the OCDMA scheme based upon the spectral-phase coding of ultrashort coherent pulses (Section 2.5).

5.4 SPECTRAL-AMPLITUDE OCDMA WITH COHERENT SOURCE ARRAY

Another alternative to an incoherent broadband thermal source for spectral-amplitude OCDMA is an array of coherent diode lasers, one for each spectral code element. Considering this form of source here further highlights the conditions under which SNR limits of the form observed in Chapter 3 do or do not occur.

Under the assumptions that each laser in the source arrays is lasing within the appropriate spectral slice and that the power level when transmitting is constant, and zero otherwise, then the basic functionality of the system is identical to that assumed in Chapter 3. However, in

order to determine the noise level at the receiver, it is necessary to be more specific about the light from each laser. Assuming, as for the thermal source case, that the spectral-slice width is significantly greater than the receiver electrical bandwidth, then any PIIN appearing in the received signal is from the mixing of the light within the same spectral slice. Hence, the critical issue is whether the mixing of the light from several different users within the same spectral slice produces PIIN at the receiver.

If the spectrum of each diode laser is identical to that of the corresponding lasers in every other array, and if these spectra are still broad with respect to the receiver bandwidth, then PIIN of the same order as that from thermal sources is generated, due to the independent phase noise of each source. Hence, an SNR limit of the form of Equation 3.29 still arises. The analysis is simply equivalent to neglecting the terms with $k = l$ in Equation 3.27, since these then correspond to the self-intensity noise of each diode laser, and it follows that $(K+1)$ is replaced by $(K-1)$ in Equation 3.29. In the worst case of each source being fully polarised, and all polarisations at the receiver being identical, then a further factor of two appears in the denominator of Equation 3.29. Practically, however, the condition of identical polarisations at the receiver is highly unlikely, and if the polarisations of each laser field at the receiver are considered to be completely random, then this factor of two can be reasonably neglected. Note that the optical bandwidth measure $\Delta\nu$ must reflect the actual laser spectral profiles, rather than the full width of the spectral coding indicated in Figure 3.1, as discussed in Section 3.6.3. This reduction in optical bandwidth is simply gauged by the ratio of the coherence time of an ideal rectangular spectral slice to the coherence time of the source-array lasers.

The clearest configuration of a coherent source array that significantly exceeds the SNR limit of a thermal source is if the laser spectra within each slice are separated by the receiver bandwidth or more. In this case, the PIIN spectrum from any pair of sources simply falls outside the receiver bandwidth. Note, however, that arrays of highly coherent lasers are not cheap, and achieving this fine-scale wavelength division to avoid in-band PIIN is even more demanding.

If each laser source is highly coherent, where the coherence time is greater than the bit period, and if the source spectra within each single slice are all within the receiver bandwidth of each other, then there is significant coherent interference in the received signal. This interference may be highly correlated between adjacent bits, depending upon the corresponding data symbols of each interfering user. In the worst case, the fields from each source within the same slice have the same polarisation and are completely coherent over a bit period, differing only by some phase shift. If this is the case for all slices, and assuming that all the phase shifts are independent and uniformly distributed on 0-2π, then the average signal-to-interference ratio is limited (Appendix C) to

$$\mathrm{SIR} \approx \frac{N}{K(K-1)} \tag{5.4}$$

This SIR differs from that of polarisation-matched thermal sources (Equation 3.29 less 3 dB)

by a factor of approximately $\frac{2NB_e}{\Delta\nu}$. An initial assumption was that the spectral slice width was significantly greater than the electrical bandwidth, that is $\frac{\Delta\nu}{N} \gg B_e$. Hence, this SIR limit is expected to be at least as poor as that with otherwise similar thermal sources.

The combination of duty-cycle reduction with coherent source arrays may also allow an improvement in the SNR limit. The crucial difference from the thermal source case is that each array source has negligible intensity noise, and so any interference is simply proportional to $K(K-1)$, the number of pairings between K transmitting users. When K is small the interference level is noticeably less than that given by the approximation K^2, under which there is no advantage in duty-cycle reduction. Clearly there is no such interference if only one signal is being transmitted. Consequently, duty-cycle reduction can improve the average SNR if it results in there being few simultaneous transmissions during each bit period. Note however that the SNR reduction is only on average, and in an asynchronous system significant variation in the SNR is expected. This leads to poorer performance than the average SNR might suggest, since low-SNR events tend to dominate the bit-error rate, which is generally a highly nonlinear function of SNR.

5.5 SUMMARY

In this chapter spectral-amplitude OCDMA has been considered with alternative sources and signalling methods. The use of thermal sources with simple duty-cycle reduction does not give any advantage over the configuration in Chapter 3 unless an ideal time gate is used at the receiver. The consequent gains with respect to the PIIN limit are at the expense of the modulation and detection bandwidths (including the bandwidth of the time gate if it is optical), the dispersion sensitivity, and also the SNRs relative to shot and receiver noise in general. The use of ultrashort coherent pulses with spectral-amplitude OCDMA has been shown to result in the same form of SNR limit if the system is otherwise unchanged from that in Chapter 3. Arrays of coherent sources have also been considered as an alternative to broadband thermal sources. If these arrays are spectrally matched, then exactly the same order of SNR limit arises from the mixing between the light fields. If these sources were arranged to be spectrally separated from every other source by at least the receiver bandwidth, then the limit found in Chapter 3 is avoided, since the system has effectively become a wavelength-division scheme. However, this approach would be very demanding and expensive.

Chapter 6

SPECTRAL-AMPLITUDE OCDMA WITH PPM SIGNALLING

6.1 INTRODUCTION

In Chapter 5 it was shown that simple duty-cycle reduction alone cannot improve the SNR limit when there are many users, but with increased modulation and receiver bandwidth, an increase in the high-power average SNR limit is possible. Pulse-position modulation (PPM) is a signalling format that also reduces the transmission duty cycle in general, but due to the information then carried by the pulse positions, it is more efficient than simple duty-cycle reduction. This chapter proposes and analyses the use of pulse-position modulation (PPM) of the broadband incoherent sources in the spectral-amplitude OCDMA system of Chapter 3. It is shown that the simple modifications necessary for PPM signalling allow performance beyond the SNR limit found in Chapter 3, without requiring expensive broadband coherent sources, nor significantly increased modulation and detection bandwidths. In particular, a simple PPM scheme with a word length of two is described which can improve the system throughput using incoherent sources without any changes, at least relative to the data rate, to either the modulation bandwidth, the detection bandwidth, or the dispersion sensitivity. This improvement is also possible in other OCDMA systems whose SNR is limited in the same manner, including those based upon coherence multiplexing.

6.2 PPM WITH SPECTRAL-AMPLITUDE OCDMA

In this section the use of pulse-position modulation with spectral-amplitude OCDMA, as per Chapter 3, is proposed. The corresponding changes and additions to the spectral-amplitude OCDMA system are described, and the potential performance improvements are analysed. The shortest possible PPM word length M is two, and the use of $M = 2$ PPM is considered first due to its simplicity.

6.2.1 Two Slots per PPM Word

In pulse-position modulation with a PPM word length of $M = 2$ slots, a symbol is transmitted in either the first or last of the two slots that comprise the PPM word. In the spectral-amplitude

OCDMA system described and analysed in Chapter 3, and assuming complementary keying, then in each bit period the data $d = +1$ or $d = -1$ is sent, corresponding to transmission with the coded spectrum or its complement respectively. Combining $\mathsf{M} = 2$ PPM with this system, there are now four possibilities for a two-slot PPM word, these being $[1, 0]$, $[-1, 0]$, $[0, 1]$, and $[0, -1]$. Here ± 1 corresponds to transmitting the coded spectrum or its complement as before, and the case 0 represents no transmission in that slot. Hence, if the slot duration is exactly equal to the bit period T_{bit} of the original OCDMA system, then there are four possible PPM words for each $2T_{\text{bit}}$ interval. Consequently, in this case the same data rate as the original system can be maintained without increasing the signalling rate.

The original spectral-amplitude OCDMA proposal of [Zaccarin and Kavehrad 1993] considered the data keying to be performed by on-off modulation of the broadband source, and the structure of the transmitter in [Nguyen *et al.* 1995] allows complementary keying by on-off modulation of two sources in complement. In both of these cases, performing PPM at the same symbol rate does not require any transmitter modifications, since electronic PPM coding before the modulator(s) is simply sufficient.

In order to decode the PPM modulation at the receiver, the simple and robust decoding structure of Figure 6.1 is proposed to follow the original OCDMA receiver. The diode pair is that from the last stage of the receiver in Figure 3.1, and T represents a delay by the slot period, which is equal to the bit period in this case. The two simple decision units perform binary choices according to the sign of their input. The decoder in Figure 6.1 has been designed to

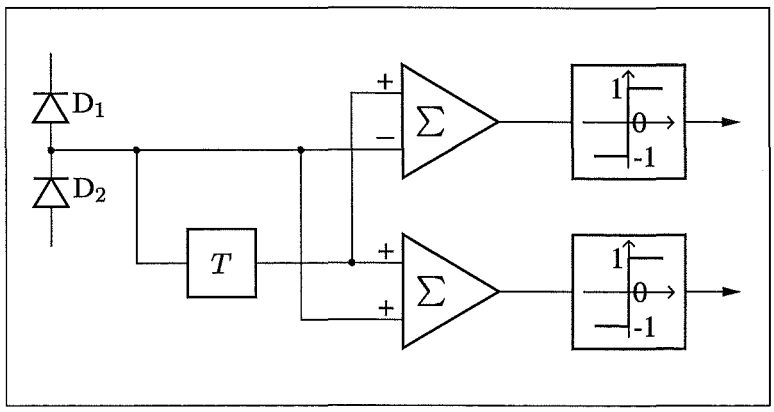

Figure 6.1 Decoder for $\mathsf{M} = 2$ PPM

compare the two received symbols in each PPM word, and this requires word synchronisation. It is assumed that synchronisation can be simply achieved because there is always a transition in the middle of each word, similar to Manchester coding. With synchronisation, for each of the four possible PPM words, the decoder gives a unique two-bit output. The mapping from the incoming data to the possible PPM words represented in Table 6.1 could be simply performed, assuming the first PPM symbol is transmitted first, in which case the upper and lower outputs of the decoder correspond directly to the input data bits.

In order to simply analyse the performance of the combined PPM-OCDMA system, ap-

Input Bits	PPM Word
$+1, +1$	$+1, 0$
$+1, -1$	$0, -1$
$-1, +1$	$0, +1$
$-1, -1$	$-1, 0$

Table 6.1 Suggested PPM Word Assignment

propriate comparison with the OCDMA system analysis in Chapter 3 is made. It is first noted that the processing in Figure 6.1 requires the same electrical bandwidth B_e as in the receiver of Figure 3.1, since both effectively integrate the photocurrent over a single slot period T_{bit}. If the received PPM word is represented as an ideal PPM signal with additive noise x_1 in the first slot, and x_2 in the second, then these noise terms are independent since the source coherence time is much less than T_{bit}. From Figure 6.1, the noise at the two decision units is given by $y_1 = x_1 - x_2$ and $y_2 = x_1 + x_2$. It is assumed that the photocurrent noise is Gaussian under the conditions of interest. Hence, x_1 and x_2 are considered to be independent zero-mean Gaussian-distributed variables, with variances denoted by σ_1^2 and σ_2^2. Under these conditions, y_1 and y_2 are also zero-mean Gaussian-distributed variables, with a covariance matrix

$$\begin{bmatrix} \sigma_1^2 + \sigma_2^2 & \sigma_1^2 - \sigma_2^2 \\ \sigma_1^2 - \sigma_2^2 & \sigma_1^2 + \sigma_2^2 \end{bmatrix} \tag{6.1}$$

The off-diagonal terms of Equation 6.1 give the cross-covariance of y_1 and y_2, and if they were zero, then y_1 and y_2 would be independent. However, due to the PPM regime, the signal power from the desired user arrives in only one of the two slots, and hence, in general, x_1 and x_2 do not have the same variance. Consequently, there is in general some correlation between the noise at each decision unit. In the extreme case of only one active user, the signal and corresponding noise are confined to a single slot, and with ideally zero noise in the empty slot, any error then affects both outputs simultaneously. However, this is extremely unlikely to occur, since such a system would, in general, be designed to have a very low error probability with many active users. In contrast, as the number of simultaneous users increases, σ_1^2 and σ_2^2 tend toward the same value, and hence pairs of errors become less likely.

6.2.1.1 Synchronous Case

It is initially assumed, for simplicity, that all the users are word synchronous. If there are K active users in the network, with independent equiprobable data, then it may be said that $\mathcal{L}$ users are transmitting in the first slot of each PPM word, where $\mathcal{L}$ is binomially distributed between 0 and K. Correspondingly, the number of users transmitting in the second slot is then $K - \mathcal{L}$. Hence, using Equation 3.27, the limiting noise at the decision thresholds, conditioned

upon $\mathcal{L}$, is expressed as

$$\sigma_I^2|_{\mathcal{L}} = \frac{B_e R^2 P_r^2}{4\Delta\nu}[\mathcal{L}(\mathcal{L}+1) + (K-\mathcal{L})(K-\mathcal{L}+1)] \tag{6.2}$$

The corresponding signal levels are still $\pm RP_r/2$. In general, the noise levels at each decoder output are correlated, and the worst-case scenario is that both outputs are in error when an error occurs. This factor of two, at worst, is ignored in the following equation since a simple performance approximation is desired. Under the assumptions that the transmitted data is equiprobable and that the noise is Gaussian, and using Equation 6.2 with the binomial distribution of $\mathcal{L}$, the probability of error is approximated by

$$P_{be} \approx 2^{-(K+1)} \sum_{\mathcal{L}=0}^{K} \binom{K}{\mathcal{L}} \operatorname{erfc}\left(\sqrt{\frac{\Delta\nu}{2B_e[\mathcal{L}(\mathcal{L}+1) + (K-\mathcal{L})(K-\mathcal{L}+1)]}}\right) \tag{6.3}$$

In Figure 6.2 an example of the synchronous performance according to Equation 6.3 is plotted, where $\frac{\Delta\nu}{B_e} = 50000$. This ratio corresponds, for example, to a system with an optical bandwidth of 20 nm around 1550 nm, and a per-user bit rate of 100 Mb s^{-1}. The corresponding limits of the original asynchronous OCDMA system are plotted for comparison in Figure 6.2, both using on-off keying (OOK) with a fixed threshold, as originally proposed for this system, and in the case of complementary keying (CompK), which was plotted previously as curve (e) of Figure 3.4. An estimate of the asynchronous performance from the following section is also included in Figure 6.2.

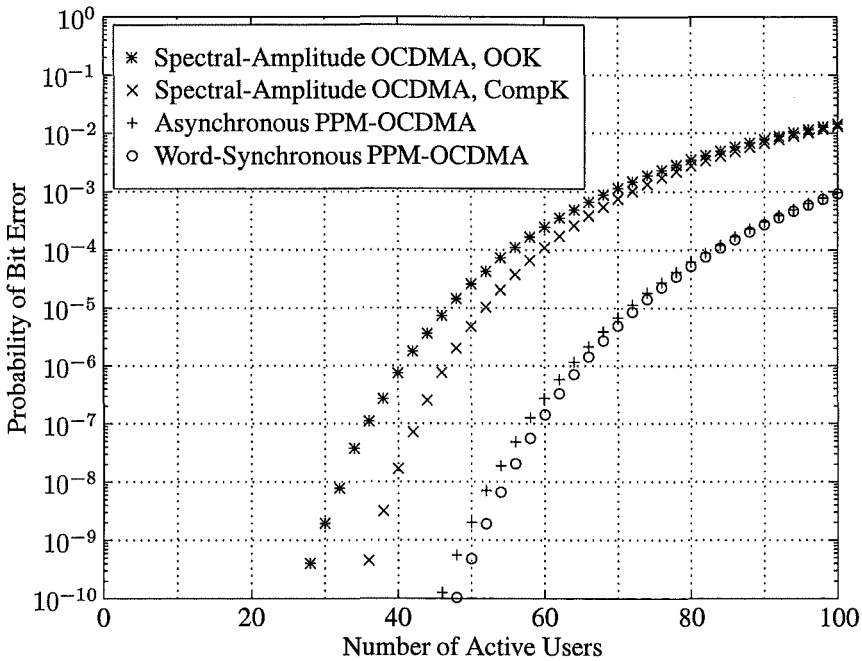

Figure 6.2 Estimates of the PIIN-Limited Error Rate, $\frac{\Delta\nu}{B_e} = 50000$, M = 2

6.2.1.2 Asynchronous Case

Without word synchronism, although there are still the same number of interfering transmissions on average, there is a wider variation in the dominant noise level over each word interval. Due to the highly nonlinear dependence of the error rate upon SNR, a wider spread of SNR values with the same mean causes the average error rate to rise, since the smaller SNR values dominate. Hence, the asynchronous case is expected to be worse than the synchronous case.

Numerical simulation of the asynchronous system was performed to get an estimate of the distribution of the noise variance at the receiver. Plotted in Figure 6.2 is the estimate of the error probability corresponding to this distribution, assuming Gaussian noise, and ignoring correlated error pairs. In the case of only two asynchronous users, the distribution of the limiting noise variance can be calculated directly. Under the Gaussian noise assumption it is thus found that the ratio $\frac{\Delta\nu}{B_e} = 239.1$ is necessary to achieve a probability of error of 10^{-9}, compared to the simulation estimate of $\frac{\Delta\nu}{B_e} = 240.6$. Furthermore, as the number of users becomes large, Figure 6.2 shows a convergence of the asynchronous and synchronous performance estimates, confirming the accuracy of the results from the numerical simulation.

As an example, from Figure 6.2, it can be seen that at an error rate of less than 10^{-9}, and with an optical bandwidth of 20nm, at most 29 users can transmit simultaneously at $100\,\mathrm{Mb\,s^{-1}}$ using spectral-amplitude OCDMA as originally proposed, which was with on-off keying (OOK). Spectral-amplitude OCDMA with the complementary keying (CompK) arrangement detailed in Chapter 3 permits up to 36 users under these conditions. With asynchronous PPM-OCDMA however, up to 49 users would be possible under the same conditions, and word-synchronous PPM-OCDMA would permit up to 51 users.

In Figure 6.3, at a raw error probability of 10^{-9}, the bandwidth ratio $\frac{\Delta\nu}{B_e}$ required by the PPM-OCDMA system is compared with this ratio for the system without PPM. It is clear that the PPM-OCDMA system is more bandwidth-efficient than the original system. This improvement in bandwidth use is tending towards a factor of two as the number of users increases. Figure 6.3 represents the possible increase in per-user bit rate that would be available using PPM signalling, in the absence of shot noise, thermal noise, and other such factors which may preclude increasing the data rate directly. Equivalently, it represents the reduction in optical bandwidth that is possible in the absence of other factors which may prevent the direct reduction of the optical bandwidth. In the case of two or three active users, the best asynchronous PPM-OCDMA system performance is worse than spectral-amplitude OCDMA using complementary keying, but it is still significantly better than that using only the on-off keying of the original proposal (see Figure 3.8, for example).

6.2.2 Greater PPM Word Lengths

For PPM word lengths greater than $\mathsf{M} = 2$, less information can be transmitted at the same signalling rate. Standard PPM encodes $\log_2\mathsf{M}$ bits of information in M slots, and if bipolar

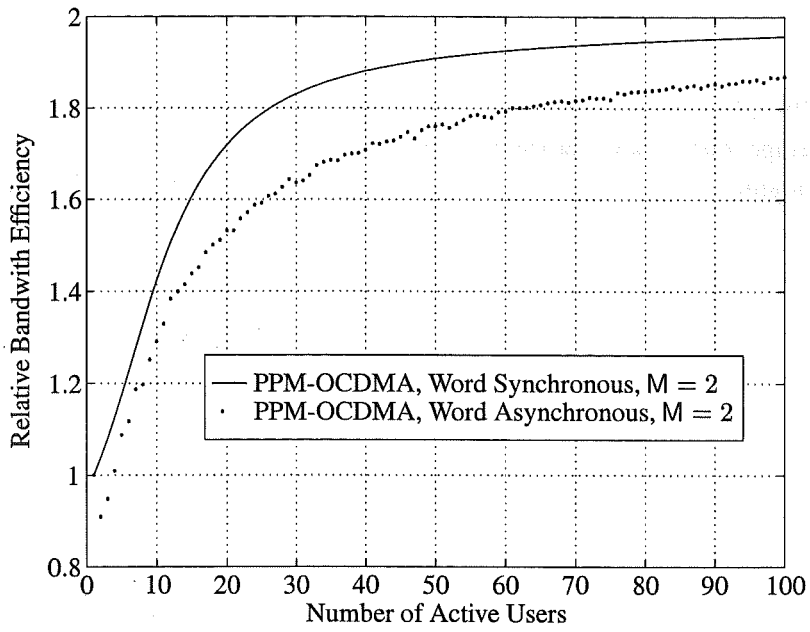

Figure 6.3 Bandwidth Efficiency compared to Spectral-Amplitude OCDMA using Complementary Keying

symbols are used, then $\log_2 M+1$ bits can be encoded. Thus, PPM with bipolar signalling can be viewed as having a coding rate of $\frac{\log_2 M+1}{M}$. For the cases $M = 4$ and $M = 8$, the effective coding rates are thus $\frac{3}{4}$ and $\frac{1}{2}$ respectively. The OCDMA system without PPM signalling may also be considered to use PPM signalling with $M = 1$, which is convenient for some later comparisons on the basis of M.

A differential form of PPM decoder is considered for the $M = 4$ and $M = 8$ cases, similar in structure to the decoder of Figure 6.1. This decoder structure is shown for the case $M = 4$ in Figure 6.4. For each bipolar PPM word, in the absence of errors, one decoder output has a

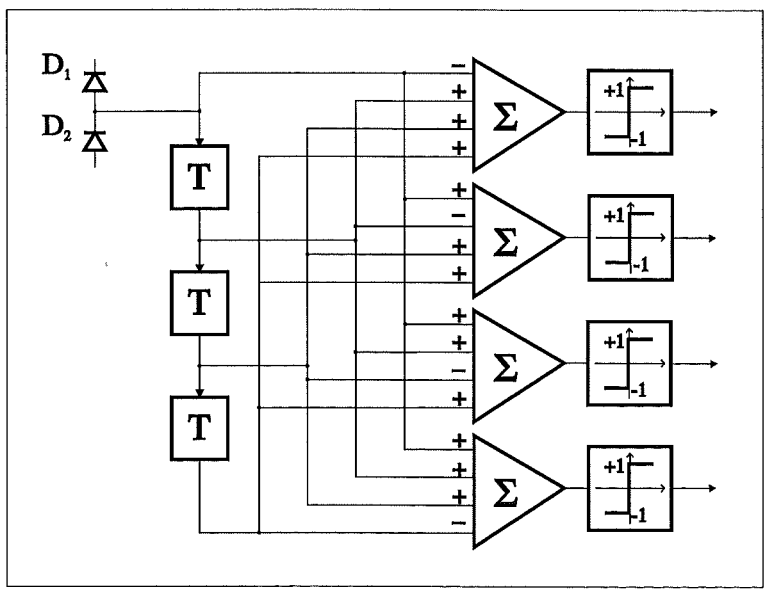

Figure 6.4 Decoder for $M = 4$ PPM

different sign to all the others. The position of the output with the different sign gives $\log_2 M$ bits of information, and together with the actual sign of this output, the $\log_2 M+1$ information bits per word can be recovered. Note that the logic needed to perform this mapping has not been shown in Figure 6.4. Achieving word synchronisation to the desired user is no longer as simple as in the $M = 2$ case, but it is assumed that this is still achievable. Such synchronisation could be performed by detecting a known signal preamble, and then tracking subsequent timing variations, for example. It may also be possible to exploit the parallel structure of the decoder to lock more rapidly to such a preamble.

In the same manner as the $M = 2$ case, for decoders of the form of Figure 6.4, different noise levels in each slot cause correlation between the noise at each decision unit. A consequence of the decoding process is that any single error in the M decision units can be detected, since an invalid output pattern occurs. Such an error does however, in general, render all $\log_2 M+1$ information bits in error, corresponding to the erroneous decoding of the whole word.

Numerical simulation of the asynchronous system was performed for both $M = 4$ and $M = 8$. A performance estimate was obtained by assuming a system bit-error rate ($\log_2 M+1$) times larger than the probability of error in one decoder output. In Figure 6.5 the network capacities of the combined PPM-OCDMA schemes with $M = 2, 4$, and 8, are compared to the original spectral-amplitude OCDMA scheme (SA-OCDMA), using both the originally proposed on-off keying with fixed detection threshold, and the complementary keying arrangement considered in Chapter 3. The network capacity is given by the possible number of simultaneous users multiplied by the bit rate per user, which is reduced for $M > 2$ as previously detailed. It is

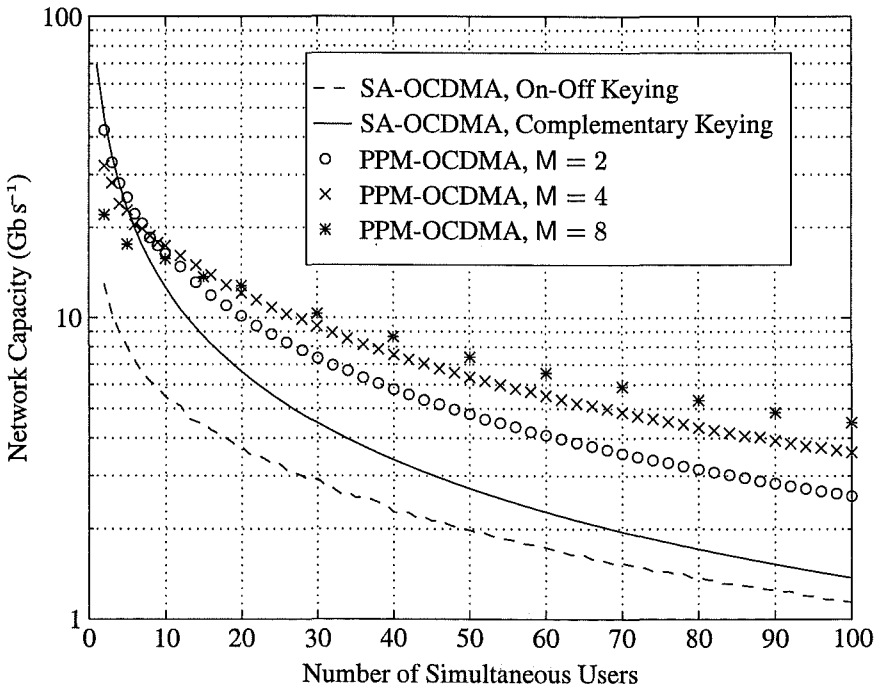

Figure 6.5 Asynchronous Network Capacity Limits, $\Delta\nu = 2.5$ THz (20 nm bandwidth @ 1550 nm), BER=10^{-9}

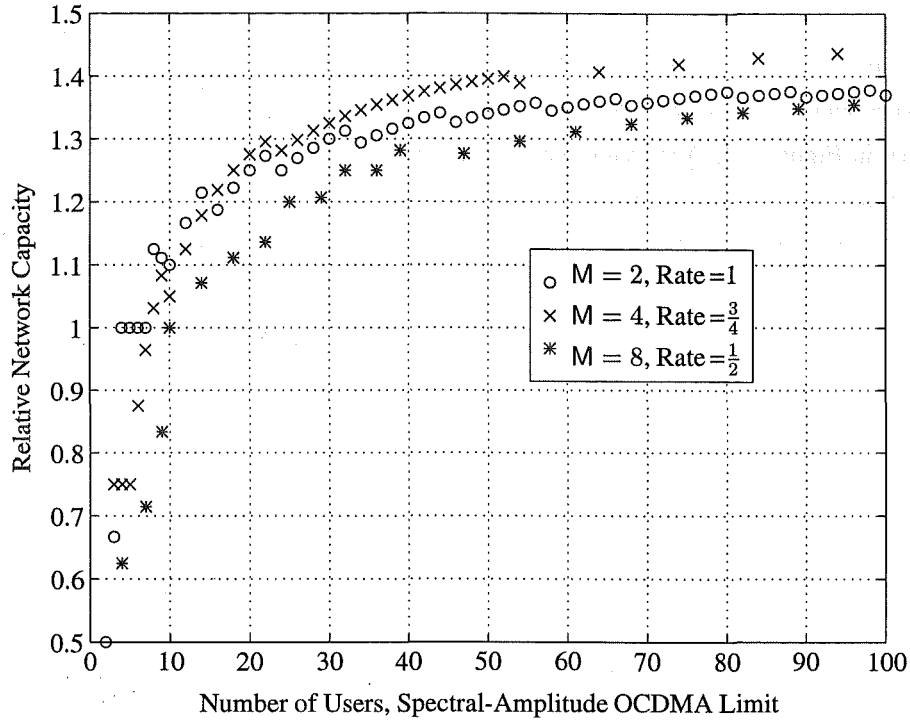

Figure 6.6 Asynchronous Network Capacity Increase when Adding Users, $\Delta\nu = 2.5$ THz, BER=10^{-9}

clear from Figure 6.5 that as the number of simultaneous users increases, the combined PPM-OCDMA system is more bandwidth-efficient than the spectral-amplitude OCDMA scheme without PPM. It is also apparent that the possible gains in spectral efficiency decrease as M increases, and this is due to the increasing coding-rate penalty.

In Figure 6.6, the performance limits of the spectral-amplitude OCDMA system with and without PPM are compared again. In this case, however, the signalling rate is assumed to be the same for each system, and the number of simultaneous users in the PPM-OCDMA system is increased, if possible, with respect to the number possible without PPM and using complementary keying. The number of users possible with PPM-OCDMA is then scaled by the code rate, so that the vertical axis of Figure 6.6 represents the network capacity relative to that using the original OCDMA system, assuming complementary keying.

From Figure 6.5 it can be seen that the $M = 8$ PPM-OCDMA case can achieve greater spectral efficiency than the $M = 4$ and $M = 2$ cases. However, by increasing the number of users at the same signalling rate, as in Figure 6.6, the $M = 8$ PPM-OCDMA case performs worse than both the $M = 4$ and $M = 2$ cases. This difference is due to the linear dependence of the limiting noise upon receiver bandwidth, compared to the quadratic dependence upon the number of users.

As M increases, the transmitted power is being confined to a smaller fraction of each word interval. Although this allows the maximum spectral efficiency to increase, the relative effects of shot noise and receiver noise must also be considered. It is most likely that the necessary

broadband sources are maximum-power limited, and hence the ratio of signal to shot noise then decreases in proportion to M. The relative effects of photodiode dark current and receiver thermal noise are also increased by at least a factor of M, due to the decoder structure having M similar paths.

The complexity of the PPM decoder structure considered here is proportional to M. The increase in complexity from $M = 2$ to $M = 4$ may be worthwhile if the received power is still sufficiently high, so that much of the possible gains indicated in Figure 6.5 and Figure 6.6 can be realised. However, even with high received power, the PPM-OCDMA system with $M = 8$ is probably not worth the increase in complexity.

6.3 APPLICABILITY TO OTHER OCDMA SYSTEMS

The use of PPM and differential detection, particularly in the case of $M = 2$, is successful in improving the PIIN-limited performance of spectral-amplitude OCDMA because the limiting noise depends upon the square of the number of simultaneous users. If this was a linear relationship, then the gain due to the duty-cycle reduction with PPM would be lost in the PPM detection process. It it is then natural to wonder whether this idea can be successfully applied to other systems with the same form of noise relationship.

The scheme of coherence multiplexing (Section 2.7) is also limited by PIIN in a similar manner to spectral-amplitude OCDMA, but the coding and decoding takes the simple form of an unbalanced interferometer. The main potential difficulties with this scheme are that the relative polarisations in each interferometer path must be maintained, and the path-length difference of the receiver interferometer must be actively controlled to match that of the desired transmitter to within a fraction of the optical wavelength. However, both of these conditions can be met in practice, and the most impressive OCDMA-like demonstrations to date are indeed based upon coherence multiplexing [Sampson *et al.* 1997].

To use PPM with bipolar signalling, as described in this chapter, within a coherence-multiplexed system requires both phase-shift keying (PSK) at the transmitter (as indicated in Figure 2.4), and also amplitude-shift keying (ASK) of the source. The PSK of the interferometer path is then equivalent to the keying with complementary spectral codes in Section 6.2, and the ASK of the source according to the PPM word is the same for both systems. The adequate performance of the receiver phase-feedback control has been demonstrated both with data modulation using ASK of the source [Pendock *et al.* 1995], and with PSK in the transmitter interferometer [Pendock and Sampson 1995]. Assuming that any path-length fluctuations are much slower than the desired bit rate, the combination of both ASK and PSK together is unlikely to affect the possibility of adequate feedback control, although it may necessitate slight modifications to the control system. The PPM decoder could be applied after the balanced detection exactly as in Section 6.2, with the same functionality and operation. While it is not undertaken here to examine this modified system in detail, it is expected that with all the

interferometer delays small with respect to the bit period, and in the case of many users, that gains very similar to those indicated in Figure 6.5 may be achieved for this system also.

Both spectral-amplitude OCDMA and coherence-multiplexed systems require spectrally matched sources, which is one of the necessary conditions for the form of SNR limit that arises in both of these cases. As detailed in Chapter 7, there are a number of OCDMA systems based upon temporal coding that are also subject to the same SNR limits if the sources have identical spectra, but this is not necessary for the function of these systems. PPM coding as considered in this chapter, especially with $M = 2$, could also be applied to such temporal-coding systems if necessary.

6.4 SUMMARY

In this chapter the use of pulse-position modulation has been introduced as a method of improving the performance of a spectral-amplitude OCDMA system beyond the limit imposed by the mixing of light from thermal sources, as found in Chapter 3. The necessary system modifications for the combined PPM-OCDMA system have been detailed, and the potential performance improvements have been investigated through analysis and numerical simulation. In particular, it has been shown that using PPM signalling with a word length of two, along with a simple and robust extra decoding stage, permits an increase in spectral efficiency of up to a factor of two. This increase is possible without changing, at least relative to the data rate, neither the modulation bandwidth, nor the detection bandwidth, nor the dispersion sensitivity. Further gains are possible with higher-order PPM signalling, but the increasing coding-rate penalty and decoder complexity, along with the relative increase in other noise levels, make these higher-order PPM-OCDMA systems less attractive. This PPM scheme can also be applied to other systems which have the same form of performance limit, such as systems based upon coherence multiplexing, and similar improvements are expected.

Chapter 7

GENERAL OCDMA ANALYSIS

7.1 INTRODUCTION

There are a wide variety of approaches to OCDMA, as detailed in Chapter 2, and it would be good to have a framework in which they all can be treated. There has been such an attempt to define a common structure for all OCDMA schemes, and a corresponding analytical basis for their comparison [Iversen *et al.* 1996]. However, the authors fail to deal adequately with the mixing of light from independent sources, which has clearly been shown to limit the performance of many OCDMA systems [Sampson *et al.* 1997]. In this chapter, the common framework introduced by Iversen *et al.* [1996] is employed, but the received signals are analysed in much more detail, and in particular, the mixing of light from each user is correctly treated. This analysis is then used to identify the crucial characteristics of systems that are limited by this mixing, such as the system analysed in Chapter 3, and the known such limit for coherence multiplexing is also shown to arise from this analysis. A number of OCDMA schemes, and in particular, those incoherent schemes which use bipolar codes, are shown to be ultimately limited by the mixing of light from independent sources, and the corresponding capacity limits are identified.

7.2 GENERAL OCDMA STRUCTURE

Figure 7.1 shows a general star-topology OCDMA structure into which almost all OCDMA schemes that use optical coding can be fitted, following the work of Iversen *et al.* [1996]. The transmitter consists of an optical source with coherence time τ_c, and an encoder, into which the data modulation and encoding are lumped. The optical fields $\boldsymbol{E}_k$ are combined together and distributed amongst the M receivers, and the fields are here represented in complex form. The receiver structure permits both single-ended and balanced detection, and also mixing with a local oscillator field, according to the definitions of the local oscillator field $\boldsymbol{E}_{\mathrm{lo}}$, the coupler power-splitting ratio α, and the decoding functions $\boldsymbol{D}_g$ and $\bar{\boldsymbol{D}}_g$, where the decoder subscript indicates the encoder to which the decoder is matched. For analytical and notational convenience, all the optical fields are represented and scaled so that $\frac{1}{A_d}\iint_{A_d}|\boldsymbol{E}|^2 \mathrm{d}A$ is equal to the total instantaneous optical power normally incident on an area A_d, and the field dependence

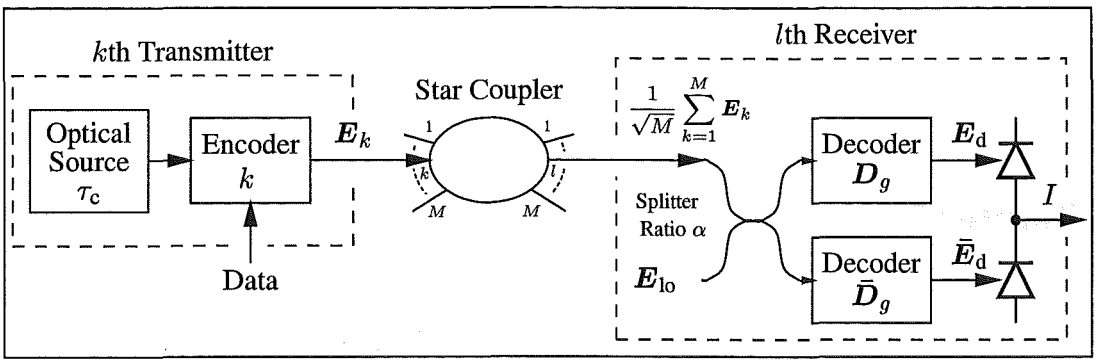

Figure 7.1 General OCDMA Structure

upon spatial location and time is implicit. When full spatial coherence is known or assumed, and the incident area fully encompasses the field distribution, the integral over the area is implicitly assumed, and the total instantaneous power is simply written $|\boldsymbol{E}|^2$.

The outputs of the receiver coupler, with power-splitting ratio α, are given by the product of the two inputs with the following transfer matrix [Iversen *et al.* 1996]

$$\begin{bmatrix} \sqrt{\alpha} & j\sqrt{1-\alpha} \\ j\sqrt{1-\alpha} & \sqrt{\alpha} \end{bmatrix} \tag{7.1}$$

The difference between the photocurrents from each detector gives the balanced receiver photocurrent

$$I = \frac{R}{T_D}\int_{T_D}\left[\frac{1}{A_1}\iint_{A_1}|\boldsymbol{E}_d(t)|^2\,dA - \frac{1}{A_2}\iint_{A_2}|\bar{\boldsymbol{E}}_d(t)|^2\,dA\right]dt \tag{7.2}$$

where R represents the photodiode responsivity, T_D is the effective integration time of the photodiodes, and A_1 and A_2 are the photodiode surface areas, which, in all cases, are assumed large enough to fully encompass the incident fields. The integration over, and division by, interval T_D represents the lowpass filtering inherent in the photodetection process, since any receiver electrical bandwidth is very much less than optical frequencies. However, at times in this chapter this ideal integration form is too restrictive, and the finite receiver bandwidth is accounted for in a different manner - in these cases this average over T_D serves only as a reminder that the receiver bandwidth limitation must be addressed.

The detected fields are given by

$$\boldsymbol{E}_d = \boldsymbol{D}_g\left(\sqrt{\frac{\alpha}{M}}\sum_{k=1}^{M}\boldsymbol{E}_k\right) + \boldsymbol{D}_g(j\sqrt{1-\alpha}\boldsymbol{E}_{lo}) \tag{7.3}$$

$$\bar{\boldsymbol{E}}_{\mathrm{d}} = \bar{\boldsymbol{D}}_g\Big(j\sqrt{\frac{1-\alpha}{M}}\sum_{k=1}^{M}\boldsymbol{E}_k\Big) + \bar{\boldsymbol{D}}_g(\sqrt{\alpha}\boldsymbol{E}_{\mathrm{lo}}) \tag{7.4}$$

where $\boldsymbol{D}_g(\boldsymbol{E})$ is the output from decoder $\boldsymbol{D}_g$ with input $\boldsymbol{E}$. If the receiver decoders are linear, then the detected fields can be written

$$\boldsymbol{E}_{\mathrm{d}} = \sqrt{\frac{\alpha}{M}}\sum_{k=1}^{M}\boldsymbol{D}_g(\boldsymbol{E}_k) + j\sqrt{1-\alpha}\boldsymbol{D}_g(\boldsymbol{E}_{\mathrm{lo}}) \tag{7.5}$$

$$\bar{\boldsymbol{E}}_{\mathrm{d}} = j\sqrt{\frac{1-\alpha}{M}}\sum_{k=1}^{M}\bar{\boldsymbol{D}}_g(\boldsymbol{E}_k) + \sqrt{\alpha}\bar{\boldsymbol{D}}_g(\boldsymbol{E}_{\mathrm{lo}}) \tag{7.6}$$

Note that this linear formulation excludes any OCDMA systems that use hard-limiting, and in particular, those systems described in Section 2.4, for which hard-limiting gives significant performance increase, and hence these systems are discussed later in Section 7.4.2. Under the linear decoder assumption, Equation 7.2 becomes

$$\begin{aligned} I = \frac{R}{T_{\mathrm{D}}}\int_{T_{\mathrm{D}}}\Bigg[\frac{1}{A_1}\iint_{A_1}\Bigg\{\frac{\alpha}{M}\Big|\sum_{k=1}^{M}\boldsymbol{D}_g(\boldsymbol{E}_k)\Big|^2 + (1-\alpha)|\boldsymbol{D}_g(\boldsymbol{E}_{\mathrm{lo}})|^2 - \\ 2\sqrt{\frac{\alpha(1-\alpha)}{M}}\sum_{k=1}^{M}\Im\{\boldsymbol{D}_g(\boldsymbol{E}_k)\boldsymbol{D}_g^*(\boldsymbol{E}_{\mathrm{lo}})\}\Bigg\}\mathrm{d}A - \frac{1}{A_2}\iint_{A_2}\Bigg\{\frac{1-\alpha}{M}\Big|\sum_{k=1}^{M}\bar{\boldsymbol{D}}_g(\boldsymbol{E}_k)\Big|^2 + \\ \alpha|\bar{\boldsymbol{D}}_g(\boldsymbol{E}_{\mathrm{lo}})|^2 - 2\sqrt{\frac{\alpha(1-\alpha)}{M}}\sum_{k=1}^{M}\Im\{\bar{\boldsymbol{D}}_g(\boldsymbol{E}_k)\bar{\boldsymbol{D}}_g^*(\boldsymbol{E}_{\mathrm{lo}})\}\Bigg\}\mathrm{d}A\Bigg]\mathrm{d}t \end{aligned} \tag{7.7}$$

where * represents complex conjugation, and $\Im\{x\}$ is the imaginary part of x.

In writing Equation 7.7 the shot noise and dark currents from the photodetectors have been neglected, along with the inevitable receiver thermal noise. In the following the effects of these realities are either discussed in the text, or else it is assumed that they are negligible due to sufficiently high received power.

7.2.1 Coherent Detection

Following the system description in the previous section, in the case of heterodyne or homodyne detection, usually $\alpha = \frac{1}{2}$, $\boldsymbol{D}_g(\boldsymbol{E}) = \bar{\boldsymbol{D}}_g(\boldsymbol{E})$, and the optical fields are all spatially coherent. Hence, assuming balanced detection, Equation 7.7 becomes

$$I = \frac{2R}{T_{\mathrm{D}}\sqrt{M}}\sum_{k=1}^{M}\int_{T_{\mathrm{D}}}\Im\{\boldsymbol{D}_g(\boldsymbol{E}_k)\boldsymbol{D}_g^*(\boldsymbol{E}_{\mathrm{lo}})\}\mathrm{d}t \tag{7.8}$$

which is linear with respect to the signals from each different user. Such coherent detection would be appropriate for an OCDMA system based upon direct BPSK modulation of coherent laser light. In this case the receiver could consist of further BPSK modulation by the spreading sequence, heterodyne or homodyne detection with a matched local oscillator, and appropriate filtering to extract the single despread signal from amongst all the other spread signals. In this manner, the system functions exactly as a radio spread-spectrum multiple-access system. There are a couple of practical differences between coherent BPSK-based OCDMA and a similar radio system however, primarily related to the enormous difference in carrier frequency between the two cases. This frequency difference manifests itself in the form of significant shot noise in the optical case, due to the much higher energy photons. There is also a significant increase in phase noise from the optical sources with respect to radio-frequency carriers, since absolute linewidth specifications cannot be easily maintained when the carrier frequency is increased by several orders of magnitude. However, at worst, the shot noise and the contributions from this phase noise increase only linearly with respect to the number of users. Since the local optical source in the receiver typically has significantly greater power than any of the received signals, the effects of any residual intensity noise in the optical sources are dominated by that of the source in the receiver.

If the receiver is not ideally balanced, then some small fraction of any source intensity noise and possible phase-induced intensity noise (PIIN) does remain in the photocurrent difference. However, as just explained, all of any source intensity noise is generally small with respect to that of the local oscillator, and a similar argument applies to the PIIN generated between the light from each transmitter source, even when they have identical power spectra. Hence, the assumption of ideal balanced detection is reasonable with respect to the mixing noise arising in this coherent case.

7.2.2 Incoherent Detection

In most OCDMA systems heterodyne or homodyne detection is not appropriate, so in Equation 7.7 $\boldsymbol{E}_{\mathrm{lo}} = 0$. Note that although this section is entitled "Incoherent Detection", the possibility of the decoders being coherently matched to the encoders or the encoded signals has not been excluded, and the typical effects of such matching are considered later in Section 7.2.7. From Equation 7.7 with $\boldsymbol{E}_{\mathrm{lo}} = 0$, the balanced photocurrent becomes

$$I = \frac{R}{MT_{\mathrm{D}}} \int_{T_{\mathrm{D}}} \Bigg[\overbrace{\alpha \sum_{k=1}^{M} |\boldsymbol{D}_g(\boldsymbol{E}_k)|^2}^{\text{(a)}} - \overbrace{(1-\alpha) \sum_{k=1}^{M} |\bar{\boldsymbol{D}}_g(\boldsymbol{E}_k)|^2}^{\text{(b)}} + \overbrace{\frac{\alpha}{A_1} \sum_{k=1}^{M} \sum_{\substack{l=1 \\ k \neq l}}^{M} \iint_{A_1} \boldsymbol{D}_g(\boldsymbol{E}_k) \boldsymbol{D}_g^*(\boldsymbol{E}_l) \mathrm{d}A}^{\text{(c)}} - \overbrace{\frac{1-\alpha}{A_2} \sum_{k=1}^{M} \sum_{\substack{l=1 \\ k \neq l}}^{M} \iint_{A_2} \bar{\boldsymbol{D}}_g(\boldsymbol{E}_k) \bar{\boldsymbol{D}}_g^*(\boldsymbol{E}_l) \mathrm{d}A}^{\text{(d)}} \Bigg] \mathrm{d}t \tag{7.9}$$

In Equation 7.9, it can be seen that the balanced receiver photocurrent has four terms, where (a) and (b) correspond to the signal power from each user after decoding. In normal operation, the light from the desired user $\boldsymbol{E}_{k=g}$ is matched in some sense by the decoders $\boldsymbol{D}_g$ and $\bar{\boldsymbol{D}}_g$, and terms (a) and (b) give a large signal component in I. Each of the unmatched users ($k \neq g$) are not being despread by the decoder(s), so only a small fraction of their power appears in $I(t)$ from terms (a) and (b), and this is the usual MAI contribution. However, there are two further terms in Equation 7.9, (c) and (d), and these represent mixing between the detected light fields from each user and that from every other user. In almost all OCDMA schemes, each user has an independent light source, since one of the motivations behind CDMA is to avoid coordination and synchronisation amongst all the users. With independent light sources, there is no temporal coherence between the detected light fields from different users. Hence, the relative phase noise between each incoherent pair of detected light fields can generate phase-induced intensity noise (PIIN) due to the mixing represented by terms (c) and (d) of Equation 7.9. This is particularly significant, since the number of these potential noise terms is of the order of K^2 rather than linear with respect to K, where K is the number of users that are actually transmitting simultaneously, and of course $K \leq M$. Consequently, this noise has been shown to severely limit OCDMA systems based upon coherence multiplexing [Healey 1987], coherence coding [Griffin *et al.* 1995][1], or spectral-amplitude coding [Smith *et al.* 1995]. Iversen *et al.* [1996] note that such unwanted mixing terms appear in the case of single-ended detection, but it is erroneously claimed that these mixing terms can be suppressed by balanced detection (termed differential detection in their work).

Clearly then, the conditions under which these mixing terms may or may not be neglected need to be carefully examined. The most obvious situations in which the mixing terms (c) and (d) of Equation 7.9 may be neglected are those in which the fields from different users are orthogonal in some domain. In Section 7.2.3 through Section 7.2.7, orthogonality or otherwise is considered for the temporal, spectral, and spatial domains, along with other considerations which affect the significance of terms (c) and (d).

7.2.3 Temporal Orthogonality

If the optical fields from each source arrive at the photodetectors at different times, then there cannot be any mixing between them, - they are orthogonal in time, as correctly observed in [Iversen *et al.* 1996]. Ideal temporal orthogonality occurs, for example, in a time-division multiple-access (TDMA) system, in which each user is allocated exclusive access to a different time slot, and hence every user must be synchronised. However, in general, CDMA systems are designed to avoid the need for synchronisation between users, and this is also desirable, or in fact more so, in optical networks. Hence, there are no OCDMA system proposals that have ideal temporal orthogonality between users' signals. Without attempting to achieve

[1]Note however that the SNR limit given in this work is in error, and that the actual SNR limit is 6 dB worse than reported therein, as detailed in Section 7.3.2.

full temporal orthogonality, however, the principle of reducing the mixing between signals by reducing their temporal extent can be advantageously applied to some OCDMA systems, as demonstrated in Chapters 5 and 6. Incoherent unipolar OCDMA systems also effectively use a form of temporal separation between users' signals through their sparse coding sequences, with a corresponding improvement with respect to mixing noise, as discussed later in Section 7.4.2.

7.2.4 Spectral Orthogonality

Similar to the previous section, if each separate light field is significantly different in wavelength, or equivalently, optical frequency, then their mixing can be neglected, as in a typical wavelength-division multiple-access (WDMA) system. Technically, pure spectral orthogonality does not actually eliminate mixing between the light fields, it merely assures that most or all of the mixing products are beyond the receiver bandwidth. Due to the extremely high optical frequencies, any mixing noise (PIIN) within a receiver bandwidth B_e can only be generated by the mixing of two optical field components whose centre frequencies differ by less than B_e. Hence, 'spectral orthogonality', in the sense that no in-band mixing terms appear, requires that the spectra of the fields received from different sources must be separated by at least B_e in frequency from all the spectral components of the other sources, where B_e is the maximum input frequency of the receiver.

In some OCDMA systems, including those based upon coherence multiplexing, coherence coding, spectral-amplitude coding, and coherent spectral-phase encoding, the light from each user is designed to have exactly the same spectral range, and hence spectral orthogonality is either impractical or impossible for these systems.

Many of the incoherent OCDMA systems, as discussed in Sections 2.4 and 2.9, assume incoherent sources of light pulses, where the coherence time is much shorter than the actual pulse length. Gain-switched Fabry-Perot semiconductor lasers have been identified as perhaps the only suitable such sources, capable of providing approximately 20 ps pulses with a time-bandwidth product of around 50 [Sampson *et al.* 1997]. The coherence time of such pulses is less than 1 ps, and it should be noted that the spectral width is significant, of the order of $\frac{50}{20\,\mathrm{ps}} = 2.5\,\mathrm{THz}$, which corresponds to several nanometres in width, depending upon the centre wavelength and the spectral shape. Hence, if many such sources are used together in an OCDMA network, it becomes quite likely that a significant proportion of them then occupy the same spectral regions. It is therefore prudent to consider the effects of any mixing between the light from these sources, since they can generate in-band components at the receiver.

7.2.5 Spatial Coherence

A necessary condition for terms (c) and (d) of Equation 7.9 to be non-negligible is that the different light fields must be spatially coherent. If the fields from any pair of different sources

at the photodetectors have no spatial coherence, then the integrals across their field distributions $\iint_{A_1} \Re\{\boldsymbol{D}(\boldsymbol{E}_k)\boldsymbol{D}^*(\boldsymbol{E}_l)\}\mathrm{d}A$ and $\iint_{A_2} \Re\{\bar{\boldsymbol{D}}(\boldsymbol{E}_k)\bar{\boldsymbol{D}}^*(\boldsymbol{E}_l)\}\mathrm{d}A$ are zero, and hence this can be viewed as spatial orthogonality. This is exactly the case in the uplink of the terrestrial-satellite OCDMA system discussed in Section 2.9.1.

As discussed in Section 2.4, there have been several OCDMA proposals that use multiple fibres to and from each user. Conceptually, this just requires the paths and components shown in Figure 7.1 and the field representations to each have an extra spatial dimension. This would further complicate the current notation and for this reason multi-fibre cases are not treated here in analytical detail. However, the effect of this extra spatial dimension upon the mixing between incoherent fields can be simply determined. Generally, the multiple fibres in such proposals are brought to separate detectors, so there is no coherence over this extra spatial dimension. It is hence reasonable to expect that the mixing terms (c) and (d) of Equation 7.9 can be reduced by a factor equal to the number of multiple fibres. This is in fact the case, provided that the signals are evenly distributed amongst the multiple fibres and that there are the same number of fields mixing within each fibre as in a single-fibre implementation. It is also necessary that the PIIN from each fibre is independent, and this is the case except if the signals in each parallel path are coherently related, as in a holographic system such as [Salehi and Paek 1995]. Such a holographic system is of course coherent, in which case the mixing between independent fields is generally of little significance, as discussed in Sections 7.2.7 and 7.4, and in fact the experiments reported in [Salehi and Paek 1995] did not use independent sources for each user.

In an OCDMA system with single path, single-mode fibres (SMF) and couplers throughout, the issue of spatial coherence is essentially determined by the relative states of polarisation (SOP) of the light fields, since there are two orthogonal polarisation modes that are guided by cylindrical SMF. The worst-case scenario is that all the fields are fully polarised, and that they all have the same polarisation state. This is the case assumed, for example, in the analysis of the performance limits of coherence-multiplexed OCDMA systems [Pendock and Sampson 1997]. If all the light is unpolarised, then the light is split evenly between two orthogonal modes, and terms (c) and (d) in Equation 7.9 may be split into two terms each, one for each orthogonal polarisation component. The PIIN power that results from these terms is 3 dB less than the case of full and matched polarisations, since mixing between orthogonal field components does not occur. In the case of fully polarised fields but no polarisation control, then the size of terms (c) and (d) varies as the polarisation state of each field changes with environmental influences. The upper limit of this variation is of course the case of full and matching polarisations just discussed, and for large numbers of users, the overall effect of mixing between different sources tends towards that of unpolarised sources. It should be noted, however, that any source intensity noise and any mixing between the light from the same source is still that corresponding to polarised sources.

If the sizes of the OCDMA system and the optical bandwidths are small enough that multimode fibre (MMF) may be used, then there is a significant reduction in the spatial coherence

of the light in the MMF due to the orthogonal MMF modes. There is a corresponding reduction in the size of terms (c) and (d) of Equation 7.9, according to the power distribution amongst the spatially-orthogonal modes of the MMF, as investigated in Section 4.3. The use of MMF is one way of reducing the spatial coherence of the mixing fields, but it increases the dispersion significantly, and there are not many optical MMF devices to choose from. If the transmitters and output fibres are single-mode, then there has to be sufficient MMF length before the MMF star coupler and the output MMFs to each multimode receiver so that the light is widely distributed amongst the modes before the mixing occurs in the star coupler. The rest of the paths from the transmitters may still remain in SMF if necessary, to avoid the extra dispersion, for example. Another way of possibly achieving a similar effect is to have an $M \times nM$ star coupler rather than $M \times M$, where n is an integer, and there are n SMF paths to n receivers in parallel at each user. The different relative phase delays between each coupler output should ensure that the mixing noise detected in each receiver is uncorrelated or of low correlation[2]. By combining the received signals after photodetection, a reduction in the mixing noise of order n is achieved for uncorrelated mixing noise in each branch. Clearly, however, there is also an increase in shot and dark-current noise of order n, and the receiver duplication is very expensive, and hence this method of reducing PIIN is only useful conceptually.

One of the major disadvantages of optical tapped delay-lines is that the balanced addition of z tap outputs has an inherent power loss of z, also referred to as the combining loss, corresponding to the use of a single output of a $z \times z$ coupler, for example. In some systems of the form of Figure 2.2 or Figure 2.5, each delay-line tap is immediately incident upon a photodiode. In such cases, the recombination of the tap outputs into a single fibre is not required, since it is merely the power from each tap that is required, and hence an array of photodiodes may be used, for example. This eliminates the combining loss of z, since all the power is detected. There is, however, an increase in dark-current associated with the larger total photodetector area, and a similar bandwidth reduction or noise increase due to the extra photodiode capacitance is likely. Another advantage of this arrangement is that there is no spatial coherence of the fields from each fibre. In this manner, mixing between the fields from different delay-line taps may be greatly reduced or eliminated. In Section 7.3.3 the effect of eliminating this mixing is quantified for some particular cases, and the effects upon incoherent unipolar OCDMA systems are discussed in Section 7.4.2.

7.2.6 Temporal Coherence

As has already been stated, it is the mixing of temporally incoherent fields within the same spatial mode that can lead to the PIIN that limits a number of OCDMA systems. This incoherence, by definition, means that the average mixing between two such fields is zero. However, technically that is an ensemble average, and under the assumption of ergodicity, it is equivalent to

[2]Zero correlation between the coupler outputs occurs, for example, if the phase delays in the coupler represent an orthogonal transformation, and each transmitted field is a Gaussian random variable with the same variance.

an average over all time, but in practice, the result of the mixing over finite time intervals is of concern. In Equation 7.9, the integral of the mixing fields over the time T_D is required, and as detailed in Section 3.2, the critical factor is the number of coherence cells $\mathcal{M}$ of the light fields that influence the measurement over time T_D, and for $T_D \gg \tau_c$, $\mathcal{M} \approx \frac{T_D}{\tau_c}$. As $\mathcal{M}$ increases, the integral over T_D can be thought of as averaging over a greater number of coherence lengths, and the resulting noise variance is then smaller. This applies regardless of whether the noise is due to source intensity noise or from the mixing of incoherent fields, and hence the total intensity noise in the balanced photocurrent of Equation 7.9 is proportional to $\frac{\tau_c}{T_D}$. Clearly then, if lower coherence sources are used, then any PIIN and source intensity noise are reduced. Of course, reducing the electrical bandwidth also reduces any intensity noise, since T_D is increased. Note that decreasing the coherence time must also correspond to increasing the spectral width, with the resulting increase in dispersion and possible increase in the overlap of source spectra.

In the general analysis of Iversen *et al.* [1996], it is stated that mixing between the light fields from different users is suppressed in the case $\tau_c \ll T_D$. However, this is quite misleading, since the intensity noise is actually just proportional to $\frac{\tau_c}{T_D}$, and merely achieving $\tau_c \ll T_D$ does not ensure that the results of such mixing are sufficiently suppressed to be negligible. In fact, in the OCDMA systems based upon coherence multiplexing, coherence coding, and spectral-amplitude coding, the source coherence times are typically shorter than the receiver integration times by several orders of magnitude, yet mixing between incoherent light still severely limits the performance of these systems [Chu and Dickey 1991, Griffin *et al.* 1995, Smith *et al.* 1995].

7.2.7 Relative Signal Magnitude

There are a total of $2M(M-1)$ terms in parts (c) and (d) of Equation 7.9, which each express the mixing between the independent light fields of each transmitting user. If each of these terms represent independent and identically distributed PIIN components that are within the detector bandwidth, then their contribution to the receiver noise is approximately proportional to the square of the number of active users, K^2. This order of noise dependence can lead to serious performance limitations, as, for example, seen in Chapter 3, where this PIIN makes the received light appear thermal as K increases. However, if the power from the desired user is much larger than that from any other user in at least some fraction of a particular domain, then any field mixing in that location is dominated by mixing with the field of the desired user. Consequently, by limiting the decision-variable scope to just that location, any effects of such mixing then only have linear dependence upon K. Assuming that the received power level from each user is equal, the general way by which to achieve such distinction is to have a decoder that is a coherent matched filter to the encoded signal, that is to coherently despread the signal. This type of decoder thus coherently combines the components of the desired signal, but all the other signals either undergo significant coherent cancellation, or else they combine incoherently on average. Such distinction can also occur in an incoherent system when the signals are sufficiently separated temporally, for example, as in the case of sparse unipolar

codes. These systems are designed so that even when collecting the power from the desired user with an incoherent decoder, the power from the other users is likely to be much smaller, at least in the interval when the signal power is greatest. However, such distinction with an incoherent decoder is only possible when the signals from each user are significantly separated in some domain, and this distinction thus arises out of that separation, rather than it being due to any incoherent decoding scheme.

7.3 SYSTEMS WITH SIGNIFICANT PIIN

In this section, OCDMA systems are considered in the light of the contributing factors to optical mixing noise, and those systems that are significantly affected by optical mixing are identified and considered in detail.

7.3.1 Coherence Multiplexing

Considering the OCDMA-like system of coherence multiplexing described in Section 2.7, it can be fitted to the structure of Figure 7.1 by defining $\boldsymbol{E}_k = \frac{1}{\sqrt{2}}[\boldsymbol{S}_k(t) + d_k(t)\boldsymbol{S}_k(t-\tau_k)]$, where $\boldsymbol{S}_k$ is the fully polarised light field of the kth user's source, $d_k(t)$ represents the kth user's ± 1 data sequence, and τ_k is the delay in the MZI encoder of the kth user. The appropriate decoding functions of the receiver matched to the gth transmitter are defined as $\boldsymbol{D}_g(\boldsymbol{E}_k) = \frac{1}{\sqrt{2}}[\boldsymbol{E}_k(t) + \boldsymbol{E}_k(t-\tau_g)]$, and $\bar{\boldsymbol{D}}_g(\boldsymbol{E}_k) = \frac{1}{\sqrt{2}}[\boldsymbol{E}_k(t) - \boldsymbol{E}_k(t-\tau_g)]$. Furthermore, $\alpha = \frac{1}{2}$ is required, and it is assumed that the polarisation states of the light from each source are completely aligned and that they remain so throughout the network.

Under these definitions and conditions, the receiver balanced photocurrent becomes

$$
\begin{aligned}
I(t) = \frac{R}{2MT_{\mathrm{D}}} \int_{T_{\mathrm{D}}} \Bigg[\sum_{k=1}^{M} \Re\{ & \underbrace{\boldsymbol{S}_k(t)\boldsymbol{S}_k^*(t-\tau_g)}_{\text{(i)}} + \underbrace{d_k(t-\tau_g)\boldsymbol{S}_k(t)\boldsymbol{S}_k^*(t-\tau_g-\tau_k)}_{\text{(ii)}} \\
& + \underbrace{d_k(t)\boldsymbol{S}_k(t-\tau_k)\boldsymbol{S}_k^*(t-\tau_g)}_{\text{(iii)}} + \underbrace{d_k(t)d_k(t-\tau_g)\boldsymbol{S}_k(t-\tau_k)\boldsymbol{S}_k^*(t-\tau_g-\tau_k)}_{\text{(iv)}} \} \\
+ \sum_{\substack{k=1 \\ k\neq l}}^{M} \sum_{l=1}^{M} \Re\{ & \underbrace{\boldsymbol{S}_k(t)\boldsymbol{S}_l^*(t-\tau_g)}_{\text{(a)}} + \underbrace{d_l(t-\tau_g)\boldsymbol{S}_k(t)\boldsymbol{S}_l^*(t-\tau_g-\tau_l)}_{\text{(b)}} \\
& + \underbrace{d_k(t)\boldsymbol{S}_k(t-\tau_k)\boldsymbol{S}_l^*(t-\tau_g)}_{\text{(c)}} + \underbrace{d_k(t)d_l(t-\tau_g)\boldsymbol{S}_k(t-\tau_k)\boldsymbol{S}_l^*(t-\tau_g-\tau_l)}_{\text{(d)}} \} \Bigg] \mathrm{d}t
\end{aligned}
\tag{7.10}
$$

where the cross terms (a)-(d) are expressed separately from the terms with $k = l$, as per Equation 7.9, although the combined form is simpler. The decoder is matched to that of user $k = g$, and it is assumed that all other users are distinct and unmatched, with $|\tau_g - \tau_k| \gg \tau_{\mathrm{c}}$, $k \neq g$. Each source field $\boldsymbol{S}_k(t)$ is assumed to have the same average power P_{s}. Hence,

term (iii) in Equation 7.10 with $k = g$ gives the signal component of $d_g(t).\frac{RP_s}{2M}$, along with a possible contribution from any source intensity noise. In fact, each term in Equation 7.10 may contribute to the total noise of $I(t)$, and these contributions can be determined by considering the power spectral density (PSD) of $I(t)$ over the receiver bandwidth in general (rather than simply averaging over the bit period as shown in Equation 7.10). This PSD is of course given by the Fourier transform of the autocorrelation $\mathrm{E}\big[I(t)I(t+\tau)\big]$. Assuming identical ideal thermal sources, data modulation at a rate $\frac{1}{T_D} \ll \frac{1}{\tau_c}$, and that all interferometer delays τ are small with respect to the bit period T_{bit}, this analysis is straightforward, and a neat calculation of the noise power following this approach is given in [Pendock and Sampson 1997]. Here, however, the total noise is calculated by the careful addition of the noise associated with each term in Equation 7.10, through the use of Equation 3.16, which was derived by calculation of the noise PSD.

The conditions assumed here are that of distinct matched and unmatched users $|\tau_g - \tau_k| \gg \tau_c$ for $k \neq g$, where τ_c is the coherence time of the identical and independent sources, and that all the interferometer delays τ_g, τ_k and τ_l are small with respect to the bit period T_{bit}. As detailed shortly, this last assumption ensures that the noise spectrum is approximately flat across the receiver bandwidth B_e, where this is assumed to be of order $\frac{1}{2T_{bit}}$. This assumption is certainly analytically convenient, but it is also likely to be reasonable in practice, since short interferometer delays are desirable for minimising the encoder and decoder sizes in an optical integrated-circuit realisation. Furthermore, this assumption is worst case, since the actual noise PSD tends to decrease from its zero-frequency level.

Each of terms (a)-(d) in Equation 7.10 represent the interference of two independent broadband fields with the same power spectrum and average power, effectively with total incident power $\frac{P_s}{2M}$ upon a single photodiode with responsivity R. Furthermore, since all of the interferometer delays τ_g, τ_k and τ_l are much greater than the source coherence time, and each source is independent, these PIIN terms are uncorrelated. There are $4K(K-1)$ such terms, each contributing PIIN power

$$\sigma^2_{\text{term}} = \frac{R^2 P_s^2 \tau_c B_e}{4M^2} \tag{7.11}$$

according to Equation 3.16, and this PIIN dominates the total noise. In using Equation 3.16 the average over the photodiode integration time T_D indicated in Equation 7.10 has been replaced by the assumption that the noise spectrum is flat over the receiver bandwidth, which is reasonable since $\tau_c \ll T_{bit}$, and hence the noise power is proportional to the receiver bandwidth B_e in general. When $k = g$, the excess noise associated with the signal term (iii) has power $2\sigma^2_{\text{term}}$ if source $\boldsymbol{S}_g$ is thermal (Equation 3.10), and when $k \neq g$, this zero-mean term represents PIIN which contributes half that power. Term (ii) represents zero-mean PIIN of power σ^2_{term} for each k. Finally, terms (i) and (iv) are correlated under the assumed condition that $\tau_g \ll T_{bit}$, and hence they produce a noise power spectrum with cosine-squared modulation, of periodicity $\frac{1}{\tau_k}$. The delays τ_k have also been assumed small compared to the bit period, so the noise spectrum

from these correlated terms is still considered flat over the receiver bandwidth B_e, giving PIIN of power $4\sigma^2_{term}$ for each k. Another way of viewing the condition $T_{bit} \gg \tau_k, \forall k$, is that the frequencies of interest are sufficiently low that the time shifts τ_k between (i) and (iv) correspond to quite small phase differences, and hence the noise from terms (i) and (iv) is almost completely correlated over the bandwidth of interest B_e. Calculation on the basis of complete correlation as above is therefore worst case. There is no other correlation between any of the aforementioned PIIN and thermal noise terms, and so the noise powers may be simply added, giving the total noise power of

$$\sigma_I^2 = \frac{R^2 P_s^2 \tau_c B_e}{4M^2}(4K^2 + 2K + 1) \tag{7.12}$$

The result of Equation 7.12 is equal to that derived neatly in [Pendock and Sampson 1997], substituting $I_0^2 = 4R^2P_s^2$ and $N = M = K$. Recalling that the signal level $\mathrm{E}[I(t)] = \pm\frac{RP_s}{2M}$, the PIIN-limited SNR is then given by

$$\rho_{CM.pol} = \frac{\mathrm{E}[I(t)]^2}{\sigma_I^2} = \frac{1}{\tau_c B_e(4K^2 + 2K + 1)} \approx \frac{1}{4\tau_c B_e K^2} \tag{7.13}$$

in agreement with [Pendock and Sampson 1997], and where the approximation is reasonable for large K.

Note that a much simpler way of getting a noise estimate close to that of Equation 7.12 is simply to assume that all the incident light has purely thermal characteristics only, and with coherence time τ_c. The photodiode with the incident signal light receives power $\frac{P_s(2K+1)}{4M}$, and the other photodiode $\frac{P_s(2K-1)}{4M}$. Simply calculating the intensity noise of each and adding their power gives a total noise estimate of $(4K^2 + 1)\sigma^2_{term}$. The only difference from Equation 7.12 is the absence of the $2K$ term, which corresponds to the case where correlation between terms (i) and (iv) may be neglected.

If each source is unpolarised, and polarisation-independent devices are used throughout the network, then the PIIN and the source intensity noise are reduced by 3 dB, giving a PIIN-limited SNR of

$$\rho_{CM.unpol} = \frac{2}{\tau_c B_e(4K^2 + 2K + 1)} \approx \frac{1}{2\tau_c B_e K^2} \tag{7.14}$$

In the case of broad-linewidth laser sources that have negligible self-intensity noise, the only difference in the case of balanced detection is that the signal term (iii) for $k = g$ is ideally noiseless, resulting in the factor $4K^2 + 2K - 1$ rather than $4K^2 + 2K + 1$ in Equations 7.12 - 7.14.

Recent analysis has drawn attention again to the performance of coherence multiplexing with single-ended detection [Gupta *et al.* 1997]. Although the case of balanced detection is both superior and much more practical for a multiple-access system, the single-ended case is also considered here in order to identify and correct the deficiencies in [Gupta *et al.* 1997].

7.3.1.1 Single-Ended Detection

The case of coherence multiplexing with single-ended detection has the same definitions as the balanced case of $\boldsymbol{E}_k = \frac{1}{\sqrt{2}}[\boldsymbol{S}_k(t) + d_k(t)\boldsymbol{S}_k(t-\tau_k)]$, $\boldsymbol{D}(\boldsymbol{E}_k) = \frac{1}{\sqrt{2}}[\boldsymbol{E}_k(t) + \boldsymbol{E}_k(t-\tau_g)]$, and $\alpha = \frac{1}{2}$, but now $\bar{\boldsymbol{D}}(\boldsymbol{E}_k) = 0$. It is still assumed that the polarisation states of the light from each source are completely aligned and that they remain so throughout the network. The source powers are again assumed sufficiently large that shot noise and receiver noise may be neglected. All further assumptions in the analysis of the balanced case also apply in the single-ended case unless stated otherwise.

Under these definitions and conditions, the detector photocurrent in terms of $\boldsymbol{E}_k$ becomes

$$I(t) = \frac{R}{4M}\frac{1}{T_\mathrm{D}}\int_{T_\mathrm{D}}\left[\sum_{k=1}^{M}\left\{\underbrace{\left|\boldsymbol{E}_k(t)\right|^2}_{\text{(i)}} + \underbrace{\left|\boldsymbol{E}_k(t-\tau_g)\right|^2}_{\text{(ii)}} + \underbrace{2\Re\{\boldsymbol{E}_k(t)\boldsymbol{E}_k^*(t-\tau_g)\}}_{\text{(iii)}}\right\} + \right.$$
$$\left. 2\sum_{k=1}^{M-1}\sum_{l=k+1}^{M}\Re\left\{\underbrace{\boldsymbol{E}_k(t)\boldsymbol{E}_l^*(t)}_{\text{(a)}} + \underbrace{\boldsymbol{E}_k(t)\boldsymbol{E}_l^*(t-\tau_g)}_{\text{(b)}} + \underbrace{\boldsymbol{E}_k(t-\tau_g)\boldsymbol{E}_l^*(t)}_{\text{(c)}} + \underbrace{\boldsymbol{E}_k(t-\tau_g)\boldsymbol{E}_l^*(t-\tau_g)}_{\text{(d)}}\right\}\right]\mathrm{d}t \tag{7.15}$$

where the form of Equation 7.10 has been maintained, and the definition of $\boldsymbol{E}_k$ has not yet been substituted to here avoid the cumbersome representation so obtained, which appears in Appendix D. In the case of balanced detection, only terms (iii), (b) and (c) remained, since terms (i), (ii), (a), and (d) are then common to both photodiodes. Although Equation 7.15 even in this form is more cumbersome than the representation in [Pendock and Sampson 1997], this form is useful in Appendix D because the effects of data modulation can be clearly deduced.

The noise calculations performed in [Gupta *et al.* 1997] assume sources with negligible self-intensity noise, so the intensity terms arising from (i) and (ii), along with the signal intensity from (iii), contribute no noise. Every other term arising from Equation 7.15 consists either of mixing between different source fields, or of mixing between a source field and that field with a time delay much greater than the coherence time, and these all contribute PIIN. However, in [Gupta *et al.* 1997] each of these terms is assumed to contribute mutually uncorrelated PIIN, so the total noise calculation is simply a matter of counting the PIIN terms in the expanded form of Equation 7.15 (Equation D.2 in Appendix D), resulting in a total noise estimate proportional to $8K^2 - 2K - 1$. The case where the wavelength separations between the different sources are such that their interference is out-of-band is also considered in [Gupta *et al.* 1997], and this amounts to assuming that all PIIN arising from terms (a)-(d) in Equation 7.15 is not within the receiver bandwidth, and hence may be neglected. The noise power is thus found to be proportional to $6K - 1$ in [Gupta *et al.* 1997]. The corresponding signal-to-interference-noise ratios are given as

$$\mathrm{SIR} = \frac{8}{8K^2 - 2K - 1}\frac{\delta\nu}{B_\mathrm{e}} \tag{7.16}$$

for the case of identical sources, and for sufficient wavelength separation

$$\mathrm{SIR} = \frac{8}{6K-1}\frac{\delta\nu}{B_\mathrm{e}} \tag{7.17}$$

where B_e is the receiver bandwidth, and $\delta\nu$ is the source linewidth [Gupta *et al.* 1997]. However, it is shown here that the PIIN from each term within Equation 7.15 cannot all be uncorrelated under practical operating conditions, and certainly not under those considered in [Gupta *et al.* 1997], and hence the K-dependence found here is different from that in Equations 7.16 and 7.17. For the case of identical sources and single-ended detection, Equation 7.16 appears to be larger than the known limit for differential detection, which is Equation 7.13. However, the definition of signal level in the calculations in [Gupta *et al.* 1997] leading to Equations 7.16 and 7.17 is twice that which is used in the SNR calculations here and in other coherence-multiplexing analyses, and hence these SIRs must be reduced by a factor of four before such comparison. Apart from the different K-dependence, as detailed shortly, and this factor of four in signal power, Equation 7.16 can be reconciled to the limits appearing in [Chu and Dickey 1991] and [Pendock and Sampson 1997] for large K so long as $\tau_\mathrm{c} = \frac{1}{2\delta\nu}$. This conversion between coherence time and linewidth is numerically between those which exist for Lorentzian and Gaussian spectral shapes when the linewidth measure is the full width at half maximum power (FWHM). Hence, this conversion is not unreasonable, but the spectral shapes of the sources and the particular type of linewidth measure used for $\delta\nu$ are not actually specified in [Gupta *et al.* 1997].

In the case of coherence multiplexing with balanced detection, it was noted that with all interferometer delays $\tau \ll T_\mathrm{bit}$, the terms (i) and (iv) of Equation 7.10 differ predominantly by only a simple time-shift. These two terms also appear in the expansion of term (iii) of Equation 7.15, along with many other such correlated terms in Equation 7.15, as detailed in Appendix D, and hence they produce a periodic modulation in the noise spectrum. Theoretically, if the interferometer delays are large enough that either an integer number or a large number of such modulation periods fall within the receiver bandwidth, then it is reasonable to simply add the power from each term as though they were uncorrelated, as per [Gupta *et al.* 1997], provided the receiver spectral response is flat, since the noise spectrum is then no longer flat. However, the examples considered in [Gupta *et al.* 1997] use a receiver bandwidth of 5 MHz, and assuming the corresponding data rate is approximately 10 Mb s^{-1}, the bit period is then 100 ns or so. In a medium with refractive index of about 1.5, the propagation delay is about 5 ns m^{-1}, and hence, recalling that the transmitter and receiver interferometers must be stabilised and matched to within a fraction of the optical wavelength, the delay in any practical interferometer length must be much smaller than this bit period. Consequently, terms in Equation 7.15 of the form of (i) and (iv) in Equation 7.10 are definitely almost completely correlated, and the neglect of such correlations in [Gupta *et al.* 1997] gives incorrect results (Equations 7.16 and 7.17) therein.

The details of calculating the noise power from Equation 7.15 appear in Appendix D.

It is sufficient here to note that strong correlation clearly exists between terms (i) and (ii) of Equation 7.15, and also between terms (a) and (d), and all further details are consigned to Appendix D. Taking all possible correlations into account, the following total noise variance is found for the case of identical thermal sources

$$\sigma_I^2 = \frac{R^2 P_s^2 \tau_c B_e}{16M^2}\left(12K^2 + 6K + 1 + 8(K+1)d_g(t)\right) \tag{7.18}$$

The term $8(K+1)d_g(t)$ in Equation 7.18 indicates that the noise power is actually dependent upon the bipolar data of the matched (gth) user, and this is a second order effect that has not been clearly reported to date. Hence, a detection threshold midway between the signal levels for a 'zero' and a 'one' is theoretically sub-optimum for the single-ended case, but this is of little significance when the number of simultaneous users is large.

If independent and identical sources with no self-intensity noise are used, then the photocurrent noise level is (Appendix D)

$$\sigma_I^2 = \frac{R^2 P_s^2 \tau_c B_e}{16M^2}(12K^2 - 2K - 1 + 8Kd_g(t)) \tag{7.19}$$

The signal in the single-ended case is given by $\pm\frac{RP_s}{4M}$, which is half that in the balanced case, but there is now also an average level of $\frac{RP_sK}{2M}$, and hence for the noiseless-source case the signal-to-average-noise ratio becomes

$$\frac{\left(\pm\frac{RP_s}{4M}\right)^2}{\mathrm{E}[\sigma_I^2]} = \frac{1}{\tau_c B_e(12K^2 - 2K - 1)} \tag{7.20}$$

to be compared with Equation 7.16 from [Gupta *et al.* 1997]. In the limit of large K, the difference between Equations 7.18 and 7.19 is negligible, giving the signal-to-average-noise ratio limit

$$\rho \approx \frac{1}{12\tau_c B_e K^2} \tag{7.21}$$

which agrees with [Pendock and Sampson 1997] and [Chu and Dickey 1991] in the limit of large K.

In the case where each source has no self-intensity noise and is sufficiently separated in wavelength from every other source, then the noise power and 'average' SNR are given by (Appendix D)

$$\sigma_I^2 = \frac{R^2 P_s^2 \tau_c B_e}{16M^2}(10K - 1 + 8d_1(t)) \quad , \qquad \rho = \frac{1}{\tau_c B_e(10K-1)} \tag{7.22}$$

which again differs from that of Equation 7.17 from [Gupta *et al.* 1997].

If each source is completely unpolarised, and there are no polarisation-dependent components in the system, then each of the previous expressions of noise power for single-ended

detection are reduced by 3 dB, with a corresponding increase in the SNR by 3 dB. If all the sources are fully polarised, but they are all considered to have random polarisation states at the receiver, then on average the sum of the PIIN from the mixing of light from different sources is reduced by 3 dB, whereas any source intensity noise and the mixing between light from the same source is unaffected (Appendix D).

7.3.2 Coherence Coding

An OCDMA system closely related to coherence multiplexing is that termed coherence coding [Griffin *et al.* 1993, Griffin *et al.* 1995]. This system has the same structure as coherence multiplexing, apart from the use of a controllable dispersive element in one branch of both the transmitter and receiver interferometers. This dispersive element is a spectral-phase encoder, of the type used in [Weiner *et al.* 1988].

This system can be analysed in a similar manner to a coherence-multiplexing system, and the dominant mixing noise arises in the same fashion as for that system. This leads to the same order of limit

$$\rho_{\text{CC.pol}} \approx \frac{1}{4\tau_c B_e K^2} \tag{7.23}$$

for fully polarised and polarisation-matched fields. Equation 7.23 is in agreement with [Sampson *et al.* 1997], in which it is stated that the analysis of the PIIN limit of coherence coding is the same as that for coherence multiplexing. In the earlier work of [Griffin *et al.* 1995], the noise level was miscalculated, resulting in an incorrect SNR limit approximately four times larger than Equation 7.23.

7.3.3 Incoherent Systems using Bipolar Coding

The basic structure of incoherent OCDMA systems using bipolar coding has been detailed in Section 2.9, and a particular example of such a system has been treated in detail in Chapter 3. Comparing Figures 2.5 and 7.1, it can be seen that matching these structures simply requires that decoders $\boldsymbol{D}_k$ and $\bar{\boldsymbol{D}}_k$ perform correlations with $\boldsymbol{A}_k$ and $\bar{\boldsymbol{A}}_k$ respectively, where these are the complementary sequences used by the kth transmitter, to which $\boldsymbol{D}_k$ and $\bar{\boldsymbol{D}}_k$ are matched. The manner in which this is performed for one particular case can be clearly seen in Figure 3.1. The only exceptions to this correlation structure are the cases of [Tančevski *et al.* 1994], where $\bar{\boldsymbol{D}}_k$ effectively gives only an output proportional to the average power in the transmitted signals, and [Neusy and Kavehrad 1990], where $\bar{\boldsymbol{D}}_k = 0$. However, if $\bar{\boldsymbol{D}}_k$ did perform a correlation with $\bar{\boldsymbol{A}}_k$ in the scheme of [Tančevski *et al.* 1994], then this satisfies their assumed condition, but it also doubles the signal level, so the scheme of [Tančevski *et al.* 1994] effectively has the same structure as all the others, but is unnecessarily inefficient. The same can be said for the scheme of [Neusy and Kavehrad 1990], but, as discussed in Section 2.9.4, this work simply ignores the need to at least compensate for the offset due to the average incident signal

powers. Since a number of crucial aspects of the proposal by Neusy and Kavehrad [1990] have not been addressed therein, this scheme is not specifically treated in the rest of this section. All these schemes are incoherent, with $\boldsymbol{E}_{\mathrm{lo}} = 0$, and in all but the scheme of [Khaleghi and Kavehrad 1996], the coupler splitting ratio $\alpha = \frac{1}{2}$. The order of effect of $\alpha \neq \frac{1}{2}$ upon mixing noise is discussed later in this section.

The transmitted field is represented by $\boldsymbol{E}_k = \boldsymbol{S} \odot \boldsymbol{A}_k$ or $\boldsymbol{E}_k = \boldsymbol{S} \odot \bar{\boldsymbol{A}}_k$, according to the data, where $\odot$ represents the time or frequency multiplication between the source field and the transmitted code. As in Section 2.9, this can be neatly expressed as $\boldsymbol{E}_k = \boldsymbol{S} \odot \frac{1-d_k \boldsymbol{a}_k}{2}$, where $\boldsymbol{a}_k$ is the bipolar representation of the kth user's code, and d_k is the bipolar data sequence. The first incoherent bipolar OCDMA proposal (Section 2.9.1) did not have any spatial coherence between the fields from each user, so any mixing between the fields could be simply neglected. However, spatial coherence must be considered with a fibre network, and hence, assuming that all the fields are fully polarised and spatially coherent, terms (c) and (d) of Equation 7.9 then reduce to

$$\frac{R}{2MT_{\mathrm{D}}} \int_{T_{\mathrm{D}}} \left\{ \sum_{\substack{k=1 \\ k \neq l}}^{M} \sum_{l=1}^{M} \boldsymbol{a}_g \, \Re\left\{ \left[\boldsymbol{S}_k \odot \left(\frac{1 - d_k \boldsymbol{a}_k}{2} \right) \right] \left[\boldsymbol{S}_l^* \odot \left(\frac{1 - d_l \boldsymbol{a}_l}{2} \right) \right] \right\} \right\} \mathrm{d}t \qquad (7.24)$$

where $\boldsymbol{a}_g$ is the bipolar representation of the receiver code (matched to the gth user), and the time dependence and possible frequency dependence of the arguments remains implicit for convenience.

To estimate the significance of the noise from Equation 7.24, attention is restricted to the interval T_{D} over which the decision variable is determined (which can be a fraction of the bit period). Within this interval, the received signals can be split into the N time or frequency slots corresponding to the N individual elements of the receiver code, and these are here termed chips. Note that this definition includes the possibility of a chip representing a fraction $\frac{1}{N}$ of the signal spectral width, as well as the usual temporal case. Throughout the following it is assumed that integration over any time T_{D} is equivalent to an effective bandwidth of $\frac{1}{2T_{\mathrm{D}}}$. Neglecting fibre and connection losses, the effective received power from a single user within a single such chip is denoted P_{c}, the coherence time of the corresponding optical field is denoted τ_{cc} and the temporal extent of the chip is denoted T_{c}. This notation allows the simultaneous derivation of the SNR limits for various incoherent bipolar system configurations. The differences between such systems are expressed in the definitions of P_{c}, τ_{cc} and T_{c}, along with the use of single-ended or balanced detection, and possible coupler combining in the receiver.

The worst-case condition of sources with the same power spectrum and the same (fully polarised) polarisation state is considered in the following. This may not be the case, especially if the bandwidths involved are small, and also, in such low-bandwidth cases, any limits due to PIIN may not be of great significance even with matched spectra. However, source availability and the necessary optical bandwidths required for high-rate systems may ultimately lead to similar source spectra, and it is prudent to consider the effects of this.

It is assumed that the codes are balanced, either directly or via Manchester encoding, and that complementary keying is performed. Hence, and assuming chip synchronism if the coding is temporal, each of K users is transmitting in exactly half of the chips at any particular time. The one exception to this is the scheme of [Andonovic *et al.* 1994], where there are just 50% more empty chips, and this does not reduce the interference since synchronism is required for this system[3]. Furthermore, assuming ideal orthogonality between codes, even with data keying, it is assumed that there are always exactly $\frac{K}{2}$ users transmitting within each of the N chips. This can never be true in practice, since it requires ideal periodic and aperiodic orthogonality, but it allows a simple conservative estimate of the mixing noise.

A crucial characteristic of the receiver design is whether the light fields corresponding to each chip in the receiver code are recombined into a single fibre before photodetection. For example, in Figure 2.2 both the transmitter and receiver contain a tapped delay-line, and in the transmitter each delayed output must be recombined into a single fibre for transmission into the network, thus incurring a significant power loss. It has been rightly noted that this combining power loss in both transmitter and receiver is a serious limitation of many such OCDMA proposals based upon incoherent optical tapped delay-lines, and indeed this has directed research elsewhere [Sampson *et al.* 1997]. However, in the receiver this recombination is not necessary, provided that merely the sum of the optical power in each delayed branch is required for the decoding process. If this is the case, then separate detection of the light from each branch allows all the received power to be detected, and any mixing between this light is avoided, although a price is paid in terms of receiver noise and bandwidth in general. If this recombination into a single fibre is avoided, then PIIN can only be generated by the mixing of pairs of different light fields within the same chip location, and, as discussed in Section 7.2.4, the PIIN can only fall within the receiver bandwidth when these fields are spectrally similar. In the worst case when each source has the same power spectrum, and under the assumption that $T_c \gg \tau_{cc}$, the PIIN from each pair of such sources is given by Equation 3.16, and hence the PIIN power from the mixing of the $\frac{K}{2}$ fields within one chip is given by

$$\sigma_c^2 \approx \frac{\frac{K}{2}\left(\frac{K}{2}-1\right)}{2} \cdot (2RP_c)^2 \cdot \frac{\tau_{cc}}{2T_c} \tag{7.25}$$

where the effective electrical bandwidth is given by $\frac{1}{2T_c}$. The assumption of $T_c \gg \tau_{cc}$ also leads to the noise generated within each chip (of temporal extent T_c) being independent, and half of the chips are associated with each photodiode due to the correlations with $\boldsymbol{A}$ and $\bar{\boldsymbol{A}}$. Adding together all of these contributions, and integrating over the interval T_D, the total PIIN power for each photodiode is given by

$$\sigma_D^2 = \sigma_c^2 \frac{N}{2}\left(\frac{T_c}{T_D}\right)^2 \approx \frac{R^2 P_c^2 NK(K-2)T_c\tau_{cc}}{8T_D^2} \tag{7.26}$$

[3]It is also possible to slightly modify the correlator form in [Andonovic *et al.* 1994] so that these extra empty chips are not required, as shown in Appendix E.

where it is assumed that the actual receiver electrical bandwidth is $B_e = \frac{1}{2T_D}$.

The alternative situation of $\frac{N}{2}$ chips being recombined before incidence upon each photodiode can only affect the temporal coding case, since the light from each chip is spectrally dissimilar in the case of spectral coding. In these cases the receiver correlator structure is effectively a single tapped delay-line, with the taps being directed to one or other of a balanced photodiode pair, according to the receiver code. If each half of these taps are recombined into a single fibre before the appropriate photodetector, then mixing can now occur between the fields from different taps. There is also an associated combining loss of $\frac{N}{2}$. This is referred to here as *lossy mixing*. During a single chip period $T_D = T_c = \frac{T_{bit}}{N}$, it is assumed that there are on average $\frac{K}{2}$ chips from different users in each of the $\frac{N}{2}$ taps which are combined and incident onto each photodetector. Hence, using Equation 3.16, for each photodiode the PIIN power is

$$\sigma_D^2 \approx \frac{\frac{KN}{4}\left(\frac{KN}{4}-1\right)}{2} \cdot (2RP_c)^2 \cdot \frac{\tau_{cc}}{2T_c} \approx \frac{R^2 P_c^2 N^2 K^2 \tau_{cc}}{16 T_c} \tag{7.27}$$

The signal from the desired user, corresponding to the expected value of terms (a) and (b) of Equation 7.9, is given by $\frac{N}{2}$ chips of power P_c and temporal extent T_c, across the interval T_D. This applies both with and without lossy mixing, and hence the signal is given by

$$\mathrm{E}[I] = d_g \frac{NRP_cT_c}{2T_D} \tag{7.28}$$

where $d_g = \pm 1$ is the bipolar data bit of the matched user. Using Equation 7.26 for each photodiode, together with Equation 7.28, the SNR limit due to PIIN for systems without lossy mixing is given by

$$\rho_{noLM} = \frac{\left(\mathrm{E}[I]\right)^2}{\sigma_I^2} \approx \frac{NT_c}{\tau_{cc}K(K-2)} \approx \frac{NT_c}{\tau_{cc}K^2} \tag{7.29}$$

Alternatively, using Equation 7.28 along with Equation 7.27 for each photodiode, and with $T_c = T_D = \frac{T_{bit}}{N}$ and $\tau_{cc} = \tau_c$, the SNR limit due to PIIN in the case of lossy mixing is given by

$$\rho_{LM} \approx \frac{2T_{bit}}{N\tau_{cc}K(K-\frac{4}{N})} \approx \frac{2T_{bit}}{N\tau_cK^2} \tag{7.30}$$

Note that this expression is based upon the assumption that detection is based purely upon the noise within the single chip period during which the signal peak occurs. If, for example, both the signal and noise contributions from the whole bit period are compared, then the SNR expression is worse than that of Equation 7.30 by a factor of N.

In Table 7.1, the first seven rows treat each of the main incoherent bipolar OCDMA configurations, listing the per-chip values of coherence time, temporal extent, and optical power. Apart from the scheme considered in detail in Chapter 3, these schemes are all briefly described and discussed in Section 2.9. The optical power of each chip P_c is given in terms of P_s, which

System Description	Chip Power	Chip Period	Chip Coherence Time	Approximate SNR Limit (worst case)
Spectral Coding [Kavehrad and Zaccarin 1995], [Nguyen *et al.* 1995]	$P_c = \frac{P_s}{2MN}$	$T_c = T_{bit}$	$\tau_{cc} = N\tau_c$	$\frac{T_{bit}}{\tau_c K^2}$
Temporal Coding, Active Correlation [O'Farrell and Lochmann 1995]	$P_c = \frac{P_s}{2M}$	$T_c = \frac{T_{bit}}{N}$	$\tau_{cc} = \tau_c$	$\frac{T_{bit}}{\tau_c K^2}$
Temporal Coding, Active Correlation [Khaleghi and Kavehrad 1996]	$\mathrm{E}[P_c] = \frac{P_s}{2M}$	$T_c = \frac{T_{bit}}{N}$	$\tau_{cc} = \tau_c$	$\frac{4\alpha(1-\alpha)T_{bit}}{\tau_c K^2}$
Temporal Coding, Passive Correlation, with lossy mixing [O'Farrell and Lochmann 1994a]	$P_c = \frac{2P_s}{MN^2}$	$T_c = \frac{T_{bit}}{N}$	$\tau_{cc} = \tau_c$	$\frac{2T_{bit}}{N\tau_c K^2}$
Temporal Coding, Passive Correlation, with lossy mixing [Andonovic *et al.* 1994]	$P_c = \frac{9P_s}{5MN^2}$	$T_c = \frac{T_{bit}}{N}$	$\tau_{cc} = \tau_c$	$\frac{2T_{bit}}{N\tau_c K^2}$
Temporal Coding, Passive Correlation, Single ended, with lossy mixing [Tančevski *et al.* 1994]	$P_c = \frac{4P_s}{MN^2}$	$T_c = \frac{T_{bit}}{N}$	$\tau_{cc} = \tau_c$	$\frac{T_{bit}}{N\tau_c K^2}$
Temporal Coding, with lossy mixing, [Zaccarin and Kavehrad 1994b]	$P_c = \frac{2P_s}{MN_{is}^2}$	$T_c = \frac{T_{bit}}{N}$	$\tau_{cc} = \tau_c$	$\frac{2T_{bit}}{N_{is}^2\tau_c K^2}$
Temporal Coding, Passive Correlation [O'Farrell and Lochmann 1994a], without lossy mixing	$P_c = \frac{P_s}{MN}$	$T_c = \frac{T_{bit}}{N}$	$\tau_{cc} = \tau_c$	$\frac{T_{bit}}{\tau_c K^2}$
Temporal Coding, Passive Correlation, Single Ended [Tančevski *et al.* 1994], without lossy mixing	$P_c = \frac{2P_s}{MN}$	$T_c = \frac{T_{bit}}{N}$	$\tau_{cc} = \tau_c$	$\frac{T_{bit}}{2\tau_c K^2}$
Temporal Coding [Zaccarin and Kavehrad 1994b], without lossy mixing	$P_c = \frac{P_s}{MN_{is}}$	$T_c = \frac{T_{bit}}{N}$	$\tau_{cc} = \tau_c$	$\frac{T_{bit}}{N_{is}\tau_c K^2}$

Table 7.1 Incoherent Bipolar OCDMA System Chip Definitions

is the effective source power level at the transmitter output, and neglecting fibre and connection losses. Hence, P_c reflects the splitting loss in the star coupler and the splitting and other possible losses within the receiver structure. The corresponding forms of the PIIN limit in each case are also listed, in terms of the bit time, source coherence time, number of users, and the code length. The last three rows of Table 7.1 are included to indicate that these three proposals can each be simply implemented without the lossy mixing of the original proposals considered earlier in Table 7.1, in which case both the received power and the approximate SNR limit are improved by the factor $\frac{N}{2}$.

It should be noted that the power levels listed in Table 7.1 are in many cases 3 dB (optical) smaller than is actually possible. Earlier in this section it was observed that the two decoders in Figure 7.1 are typically performing correlations with complementary unipolar sequences in schemes of this type. Hence, each fraction of the received light power should be incident on one photodiode or the other, according to the code sequences. As originally proposed in many of these schemes, the use of a 3 dB coupler and two separate unipolar correlations wastes 50% of the received power, since the power arriving at a unipolar correlator that does not match the

unipolar code is not redirected to the other photodiode.

The SNR limit of

$$\rho_{\text{PIIN}} \approx \frac{T_{\text{bit}}}{\tau_{\text{c}} K^2} \tag{7.31}$$

in the first two rows of Table 7.1 arises directly from Equation 7.29 using the listed parameters. Equation 7.31 is smaller by a factor of two than that derived in Chapter 3 for spectral-amplitude OCDMA, substituting $B_{\text{e}} = \frac{1}{2T_{\text{bit}}}$ and $\Delta\nu = \frac{1}{\tau_{\text{c}}}$ in that case. This factor of two arises because fully polarised and polarisation-matched fields were assumed in reaching Equation 7.31, whereas unpolarised fields were assumed in reaching the limit of Equation 3.29. This improvement in the PIIN-limited SNR by 3 dB with unpolarised fields compared to those with fully polarised and polarisation-matched fields arises in general, since there is no mixing between the light in the two orthogonal (polarisation) modes of single-mode fibre. The spectral-amplitude OCDMA system of [Nguyen *et al.* 1995] has been listed as the same as that of [Kavehrad and Zaccarin 1995] in the first row of Table 7.1, since under the assumption of complementary keying the only difference between the two is then merely a doubling of code lengths in [Nguyen *et al.* 1995].

The scheme listed in the third row of Table 7.1 is almost identical to that in the second row. The only differences are that unbalanced codes may be used in [Khaleghi and Kavehrad 1996], and that the splitting ratio α of the receiver coupler is then determined by the level of receiver code imbalance. If the splitting ratio is set to be equal to the receiver code imbalance, then the extra factor $4\alpha(1-\alpha)$ arises in the SNR limit due to PIIN, as shown in Table 7.1, and the average chip power $\mathrm{E}[P_{\text{c}}]$ is indicated since P_{c} then varies according to the code imbalance and the transmitted data.

The system proposals appearing in rows four to six of Table 7.1 each have lossy mixing, and this generally results in an overall power loss of $\frac{N}{2}$ with respect to such systems without the extra coupling. More importantly, however, due to the combination of the fields from each delay-line tap, Equation 7.30 shows that the extra mixing that occurs with identical sources results in a further degradation of the SNR limit by the factor $\frac{N}{2}$ from that of Equation 7.31. There is a further reduction by a factor of two in the SNR limit in the case of [Tančevski *et al.* 1994], since this system effectively uses only single-ended photodetection. As noted previously, however, a balanced detection system following Figure 2.5 is a reasonable and practical way to implement the structure of [Tančevski *et al.* 1994], and it avoids this 3 dB penalty. In the case of [Andonovic *et al.* 1994], minimum possible losses within their receiver structure have been assumed, while ensuring the same power is incident upon each photodiode. Since N appears in the SNR limit for [Andonovic *et al.* 1994], if their correlator structure is modified to require only standard Manchester coding, the SNR improves due to the codes being shorter by one third (Appendix E).

In row seven of Table 7.1 the scheme of [Zaccarin and Kavehrad 1994b] is considered, and this has lossy mixing similar to the previous three systems. However, this scheme combines

both optical and electrical encoding, where N_{is} is the length of the optically encoded inner sequence, and N remains as the overall code length. Consequently, the SNR limit is determined by N_{is}, whereas the chip period is determined by N. However, as well as the change from N to N_{is}, the SNR limit of this system is worse than that from Equation 7.30 by a further factor of N_{is}. The reason is that in this system the noise from the whole bit period contributes to the PIIN-limited SNR, rather than just that noise which occurs during the time T_c in which the signal peak occurs, as noted when Equation 7.30 was obtained. Although simpler, this detection characteristic in general also increases the MAI by the same factor, and hence is rarely considered. In the case of [Zaccarin and Kavehrad 1994b], each user employs the same Barker code or m-sequence for the inner sequence, and due to the low autocorrelation sidelobes of these codes, the MAI arising from this simpler detection process is considered small.

As previously mentioned, the final three rows of Table 7.1 indicate that avoiding the coupling into the same fibre within the receivers of these schemes is feasible, although in the latter case the form of SNR limit is still significantly worse than that of Equation 7.31. It is also possible to use balanced detection with the scheme of [Tančevski *et al.* 1994] without lossy mixing, thus removing the factor of two in the SNR limit in Table 7.1, although this requires doubling the receiver complexity from that shown in [Tančevski *et al.* 1994]. The SNRs with respect to shot noise and thermal noise are, as usual, also increased by 3 dB with balanced detection.

For all of the schemes considered in Table 7.1, each source has been assumed to have the same power spectrum, and to be mutually independent, but note that thermality has not been assumed. Furthermore, all of the most efficient schemes considered in Table 7.1 have exactly the same order of SNR limit due to PIIN as that derived in detail in Chapter 3 for spectral-amplitude coding. The analysis leading to Equations 7.30 and 7.31 does not consider the effects of any source intensity noise upon such a system, and this demonstrates that these limits arise purely due to the mixing between the light fields, rather than due to any inherent intensity fluctuations in each of these fields. The basic structure of every incoherent bipolar OCDMA proposal (shown in Figure 2.5) leads directly to the SNR limit of Equation 7.31 due to PIIN, in the limit of high K, when the sources are independent and identical and the fields spatially coherent (and avoiding any unnecessary losses and mixing in the receiver). If there is significant source intensity noise, then this results in a noise term proportional to the number of users K, but the PIIN is dominantly proportional to K^2, and hence the PIIN still dominates for large K. Note that in the limit of large K, the detected light at each photodiode may then be considered thermal, which leads to the limits in Table 7.1 in a somewhat simpler manner. Here this approach has been deliberately avoided in order to emphasise that source thermality is not a necessary condition for limits of this form. Simply assuming the detected light to be purely thermal when K is large can also give misleading estimates in some schemes, as for example in the case of coherence multiplexing with single-ended detection.

The total network capacity G for the OCDMA schemes following Equation 7.31, assuming

a desired SNR ρ_d, is given by

$$G = K \times \frac{1}{T_{bit}} \approx \frac{1}{\rho_d \tau_c K} \tag{7.32}$$

This limit shows that at a fixed SNR, the total network capacity reduces as the number of users increases, which restricts such systems with identical sources to moderate numbers of users. Decreasing the source coherence time increases the capacity, and this is reasonable since it corresponds to increasing the optical bandwidth. If the sources can be separated in wavelength sufficiently, then this form of limit does not appear at all, but this too corresponds to increasing the optical bandwidth. Greater network capacity G can of course be achieved at the expense of the SNR, and hence also the error rate. For such proposals that also include lossy mixing, the network capacity is further reduced by the factor of half the code length to give

$$G \approx \frac{2}{\rho_d \tau_c K N} \tag{7.33}$$

Along with the decrease according to K, the reduction in capacity as the code length N increases makes these schemes extremely unattractive under worst-case conditions (independent and identical sources, with spatially coherent fields).

One obvious limitation of the analysis in this section is that we have assumed ideally orthogonal code sequences, but this is not realistic in any asynchronous temporal-coding system, although it is possible in the spectral-coding case. Hence, there is also significant multiple-access interference (MAI) in each of the temporal coding systems considered in this section, represented by terms (a) and (b) of Equation 7.9 for each unmatched user. In this section the noise level due to PIIN has been the particular focus of attention since its existence has not been considered in any of the original incoherent bipolar OCDMA proposals. Since these systems are based upon bipolar coding, the levels and the statistics of the MAI are directly comparable to that of radio CDMA systems in the literature, and these have often been detailed along with the original incoherent bipolar system proposals, as for example, in [O'Farrell and Lochmann 1994a] and [Khaleghi and Kavehrad 1996]. The corresponding variance of the MAI component in the receiver photocurrent difference is then [Khaleghi and Kavehrad 1996]

$$\sigma^2_{MAI} \approx \frac{2(K-1)}{3N'} \mathrm{E}[I]^2 \tag{7.34}$$

where $\mathrm{E}[I]^2$ is the signal power and N' is the length of the bipolar codes. In the cases where direct unipolar versions of the bipolar codes are used, then $N' = N$, but when balanced unipolar codes are obtained from the bipolar codes via Manchester encoding, then $N' = \frac{N}{2}$. Including this MAI variance along with the PIIN in the SNR expression from Equation 7.31 gives

$$\rho \approx \frac{1}{\frac{2(K-1)}{3N'} + \frac{\tau_c}{T_{bit}} K^2} \tag{7.35}$$

for the worst-case scenario of fully polarised and polarisation-matched fields that have the same power spectrum.

It can be seen from Equation 7.35 that the level of MAI power reduces linearly if the code length is increased, but the PIIN is independent of the code length, and hence PIIN can seriously limit these systems. In the case of lossy mixing, the SNR expression is even worse, since the PIIN power increases linearly with code length, which renders such configurations completely untenable. As indicated in Table 7.1, several OCDMA proposals that included lossy mixing can be considered without lossy mixing. This simply involves, for example, the use of a diode array to detect the power from several fibres, rather than using a star coupler and only detecting a single output. However, this is only possible when the electrical signal required is simply in proportion to the sum of the optical power from these fibres.

The limits reached in this section have been under the worst-case condition, amongst others, of sources with the same power spectrum. While it is true that this is not necessary for the schemes using temporal coding, source availability and the necessary optical bandwidths required for high-rate systems may lead to the consideration of such systems. Furthermore, the severe SNR limits found here in many cases under the assumption of identical sources rules out these schemes if the sources are similar. All of the incoherent bipolar OCDMA schemes considered here perform no better than the particular case considered in Chapter 3 when the sources are independent and identical and the fields from each user are spatially coherent, and this arises from their essential structure. In Section 7.3.4 the origin of these limits is briefly revisited with respect to Sections 7.2.3 - 7.2.7.

7.3.4 Discussion

Each of the schemes considered here in Section 7.3, at least in the worst case, have independent light fields with similar power levels and spectra arriving at the receiver at the same time within the same spatial mode or mode pair. Under these conditions, as the number of such fields increases, the mixing between these fields generates sufficient PIIN that the received light appears near-thermal. The intensity-noise level then depends predominantly upon the total optical power, which is proportional to the number of active users K. During the detection interval of interest (either T_{bit} or some fraction thereof) the signal level from the matched user in each of these schemes is only proportional to the power from a single source, and thus of the order of $\frac{1}{K}$ of the received optical power during that interval. Hence, using Equation 3.10, SNR limits of the form $\frac{T_{\text{bit}}}{\tau_c K^2}$ always arise in such cases.

In order to avoid these limits, it is necessary to either reduce the mixing levels by exploiting some separation between signals in the temporal, spectral or spatial domains, or else to increase the signal level with respect to the optical power from all the other users during the detection interval, as discussed in Sections 7.2.3 - 7.2.7. Coherent despreading was observed in Section 7.2.7 to be the primary method by which the latter approach can be implemented, and note that this is not the same as completely-optical despreading.

It is easy to think that the critical mixing between fields occurs at the photodetectors, due to their square-law characteristics, and therefore by completing the despreading before photodetection, the desired signal then dominates, thus reducing the effects of the mixing when photodetection occurs. This is particularly applicable to incoherent OCDMA systems that utilise bipolar codes, since all such proposals to date have used the electrical domain for the subtraction required during despreading. However, whenever two fields are combined together so that they are spatially coherent, any relative phase noise between the fields causes the actual optical intensity to fluctuate. Hence, such phase-induced intensity noise (PIIN) is not simply produced at the photodetectors due to their square-law characteristic, but rather photodetection is simply the point at which this PIIN is detected. By implementing before photodetection the necessary subtraction for incoherent bipolar despreading, there is therefore no advantage with respect to PIIN, and note that achieving such incoherent optical subtraction is not impossible, as demonstrated by [Coppinger *et al.* 1997]. Fully-optical, but nonetheless incoherent, despreading can only increase the signal level relative to the optical power from all the other users in some particular location by exploiting some existing separation between the signals from each user, as discussed in Section 7.2.7.

7.4 SYSTEMS WITH INSIGNIFICANT PIIN

Considered in this section are those systems for which PIIN is either insignificant, or at least of a much-less-significant order than for those schemes of the previous section. The reasons why this is so are briefly discussed for each scheme.

7.4.1 Coherent and Coherently Matched Coding

In Section 7.2.1 it was shown that balanced heterodyne or homodyne detection in a coherent OCDMA system effectively balances out any intensity noise from the transmitter sources and any PIIN from the mixing between the light from different such sources. In practice, however, even with a poorly balanced detector, any intensity noise in the local oscillator dominates any other source intensity noise or mixing noise, since the local source is usually of significantly higher power than all of the received fields.

As outlined in Section 2.6, one class of OCDMA system proposals has optical lattice structures in the encoders and decoders that are coherently matched between communicating users. Due to the coherent recombination of the light pulses from the desired user, the signal pulse has a fixed fraction of the received signal energy (typically 50%), regardless of code length, and it is thus much more distinct from the incoherently-combining MAI than in the incoherent case. The consequence is that any in-band PIIN due to mixing between light pulses is much smaller with respect to the signal power than in an incoherent system, even if all the sources are spectrally matched. This can be seen by considering that mixing with the desired signal should dominate any mixing, thus ensuring that any in-band PIIN power has linear dependence upon

the number of users. Alternatively, considering the worst-case mixing scenario, in which the received light appears thermal, the coherently combined signal comprises much more than $\frac{1}{K}$ of the power in the detection interval (as in Section 7.3.4), and hence any SNR limit so arising is much less severe than those arising in Section 7.3.

Systems based upon the coherent spectral-phase encoding of ultrashort pulses require signals that have the same power spectrum, and hence the interference between such signals then lies within the receiver bandwidth. The ideal detection scheme involves a device triggered only by a very short high-intensity pulse, and this acts effectively as a time gate, excluding interference from other users during the rest of the bit period. The term mixing is not very appropriate here because the small contributions from each interfering user during this detection interval are completely coherent, but of random phase, and hence their combination with the desired pulse is more clearly described as coherent superposition, rather than mixing. The results of this coherent superposition lead to a dominant interference term that has linear dependence on the number of interfering users, rather than the quadratic dependencies arising in Section 7.3. Furthermore, in the analysis of [Salehi *et al.* 1990], the pulses considered are so short that even when dispersed by the spectral encoder, the extent of the spread pulse may still be a small fraction of the actual bit period. Hence, in an asynchronous such system, the signals from each user have little temporal overlap, and even without this separation, the order of interference is less severe than the limits arising in Section 7.3 due to the coherent detection in this scheme.

7.4.2 Incoherent Unipolar OCDMA Systems

As discussed in Section 7.2.7, if the desired signal has been despread and it dominates with respect to all the other spread signals in some time or frequency location, then any PIIN is dominated by mixing with the desired signal, and in general such noise is then only linear in the number of simultaneous users. This situation arises when an ideal time gate is used to limit the decision variable scope to a single chip period, this being the interval during which a peak is expected if the transmitted bit is a 'one', as described in Section 2.4. In such unipolar systems, assuming the desired error rate is very small, the sum of the contributions from all the interfering users during such a chip interval must almost always be less than the expected signal level. In the worst case, when all the light is fully polarised, with the same spectrum and polarisation state, the mixing between each co-located pulse pair does generate in-band PIIN, and this must increase the error likelihood. However, this performance degradation is not of the same order as those arising in the systems considered in Section 7.3. This advantage with respect to mixing noise can be viewed as a consequence of the temporal separation between signals from each user, by virtue of the sparse coding systems.

Many incoherent unipolar OCDMA proposals have the form shown in Figure 2.2, with a tapped delay-line in the receiver. The incoherent combination of such delay-line taps into a single-mode waveguide incurs a significant loss, and in Section 7.3.3 this was termed lossy mixing, since as well as the loss, mixing then occurs in the coupler between light which did

not arrive simultaneously at the receiver. Even when the mixing between light from different sources may be neglected, such lossy mixing then applies to the pulses from the desired user, but the corresponding SNR limit due to this mixing has not been noted in the literature, and this is briefly considered here.

Generally, a unipolar code sequence is quite sparse, having w light pulses out of n such chip intervals (Section 2.4.2). The delays in the decoder are designed to add these w pulses together in a single chip interval on an intensity basis, and their sum should then be detected as a data 'one'. The addition on a power basis is arranged by mismatching the encoder and decoder delays by significantly more than the coherence time, but still much less than the chip time[4]. Each of these w pulses are spectrally and polarisation matched, since they are from the same source, if not the same pulse, and it is reasonable to assume that any variations in polarisation state have a much larger time constant than the bit rate. Hence, assuming these pulses are fully polarised, and using Equation 3.16, the mixing between these w pulses gives a finite SNR due to PIIN of

$$\frac{(wRP_c)^2}{\frac{w(w-1)}{2}(2RP_c)^2\frac{\tau_c}{2T_c}} \approx \frac{T_c}{\tau_c} \tag{7.36}$$

whereas many analyses assume that no error can occur when a 'one' is transmitted. If the light is unpolarised, then this limit is greater by 3 dB. This clearly shows that with lossy mixing, there is significant noise associated with the peak occurring when the desired sequence should be detected. Unlike SNRs dependent on shot noise or thermal noise, this SNR limit does not increase as the source power levels are increased. The detrimental effects of this PIIN have not been included in any incoherent unipolar OCDMA analyses to date, but it only reinforces the undesirability of systems including such lossy mixing, since using a star coupler to recombine signals into a single fibre is very unattractive, purely on the basis of the optical loss. If photodetection is the operation immediately following such a coupler, and no field mixing is required, then the use of an array of photodetectors can eliminate both the combining loss and such mixing noise, although there are bandwidth and noise penalties associated with the extra photodiode area in general.

Early in the analysis in this chapter was the assumption that any optical processing in the receiver is linear. However, the incoherent unipolar systems described in Section 2.4 often include an optical hard limiter, which is certainly not linear. The arguments above show that the effects of mixing between incoherent light are generally not as severe as for the systems in Section 7.3, especially if lossy mixing is avoided. With the use of an ideal hard limiter, this is even more so, since the hard limiter functions as a logical OR gate, which gives the same output level when light pulses from one or more users are input to it. Since more than one pulse is required simultaneously for mixing to occur, the hard limiter excludes almost all such mixing-based intensity noise.

[4]This mismatching is only necessary when the tap outputs are recombined into a single-mode waveguide.

7.5 SUMMARY

In this chapter the common structure of all optically coded linear OCDMA schemes has been defined, and the corresponding receiver decision variable, being the balanced photocurrent, has been correctly expressed. The receiver decision variable in the cases of heterodyne, homodyne, and incoherent detection was then considered, and in particular, the mixing between light fields from different sources has been treated carefully. The distribution of these fields in the temporal, spectral, and spatial domains, along with the type of receiver decoding, can each influence the significance of the effects of such mixing, and the conditions under which they do so have been clearly expressed. In the light of this expression, the different classes of OCDMA schemes were examined and the corresponding significance of mixing between light fields from different sources was analysed. The known limits for coherence multiplexing with balanced detection due to such mixing have been shown to arise from this analysis, and the single-ended coherence-multiplexing case was also considered in order to highlight the deficiencies in a recent analysis of this system.

All of the proposed incoherent OCDMA systems that utilise optical coding and bipolar codes have been shown, in the case of independent and identical sources with complete spatial coherence of all the fields, to have an SNR limit of the same form or worse than that of the particular such system analysed in detail in Chapter 3. These SNR limits are due to the in-band phase-induced intensity noise arising from the mixing of the fields from each independent source. The light from each user is combined together using a single-mode star coupler in each of these schemes, and the phase-induced intensity noise actually exists from this point on. The necessary bipolar correlation at the receiver amounts to splitting the received light into two groups, according to the receiver code, and then obtaining the difference between the optical power of these two groups. The result thus depends upon all of the intensity noise of all of the received light, regardless of whether the correlation process is performed in a fully optical manner or not. Consequently, any incoherent OCDMA system that uses bipolar coding, when each independent source has the same spectrum and all the signals are combined into the same single-mode fibre, must always have an SNR limit due to phase-induced intensity noise of the form in Chapter 3 or worse.

In general, for incoherent OCDMA systems that use only one single-mode fibre (SMF) path and independent sources with the same spectrum, temporal separation is then the only possible method left by which to avoid significant limitation due to mixing between the light from each user. Since systems that simply use bipolar coding do not have any such temporal separation, then as already observed here, they are significantly limited by this mixing. Incoherent OCDMA systems using unipolar codes, however, actually exploit temporal separation between the signals from each user by virtue of their sparse temporal codes. Hence, especially when hard-limiting and lossless detection are incorporated, such systems are not affected greatly by the mixing of light from different users. However, the numbers of such sparse codes and their poor correlation properties, which result from the need for minimum temporal

overlapping, then significantly limit such systems. Consequently, incoherent OCDMA systems that use single SMFs, independent sources, and the same optical bandwidth, are always going to be particularly inefficient.

Many incoherent temporally coded OCDMA proposals utilise optical tapped delay-lines at the receiver, whether based upon unipolar or bipolar codes, and the typical structure of these delay-lines involves the incoherent combination of all the tap outputs back into a single-mode optical waveguide. As well as the significant disadvantage of the power loss that this incurs, the mixing between the light from each tap can cause further serious degradation of the SNR, especially when the sources have identical spectra.

Chapter 8

CONCLUSIONS

This thesis has presented research into the performance limits of OCDMA systems that arise due to the intensity noise caused by the mixing of independent light fields. The focus has primarily been towards incoherent OCDMA systems that use bipolar coding structures, and in particular, to the system based upon amplitude-coding of broadband optical spectra. Such systems have attracted interest due to the generally poor correlation properties of the unipolar codes developed for incoherent OCDMA systems, and the difficulties, at least perceived, in meeting the phase- and polarisation-matching requirements of coherent OCDMA systems.

The use of the spectral domain for coding has the attraction that the codes always remain in phase, even in an asynchronous such system, and thus there are many more user codes available than in asynchronous temporal CDMA systems, and ideal orthogonal code sets are also possible. However, the analysis here has shown that spectral-amplitude-coding OCDMA systems are subject to a serious limitation that restricts their performance to significantly lower levels than those claimed in the original proposals and analyses of this system. This limitation is primarily due to phase-induced intensity noise (PIIN) arising from the mixing of the light from each independent and incoherent broadband source. Unlike many other sources of noise in a real system, this PIIN cannot be overcome simply by increasing the source power, and hence the analysis here has concentrated upon this intensity noise, largely ignoring realities such as shot noise that can be overcome in this manner.

The PIIN limits the SNR of spectral-amplitude OCDMA to being proportional to the ratio of optical to electrical bandwidth, and approximately inversely proportional to the square of the number of active users. At a fixed SNR, the corresponding total network capacity of spectral-amplitude OCDMA is then proportional to the optical bandwidth, and inversely proportional to both the SNR and approximately the number of active users. The maximum total network capacity, and hence also the overall network efficiency, thus reduce as the number of active users increases, and this is a significant limitation. PIIN-based limits of the same order have been both recognised and experimentally verified in multiple-access systems based upon coherence multiplexing, and the limits found here for spectral-amplitude OCDMA only exceed those of coherence multiplexing by a factor of two at best.

It has been claimed that spectral-amplitude OCDMA can outperform a spectrum-sliced

WDM system using the same apparatus, but here this claim has been refuted by showing that the best-case SNR and capacity limits for spectral-amplitude OCDMA are worse than that of such a WDM system by a factor of at least the number of active users.

There are four characteristics in particular of the spectral-amplitude OCDMA system analysed here that together lead to the serious performance limit found for this system, and these are : each user has an independent source with the same spectrum; each user transmits at the same time; the light from each user is spatially coherent within the same single-mode fibre; and the decoding process is incoherent. In order to achieve performance beyond the PIIN limit found in Chapter 3, the system must be modified to alleviate or eliminate at least one of these characteristics. Chapters 4 - 6 of this thesis have thus presented investigations into possible such modifications, and these are summarised in the following.

The use of independent sources is essential in order that each user be independent, which is one of the motivations for a CDMA protocol, so the first possible option to eliminate the PIIN limit is to have spectrally dissimilar sources, thus moving the PIIN out of the receiver bandwidth. However, spectral-amplitude OCDMA requires each user to encode the same spectral regions, and hence achieving spectral separation between different users is not practical in general, although not completely impossible, as detailed in Chapter 5.

Spectral-amplitude OCDMA was considered in Chapter 3 with two signalling regimes, in which active users either transmitted all the time, or approximately half of the time, but the SNR and capacity limits were shown to be of the same order for both schemes. The reduction of the transmission duty-cycle to try to achieve performance beyond these limits has been considered in both Chapter 5 and Chapter 6. It has been shown that simple duty-cycle reduction alone cannot improve the performance with broadband incoherent sources, but together with the use of an ideal time-gate at the receiver, performance beyond the limits of Chapter 3 are possible. However, this requires significant increase to both the modulation and detection bandwidths. Furthermore, the dispersion sensitivity is increased by the same factor, and the signal power is also reduced in general. Such bandwidth and dispersion-sensitivity increases are not, however, actually necessary in order to improve the system performance, as shown in Chapter 6 through the use of pulse-position modulation.

In Chapter 6 it has been shown that the network capacity of spectral-amplitude OCDMA, at a given SNR, can be near-doubled from the limit found in Chapter 3 by a change to a pulse-position signalling format of 50% duty-cycle, along with the addition of a simple decoder after the original receiver. The modulation and detection bandwidths necessary for this scheme are exactly the same relative to the data rate as those in the original scheme, and further capacity gains are possible with smaller duty-cycle and greater decoder complexity.

In order to reduce the spatial coherence of the fields from each user, the use of multimode fibre rather than single-mode fibre has been proposed and investigated in Chapter 4. An experimental demonstration of the corresponding reduction in PIIN through the use of multimode fibre has also been described therein. With sufficient multimode fibre length to ensure the light

is near-evenly distributed amongst all the fibre modes, reductions in PIIN of as much as 20 dB may be possible for typical graded-index multimode fibre. However, the intermodal dispersion then restricts the product of bit rate and fibre length to much lower levels, and single-mode components can no longer be used.

Although it is conceivable to operate a spectral-amplitude OCDMA system in a fully-coherent manner, as briefly mentioned in Chapter 5, it is less difficult and more efficient to use the original coherent spectral-coding system from which incoherent spectral-amplitude OCDMA was derived. Due to the coherent despreading of both of these arrangements, the significant PIIN limits found in Chapter 3 no longer apply.

In Chapter 7 the common structure of most OCDMA systems has been analysed, and the general characteristics under which the mixing between light from different users does or does not have a significant effect have been clearly discussed. Orthogonality, or at least some degree of separation, between the light from each user in either the temporal, spectral, or spatial domains are the three clearest methods by which to eliminate or reduce the effects of this light mixing. The fourth method is to concentrate the desired signal power so that it significantly exceeds that from the other users in a fraction of some domain. This can only be done in general via coherent despreading in the decoding process, or by exploiting existing temporal, spectral, or spatial separation between the signals from each user. The manner in which these four possibilities apply to spectral-amplitude OCDMA has been seen through Chapters 4 - 6. In the light of the general analysis in Chapter 7, each category of OCDMA system has been considered to determine whether or not mixing between light from different users causes significant performance limits.

The analysis in Chapter 7 has been shown to generate the known limit due to field mixing for coherence multiplexing with balanced detection, and the single-ended case has also been considered in order to identify and correct the deficiencies in a recent published analysis. The performance limit in coherence multiplexing has the same form as that found in Chapter 3, and hence the simple method proposed in Chapter 6 for improving the performance limit of spectral-amplitude OCDMA can also be applied to coherence-multiplexing systems.

Each proposed incoherent OCDMA system that uses bipolar optical coding has been considered in the worst-case conditions of having independent and identical sources, and where the light fields from each user are spatially coherent. The orders of the performance limits in these worst-case conditions have been calculated for each such proposal to date, and it has been shown that each of these proposed systems have SNR and capacity limits of the same order or worse than those found in Chapter 3. It has been shown that such limits arise in general for any incoherent bipolar OCDMA proposal with independent and identical sources, and where the light fields from each user are spatially coherent, regardless of whether despreading is accomplished before photodetection or not.

The unipolar codes used in many incoherent OCDMA systems are designed to have minimum overlap with any other such code, regardless of relative offset. Therefore, the light trans-

mitted by different users in such systems is predominantly temporally separated, and hence such systems are not greatly affected by the mixing of light from different users, especially when hard-limiting and lossless detection are incorporated. However, due to the need to minimise the overlaps between such codes, these codes are sparse, their numbers are significantly limited, and their correlation properties are also generally poor with respect to bipolar codes. These restrictive characteristics were the original motivation behind the proposals to use bipolar codes in incoherent OCDMA. However, in using bipolar codes to overcome the unipolar code restrictions, the temporal separation between the fields from each user is eliminated, and the system may then be significantly limited by the resulting field mixing instead. Hence, for incoherent OCDMA systems using single SMF paths and independent sources with the same spectrum, the bipolar such systems are significantly limited by mixing between light from each source, whereas the unipolar schemes avoid most of such mixing, but are then limited by the resulting poor code properties. Consequently, incoherent OCDMA systems that use single SMFs, independent sources, and the same optical bandwidth, are always going to be particularly inefficient. However, since the available optical bandwidth is so large, the performance levels possible with such inefficient systems may still be attractive for some applications if they can be implemented simply and cheaply.

8.1 SUGGESTIONS FOR FUTURE WORK

The use of PPM signalling with a simple decoder structure was shown in Chapter 6 to improve the PIIN-limited performance of spectral-amplitude OCDMA, and it was stated that this scheme should allow similar improvements if applied to coherence-multiplexing systems. Such systems and their PIIN limits have been practically demonstrated recently in a number of laboratory experiments. Hence, by modifying such an experiment to incorporate the PPM signalling and extra decoding of Chapter 6, it should be possible to demonstrate experimentally that this scheme does improve the PIIN-limited performance of such a system.

Dispersion limits the possible network size in most OCDMA systems, especially for systems such as spectral-amplitude OCDMA that use large optical bandwidths. In the case of coherence multiplexing, the tradeoff between dispersion and PIIN has been shown to result in an optimum optical bandwidth for a given link length. The dispersion penalties for spectral-amplitude OCDMA should be similar to those of coherence multiplexing, but closer investigation may be warranted, for example, in the comparison of dispersion effects for on-off keying and complementary keying.

Incoherent OCDMA systems have been seen to be particularly inefficient under certain conditions, regardless of whether unipolar or bipolar codes are used, although the related limits arise in different manners. A closer comparison of two such systems, each with temporal coding, but one using sparse unipolar codes and the other using standard bipolar codes, could be made in order to determine which has the least restrictive limits. The use of nonlinear

processing in the sparse coding system, in the form of ideal optical hard limiting, may perhaps give this system an advantage.

The work in this thesis has drawn further attention to the advantage of coherent spreading in OCDMA systems. Optical phase-shift keying (PSK) can be accomplished at rates unconstrained by electronic bandwidths through cross phase modulation (XPM) with an optical pulse sequence, and this appears to be a promising area for further research. Data keying in such a system could be implemented through further XPM with a light signal corresponding to the binary data, for instance, but there may be much better ways in which to do this. The efficient generation of the necessary pulse sequences, and the requirements of the code-acquisition system at the receiver, are two areas where attention could be directed. The effects of dispersion upon such a high-rate PSK system may not be well understood, and hence closer investigation may be warranted there also.

Appendix A

SUM OF A BINOMIAL-QUADRATIC SERIES

The noise power of Equation 3.33 depends upon the number of transmitting users $\mathcal{L}$, and here this expression is averaged over the binomial distribution of $\mathcal{L}$. Equation 3.33 is first reproduced here for convenience.

$$\sigma_I^2|_{\mathcal{L}} = \frac{B_e R^2 P_r^2 \mathcal{L}(\mathcal{L}+1)}{4\Delta\nu} \tag{A.1}$$

Assuming that each of K bit-synchronous users is transmitting equiprobable data by OOK, then $\mathcal{L}$ is binomially distributed from 0 to K, and hence

$$\begin{aligned} \mathrm{E}[\sigma_I^2] &= 2^{-K} \sum_{\mathcal{L}=0}^{K} \binom{K}{\mathcal{L}} \frac{B_e R^2 P_r^2 \mathcal{L}(\mathcal{L}+1)}{4\Delta\nu} \\ &= 2^{-K} \frac{B_e R^2 P_r^2}{4\Delta\nu} \sum_{\mathcal{L}=0}^{K} \binom{K}{\mathcal{L}} \mathcal{L}(\mathcal{L}+1) \end{aligned} \tag{A.2}$$

The following series sums are known [Gradshteyn and Ryzhik 1965]

$$\sum_{r=0}^{n} \binom{n}{r} r = n2^{n-1}, \quad \sum_{r=0}^{n} \binom{n}{r} = 2^n \tag{A.3}$$

The results in Equation A.3 can be used to simplify the series sum in Equation A.2, as follows

$$\begin{aligned}
\sum_{r=0}^{n}\binom{n}{r}r(r+1) &= (n+1)\sum_{r=0}^{n}\binom{n}{r}r-\sum_{r=0}^{n}\binom{n}{r}r(n-r)\\
&= (n+1)n2^{n-1}-\sum_{r=1}^{n-1}\frac{n!r(n-r)}{(n-r)!r!}\\
&= (n+1)n2^{n-1}-\sum_{r=1}^{n-1}\frac{n(n-1)(n-2)!}{(n-r-1)!(r-1)!}\\
&= (n+1)n2^{n-1}-n(n-1)\sum_{r=0}^{n-2}\binom{n-2}{r}\\
&= 2(n+1)n2^{n-2}-n(n-1)2^{n-2}\\
&= n(n+3)2^{n-2} \qquad \text{(A.4)}
\end{aligned}$$

Using Equation A.4, Equation A.2 becomes

$$\begin{aligned}
\mathrm{E}[\sigma_I^2] &= 2^{-K}\frac{B_e R^2 P_r^2}{4\Delta\nu}\ 2^{K-2}K(K+3)\\
&= \frac{B_e R^2 P_r^2 K(K+3)}{16\Delta\nu} \qquad \text{(A.5)}
\end{aligned}$$

which gives Equation 3.34.

Appendix B

SPECTRAL-AMPLITUDE OCDMA WITH SHORT COHERENT PULSE SOURCES

Spectral-amplitude OCDMA is here considered with ultrashort coherent pulses rather than broadband incoherent thermal sources. In order to understand the effects of any interaction between pulses from different users which arrive simultaneously at the receiver, the pulse-synchronous case is first considered.

B.1 SYNCHRONOUS CASE

It is here assumed that the encoded pulses from different users arrive at the receiver almost simultaneously, such that they can be considered time-synchronous, but with random optical phase. Hence, using Equation 5.1, the total field approaching the receiver is expressed as

$$\boldsymbol{E} = \sum_{k=1}^{K} q e^{j\phi_k} = \frac{\sqrt{P_{\mathrm{p}}}}{N} e^{j2\pi\nu_o t} \operatorname{sinc}\left(\frac{\Delta\nu t}{N}\right) \sum_{k=1}^{K} e^{j\phi_k} \sum_{i=1}^{N} c_k(i) e^{-j\frac{2\pi\Delta\nu t}{N}(i-\frac{N+1}{2})} \tag{B.1}$$

where the ϕ_k are each assumed to be independent and uniformly distributed on 0-2π. Denoting the receiver amplitude code for the upper photodetector as $\boldsymbol{c}_+$, the photocurrent at the upper photodetector is given by

$$I_+ = \frac{RP_{\mathrm{p}}}{N^2} \operatorname{sinc}^2\left(\frac{\Delta\nu t}{N}\right) \sum_{k=1}^{K}\sum_{l=1}^{K} e^{j(\phi_k-\phi_l)} \sum_{i=1}^{N}\sum_{i'=1}^{N} c_+(i)c_+(i')c_k(i)c_l(i')e^{-j\frac{2\pi\Delta\nu t}{N}(i-i')} \tag{B.2}$$

where R is the photodiode responsivity, and $\operatorname{sinc}^2(x) = \frac{\sin^2(\pi x)}{\pi^2 x^2}$.

Assuming that the width of each spectral division $\frac{\Delta\nu}{N}$ is significantly greater than the receiver bandwidth, any terms in Equation B.2 with $i \neq i'$ do not appear in the received signal. An identical expression arises for the current I_- from the lower photodetector, except for the substitution of $\boldsymbol{c}_-$ for $\boldsymbol{c}_+$. Assuming that the receiver is matched to the gth code, then $c_+(i) = \frac{1-h_g(i)}{2}$, $c_-(i) = \frac{1+h_g(i)}{2}$, where $h_g(i)$ is the bipolar representation of the code of user g, and for convenience, ϕ_g is taken to be zero[1]. Performing the difference between the upper

[1]Note that denoting $\phi_g = 0$ does not mean that the receiver needs to be optically phase-synchronous with the

and lower photodiode currents, and removing all terms with $i \neq i'$, gives

$$I_+ - I_- = -\frac{RP_p}{N^2}\,\mathrm{sinc}^2\left(\frac{\Delta\nu t}{N}\right) \underbrace{\sum_{k=1}^{K}\sum_{l=1}^{K} e^{j(\phi_k-\phi_l)} \sum_{i=1}^{N} h_g(i)c_k(i)c_l(i)}_{\text{(A)}} \tag{B.3}$$

Assuming that the data is represented by code complementation rather than on-off keying, the codes $\boldsymbol{c}_k$ are given by

$$c_k(i) = \frac{1 - d_k h_k(i)}{2} \qquad i = 1, 2, \ldots, N \tag{B.4}$$

where d_k is the bipolar data bit of the kth user and $h_k(i)$ is the ith element of the bipolar code $\boldsymbol{h}_k$ of the kth user.

The triple sum (A) in Equation B.3 can be evaluated only when the code properties are defined, and for the case of codes based upon Hadamard matrices, this is straightforward. This is due to the basic property of a Hadamard matrix, that the number of elements in agreement between any two distinct rows or columns is equal to the number of such elements in disagreement. This property still holds if the same operation is applied to each row or column. For the case $k = l$, (A) of Equation B.3 becomes

$$(\mathrm{A})_{k=l} = \sum_{k=1}^{K}\sum_{i=1}^{N} h_g(i)c_k(i) = \begin{cases} -d_g\frac{N}{2}, & k = g \\ 0, & k \neq g \end{cases} \tag{B.5}$$

which simply gives the data of the matched user when $k = g$, and zero otherwise. In the case where $k = g$ or $l = g$ and $k \neq l$, the corresponding terms of (A) become

$$\begin{aligned}(\mathrm{A})_{l\neq k=g} + (\mathrm{A})_{k\neq l=g} &= \sum_{i=1}^{N} h_g(i)\left[\sum_{\substack{l=1\\ l\neq g}}^{K} e^{-j\phi_l}c_g(i)c_l(i) + \sum_{\substack{k=1\\ k\neq g}}^{K} e^{j\phi_k}c_k(i)c_g(i)\right] \\ &= -d_g\frac{N}{2}\sum_{\substack{k=1\\ k\neq g}}^{K}\cos(\phi_k)\end{aligned} \tag{B.6}$$

The result in Equation B.6 consists of a contribution to the signal from each interfering user, according to their relative phase. This is unusual, and note that it implies that if all the users were phase-synchronous ($\phi_k = 0$), then the signal power increases as the number of interfering users increases. The physical reason for this term is that in the ideal bit-synchronous case, the light from each different source within a single spectral slice differs only by each phase term $e^{j\phi_k}$, so they are coherent and hence they do not simply add on a power basis. This term can easily be greater in magnitude than the signal itself, and hence it is the dominant limitation of this particular configuration. By assuming relative phases that are uniformly distributed on

matched transmitter, it is merely a convenient choice of phase reference.

0-2π, and, more importantly, that these are independent from bit to bit, then Equation B.6 can be considered an interference term with zero mean, and a variance of $\frac{N^2(K-1)}{8}$.

In the case of $k, l \neq g$ and $k \neq l$, (A) becomes

$$(\mathrm{A})_{k\neq g, l\neq g, k\neq l} = 2 \sum_{\substack{k=1 \\ k\neq g}}^{K-1} \sum_{\substack{l=k+1 \\ l\neq g}}^{K} \cos(\phi_k - \phi_l) \sum_{i=1}^{N} h_g(i) c_k(i) c_l(i) \tag{B.7}$$

Using the property that the multiplication of any row of a Hadamard matrix by another such row also gives a row in the Hadamard matrix, the final sum in Equation B.7 is zero if and only if $\boldsymbol{h}_k.\boldsymbol{h}_l \neq \boldsymbol{h}_g$, where . denotes element-wise multiplication. For all $k \neq g$, there are at most $\lfloor \frac{K-1}{2} \rfloor$ unique pairs k, k' for which $\boldsymbol{h}_k.\boldsymbol{h}_{k'} = \boldsymbol{h}_g$, where $\lfloor x \rfloor$ is the floor of x, and in which case the last sum in Equation B.7 becomes $d_k d_{k'} \frac{N}{4}$. Hence, the value of Equation B.7 depends not only upon the relative phases and data bits of the interfering users, but also upon which specific users they are. Using the upper bound that there are exactly $\frac{K-1}{2}$ unique pairs $k, k' \neq g$ in $1, 2, \ldots, K$ for which $\boldsymbol{h}_k.\boldsymbol{h}_{k'} = \boldsymbol{h}_g$, and assuming equiprobable data and uniformly distributed relative phases, Equation B.7 is found to be zero-mean, with variance of approximately $\frac{N^2(K-1)}{16}$.

The random variables from Equation B.6 and Equation B.7 are independent, giving the result that

$$\frac{N^2(K-1)}{8} \leq \sigma^2_{(\mathrm{A})} \leq \frac{3N^2(K-1)}{16} \tag{B.8}$$

It has already been assumed that the receiver bandwidth is significantly smaller than that of a spectral slice $\frac{\Delta\nu}{N}$, and note that this corresponds to an ideal integration time T_D which significantly exceeds the width of the main lobe of the signal envelope $\mathrm{sinc}^2(\frac{\Delta\nu t}{N})$. Hence, this assumption means that the integration time of the photodiodes encompasses the significant signal power. The signal photocurrent is given by

$$\mathrm{E}[I_+ - I_-] = \mathrm{E}[(\mathrm{A})] \frac{-RP_\mathrm{p}}{N^2 T_\mathrm{D}} \int_{-\frac{T_\mathrm{D}}{2}}^{\frac{T_\mathrm{D}}{2}} \mathrm{sinc}^2(\frac{\Delta\nu t}{N}) \mathrm{d}t = d_g \frac{RP_\mathrm{p}}{2NT_\mathrm{D}} \int_{-\frac{T_\mathrm{D}}{2}}^{\frac{T_\mathrm{D}}{2}} \mathrm{sinc}^2(\frac{\Delta\nu t}{N}) \mathrm{d}t \tag{B.9}$$

and the photocurrent variance is simply

$$\sigma_I^2 = \sigma^2_{(\mathrm{A})} \left[\frac{RP_\mathrm{p}}{N^2 T_\mathrm{D}} \int_{-\frac{T_\mathrm{D}}{2}}^{\frac{T_\mathrm{D}}{2}} \mathrm{sinc}^2(\frac{\Delta\nu t}{N}) \mathrm{d}t \right]^2 \tag{B.10}$$

giving the SIR limit

$$\frac{4}{3(K-1)} \leq \mathrm{SIR} \leq \frac{2}{(K-1)} \tag{B.11}$$

B.2 ASYNCHRONOUS CASE

In the asynchronous case, the received signal representation becomes

$$\boldsymbol{E} = \frac{\sqrt{P_{\mathrm{p}}}}{N}\sum_{k=1}^{K} e^{j2\pi\nu_o(t-\tau_k)}\,\mathrm{sinc}\Big(\frac{\Delta\nu(t-\tau_k)}{N}\Big)e^{j\phi_k}\sum_{i=1}^{N} c_k(i)e^{-j\frac{2\pi\Delta\nu(t-\tau_k)}{N}(i-\frac{N+1}{2})} \tag{B.12}$$

where $-\frac{T_{\mathrm{bit}}}{2} < \tau_k \leq \frac{T_{\mathrm{bit}}}{2}$ represents the time offset of the kth user. Assuming that the spectral width $\frac{\Delta\nu}{N}$ is significantly greater than the receiver bandwidth, and integrating the difference between the upper and lower photodiode currents over the photodiode integration time, gives

$$\begin{aligned} I = -\frac{RP_{\mathrm{p}}}{N^2T_{\mathrm{D}}}\int_{-\frac{T_{\mathrm{D}}}{2}}^{\frac{T_{\mathrm{D}}}{2}}\sum_{k=1}^{K}\sum_{l=1}^{K}\mathrm{sinc}\Big(\frac{\Delta\nu(t-\tau_k)}{N}\Big)\,\mathrm{sinc}\Big(\frac{\Delta\nu(t-\tau_l)}{N}\Big)e^{j(\phi_k-\phi_l)-j2\pi\nu_o(\tau_k-\tau_l)}\cdot \\ \sum_{i=1}^{N} h_g(i)c_k(i)c_l(i)e^{-j\frac{2\pi\Delta\nu(\tau_k-\tau_l)}{N}(i-\frac{N+1}{2})}\;\mathrm{d}t \quad = I_{k=l=g} + I_{k=l\neq g} + I_{k\neq l} \end{aligned} \tag{B.13}$$

where the receiver is matched to sequence $\boldsymbol{h}_g$, and $\tau_g = 0$.

In the cases $k = l$, the only difference between Equations B.3 and B.13 is the time offset of the squared sinc function, and the result $I_{k=l\neq g}$ is still zero for each unmatched user. In the case of the matched user, the bipolar signal

$$I_{k=l=g} = -d_k\frac{RP_{\mathrm{p}}}{2NT_{\mathrm{D}}}\int_{-\frac{T_{\mathrm{D}}}{2}}^{\frac{T_{\mathrm{D}}}{2}}\mathrm{sinc}^2\Big(\frac{\Delta\nu t}{N}\Big)\mathrm{d}t \tag{B.14}$$

is still achieved. However, for the cases $k \neq l$, the differences between Equations B.3 and B.13 are certainly significant. Firstly, the product of the two sinc functions in Equation B.13 across the bit period represents the general reduction of mixing-term amplitudes due to the asynchronism. Furthermore, each term in the final sum of Equation B.13 now has a phase dependent on i as well as k and l, which means this sum cannot be simply determined as in the synchronous case.

With $k \neq l$, there are only $\frac{N}{4}$ non-zero terms in the sum over i in Equation B.13, and the overall phase of each term depends upon variables ϕ_k, ϕ_l, τ_k, τ_l, i, and also the data bits d_k and d_l. If it is assumed that

$$e^{j(\phi_k-\phi_l)-j2\pi\nu_o(\tau_k-\tau_l)}\sum_{i=1}^{N} h_g(i)c_k(i)c_l(i)e^{-j\frac{2\pi\Delta\nu(\tau_k-\tau_l)}{N}(i-\frac{N+1}{2})} \approx \sum_{i'=1}^{\frac{N}{4}} e^{j\phi_{i',k,l}} \tag{B.15}$$

where the $\phi_{i',k,l}$ are random variables that are distributed uniformly on 0-2π and independent

for each i',k,l, then the terms from Equation B.13 with $k \neq l$ become

$$I_{k\neq l} \approx \frac{2RP_{\mathrm{p}}}{N^2T_{\mathrm{D}}} \sum_{k=1}^{K-1} \sum_{l=k+1}^{K} \int_{-\frac{T_{\mathrm{D}}}{2}}^{\frac{T_{\mathrm{D}}}{2}} \mathrm{sinc}\left(\frac{\Delta\nu(t-\tau_k)}{N}\right) \mathrm{sinc}\left(\frac{\Delta\nu(t-\tau_l)}{N}\right) \mathrm{d}t \sum_{i'=1}^{\frac{N}{4}} \cos(\phi_{i',k,l}) \tag{B.16}$$

From Equation B.16, the variance of $I_{k\neq l}$ is then given by $\frac{K(K-1)}{2}$ terms of variance

$$\frac{R^2P_{\mathrm{p}}^2}{2N^3} \underbrace{\left[\frac{1}{T_{\mathrm{D}}} \int_{-\frac{T_{\mathrm{D}}}{2}}^{\frac{T_{\mathrm{D}}}{2}} \mathrm{sinc}\left(\frac{\Delta\nu(t-\tau_k)}{N}\right) \mathrm{sinc}\left(\frac{\Delta\nu(t-\tau_l)}{N}\right)\right]^2}_{\text{(A)}} \tag{B.17}$$

The photodiode integration time T_{D} is ideally equal to the bit period T_{bit}, and the relative delays τ_k and τ_l are assumed to be uniformly distributed from $-\frac{T_{\mathrm{bit}}}{2}$ to $\frac{T_{\mathrm{bit}}}{2}$. Evaluating the expected value of the term (A) in Equation B.17 over the relative delays τ_k and τ_l and using $T_{\mathrm{D}} = T_{\mathrm{bit}}$, it is found[2] that

$$\mathrm{E}[(\mathrm{A})] \approx \frac{N}{T_{\mathrm{bit}}\Delta\nu} \left[\frac{1}{T_{\mathrm{bit}}} \int_{-\frac{T_{\mathrm{bit}}}{2}}^{\frac{T_{\mathrm{bit}}}{2}} \mathrm{sinc}^2\left(\frac{\Delta\nu t}{N}\right)\right]^2 \tag{B.18}$$

and that this approximation becomes more accurate as $\frac{T_{\mathrm{bit}}\Delta\nu}{N}$ increases. Note that $T_{\mathrm{bit}} \gg \frac{N}{\Delta\nu}$ has already been assumed.

The signal power is given by

$$I_{k=l=g}^2 = \frac{R^2P_{\mathrm{p}}^2}{4N^2T_{\mathrm{bit}}^2} \left[\int_{-\frac{T_{\mathrm{bit}}}{2}}^{\frac{T_{\mathrm{bit}}}{2}} \mathrm{sinc}^2\left(\frac{\Delta\nu t}{N}\right)\right]^2 \tag{B.19}$$

and hence an SIR estimate of

$$\mathrm{SIR} \approx \frac{\Delta\nu T_{\mathrm{bit}}}{K(K-1)} \tag{B.20}$$

is found under the assumption of Equation B.15.

In order to validate the assumption represented in Equation B.15, Monte Carlo simulation of ideal asynchronous received signals (Equation B.12) was performed, recording the corresponding interference levels. In Figure B.1 the interference estimates from a number of simulations are compared with the predictions according to Equation B.20. Each point in Figure B.1 represents the average interference level over 10000 trials. In a single trial, each user was assumed to have equiprobable binary data, uniformly-distributed random relative optical phase, and a random time delay uniformly distributed over the bit period. The interference level was calculated assuming ideal spectral-amplitude coding and balanced detection at the

[2]This was via algebraic manipulation into tabulated integrals, and subsequent numerical evaluation.

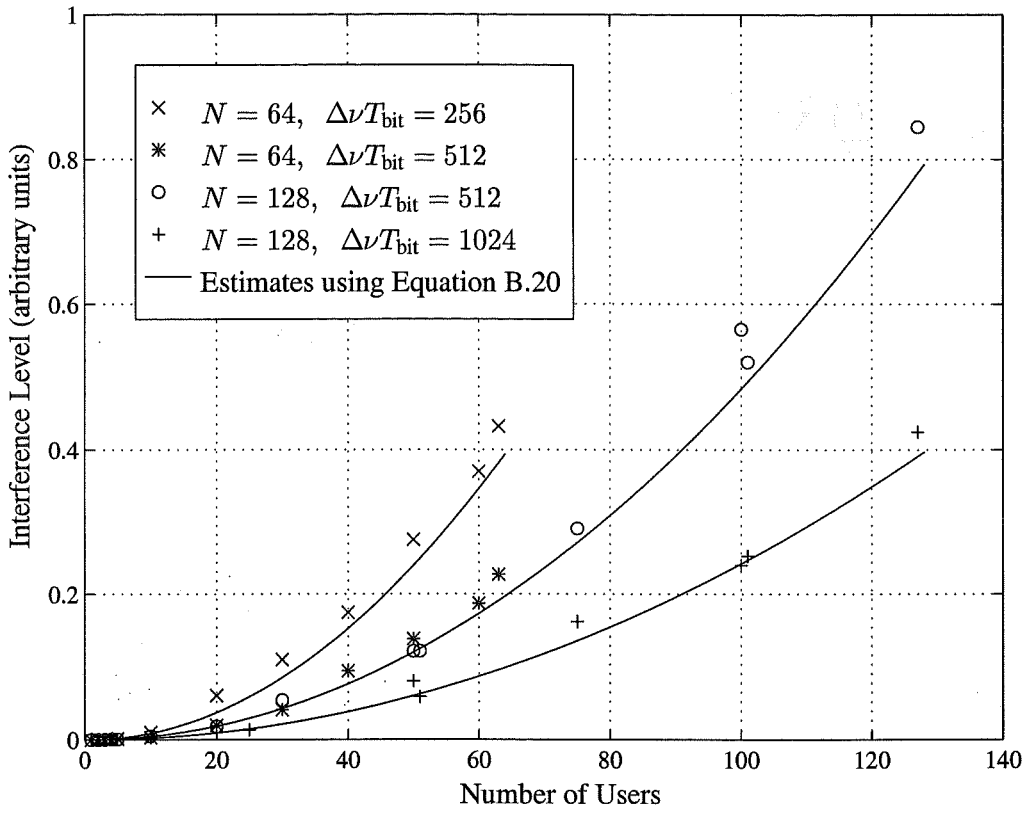

Figure B.1 Comparison of Simulation Results with Analytical Estimate

receiver, and the finite receiver bandwidth was represented by ideal integration over the bit period. Hadamard codes based on the cyclic shifts of m-sequences were used, and the binary data keying was by code complementation. Good correspondence between the estimates from Equation B.20 and the numerical simulation results can be seen in Figure B.1.

Appendix C

SPECTRAL-AMPLITUDE OCDMA WITH HIGHLY COHERENT SOURCE ARRAYS

Here, the SIR limit is estimated for the case of spectral-amplitude OCDMA using highly coherent laser array sources. In the worst case, the fields from each source within the same slice have the same polarisation and are completely coherent over a bit period, differing only by some phase shift. Under the assumption that the spectral slice width is significantly greater than the receiver electrical bandwidth, the only significant interference is between light within the same slice, and the contributions from each slice are independent. Hence, for the purpose of interference estimation over the bit period, the received fields can be simply represented as

$$\boldsymbol{E} = \sqrt{\frac{P_s}{N}} \sum_{k=1}^{K} \sum_{i=1}^{N} c_k(i) e^{j\phi_{ki}} \tag{C.1}$$

incident upon a single detector. In Equation C.1, the amplitude is scaled such that $R|\boldsymbol{E}|^2$ gives the photocurrent, where R is the photodiode responsivity, and $c_k(i)$ is the ith unipolar code element of the kth user, following the notation in Chapter 3. Random variables ϕ_{ki} are independent over all k,i and are each uniformly distributed on 0-2π. The actual spectral coding and balanced detector structure would weight the terms in Equation C.1 by $h_g(i)$, the bipolar elements of the gth code, but it is assumed that these signs are incorporated into ϕ_{ki}.

The photocurrent difference is given by

$$R|\boldsymbol{E}|^2 = \frac{RP_s}{N} \sum_{k=1}^{K} \sum_{l=1}^{K} \sum_{i=1}^{N} c_k(i) c_l(i) e^{j(\phi_{ki} - \phi_{li})} \tag{C.2}$$

In Equation C.2, the terms with $k = l$ give the desired signal and any direct MAI when the balanced receiver structure is properly represented, but the MAI is ideally zero with Hadamard-based codes. Consequently, the terms with $k = l$ are neglected, and the remaining terms from Equation C.2 can be expressed as

$$\frac{2RP_s}{N} \sum_{k=1}^{K-1} \sum_{l=k+1}^{K} \sum_{i=1}^{N} c_k(i) c_l(i) \cos(\phi_{ki} - \phi_{li}) \tag{C.3}$$

To estimate the variance of the interference represented by Equation C.3, note first that the variance of the cosine term is $\frac{1}{2}$ under the aforementioned assumptions on ϕ_{ki}. With Hadamard-based codes, there are only $\frac{N}{4}$ non-zero values of $c_k(i)c_l(i)$ over all $i = 1 \ldots N$ with $k \neq l$. Hence, the variance of Equation C.3 is estimated as

$$\sigma_I^2 \approx \left(\frac{2RP_s}{N}\right)^2 \cdot \frac{K(K-1)}{2} \cdot \frac{N}{4} \cdot \frac{1}{2} = \frac{R^2 P_s^2 K(K-1)}{4N} \tag{C.4}$$

The signal is given by $\pm\frac{RP_s}{2}$, giving an SIR estimate of

$$\text{SIR} \approx \frac{N}{K(K-1)} \tag{C.5}$$

Appendix D

COHERENCE MULTIPLEXING WITH SINGLE-ENDED DETECTION

Equation 7.15 is reproduced here for convenience.

$$I(t) = \frac{R}{4M}\frac{1}{T_{\mathrm{D}}}\int_{T_{\mathrm{D}}}\left[\sum_{k=1}^{M}\left\{\left|\boldsymbol{E}_k(t)\right|^2 + \left|\boldsymbol{E}_k(t-\tau_g)\right|^2 + 2\Re\{\boldsymbol{E}_k(t)\boldsymbol{E}_k^*(t-\tau_g)\}\right\} + 2\sum_{k=1}^{M-1}\sum_{l=k+1}^{M}\Re\left\{\boldsymbol{E}_k(t)\boldsymbol{E}_l^*(t) + \boldsymbol{E}_k(t)\boldsymbol{E}_l^*(t-\tau_g) + \boldsymbol{E}_k(t-\tau_g)\boldsymbol{E}_l^*(t) + \boldsymbol{E}_k(t-\tau_g)\boldsymbol{E}_l^*(t-\tau_g)\right\}\right]\mathrm{d}t \tag{D.1}$$

Substituting $\boldsymbol{E}_k = \frac{1}{\sqrt{2}}[\boldsymbol{S}_k(t) + d_k(t)\boldsymbol{S}_k(t-\tau_k)]$ and regrouping some terms, Equation D.1 becomes

$$\begin{aligned} I(t) = \frac{R}{4MT_{\mathrm{D}}}\int_{T_{\mathrm{D}}}\Bigg[\sum_{k=1}^{M}\sum_{l=1}^{M}\Re\Big\{&\underbrace{\boldsymbol{S}_k(t)\boldsymbol{S}_l^*(t-\tau_g)}_{\text{(i)}} + \underbrace{d_l(t-\tau_g)\boldsymbol{S}_k(t)\boldsymbol{S}_l^*(t-\tau_g-\tau_l)}_{\text{(ii)}} + \\ &\underbrace{d_k(t)\boldsymbol{S}_k(t-\tau_k)\boldsymbol{S}_l^*(t-\tau_g)}_{\text{(iii)}} + \underbrace{d_k(t)d_l(t-\tau_g)\boldsymbol{S}_k(t-\tau_k)\boldsymbol{S}_l^*(t-\tau_g-\tau_l)}_{\text{(iv)}} + \underbrace{d_l(t)\boldsymbol{S}_k(t)\boldsymbol{S}_l^*(t-\tau_l)}_{\text{(v)}} + \\ &\underbrace{d_l(t-\tau_g)\boldsymbol{S}_k(t-\tau_g)\boldsymbol{S}_l^*(t-\tau_g-\tau_l)}_{\text{(vi)}}\Big\} + \sum_{k=1}^{M-1}\sum_{l=k+1}^{M}\Re\Big\{\underbrace{\boldsymbol{S}_k(t)\boldsymbol{S}_l^*(t)}_{\text{(a)}} + \underbrace{d_k(t)d_l(t)\boldsymbol{S}_k(t-\tau_g)\boldsymbol{S}_l^*(t-\tau_g)}_{\text{(b)}} + \\ &\underbrace{\boldsymbol{S}_k(t-\tau_k)\boldsymbol{S}_l^*(t-\tau_l)}_{\text{(c)}} + \underbrace{d_k(t-\tau_g)d_l(t-\tau_g)\boldsymbol{S}_k(t-\tau_g-\tau_k)\boldsymbol{S}_l^*(t-\tau_g-\tau_l)}_{\text{(d)}}\Big\} + \frac{1}{2}\sum_{k=1}^{M}\Big\{\underbrace{\left|\boldsymbol{S}_k(t)\right|^2}_{\text{(e)}} + \\ &\underbrace{\left|\boldsymbol{S}_k(t-\tau_g)\right|^2}_{\text{(f)}} + \underbrace{\left|\boldsymbol{S}_k(t-\tau_k)\right|^2}_{\text{(g)}} + \underbrace{\left|\boldsymbol{S}_k(t-\tau_g-\tau_k)\right|^2}_{\text{(h)}}\Big\}\Bigg]\mathrm{d}t \end{aligned} \tag{D.2}$$

The average of Equation D.2 is given by

$$\mathrm{E}[I(t)] = \frac{RP_{\mathrm{s}}K}{2M} + d_g(t)\frac{RP_{\mathrm{s}}}{4M} \tag{D.3}$$

The first term of Equation D.3 is simply the DC photocurrent level due to the incident light power represented by terms (e)-(h), and the latter term in Equation D.3 is the signal component, from term (iii) with $k = l = g$.

As for the balanced case in Section 7.3.1, it is assumed that all interferometer delays and their differences are small with respect to the bit period, but much greater than the coherence time of the sources, and that the receiver bandwidth is of the order of $\frac{1}{T_{\text{bit}}}$. These assumptions mean that any data modulation $d_k(t)$ is approximately equal to the delayed modulation $d_k(t-\tau)$ over each whole bit period, where τ is any interferometer delay or delay difference. Furthermore, the correlated noise within the receiver bandwidth B_{e} arising from two terms that differ by only such a time shift τ is considered completely correlated within the receiver bandwidth B_{e}, since the time delays τ are much smaller than the bit period. The noise spectrum both from each term and in total is then approximately flat over the receiver bandwidth, and it is assumed to be ideally flat in this region. These are all worst case noise conditions.

Terms (e)-(h), along with term (iii) when $k = l = g$, are source intensity terms, contributing the mean photocurrent as already noted, and these are constant if each source has negligible intensity noise. However, if each source is thermal, then these terms have significant intensity noise according to Equation 3.10, and they are all highly correlated. Term (iii) is also data dependent, and assuming complete correlation between the noise from these terms within B_{e}, the excess noise power from these terms with $k = g$ is then $(10 + 8d_g(t))\sigma^2_{\text{term}}$, where σ^2_{term} is given by

$$\sigma^2_{\text{term}} = \frac{R^2 P_{\text{s}}^2 \tau_{\text{c}} B_{\text{e}}}{16M^2} \tag{D.4}$$

For $k \neq g$, the remaining thermal noise power from terms (e)-(h) is simply $8(K-1)\sigma^2_{\text{term}}$.

When $k = l \neq g$, terms (i)-(vi) represent the mixing between each optical field and a delayed version of itself, which generates PIIN, and these are here said to be *self-mixing* terms. Note that terms (ii) and (iii) are uncorrelated with any other terms when $k = l \neq g$, but (i) and (iv) are correlated, and also (v) and (vi). Treating each of these terms as representing two similar independent fields incident with total power $\frac{RP_{\text{s}}}{4M}$ upon a single photodiode, the PIIN levels are simply calculable by Equation 3.16. Assuming complete correlation between the noise within B_{e} from the correlated terms, the total self-mixing PIIN power from these terms is then given by $10(K-1)\sigma^2_{\text{term}}$. In the case $k = l = g$, terms (i) and (iv) are still correlated, but now they differ from (v) and (vi) by only the data of the matched user $d_g(t)$, and (iii) is the signal intensity term which was dealt with earlier. The noise power of these five terms with $k = l = g$ is thus given by $(9 + 8d_g(t))\sigma^2_{\text{term}}$.

In the case where $k \neq l$, each term (i)-(vi) and (a)-(d) represents the mixing of optical fields from different sources, they generate PIIN according to Equation 3.16, and these are referred to here as *cross-mixing* terms. If the optical frequency range of each field is separated from that of every other field by at least the receiver bandwidth, then all such cross-mixing PIIN contributions are out-of-band at the receiver, and ideally contribute no PIIN to the received

signal. If each source has an identical power spectrum, however, then the cross-mixing terms do produce PIIN within the receiver bandwidth.

In the case of identical sources and $k \neq l$, term (ii) is uncorrelated with all other terms, and thus contributes PIIN of power $K(K-1)\sigma^2_{\text{term}}$ over all $k \neq l$. Terms (a)-(d) are highly correlated, but they depend upon the data-modulation product $d_k(t)d_l(t)$. Assuming each user has independent equiprobable data distributions, the average PIIN power from these terms is $4K(K-1)\sigma^2_{\text{term}}$, as though they were uncorrelated. When $k \neq l$ and $k, l \neq g$, terms (i), (iii) and (iv) are uncorrelated with all other terms, but terms (v) and (vi) are still highly correlated, giving worst case PIIN power $7(K-1)(K-2)\sigma^2_{\text{term}}$. In the case $k \neq l = g$, terms (v) and (vi) are still correlated, terms (iii) and (iv) are uncorrelated with any other term, but now term (i) differs from (v) by only $d_g(t)$, the data of the matched user. Hence the worst case PIIN power from these terms in this case is $(7 + 4d_g(t))(K-1)\sigma^2_{\text{term}}$. Finally, for the case $l \neq k = g$, terms (iv) and (vi) differ by the data modulation of the matched user $d_g(t)$, term (v) is still correlated with (vi), (i) is uncorrelated with any other term, and now (iii) differs from (b) by only the data-modulation term $d_l(t)$. Assuming each unmatched user has independent equiprobably-distributed data ($d_l(t)$), then the correlation between (iii) and (b) with $l \neq k = g$ can be neglected on average. Hence, the PIIN power from these terms with $l \neq k = g$ is the same as with $k \neq l = g$, that is $(7 + 4d_g(t))(K-1)\sigma^2_{\text{term}}$.

Collecting together all the contributions above, if the sources are thermal, the self-intensity terms contribute source intensity noise power

$$\sigma^2_{I_{\text{si}}} = \frac{R^2 P_s^2 \tau_c B_e}{16M^2}(8K + 2 + 8d_g(t)) \tag{D.5}$$

the self-mixing terms always contribute PIIN power

$$\sigma^2_{I_{\text{sm}}} = \frac{R^2 P_s^2 \tau_c B_e}{16M^2}(10K - 1 + 8d_g(t)) \tag{D.6}$$

and if all the sources have the same power spectrum then the cross-mixing terms contribute PIIN power

$$\sigma^2_{I_{\text{cm}}} = \frac{R^2 P_s^2 \tau_c B_e}{16M^2}(12K + 8d_g(t))(K-1) \tag{D.7}$$

The total noise in the case of identical thermal sources is simply the sum of Equations D.5 - D.7, giving Equation 7.18

$$\sigma^2_I = \frac{R^2 P_s^2 \tau_c B_e}{16M^2}(12K^2 + 6K + 1 + 8(K+1)d_g(t)) \tag{D.8}$$

If independent and identical sources with no self-intensity noise are used, then the noise

power σ_I^2 is simply the sum of Equations D.6 and D.7, giving Equation 7.19

$$\sigma_I^2 = \frac{R^2 P_s^2 \tau_c B_e}{16M^2}(12K^2 - 2K - 1 + 8K d_g(t)) \tag{D.9}$$

Similarly, in the case of sources which are sufficiently separated in wavelength, the cross-mixing terms are zero, and with no self-intensity noise, σ_I^2 is simply given by Equation D.6, and if the sources are thermal, then σ_I^2 is given by the sum of Equations D.5 and D.6.

The 'average' SNR[1] in each of the above cases is then simply calculable by assuming $\mathrm{E}[d_g(t)] = 0$ and using the signal power from the squared latter term in Equation D.3. In the case of each source being unpolarised and the whole network being polarisation independent, all of the above noise expressions are multiplied by a factor of one half, which is a 3 dB reduction in noise power. If each source is fully polarised, but they are all considered to have random polarisation states at the receiver, then just the cross-mixing noise is reduced by 3 dB on average, but any self-intensity noise and self-mixing noise remains the same.

[1]The single quotes appear because a signal-to-average-noise ratio is used, rather than an actual average of the SNR.

Appendix E

MODIFIED INCOHERENT BIPOLAR CORRELATOR

Here the receiver correlator structure of [Andonovic *et al.* 1994] is described, and a straightforward modification of this is given that allows this scheme to match the common form of incoherent and bipolar OCDMA used in Section 7.3.3. Although there are remaining practical problems with this correlator, which are mentioned briefly, no attempts to address them here are made.

The receiver correlator in [Andonovic *et al.* 1994] has the basic structure shown in Figure E.1. Each directional coupler switch in the delay-line of Figure E.1 can be switched to route the inputs according to either the cross state $\times$ or the bar state =, corresponding to unipolar code elements 'one' and 'zero' respectively. These couplers are in pairs of opposite state, corresponding to either the unipolar elements [0,1] or [1,0], and there are as many pairs as elements in the original bipolar code. The delay T is the pulse or chip period, and it is assumed that all other delays in the delay-line configuration are small with respect to T. Each element of the bipolar code is represented by the unipolar pulse sequence of either [0,1,0] or [1,0,0], according to the element sign. This is effectively Manchester encoding of each code element, along with an extra empty space. This empty pulse space corresponds to the delay of $2T$ between each pair of switches in Figure E.1, rather than just T, since it is assumed that the

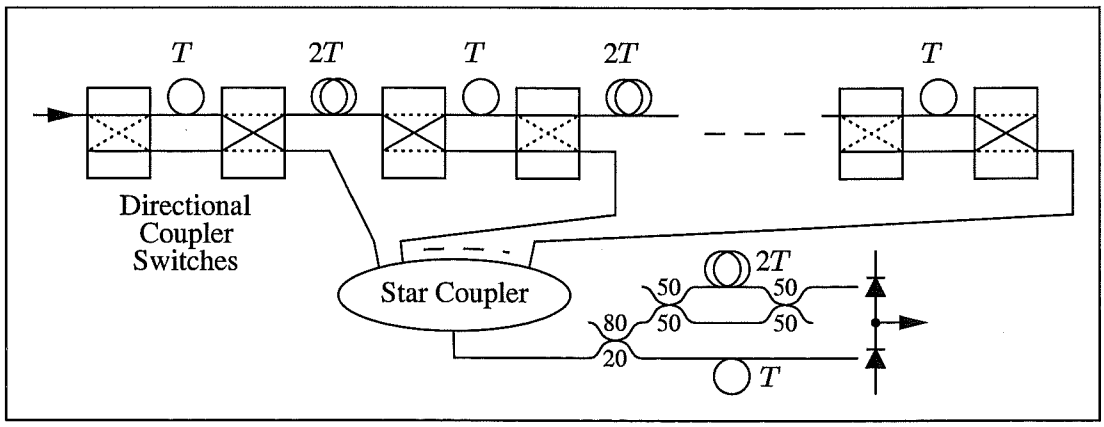

Figure E.1 Receiver Correlator Structure of [Andonovic *et al.* 1994]

total unipolar code sequence is loaded serially into the delay-line of Figure E.1[1]. When the unipolar code is correctly aligned in the delay-line, there will be a pulse output from only the switch pairs whose state matches that of the corresponding unipolar code elements. These outputs are then gathered by the star coupler. For all the switch pairs whose states do not match those of the corresponding unipolar code elements, there will instead be a pulse output either leading or trailing the matched outputs by T. This is the reason for the structure beyond the star coupler, since the two 50/50 couplers with the $2T$ delay adds these pulses corresponding to code mismatches, and the other path delivers the pulses corresponding to code matches to the other photodiode at the same time [Andonovic *et al.* 1994]. Minimising the loss using this configuration and ensuring that the same power occurs at each photodiode requires the 2×2 coupler immediately after the star coupler to have an 80/20 splitting ratio, and this value is assumed both here and in Section 7.3.3, whereas the splitting ratios are not specified in [Andonovic *et al.* 1994]. In this manner, during the appropriate interval T, the balanced detector output is proportional to the difference between the number of code disagreements and the number of code agreements, as required for the effective bipolar correlation (Section 2.9). The extra element [0] between each Manchester-encoded unipolar pair is necessary so that when there is a code match with the switch-pair state, no pulse occurs either side of the pulse that indicates the match, because these locations are used to indicate a mismatch.

To overcome the need for the extra zero code elements in [Andonovic *et al.* 1994], which increase the code length by 50%, it is necessary to collect the pulses corresponding to code mismatches in the delay-line of Figure E.1 in a slightly better fashion. If the same form of delay-line is considered, but with only T delay between each pair rather than $2T$, as in Figure E.2, and the extra zero unipolar code elements removed, then the pulses corresponding to code matches appear as before. The pulses corresponding to code mismatches still occur either immediately before or after this matched-pulse position, but the time slot T on the other side of the matched-pulse position may or may not contain a pulse, according to the adjacent code element. Whether the mismatched pulse occurs before or after the matched-pulse position is simply due to which state the switch pair is in, and the modified correlator structure makes use of this information.

In Figure E.2, if the first switch in each pair is in the cross state, then the output of this pair is routed to the left star coupler, otherwise the output from each pair is directed to the right star coupler. The pulses corresponding to code matches are thus split between the two star couplers, and so these two outputs are coupled together and incident upon the upper photodiode, albeit delayed by T. The pulses corresponding to code mismatches either appear at the left star coupler output immediately before the matched-pulse position, or at the right star coupler output immediately after the matched-pulse position. Hence, the left star-coupler output is retarded by T relative to the matched-pulse position and incident upon the lower photodiode, along with the right star-coupler output advanced by T relative to the matched-pulse position. In this

[1]Presumably all the switches would be in the bar state during this loading, but this is not discussed in [Andonovic *et al.* 1994]

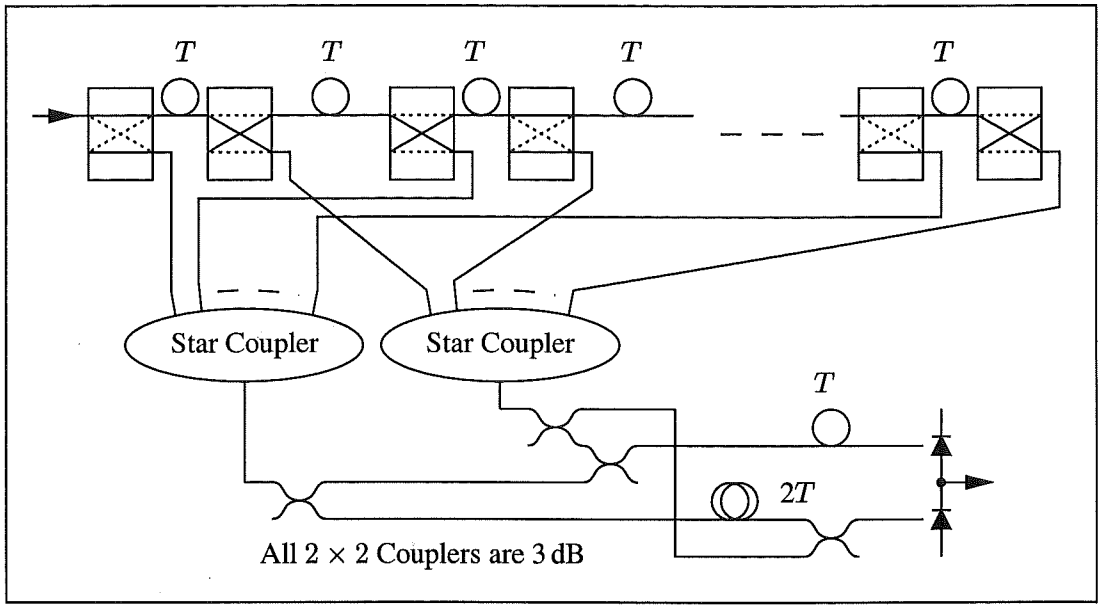

Figure E.2 Modified Receiver Correlator Structure

manner, the same output as Figure E.1 is achieved, although it is simply inverted according to the drawn polarity.

The most significant differences in these two configurations are the doubling of the number of delay-line taps and the use of an extra star coupler to gather these taps together in Figure E.2. However, only half of these taps are actually used while performing the desired correlation in Figure E.2, matching those in Figure E.1. The signal appearing at each photodiode in Figure E.1 is 20% of the star coupler output, and in Figure E.2 the signal appearing at each photodiode is 25% of the star coupler outputs. The star coupler size is the same in each configuration, so Figure E.2 has a slight power advantage over Figure E.1 as represented therein. However, both these structures are drawn with unused 2×2 coupler outputs, and if these are utilised appropriately (using extra photodiodes, for example), then the modified structure is actually 50% more efficient in terms of optical power, as well as having codes which are 33% shorter.

The highly undesirable loss of the star coupler(s) in each configuration is noted, but this is not addressed here. Another practical issue with the structure of both Figures E.1 and E.2 is that even if all the switches are in the bar state while the received code is serially input into the delay-line, the tap outputs over three successive pulse periods are required, rather than just over a single pulse period. The power appearing from the delay-line taps during one pulse period in practice clearly affects the tap outputs in subsequent pulse periods, and this is not addressed here nor in [Andonovic *et al.* 1994].

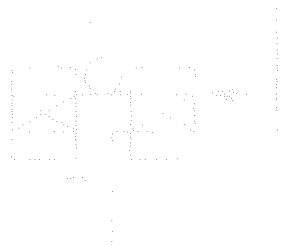

REFERENCES

Agrawal, G.P. (1989), *Nonlinear Fiber Optics*, Academic Press, Inc., 1989.

Agrawal, G.P. (1992), *Fiber-Optic Communication Systems*, John Wiley & Sons, Inc., 1992.

Aisawa, S., Sakamoto, T., Fukui, M., Kani, J., Jinno, M. and Oguchi, K. (1998), "Ultra-wideband, long distance WDM demonstration of 1 Tbit/s (50 × 20Gbit/s), 600km transmission using 1550nm and 1580nm wavelength bands," *Electronics Letters*, Vol. 34, No. 11, May 1998, pp. 1127–1129.

Andonovic, I. and Tančevski, L. (1996), "Incoherent optical code division multiple access systems," *Proceedings of the 1996 IEEE International Symposium on Spread Spectrum Techniques and Applications, ISSSTA'96*, Vol. 1, September 1996, pp. 424–430.

Andonovic, I., Tančevski, L., Shabeer, M. and Bazgaloski, L. (1994), "Incoherent all-optical code recognition with balanced detection," *Journal of Lightwave Technology*, Vol. 12, No. 6, June 1994, pp. 1073–1080.

Andrekson, P.A., Olsson, N.A., Simpson, J.R., Logan, R.A. and Haner, M. (1991), "16 Gbit/s all-optical demultiplexing using four-wave mixing," *Electronics Letters*, Vol. 27, No. 11, May 1991, pp. 922–924.

Andrekson, P.A., Olsson, N.A., Simpson, J.R., Digiovanni, D.J., Morton, P.A., Tanbun-Ek, T., Logan, R.A. and Wecht, K.W. (1992), "64 Gb/s all-optical demultiplexing with the nonlinear optical-loop mirror," *IEEE Photonics Technology Letters*, Vol. 4, No. 6, June 1992, pp. 644–647.

Argon, C. and Ergül, R. (1995), "Optical CDMA via shortened optical orthogonal codes based on extended sets," *Optics Communications*, Vol. 116, 1995, pp. 326–330.

Ayadi, F. and Rusch, L.A. (1997), "Coherent optical CDMA with limited phase excursion," *IEEE Communications Letters*, Vol. 1, No. 1, January 1997, pp. 28–30.

Ayadi, F., Hayes, J.F. and Kavehrad, M. (1995), "Throughput calculation of an optical CDMA system using coherent modulation," *Proceedings of the 1995 Canadian Conference on Electrical and Computer Engineering*, Vol. 1, 1995, pp. 83–86.

Azizoglu, M.Y., Salehi, J.A. and Li, Y. (1990), "On the performance of fiber-optic CDMA systems," *Proceedings of the 1990 IEEE Global Telecommunications Conference, GLOBECOM'90*, Vol. 3, December 1990, pp. 1861–1865.

Benedetto, S. and Olmo, G. (1991), "Performance evaluation of coherent optical code division multiple access," *Electronics Letters*, Vol. 27, No. 22, October 1991, pp. 2000–2002.

Brady, D. and Verdú, S. (1991), "A semiclassical analysis of optical code division multiple access.," *IEEE Transactions on Communications*, Vol. 39, No. 1, January 1991, pp. 85–93.

Brandt-Pearce, M. and Aazhang, B. (1993), "Optical spectral amplitude code division multiple access system," *Proceedings of the 1993 IEEE International Symposium on Information Theory, ISIT'93*, 1993, P. 379.

Brandt-Pearce, M. and Aazhang, B. (1994), "Performance analysis of single-user and multiuser detectors for optical code division multiple access communication systems.," *IEEE Transactions on Communications*, Vol. 43, No. 2/3/4, February/March/April 1994, pp. 435–444.

Brooks, J.L., Wentworth, R.H., Youngquist, R.C., Tur, M., Kim, B.Y. and Shaw, H.J. (1985), "Coherence multiplexing of fiber-optic interferometric sensors," *Journal of Lightwave Technology*, Vol. 3, No. 5, October 1985, pp. 1062–1071.

Burns, W.K., Moeller, R.P. and Dandridge, A. (1990), "Excess noise in fiber gyroscope sources," *IEEE Photonics Technology Letters*, Vol. 2, No. 8, August 1990, pp. 606–608.

Cahill, M.J.L., Pendock, G.J. and Sampson, D.D. (1997), "Hybrid coherence multiplexing/coarse wavelength-division multiplexing passive optical network for customer access," *IEEE Photonics Technology Letters*, Vol. 9, No. 7, July 1997, pp. 1032–1034.

Chang, Y.L. and Marhic, M.E. (1990), "2^n codes for optical CDMA and associated networks," *IEEE/LEOS Summer Topical Meetings, Technical Digest*, July 1990, pp. 23–24.

Chang, Y.L. and Marhic, M.E. (1992), "Fiber-optic ladder networks for inverse decoding coherent CDMA," *Journal of Lightwave Technology*, Vol. 10, No. 12, December 1992, pp. 1952–1962.

Chang, C.C., Sardesai, H.P. and Weiner, A.M. (1998), "Code-division multiple-access encoding and decoding of femtosecond optical pulses over a 2.5-km fiber link," *IEEE Photonics Technology Letters*, Vol. 10, No. 1, January 1998, pp. 171–173.

Chu, K.W. and Dickey, F.M. (1991), "Optical coherence multiplexing for interprocessor communications," *Optical Engineering*, Vol. 30, No. 3, March 1991, pp. 337–344.

Chung, H.C. and Kumar, P.V. (1990), "Optical orthogonal codes - new bounds and an optimal construction," *IEEE Transactions on Information Theory*, Vol. 36, No. 4, July 1990, pp. 866–873.

Chung, F.R.K., Salehi, J. and Wei, V.K. (1989), "Optical orthogonal codes: design, analysis, and applications," *IEEE Transactions on Information Theory*, Vol. 35, No. 3, May 1989, pp. 595–604.

Cielo, P. and Delisle, C. (1976), "Multiplexage en communication optique par interféromètrie à grande différence de marche en lumière blanche," *Canadian Journal of Physics*, Vol. 54, No. 23, 1976, pp. 2322–2331.

Coppinger, F., Yegnanarayanan, S., Trinh, P.D. and Jalali, B. (1997), "All-optical incoherent negative taps for photonic signal processing," *Electronics Letters*, Vol. 33, No. 11, May 1997, pp. 973–975.

Davenport Jr, W.B. and Root, W.L. (1958), *An Introduction to the Theory of Random Signals and Noise*, McGraw-Hill, 1958.

Davies, P.A. and Shaar, A.A. (1983), "Asynchronous multiplexing for an optical-fibre local-area network," *Electronics Letters*, Vol. 19, No. 10, May 1983, pp. 390–392.

DeCusatis, C.M. and Das, P.K. (1990), "Spread-spectrum techniques in optical communication using transform domain processing," *IEEE Journal on Selected Areas in Communications*, Vol. 8, No. 8, October 1990, pp. 1608–1616.

Delisle, C. and Cielo, P. (1975), "Application de la modulation spectrale à la transmission de l'information," *Canadian Journal of Physics*, Vol. 53, No. 11, 1975, pp. 1047–1053.

Desem, C. (1988), "Optical interference in lightwave subcarrier multiplexing systems employing multiple optical carriers," *Electronics Letters*, Vol. 24, No. 1, January 1988, pp. 50–52.

Elmirghani, J.M.H. and Cryan, R.A. (1994), "New PPM-CDMA hybrid for indoor diffuse infrared channels," *Electronics Letters*, Vol. 30, No. 20, September 1994, pp. 1646–1647.

Foschini, G.J. and Vannucci, G. (1988), "Using spread-spectrum in a high-capacity fiber-optic local network," *Journal of Lightwave Technology*, Vol. 6, No. 3, March 1988, pp. 370–379.

Gagliardi, R.M., Mendez, A, J., Dale, M.R. and Park, E. (1993), "Fiber-optic digital video multiplexing using optical CDMA," *Journal of Lightwave Technology*, Vol. 11, No. 1, January 1993, pp. 20–26.

Garrett, I. (1993), "Pulse-position modulation for transmission over optical fibers with direct or heterodyne detection," *IEEE Transactions on Communications*, Vol. 31, No. 4, April 1993, pp. 518–527.

Gelman, A.D. and Schilling, D.L. (1988), "A fiber optic CDMA network for real-time communication," *Proceedings of the 1988 Joint Conference of the IEEE Computer and Communications Societies, INFOCOM'88*, March 1988, pp. 62–69.

Gimlett, J.L. and Cheung, N.K. (1986), "Dispersion penalty analysis for LED/single-mode fiber transmission systems," *Journal of Lightwave Technology*, Vol. 4, No. 9, September 1986, pp. 1381–1392.

Gloge, D. (1971), "Weakly guiding fibers," *Applied Optics*, Vol. 10, No. 10, October 1971, pp. 2252–2258.

Goedgebuer, J.P. and Hamel, A. (1987), "Coherence multiplexing using a parallel array of electrooptic modulators and multimode semiconductor lasers," *IEEE Journal of Quantum Electronics*, Vol. 23, No. 12, December 1987, pp. 2224–2237.

Goodman, J.W. (1985), *Statistical Optics*, John Wiley & Sons, Inc., 1985.

Gradshteyn, I.S. and Ryzhik, I.M. (1965), *Table of Integrals, Series, and Products*, Academic Press, Inc., 1965.

Green Jr, P.E. (1993), *Fiber Optic Networks*, Prentice-Hall, Inc., 1993.

Griffin, R.A., Sampson, D.D. and Jackson, D.A. (1992a), "Demonstration of data transmission using coherent correlation to reconstruct a coded pulse sequence," *IEEE Photonics Technology Letters*, Vol. 4, No. 5, May 1992, pp. 513–515.

Griffin, R.A., Sampson, D.D. and Jackson, D.A. (1992b), "Optical phase coding for code-division multiple access networks," *IEEE Photonics Technology Letters*, Vol. 4, No. 12, December 1992, pp. 1401–1404.

Griffin, R.A., Sampson, D.D. and Jackson, D.A. (1993), "Modification of optical coherence using spectral phase coding for use in photonic code-division multiple access systems," *Electronics Letters*, Vol. 29, No. 25, December 1993, pp. 2214–2216.

Griffin, R.A., Sampson, D.D. and Jackson, D.A. (1995), "Coherence coding for photonic code-division multiple access networks," *Journal of Lightwave Technology*, Vol. 13, No. 9, September 1995, pp. 1826–1837.

Gupta, G.C., Karafolas, N. and Uttamchandani, D. (1994), "Low coherence optical CDMA for LAN," *Proceedings of the 1994 Lasers and Electro-Optics Society Annual Meeting, LEOS'94*, Vol. 2, October-November 1994, pp. 122–123.

Gupta, G.C., Legg, P.J., Uttamchandani, D. and Andonovic, I. (1997), "Capacity bounding of coherence multiplexed local area networks due to interferometric noise," *IEE Proceedings - Optoelectronics*, Vol. 144, No. 2, April 1997, pp. 67–74.

Hajela, D.J. and Salehi, J.A. (1992), "Limits to the encoding and bounds on the performance of coherent ultrashort light pulse code-division multiple-access systems," *IEEE Transactions on Communications*, Vol. 10, No. 2, February 1992, pp. 325–336.

Harwit, M. and Sloane, N.J.A. (1979), *Hadamard Transform Optics*, Academic Press, Inc., 1979.

Hasegawa, S. and Hirosaki, B. (1983), "Spread-spectrum multiple access data loop," *NEC Research and Development*, No. 71, October 1983, pp. 48–58.

Healey, P. (1987), "Dimensioning an optical-fiber spread-spectrum multiple-access communication system," *Optics Letters*, Vol. 12, No. 6, June 1987, pp. 425–427.

Hinkov, I., Hinkov, V., Iversen, K. and Ziemann, O. (1995), "Feasibility of optical CDMA using spectral encoding by acoustically tunable optical filters," *Electronics Letters*, Vol. 31, No. 5, March 1995, pp. 384–385.

Ho, C.L. (1996), "Performance analysis of optical CDMA communication systems with quadratic congruential codes," *Proceedings of the 1996 IEEE International Symposium on Spread Spectrum Techniques and Applications, ISSSTA'96*, Vol. 1, 1996, pp. 418–423.

Ho, C.L. and Wu, C. (1994), "Performance analysis of CDMA optical communication systems with avalanche photodiodes," *Journal of Lightwave Technology*, Vol. 12, No. 6, June 1994, pp. 1062–1072.

Holmes, J.K. (1982), *Coherent Spread Spectrum Systems*, Wiley Interscience, 1982.

Holmes, A.S. and Syms, R.R.A. (1991), "Switchable all-optical encoding and decoding using optical fiber lattices," *Optics Communications*, Vol. 86, January 1991, pp. 25–28.

Holmes, A.S. and Syms, R.R.A. (1992), "All-optical CDMA using "quasi-prime" codes," *Journal of Lightwave Technology*, Vol. 10, No. 2, February 1992, pp. 279–286.

Hui, J.Y. (1985), "Pattern code modulation and optical decoding - a novel code-division multiplexing technique for multifiber networks," *IEEE Journal on Selected Areas in Communications*, Vol. 3, No. 6, November 1985, pp. 916–927.

Iversen, K., Mückenheim, J. and Hampicke, D. (1996), "A basic theory of fiber-optic CDMA," *Proceedings of the 1996 IEEE International Symposium on Spread Spectrum Techniques and Applications, ISSSTA'96*, Vol. 1, 1996, pp. 431–437.

Jackson, K.P., Newton, S.A., Moslehi, B., Tur, M., Cutler, C.C., Goodman, J.W. and Shaw, H.J. (1985), "Optical fiber delay-line signal processing," *IEEE Transactions on Microwave Theory and Techniques*, Vol. 33, No. 3, March 1985, pp. 193–209.

Kao, C.K. (1988), *Optical Fibre*, Peter Peregrinus Ltd., 1988.

Karafolas, N. and Uttamchandani, D. (1994a), "Self-homodyne code division multiple access technique for fiber optic local area networks," *IEEE Photonics Technology Letters*, Vol. 6, No. 7, July 1994, pp. 880–883.

Karafolas, N. and Uttamchandani, D. (1994b), "Fiber optic spread spectrum system based on PSK spreading and self-homodyne despreading of the optical spectrum," *Optics Communications*, Vol. 111, October 1994, pp. 238–244.

Karafolas, N. and Uttamchandani, D. (1995), "Optical CDMA system using bipolar codes and based on narrow passband optical filtering and direct detection," *IEEE Photonics Technology Letters*, Vol. 7, No. 9, September 1995, pp. 1072–1074.

Karafolas, N., Gupta, G.C. and Uttamchandani, D. (1996), "Combining code division multiplexing and coherence multiplexing for optical fibre multiple access networks," *Optics Communications*, Vol. 123, January 1996, pp. 11–18.

Kavehrad, M. (1995), March 1995. Private communication.

Kavehrad, M. and Simova, E. (1996), "Optical CDMA by amplitude spectral encoding of spectrally-sliced light-emitting-diodes," *Proceedings of the 1996 IEEE International Symposium on Spread Spectrum Techniques and Applications, ISSSTA'96*, Vol. 1, 1996, pp. 414–418.

Kavehrad, M. and Zaccarin, D. (1995), "Optical code-division-multiplexed systems based on spectral encoding of noncoherent sources," *Journal of Lightwave Technology*, Vol. 13, No. 3, March 1995, pp. 534–545.

Keating, A.J. and Sampson, D.D. (1997), "Reduction of excess intensity noise in spectrum-sliced incoherent light for WDM applications," *Journal of Lightwave Technology*, Vol. 15, No. 1, January 1997, pp. 53–61.

Khaleghi, F. and Kavehrad, M. (1996), "A new correlator receiver architecture for noncoherent optical CDMA networks with bipolar capacity," *IEEE Transactions on Communications*, Vol. 44, No. 10, October 1996, pp. 1335–1339.

Kiasaleh, K. (1989), "Spread-spectrum optical on-off-keying communication system," *Proceedings of the 1989 IEEE International Conference on Communications, ICC'89*, Vol. 1, June 1989, pp. 136–140.

Kiasaleh, K. (1991), "Fiber optic frequency hopping multiple access communication system," *IEEE Photonics Technology Letters*, Vol. 3, No. 2, February 1991, pp. 173–175.

Kitayama, K. (1994), "Novel spatial spread spectrum based fiber optic CDMA network for image transmission," *IEEE Journal on Selected Areas in Communications*, Vol. 12, No. 4, May 1994, pp. 762–772.

Kostić, Z. and Titlebaum, E.L. (1994), "The design and performance analysis for several new classes of codes for optical synchronous CDMA and for arbitrary-medium time-hopping synchronous CDMA communication systems," *IEEE Transactions on Communications*, Vol. 42, No. 8, August 1994, pp. 2608–2617.

Kwon, H.M. (1991a), "Optical orthogonal code division multiple access system Part I: with APD noise and thermal noise," *Proceedings of the 1991 IEEE International Conference on Communications, ICC'91*, Vol. 2, June 1991, pp. 614–617.

Kwon, H.M. (1991b), "Optical orthogonal code division multiple access system Part II: multibits/sequence-period OOCDMA," *Proceedings of the 1991 IEEE International Conference on Communications, ICC'91*, Vol. 2, June 1991, pp. 618–621.

Kwon, H.M. (1994a), "Optical orthogonal code-division multiple-access system - Part I: APD noise and thermal noise," *IEEE Transactions on Communications*, Vol. 42, No. 7, July 1994, pp. 2470–2479.

Kwon, H.M. (1994b), "Optical orthogonal code-division multiple-access system - Part II: multibits/sequence-period OOCDMA," *IEEE Transactions on Communications*, Vol. 42, No. 8, August 1994, pp. 2592–2599.

Kwong, W.C. and Yang, G.C. (1995), "Construction of 2^n prime-sequence codes for optical code division multiple access," *IEE Proceedings on Communication*, Vol. 142, No. 3, June 1995, pp. 141–150.

Kwong, W.C., Perrier, P.A. and Prucnal, P.R. (1991), "Perfomance comparison of asynchronous and synchronous code-division multiple-access techniques for fiber-optic local area networks," *IEEE Transactions on Communications*, Vol. 39, No. 11, November 1991, pp. 1625–1634.

Kwong, W.C., Prucnal, P.R. and Liu, Y. (1992), "Ultrafast all-optical code-division multiple-access networks," *SPIE Proceedings*, Vol. 1787, 1992, pp. 121–132.

Kwong, W.C., Zhang, J.G. and G.-C., Y. (1994), "2^n prime-sequence code and its optical CDMA coding architecture," *Electronics Letters*, Vol. 30, No. 6, March 1994, pp. 509–510.

Lam, A.W. and Hussain, A.M. (1992), "Performance analysis of direct-detection optical CDMA communication systems with avalanche photodiodes," *IEEE Transactions on Communications*, Vol. 40, No. 4, April 1992, pp. 810–820.

Lee, C.E. and Taylor, H.F. (1991), "Intensity noise in long-wavelength superluminescent sources," *IEEE Journal of Quantum Electronics*, Vol. 27, No. 5, May 1991, pp. 1171–1174.

Letaief, K.B. (1995), "The performance of optical fiber direct-sequence spread-spectrum multiple-access communication systems," *IEEE Transactions on Communications*, Vol. 43, No. 11, November 1995, pp. 2662–2666.

Maeda, M.W., Sessa, W.B., Way, W.I., Yi-Yan, A., Curtis, L. and Laming, R.I. (1990), "The effect of four-wave mixing in fibers on optical frequency-division multiplexed systems," *Journal of Lightwave Technology*, Vol. 8, No. 9, September 1990, pp. 1402–1408.

Mandayam, N.B. and Aazhang, B. (1994), "Importance sampling for analysis of direct detection optical communication systems.," *IEEE Transactions on Communications*, Vol. 43, No. 2/3/4, February/March/April 1994, pp. 229–239.

Marhic, M.E. (1993), "Coherent Optical CDMA Networks," *Journal of Lightwave Technology*, Vol. 11, No. 5/6, May/June 1993, pp. 854–863.

Marhic, M.E. and Chang, Y.L. (1989), "Pulse coding and coherent decoding in fibre-optic ladder networks," *Electronics Letters*, Vol. 25, No. 22, October 1989, pp. 1535–1536.

Marić, S.V. (1993), "New family of algebraically designed optical orthogonal codes for use in CDMA fibre-optic networks," *Electronics Letters*, Vol. 29, No. 6, March 1993, pp. 538–539.

Marić, S.V., Hahm, M.D. and Titlebaum, E.L. (1995), "Construction and performance of a new family of optical orthogonal codes for CDMA fiber-optic networks," *IEEE Transactions on Communications*, Vol. 43, No. 2/3/4, February/March/April 1995, pp. 485–489.

Marom, E. and Ramer, O.G. (1978), "Encoding-decoding optical fibre network," *Electronics Letters*, Vol. 14, No. 3, February 1978, pp. 48–49.

Masuda, H., Kawai, S. and Aida, K. (1998), "Ultra-wideband hybrid amplifier comprising distributed Raman amplifier and erbium-doped fibre amplifier," *Electronics Letters*, Vol. 34, No. 13, June 1998, pp. 1342–1344.

Mendez, A.J., Lambert, J.L., Morookian, J.M. and Gagliardi, R.M. (1994), "Synthesis and demonstration of high speed, bandwidth efficient optical code division multiple access (CDMA) tested at 1 Gb/s throughput," *IEEE Photonics Technology Letters*, Vol. 6, No. 9, September 1994, pp. 1146–1149.

Mezger, F.B. and Brandt-Pearce, M. (1996), "Dispersion limited fiber-optic CDMA systems with overlapped signature sequences," *Proceedings of the 1996 Lasers and Electro-Optics Society Annual Meeting, LEOS'96*, Vol. 2, November 1996, pp. 408–409.

Mollenauer, L.F., Lichtman, E., Neubelt, M.J. and Harvey, G.T. (1993), "Demonstration, using sliding-frequency guiding filters, of error-free soliton transmission over more than 20 Mm at 10 Gbit/s, single channel, and over more than 13 Mm at 20 Gbit/s in a two-channel WDM," *Electronics Letters*, Vol. 29, No. 10, May 1993, pp. 910–911.

Morkel, P.R., Laming, R.I. and Payne, D.N. (1990), "Noise characteristics of high-power doped-fibre superluminescent sources," *Electronics Letters*, Vol. 26, No. 2, January 1990, pp. 96–98.

Moslehi, B. (1986), "Noise power spectra of optical two-beam interferometers induced by the laser phase noise," *Journal of Lightwave Technology*, Vol. 4, No. 11, November 1986, pp. 1704–1710.

Nelson, L.B. and Poor, H.V. (1995a), "Performance of Multiuser Detection for Optical CDMA - Part I: Error Probabilities," *IEEE Transactions on Communications*, Vol. 43, No. 11, November 1995, pp. 2803–2811.

Nelson, L.B. and Poor, H.V. (1995b), "Performance of Multiuser Detection for Optical CDMA - Part II: Asymptotic Analysis," *IEEE Transactions on Communications*, Vol. 43, No. 12, December 1995, pp. 3015–3024.

Neusy, P.C. and Kavehrad, M. (1990), "Proposal for an all-optical code-division multiple access for local area networks," *Electronics Letters*, Vol. 26, No. 18, August 1990, pp. 1471–1473.

Nguyen, L., Aazhang, B. and Young, J.F. (1995), "All-optical CDMA with bipolar codes," *Electronics Letters*, Vol. 31, No. 6, March 1995, pp. 469–470.

Nguyen, L., Young, J.F. and Aazhang, B. (1996), "Photoelectric current distribution and bit error rate in optical communication systems using a superfluorescent fiber source," *Journal of Lightwave Technology*, Vol. 14, No. 6, June 1996, pp. 1455–1466.

Nguyen, L., Dennis, T., Aazhang, B. and Young, J.F. (1997), "Experimental demonstration of bipolar codes for optical spectral amplitude CDMA communication," *Journal of Lightwave Technology*, Vol. 15, No. 9, September 1997, pp. 1647–1653.

O'Farrell, T. and Beale, M. (1989), "Code-division multiple-access (CDMA) techniques in optical fibre LANs," *Second IEE National Conference on Telecommunications, IEE Conference Publication*, No. 300, April 1989, pp. 111–115.

O'Farrell, T. and Lochmann, S.I. (1994a), "Performance analysis of an optical correlator receiver for SIK DS-CDMA communication systems networks with bipolar capacity," *Electronics Letters*, Vol. 30, No. 1, January 1994, pp. 63–65.

O'Farrell, T. and Lochmann, S.I. (1994b), "Optical correlator receivers for SIK DS-CDMA communication systems," *Proceedings of the 1994 IEEE International Symposium on Spread Spectrum Techniques and Applications, ISSSTA'94*, Vol. 2, July 1994, pp. 584–587.

O'Farrell, T. and Lochmann, S.I. (1995), "Switched correlator receiver architecture for optical CDMA networks with bipolar capacity," *Electronics Letters*, Vol. 31, No. 11, May 1995, pp. 905–906.

Ohtsuki, T., Sasase, I. and Mori, S. (1995), "Effects of hard-limiter and error-correction coding on performance of direct-detection optical CDMA systems with PPM signaling," *IEICE Transactions on Fundamentals of Electronics, Communications, and Computer Sciences*, Vol. E78-A, No. 9, September 1995, pp. 1092–1101.

Ohtsuki, T., Sasase, I. and Mori, S. (1996), "Access timing controlled direct-detection optical CDMA systems with PPM signaling," *IEICE Transactions on Fundamentals of Electronics, Communications, and Computer Sciences*, Vol. E79-A, No. 9, September 1996, pp. 1392–1399.

Onoda, T. and Miki, N. (1991), "Synchronous CDMA for optical subscriber systems using 'block interleave'," *Electronics Letters*, Vol. 27, No. 24, November 1991, pp. 2219–2222.

Park, E., Mendez, A.J. and Garmire, E.M. (1992), "Temporal/spatial optical CDMA networks - design, demonstration, and comparison with temporal networks," *IEEE Photonics Technology Letters*, Vol. 4, No. 10, October 1992, pp. 1160–1162.

Pendock, G.J. and Sampson, D.D. (1995), "Increasing the transmission capacity of coherence multiplexed communication systems by using differential detection," *IEEE Photonics Technology Letters*, Vol. 7, No. 12, December 1995, pp. 1504–1506.

Pendock, G.J. and Sampson, D.D. (1996a), "Capacity of coherence-multiplexed CDMA networks," *Proceedings of the 1996 Conference on Lasers and Electrooptics, CLEO'96*, 1996, pp. 401–402.

Pendock, G.J. and Sampson, D.D. (1996b), "Excess noise in transmitted pulses of ASE," *Proceedings of the 21st Australian Conference on Optical Fibre Technology, ACOFT'96*, December 1996, pp. 69–72.

Pendock, G.J. and Sampson, D.D. (1997), "Capacity of coherence-multiplexed CDMA Networks," *Optics Communications*, Vol. 143, November 1997, pp. 109–117.

Pendock, G.J., Cahill, M.J.L. and Sampson, D.D. (1995), "Multi-gigabit per second demonstration of photonic code-division multiplexing," *Electronics Letters*, Vol. 31, No. 10, May 1995, pp. 819–820.

Peterson, G.D. and Gardner, C.S. (1981), "Cross-correlation interference effects in multiaccess optical communications," *IEEE Transactions on Aerospace and Electronic Systems*, Vol. 17, No. 2, March 1981, pp. 199–207.

Petrovic, R. and Holmes, S. (1990), "Orthogonal codes for CDMA optical fibre LANs with variable bit interval," *Electronics Letters*, Vol. 26, No. 10, May 1990, pp. 662–664.

Petrovic, R. and Holmes, S. (1991), "CDMA techniques in optical fibre LANs," *Journal of Optical Communications*, Vol. 12, No. 3, September 1991, pp. 101–106.

Prucnal, P.R., Santoro, M.A. and Fan, T.R. (1986a), "Spread spectrum fiber-optic local area network using optical processing," *Journal of Lightwave Technology*, Vol. 4, No. 5, May 1986, pp. 547–554.

Prucnal, P.R., Santoro, M.A. and Sehgal, S.K. (1986b), "Ultrafast all-optical synchronous multiple-access fiber networks," *IEEE Journal on Selected Areas in Communications*, Vol. 4, No. 9, December 1986, pp. 1484–1493.

Ramo, S., Whinnery, J.R. and Van Duzer, T. (1984), *Fields and Waves in Communication Electronics*, John Wiley & Sons, Inc., 1984.

Riza, N.A., Hershey, J.E. and Hassan, A.A. (1993), "Signaling system for multiple-access laser communications and interference protection," *Applied Optics*, Vol. 32, No. 11, April 1993, pp. 1965–1972.

Salehi, J.A. (1989a), "Emerging optical code-division multiple access communications systems," *IEEE Network*, March 1989, pp. 31–39.

Salehi, J.A. (1989b), "Code division multiple-access techniques in optical fiber networks - Part I : Fundamental principles," *IEEE Transactions on Communications*, Vol. 37, No. 8, August 1989, pp. 824–833.

Salehi, J.A. and Brackett, C.A. (1989), "Code division multiple-access techniques in optical fiber networks - Part II : Systems performance analysis," *IEEE Transactions on Communications*, Vol. 37, No. 8, August 1989, pp. 834–842.

Salehi, J.A. and Paek, E.G. (1995), "Holographic CDMA," *IEEE Transactions on Communications*, Vol. 43, No. 9, September 1995, pp. 2434–2438.

Salehi, J.A., Weiner, A.M. and Heritage, J.P. (1990), "Coherent ultrashort light pulse code-division multiple access communication systems," *Journal of Lightwave Technology*, Vol. 8, No. 3, March 1990, pp. 478–491.

Sampson, D.D. and Holloway, W.T. (1994), "100mW spectrally-uniform broadband ASE source for spectrum-sliced WDM systems," *OSA Technical Digest Series*, Vol. 14, 1994, pp. pd2–1 – pd2–4.

Sampson, D.D. and Jackson, D.A. (1990a), "Coherent optical fibre communications system using all-optical correlation processing," *Optics Letters*, Vol. 15, No. 10, May 1990, pp. 585–587.

Sampson, D.D. and Jackson, D.A. (1990b), "Spread-spectrum optical fibre network based on pulsed coherent correlation," *Electronics Letters*, Vol. 26, No. 19, September 1990, pp. 1550–1553.

Sampson, D.D., Griffin, R.A. and Jackson, D.A. (1994), "Photonic CDMA by coherent matched filtering using time-addressed coding in coherent optical ladder networks," *Journal of Lightwave Technology*, Vol. 12, No. 11, November 1994, pp. 2001–2010.

Sampson, D.D., Pendock, G.J. and Griffin, R.A. (1997), "Photonic code-division multiple-access communications," *Fiber and Integrated Optics*, Vol. 16, No. 2, 1997, pp. 129–157.

Santoro, M.A. and Prucnal, P.R. (1987), "Asynchronous fiber-optic local area network using CDMA and optical correlation," *Proceedings of the IEEE*, Vol. 75, No. 9, September 1987, pp. 1336–1338.

Shaar, A.A. and Davies, P.A. (1983), "Prime sequences: quasi-optimal sequences for OR channel code division multiplexing," *Electronics Letters*, Vol. 19, No. 21, October 1983, pp. 888–889.

Shalaby, H.M.H. (1995), "Performance analysis of optical synchronous CDMA communication systems with PPM signalling," *IEEE Transactions on Communications*, Vol. 43, No. 2/3/4, February/March/April 1995, pp. 624–634.

Shalaby, H.M.H. (1996), "Optical CDMA with interference cancellation," *Proceedings of the 1996 IEEE International Symposium on Spread Spectrum Techniques and Applications, ISSSTA'96*, Vol. 2, September 1996, pp. 590–594.

Simon, M.K., Omura, J.K., Scholtz, R.A. and Levitt, B.K. (1985), *Spread Spectrum Communications*, Vol. 1, Computer Science Press, Inc., 1985.

Smith, E.D.J., Gough, P.T. and Taylor, D.P. (1995), "Noise limits of optical spectral-encoding CDMA systems," *Electronics Letters*, Vol. 31, No. 17, August 1995, pp. 1469–1470.

Snyder, A.W. and Love, J.D. (1983), *Optical Waveguide Theory*, Chapman and Hall, 1983.

Takushima, Y. and Kikuchi, K. (1994), "Photonic switching using spread spectrum technique," *Electronics Letters*, Vol. 30, No. 5, March 1994, pp. 436–438.

Tamura, S., Nakano, S. and Okazaki, K. (1985), "Optical code-multiplex transmission by Gold sequences," *Journal of Lightwave Technology*, Vol. 3, No. 1, February 1985, pp. 121–127.

Tančevski, L. and Andonovic, I. (1995), "Block multiplexing codes for optical ladder network correlators," *IEEE Photonics Technology Letters*, Vol. 6, No. 2, February 1995, pp. 309–311.

Tančevski, L. and Andonovic, I. (1994), "Wavelength hopping/time spreading code division multiple access systems," *Electronics Letters*, Vol. 30, No. 17, August 1994, pp. 1388–1390.

Tančevski, L., Bazgaloski, L., Andonovic, I. and Budin, J. (1994), "Incoherent asynchronous optical CDMA using gold codes," *Electronics Letters*, Vol. 30, No. 9, April 1994, pp. 721–723.

Taylor, H.F. (1990), "Intensity noise and spontaneous emission coupling in superluminescent light sources," *IEEE Journal of Quantum Electronics*, Vol. 26, No. 1, January 1990, pp. 94–97.

Tou, C.P. (1987), "Code division multiplexing for optical fiber communications," *Proceedings of the 1987 IEEE Pacific Rim Conference on Communications, Computers and Signal Processing*, June 1987, pp. 327–330.

Tur, M., Shafir, E. and Bløtekjaer, K. (1990), "Source-induced noise in optical systems driven by low-coherence sources.," *Journal of Lightwave Technology*, Vol. 8, No. 2, February 1990, pp. 183–189.

Vannucci, G. and Yang, S. (1989), "Experimental spreading and despreading of the optical spectrum," *IEEE Transactions on Communications*, Vol. 37, No. 7, July 1989, pp. 777–780.

Vethanayagam, N. and MacDonald, R. (1991), "Demonstration of a novel optical code-division multiple-access system at 800 megachips per second," *Optics Letters*, Vol. 16, No. 13, July 1991, pp. 1010–1012.

Viterbi, A.J. (1995), *CDMA: Principles of Spread Spectrum Communications*, Addison-Wesley Publishing Co., 1995.

Wacogne, B. and Jackson, D.A. (1996a), "Security vulnerability in coherence modulation communication systems," *IEEE Photonics Technology Letters*, Vol. 8, No. 3, March 1996, pp. 470–472.

Wacogne, B. and Jackson, D.A. (1996b), "Enhanced security in a coherence modulation system using optical path difference corruption," *IEEE Photonics Technology Letters*, Vol. 8, No. 7, July 1996, pp. 947–949.

Wallace, C.G., Kelly, A.E., Uttamchandani, D. and Andonovic, I. (1995), "New unipolar codes allowing electrooptical correlation utilizing a semiconductor laser amplifier," *IEEE Photonics Technology Letters*, Vol. 17, No. 12, December 1995, pp. 1456–1458.

Weiner, A.M., Heritage, J.P. and Salehi, J.A. (1988), "Encoding and decoding of femtosecond pulses," *Optics Letters*, Vol. 13, No. 4, April 1988, pp. 300–302.

Wentworth, R.H. (1989), "Theoretical noise performance of coherence-multiplexed interferometric sensors," *Journal of Lightwave Technology*, Vol. 7, No. 6, June 1989, pp. 941–956.

Wentworth, R.H. and Moslehi, B. (1989), "Comments on "Fringe visibility and phase noise in superluminescent diodes"," *IEEE Journal of Quantum Electronics*, Vol. 25, No. 5, May 1989, pp. 1125–1126.

Wu, J.H. and Wu, J. (1995), "Synchronous fiber-optic CDMA using hard-limiter and BCH codes," *Journal of Lightwave Technology*, Vol. 13, No. 6, June 1995, pp. 1169–1176.

Yang, G.C. and Fuja, T.E. (1995), "Optical orthogonal codes with unequal auto- and cross-correlation constraints," *IEEE Transactions on Information Theory*, Vol. 41, No. 1, January 1995, pp. 96–106.

Yang, G.C. and Jaw, J.Y. (1994), "Performance analysis and sequence designs of synchronous code-division multiple-access systems with multimedia services," *IEE Proceedings on Communications*, Vol. 141, No. 6, December 1994, pp. 371–378.

Yang, G.C. and Kwong, W.C. (1995a), "On the construction of 2^n codes for optical code-division multiple-access," *IEEE Transactions on Communications*, Vol. 43, No. 2/3/4, February/March/April 1995, pp. 495–502.

Yang, G.C. and Kwong, W.C. (1995b), "Performance analysis of optical CDMA with prime codes," *Electronics Letters*, Vol. 31, No. 7, March 1995, pp. 569–570.

Yao, X.S., Feinberg, R.L. and Maleki, L. (1993), "Limitations on peak pulse power, pulse width, and coding mask misalignment in a fiber-optic code division multiple-access system," *Journal of Lightwave Technology*, Vol. 11, No. 5/6, May/June 1993, pp. 836–846.

Yurek, A.M., Goldberg, L., Weller, J.F. and Taylor, H.F. (1987), "Fringe visibility and phase noise in superluminescent diodes," *IEEE Journal of Quantum Electronics*, Vol. 23, No. 8, August 1987, pp. 1256–1260.

Zaccarin, D. and Kavehrad, M. (1993), "An optical CDMA system based on spectral encoding of LED," *IEEE Photonics Technology Letters*, Vol. 4, No. 4, April 1993, pp. 479–482.

Zaccarin, D. and Kavehrad, M. (1994a), "Performance evaluation of optical CDMA systems using non-coherent detection and bipolar codes," *Journal of Lightwave Technology*, Vol. 12, No. 1, January 1994, pp. 96–105.

Zaccarin, D. and Kavehrad, M. (1994b), "New architecture for incoherent optical CDMA to achieve bipolar capacity," *Electronics Letters*, Vol. 30, No. 3, February 1994, pp. 258–259.

Zhang, J.G. (1996), "Strict optical orthogonal codes for purely asynchronous code-division multiple-access applications," *Applied Optics*, Vol. 35, No. 35, December 1996, pp. 6996–6999.